A test procedure for vehicle dynamic controllers

ika Report 8329

Contents

1 Introduction

In modern vehicles, wheel slip control systems from the anti-blocking system (ABS) via the traction control down to the driving-dynamics controls have been developed. In this last named system, the driving condition of the vehicle is monitored by sensorics and the vehicle stabilised in critical driving situations by purposeful interventions individual to each wheel by the brake as well as a reduction of the engine torque.

As the brake interventions can be critical to safety, a sophisticated inherent diagnosis monitors the system. In disturbances, the driving-dynamics controller can thus partly or totally be deactivated before faulty interventions result. The driver is advised of the disturbance of the system by a warning light going on. In addition, the disturbance recognised is stored in the error memory of the system. However, the inherent diagnoses cannot cover all the imaginable malfunctions, and they also react very late to creeping deteriorations of the system.

During the periodical vehicle monitoring, all the electronically controlled systems can currently only be tested insufficiently. Alongside a visual check of sensors, wiring and actuators, there is only a check of the warning lamp. However, the meaningfulness of this is only minimal, in addition only possessing an extremely low manipulation safety.

For this reason, the "International Motor Vehicle Inspection Committee (CITA)“ commissioned the "Institut für Kraftfahrwesen Aachen (ika)“ with developing a test procedure for vehicle dynamics controllers. The test procedure is to be as simple as possible and to enable a qualitatively meaningful analysis of the state of the vehicle dynamics controller within a short period. In addition, the apparatus needed for the implementation of the tests is to be within reasonable limits.

The development of this test procedure is done with the help of simulation models. For this, two vehicles are selected to start with which have a distinct difference in their vehicle class, their drive concept and the structure of the vehicle dynamics controller. This mode of procedure is to provide a certain "universality" of the results. After this, both the vehicles themselves as well as the intervention conduct of the vehicle dynamics controller are examined in test-bench and driving tests. With the help of the information gained in this way, the simulation models are drawn up and verified. The simulation models are especially well suited for drawing up a test procedure, as a large number of tests can be carried out in a short time here. In addition, the conduct of the systems in disturbances can be examined free of risks.

2 State of the art

Before we deal with the actual development of a test procedure for a vehicle dynamics controller, the current state of the art both with the systems themselves as well as in the existing test concepts is to be portrayed.

2.1 Vehicle dynamics controller

In modern vehicles, not only the anti-blocking (ABS) and traction control systems (TCS), but also vehicle dynamics controller (VDC) are part of standard equipment. These systems monitor the state of the vehicle and support the driver by purposeful brake interventions and/or a reduction of the engine torque when controlling the vehicle in borderline situations.

2.1.1 Principal mode of function

To assess the current state of driving, the driving-dynamics control system possesses various sensors as shown in Fig. 2-1. Alongside detection of the wheel speeds and the steering wheel angle, the yaw velocity and the transverse acceleration of the vehicle are measured. In order to initiate the brake interventions, a hydraulic power unit is needed. In addition, there is a connection to the engine electronics of the vehicle.

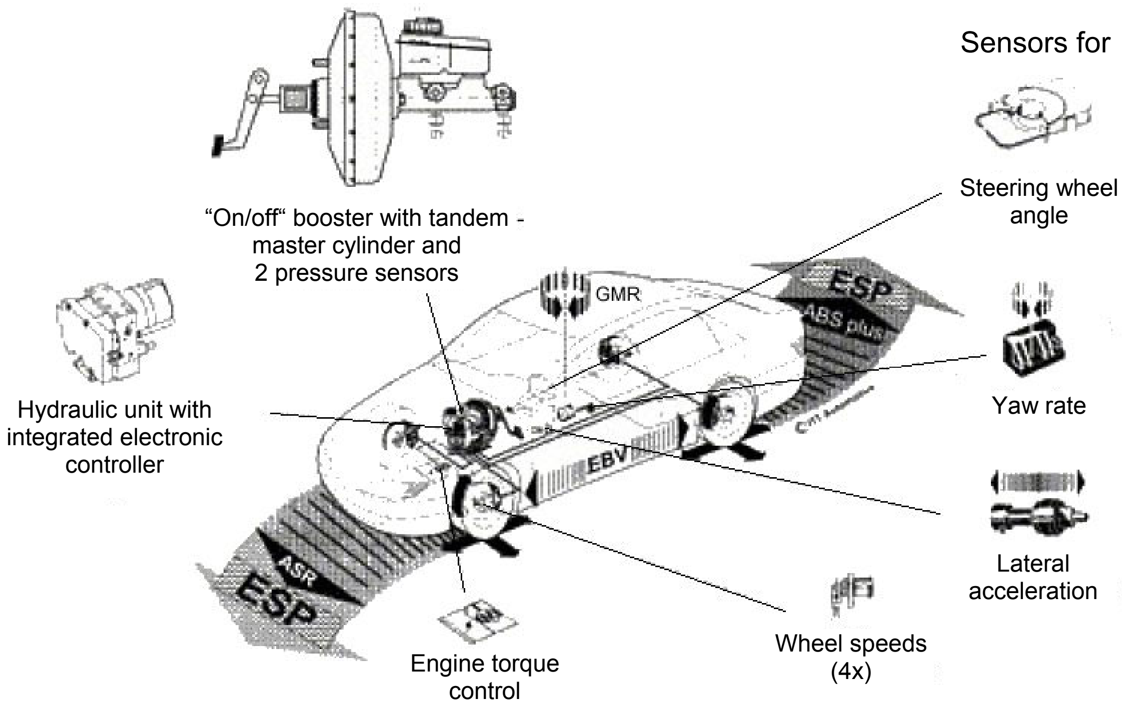

Fig. 2-1: Sensor equipment of the vehicle dynamics controller [FEN98]

If there is an understeer reaction in a vehicle, i.e. a high load of the grip on the front axle, the yaw rate is reduced. This alteration is detected by the sensors, and the vehicle dynamics controller initiates a brake intervention on the rear wheel on the inside of the bend, Fig. 2-2. As a result of the brake power acting on one side, a yaw moment is generated around the vertical axis, turning the vehicle in the direction of the inside of the bend and thus counteracting the understeer movement.

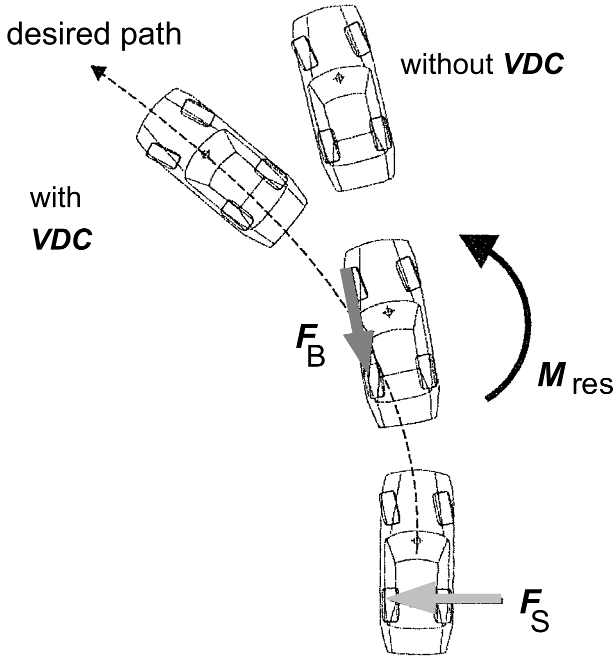

Fig. 2-2: Brake intervention of the vehicle dynamics controller while understeering

If a vehicle shows an oversteer reaction, i.e. the rear of the vehicle threatens to swerve, there is a fast increase in the yaw rate, Fig. 2-3. The vehicle dynamics controller initiates a brake power on the front wheel on the outside of the bend as a result. In this way, a yaw moment is generated which counteracts the turning movement of the vehicle around the vertical axis and thus prevents further swerving. In addition, the lateral force potential of the front wheel is weakened by the intervention, also supporting the required movement of the vehicle.

In order to generate a desired yaw movement of the vehicles, one side of the vehicle could naturally be braked on both wheels. However, a brake intervention on the axle which has already reached the adhesion limit anyway is normally avoided. The fact that each brake intervention reduces the traction of the vehicle is principally positive for the stability in driving. This alone frequently increases the driving stability.

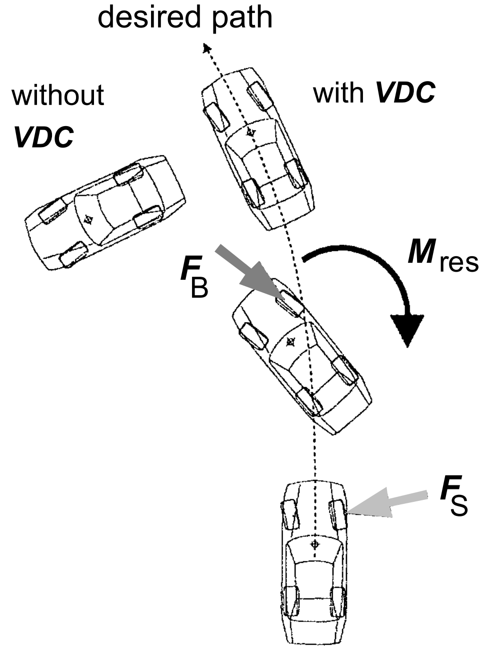

Fig. 2-3: Brake intervention of the vehicle dynamics controller while oversteering

Alongside this control of the yaw velocity, all the present systems also have standard structures to limit the vehicle's sideslip angle. The necessity of such algorithms is made clear by the movement of a vehicle on a circular journey on various coefficients of friction and with various control concepts, Fig. 2-4.

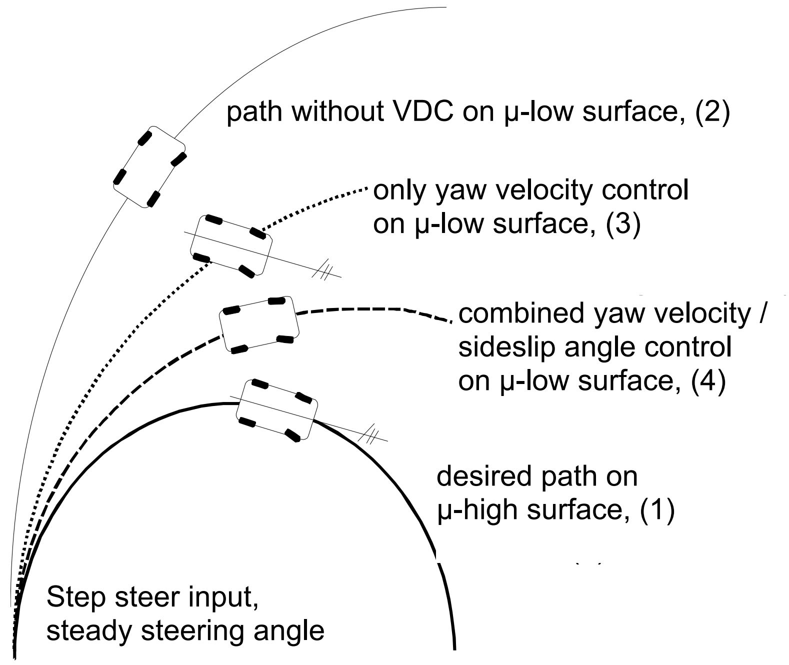

Fig. 2-4: Steady-state cornering of a vehicle on µ-low and µ-high surface with different control strategies [VAN96a,b,c]

The bottom graph (1) shows the course of the track of the vehicle when the tyre-road coefficient of friction between the road and the tyre is sufficient for the lateral forces to be transmitted. Lateral force reserves still exist, nominal and actual movement correspond. In this case, the vehicle follows the nominal course required by the driver in steady state cornering.

But if the road surface has a coefficient of friction no longer sufficient to achieve the nominal lateral acceleration stipulated by the steering angle and the vehicle velocity, a vehicle without driving-dynamics control will, as a rule, understeer and swerve out of the curve. The radius of the track will be distinctly larger than the nominal radius (2).

In a vehicle with vehicle dynamics controler, but without sideslip angle limitation (3), this situation would be evaluated as severe understeering and thus lead to a brake power on the rear wheel on the inside of the bend. With such a control, a correct yaw velocity would result, but at the same time a strong sideslip angle would be formed. All told, a pure yaw velocity control on a low coefficient of friction would lead to an unstable driving condition as a result of the intervention of the vehicle dynamics controller if the driver failed to react in good time by reducing the steering angle accordingly.

A stable vehicle movement without intervention by the driver therefore needs not only control of the yaw velocity, but also a limitation of the sideslip angle. In such a combined control, the vehicle moves stably with a limited sideslip angle on a path which corresponds to the physically possible transverse acceleration (4). The weighting of the control to yaw angle or sidselip angle is done differently in [P4305], [WIT95], [VAN94], [VAN96].

2.1.2 Structure of the controller

In the "Driver/Vehicle Environment“ control loop, disturbing variables act on the vehicle and lead to a deviation between nominal and actual course. Normally, the "vehicle" norm route is designed in such a way that these deviations can be compensated by the "driver" control alone. When approaching the threshold area of the vehicle or with a large alteration of the vehicle driving performance (e.g. due to load, low coefficients of friction), the driver can be overburdened with his control task. In such situations, the vehicle dynamics controler is to compensate the disturbances which the driver alone is no longer in a position to compensate.

To fulfil this task, the vehicle dynamics controller, as described further below, has sensors, which detect the driving condition. In a software model, all the estimated and standard variables are calculated. The actuation system is used to set the slip alterations on the tyres. The whole controls are superposed by a safety concept which is used to recognise malfunctions and to guarantee driving safety in partial or complete failure of the system, Fig. 2-5.

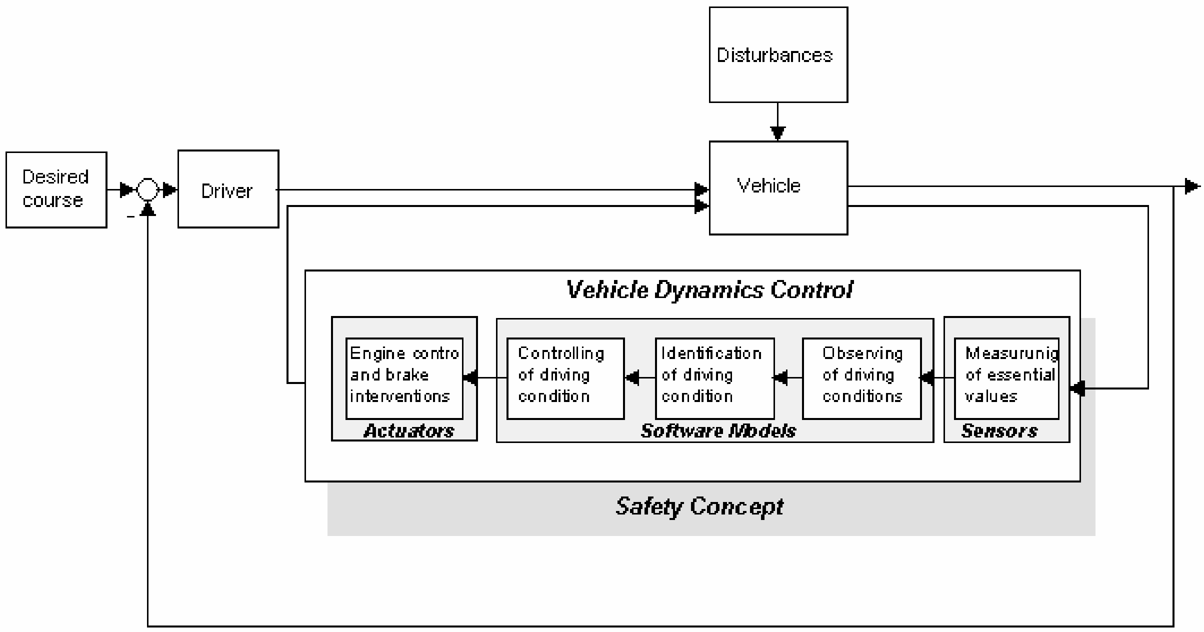

Fig. 2-5: Control loop driver-vehicle-environment

In principle, all the software elements of a vehicle dynamics controller can be assigned to the observation of driving condition, identification of driving condition and control of driving condition blocks. In the design for various vehicle concepts (front, rear and four-wheel drive) as well as quality of the control, sensors, design of control and possibilities of intervention, differences in detail naturally occur between the systems stated [ALB96], [KOI96], [VAN96].

Observation of the driving condition of the vehicle calculates and estimates all the variables not directly measurable as a function of the sensors used and the vehicle and tyre models stored in the computer. These are essentially:

- driving speed
- sideslip angle

The driving speed can be calculated quite well from the four wheel-speed sensors. In addition, modern systems normally also have a longitudinal acceleration sensor, in order further to improve the quality of the estimate of the driving speed. The sideslip angle is normally determined by means of integration of the sideslip angle velocity, which for its part is calculated from the yaw velocity $\dot{\psi}$, transverse acceleration a_y and longitudinal velocity v_x [WIT95]:

$$\dot{\beta} = \dot{\psi} - \frac{a_y}{v_x} \qquad \text{Eq. 2-1}$$

The task of Identification of the driving condition of the vehicle is to recognise a driving state critical for lateral dynamics and to activate the driving condition control. A state critical for lateral dynamics has been reached if the calculated nominal and the measured actual yaw velocity distinctly deviate from one another. For this purpose, the nominal yaw velocity to [P4305] and [WIT95] is surrounded by a tolerance band and the driving condition control is only activated if the tolerance band is exceeded. The nominal yaw velocity is calculated from longitudinal velocity v_x and steering wheel angle δ according to the linear bicycle model:

$$\dot{\psi}_{soll} = \frac{v_x}{l \cdot \left(1 + \frac{v_x^2}{v_{char}^2}\right)} \cdot \delta \qquad \text{Eq. 2-2}$$

In addition, wheel base l and the characteristic velocity of the vehicle v_{char} (driving speed with the highest yaw sensitivity of the vehicle) are needed in this equation. Further, the nominal yaw velocity is frequently limited to the predominant coefficient of friction:

$$\dot{\Psi}_{max} = \frac{g \cdot \mu}{v} \qquad \text{Eq. 2-3}$$

If the coefficient of friction is not estimated in the observer of the controls, an exclusive observation of the yaw velocity not limited as a function of the coefficient of friction can also be used in order to recognise the nominal driving state [WIT95], [VAN96].

The driving condition control determines a corrective yaw torque from the results of the driving condition recognition according to suitable control algorithms, the torque being set by individual brake and/or engine intervention. For this, hydraulics which can build up pressure independently are necessary. Brake and drive slip controls are normally subordinate to the actual vehicle dynamics controller.

To sum up, efficient lateral dynamics controls require sensors for wheel speeds, steering wheel angle and yaw velocity. With this, a good control can be designed via a yaw velocity control specifically for a high coefficient of friction [WIT95]. For adequate control with a low coefficient of friction, a lateral acceleration sensor is additionally necessary according to [WIT95], [VAN94], [VAN96]. In this way, a combined yaw velocity control / sideslip angle limitationcan be implemented.

2.1.3 Safety concept

Due to the high safety requirements made of active control systems in motor vehicles, the design of a corresponding safety concept is necessary. With this safety concept, there must be a guarantee that no unsafe system conditions can occur in measurement errors due to the failure of various parts of the electronics which can occur without being foreseeable, e.g. wear and tear.

The objective of the safety concept must be to recognise errors occurring and to master them according to the cause and effect. Depending on the error, this can lead to the system being switched off and, if need be, transfer to a safe condition. The failure of the system may not lead to an additional limitation of the vehicle safety as a matter of principle.

In practice, system safety is only partly realised by the redundant design of important system hardware components. Mainly, inherent diagnosis is used, covering the following aspects:

- interruption of the line
- physical plausibility
- analytical redundancy
- sensor self-tests

Monitoring for interruption of the line recognises both broken wires and also wires with a great increase in ohmic resistances. Physically implausible signals are, for example, sensor figures a long way outside the possible boundaries of driving physics, but also signal interferences.

In analytical redundancy, the sensors are monitored against one another during the entire stationary driving operation by model calculations examining whether the relationships between the sensor signals determined via the movement of the vehicle are not breached. These models are further used to calculate and compensate sensor offsets occurring within the sensor specifications,.

The sensor self-tests portray an active test of the sensors. The yaw velocity sensor, for example, is tested by active de-tuning of the sensor element and evaluation of the signal reply. Fig. 2-6 shows the mode of function of this test. Whenever the test function is activated, the yaw velocity sensor provides an additional amplitude of +/- 28°/s as an output signal to the control device. This signal is detected with a periodic duration of 20 ms, with the result that a decision about the functionality of the sensor can be made every 20 ms [VAN98]..

The function of the brake pressure sensor is monitored with the help of an initialisation test, Fig. 2-7. When the supply voltage is brought up, the signal voltage follows the course of the energy supply to start with until the maximum voltage of 5 V is reached, without brake pressures actually existing. About 300 ms after this maximum voltage has been reached, the sensor must output a voltage of 2.5 V for a period of about 100 ms. The signal voltage output only corresponds to the measured brake pressures after completion of this initialisation test.

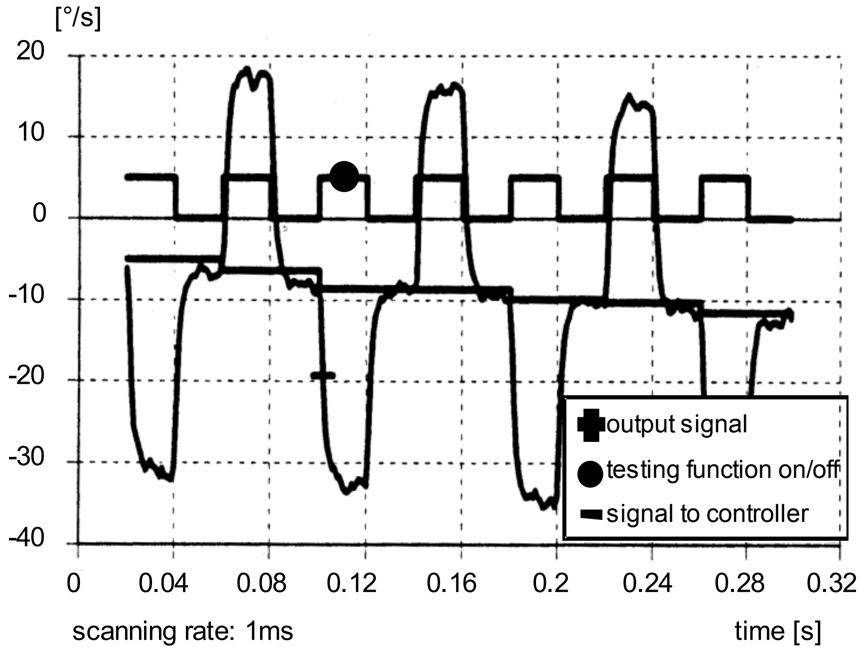

Fig. 2-6 Self-test of the yaw velocity sensor [VAN98]

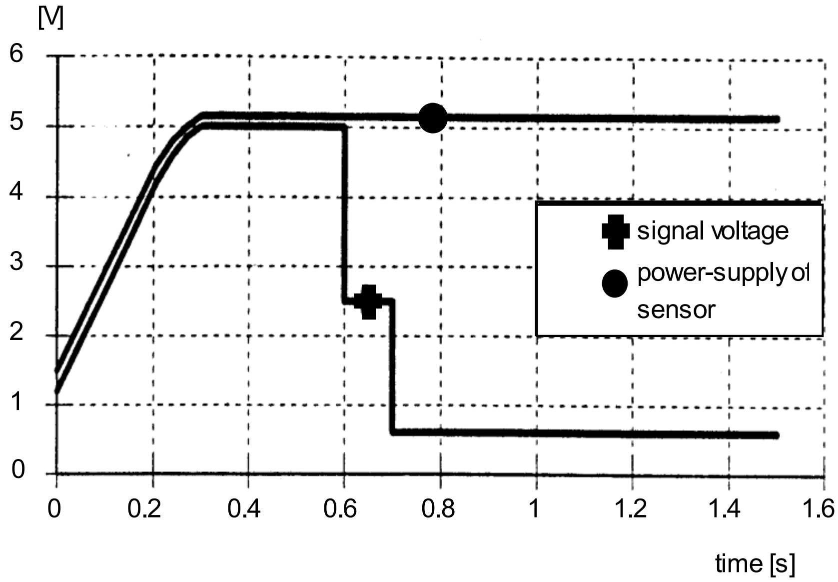

Fig. 2-7: Initialisation test of the brake pressure sensor [VAN98]

As the measurement of the steering wheel angle is state of the art and can be done reliably, the steering wheel sensor can generally be defined as the so-called "master sensor“. Starting from this sensor, all the necessary calibration procedures for the other sensors are done. For this reason, the steering wheel angle sensor must be in a position to recognise internal errors and to report them to the control device straight away via a CAN (Controller Area Network) bus [VAN98]. In this way, the CAN bus, via which the communication with other systems such as the engine management and the gearbox control functions is done, also contributes to increasing the reliability of the driving-dynamics control.

In the event of an error, the system is switched off partly or totally as a function of the kind of error. On a first relapse level, the vehicle dynamics control functions are only available with free rolling or braked wheels in the Bosch ESP. This is the case for an error in the interface to the engine management or in an error in the supercharge pump.

Treatment of errors also depends upon whether the control is active or not [WIT95]. In the event of a control device error or an electrical fault in the hydraulic components, the ESP is deactivated straight away and all the warning lamps are switched on. If errors occur in the wheel speed sensors or the pressure sensor with the control active, the function of the ESP can be maintained at least partly with emergency running programmes until the end of the system intervention. If errors occur on these sensors without the control being active, the ESP is directly deactivated.

If an error occurs on the yaw angle sensor, on the lateral acceleration sensor or on the steering wheel angle sensor, an emergency run ABS is activated, which does not depend on any of the three sensor signals in the calculation of the reference velocity. In this way, a basic ABS functionality can be maintained. Switching over to the emergency run ABS is displayed to the driver by the activation of the ESP lamp.

Even in a complete failure of the ESP and emergency run ABS, the function of the electronic brake proportioning device is maintained to start with. A relapse level can limit the brake pressure on the rear axle to uncritical values if a sufficient quantity of wheel speed signals are available. If not even this function can be maintained, the driver is notified of this in the form of a red warning light [VAN98].

2.2 Existing test concepts

Despite the complex inherent diagnosis routines, which can easily exceed the scope of the actual control logic in modern control devices, extensive tests are done with the electronically controlled system both by the suppliers of the electronics and by the vehicle manufacturers themselves. The reason for this is that many control device functions can only be tested unambiguously if not only the signals on the electrical interfaces, but also variables internal to the control devices can be observed and/or altered [KLU99]. A glance at the MIL (Malfunction Indication Light) is obviously not considered sufficient by either the supplier or the vehicle manufacturer.

Suppliers of electronically controlled systems mainly hold functional tests both as quality assurance measures accompanying the development and also for acceptance by the automobile manufacturer. In the functional test, the properties of the test object compared with defined specifications are verified. The tests are held with the help of real-time simulators, in which the real control device is fed with test signals by a simulated vehicle environment (Hardware-in-the-Loop – HIL) [KLU99].

Vehicle manufacturers subject ready fitted vehicles to a bench test at the end of the production line. But this is merely a test of the sensors, as the following illustration shows (Fig. 2-8).

Fig. 2-8: ESP test-bench at Audi AG

By rotating the vehicle around the lateral, longitudinal and yaw axis, lateral acceleration, longitudinal acceleration and yaw rate sensors are tested. The entire test is fully automatic. For one minute, stipulated profiles are run, for one minute there is free running. The requirements of the test programme run via a universal test system with communication to the control device. With the test bench at the end of the line, reproducible measurement results are achieved, thus replacing the "double S runs" on the test track necessary up to now for the initialisation of the sensors [AUD01].

3 Measurement of the test vehicles

The test vehicles selected are a Mercedes-Benz A Class and a BMW 330xi, Fig. 3-1 and Fig. 3-2.

Fig. 3-1: Mercedes-Benz A-Class (A160)

Fig. 3-2: BMW 330xi

The Mercedes-Benz A Class is a front-driven vehicle. The standard vehicle dynamics controller comes from Robert Bosch GmbH. It is called ESP (Electronic Stability Programme) at DaimlerChrysler. The BMW has a permanent four-wheel drive, with only about 33% of the drive torque being transmitted to the front axle. Thus, it is still a rather rear-dominated vehicle. The vehicle dynamics controller unit, which is also standard, is called DSC (Dynamic Stability Control) here and is produced by ContiTeves AG. Thus, two vehicles with completely differing drive and vehicle dynamics controller concepts are available for the tests.

3.1 Bench tests

In order to be able to produce the two complete vehicle simulation models, a large number of vehicle-specific data must be known. For this reason, the locations of centre of gravity, the moments of inertia for the three main axes, the axis cinematic points, the spring and shock absorber characteristics and the tyre maps and the brake proportioning are determined experimentally. For the measurements in which the state of loading of the vehicle is relevant (location of centre of gravity and moments of inertia), identical loading conditions are selected, as in the driving tests to be held later. They correspond to a driver with a passenger sitting behind him and the measurement technique, accommodated on the right-hand side of the interior in each case. Below, the individual test benches and the implementation of the measurements and their evaluation are described.

3.1.1 Location of centre of gravity

The location of centre of gravity of the test vehicle is determined in a longitudinal, lateral and vertical direction. Below, the longitudinal direction is called the x coordinate, the lateral direction y coordinate and the vertical direction z coordinate.

The location of centre of gravity in the x and y directions is determined by measuring the four wheel loads by means of wheel-load scales, onto which the vehicle is placed. Alongside the overall weight of the vehicle determined in this way, the position of the centre of gravity in an x and y direction can be calculated with the known wheel base and track width variables by production of torque equilibria.

The height of the centre of gravity is determined by weight displacement when lifting an axle. In this process, the brakes are released and the transmission is in neutral, through which the wheels can be freely turned. The efficiency lines of the axle loads pass through the wheel centre lines. To detect the axle load of the axle which has not been lifted, two wheel-load scales are used, Fig. 3-3.

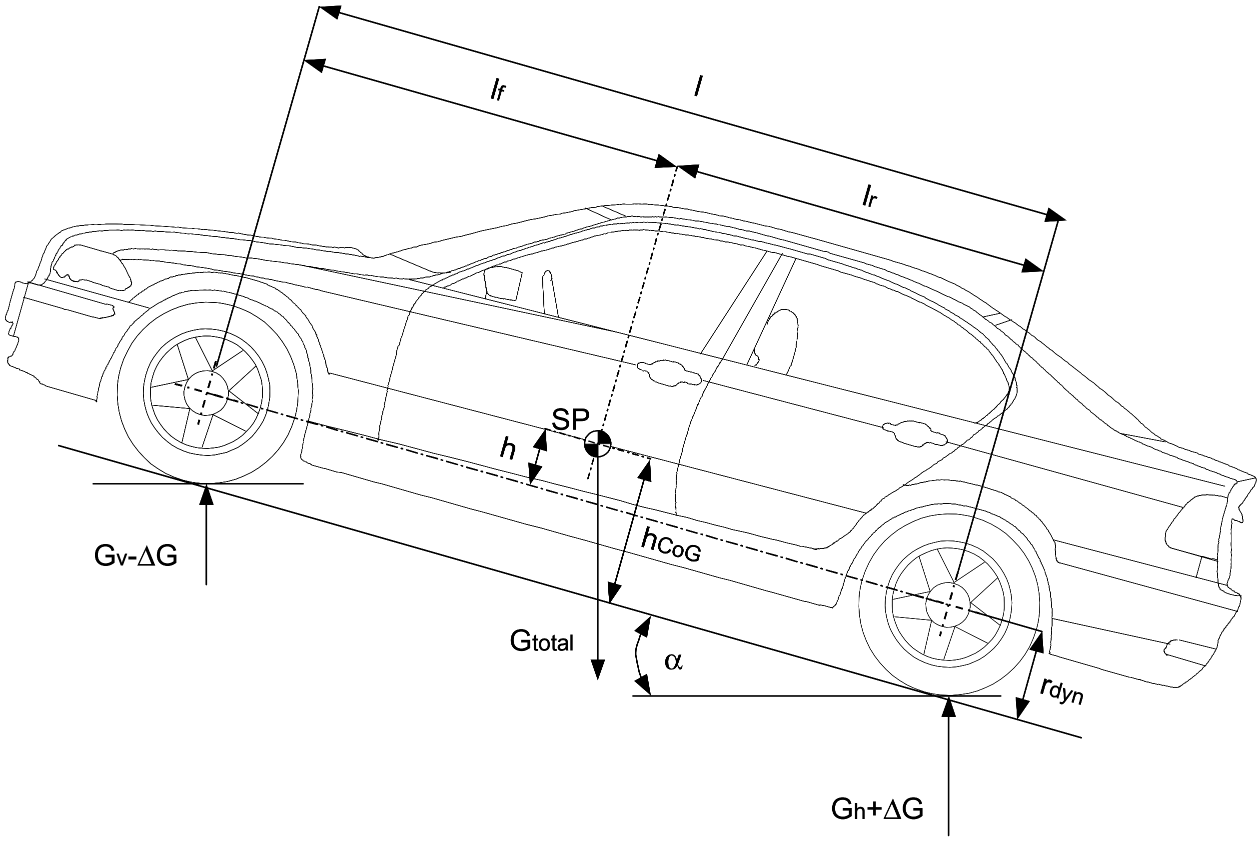

Fig. 3-3: Measurement of the vehicle's centre-of-gravity height h_S

As a function of the inclination of the vehicle, the axle loads on the front and rear axle change. The height h of the centre of gravity above the level passing through the front and rear wheel centre line can be calculated via the torque equilibrium around the rear wheel centre line from the difference of the axle loads and the angle of inclination of the vehicle in question:

$$h_{CoG} = \frac{(\Delta G \cdot l)}{(\tan(\alpha) \cdot G_{total})} + r_{dyn} \qquad \text{Eq. 3-1}$$

The dynamic wheel radius is measured with the vehicle at a standstill. Thus, the following basic values result for the two test vehicles on this basis of calculation (Fig. 3-4 and Fig. 3-5).

- **Mercedes-Benz A-Class**

Basic values	
wheel base	2423 mm
track width front	1492 mm
track width rear	1426 mm
dynamic tyre radius	280 mm
total mass	1245 kg
distance front axle - centre of gravity	1100 mm
distance rear axle - centre of gravity	1323 mm
centre-of-gravity height	580 mm

Fig. 3-4: Basic values Mercedes-Benz A-Class

- **BMW 330xi**

Basic values	
wheel base	2725 mm
track width front	1471 mm
track width rear	1478 mm
dynamic tyre radius	300.5 mm
total mass	1725 kg
distance front axle - centre of gravity	1365 mm
distance rear axle - centre of gravity	1360 mm
centre-of-gravity height	493 mm

Fig. 3-5: Basic values BMW 330xi

3.1.2 Moments of inertia

Now that the location of centre of gravity is known, the moments of inertia (MOI) around the longitudinal, lateral and vertical axes can be measured. This is done by the vehicle oscillating around the corresponding axes at the centre of gravity of the vehicle against springs of a known stiffness. By measurement of the oscillation time T, the moments of inertia can be calculated with known spring stiffness.

To determine the moments of inertia around the lateral axis of the vehicle, the vehicle is placed on a cutting line transverse to the direction of travel. The cutting line is aligned in such a way that the centre of gravity of the vehicle in a horizontal position of the vehicle is vertically above the cutting line. In the longitudinal direction of the vehicle, springs on which the vehicle supports itself via the auxiliary frame are clamped in at identical distances, Fig. 3-6.

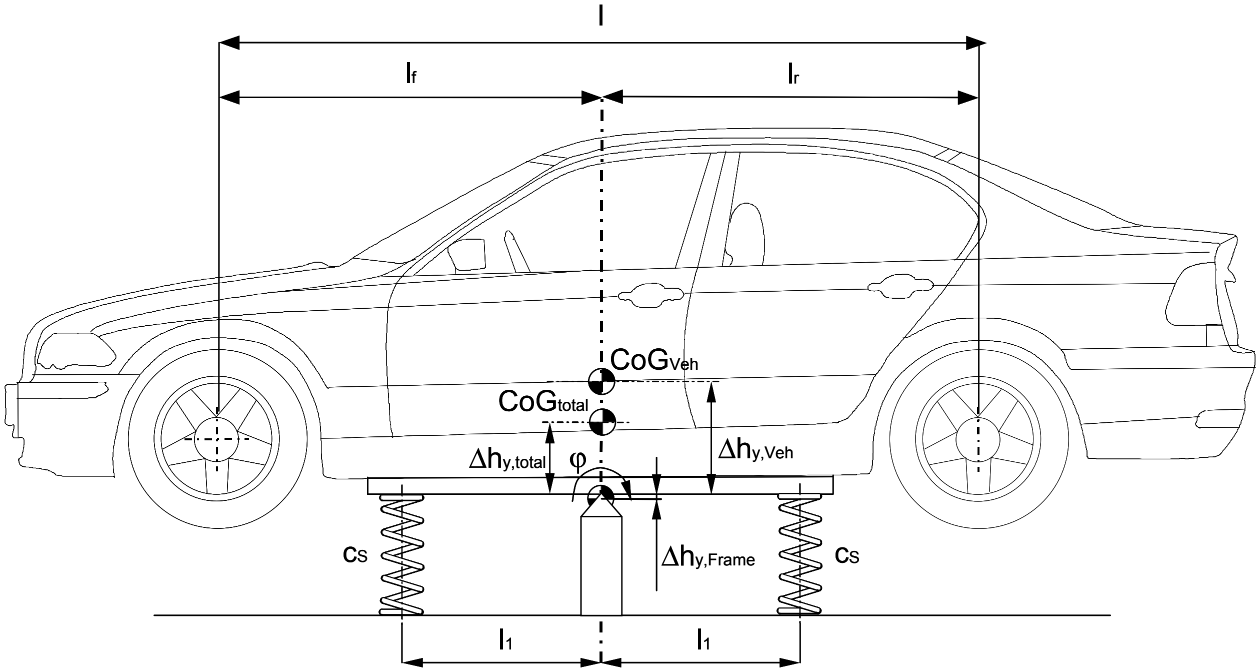

Fig. 3-6: Measurement of the MoI around the transversal vehicle axis

Euler's theorem is used to calculate the moment of inertia of the vehicle/frame unit around the cutting line axis from the frequency of the oscillations of this system:

$$\Theta_{y,total} = \frac{\left(2 \cdot c_S \cdot l_{1,total}^2 - m \cdot g \cdot \Delta h_{y,total}\right)}{(2 \cdot \pi)^2} \cdot T^2 \qquad \text{Eq. 3-2}$$

This approach for the calculation of the moment of inertia holds for the entire vehicle/frame unit around the cutting line axis. In order to obtain the MOI for the vehicle around its lateral axis passing through the centre of gravity alone, two items obtained up to now must be subtracted:

On the one hand, an item is contained corresponding to the MOI of the frame. To remove it from the result up to now, the measurement with the auxiliary frame alone is repeated and the moment of inertia of the frame around the cutting line axis $\Theta_{y,Frame}$ is calculated. By subtracting $\Theta_{y,Frame}$ from the overall moment of inertia around the cutting line $\Theta_{y,total}$, the moment of inertia of the vehicle alone around the cutting line axis, Eq. 3-3, results.

$$\Theta_{y,Veh} = \Theta_{y,total} - \Theta_{y,Frame} \qquad \text{Eq. 3-3}$$

The second item having an influence on the moment of inertia around the lateral axis is the so-called "Steiner ratio“ of the vehicle. The Steiner ratio results from the distance between the rotary axis of the cutting line and the required reference axis, the axis through the centre of gravity of the vehicle. By subtracting the Steiner ratio in Eq. 3-4, the moment of inertia in a lateral direction of the vehicle through the centre of gravity is determined.

$$\Theta_{y,CoG} = \Theta_{y,Veh} - m_{Veh} \cdot \Delta h^2_{y,Veh} \qquad \text{Eq. 3-4}$$

Fig. 3-7 shows the test set-up for the measurement of the BMW 330xi.

Fig. 3-7: Test-bench structure for the MOI measurement around the transversal axis

Each measurement of the oscillation time is done a total of ten times. Finally, the mean value of these ten measurements is used for the calculation of the MOI. An analogous procedure is used in determining the MOI around the longitudinal and vertical axis of the vehicle, with the oscillation axis being rotated by 90° each time. The entire mode of procedure is identical for both test vehicles. Fig. 3-8 and Fig. 3-9 show the results of the measurements.

- **Mercedes-Benz A-Class**

Moment of intertia in the centre-of-gravity	
around the x-axis	335 kgm²
around the y-axis	1095 kgm²
around the z-axis	1200 kgm²

Fig. 3-8: Total vehicle’s moment of inertia of Mercedes-Benz A-Class

- **BMW 330xi**

Moment of intertia in the centre-of-gravity	
around the x-axis	510 kgm²
around the y-axis	2280 kgm²
around the z-axis	2730 kgm²

Fig. 3-9: Total vehicle’s moment of inertia of BMW 330xi

3.1.3 Cinematic points

The cinematic points of the wheel suspension do not have to be determined separately in the course of this study, as they are already available from other investigations. The following data hold for the two test vehicles:

- **Mercedes-Benz A-Class**

Front and rear axle of the Mercedes-Benz A Class are shown in Fig. 3-10. The vehicle has a McPherson front axle. The wheel control is done not only by the suspension strut, but also by an A-frame arm, which is supported on the body by two rubber bearings. The connection to the wheel carrier is via a flanged joint, which is connected to the cross-member by three screws. The wheel carrier is screwed on its upper arm onto the suspension strut, which is supported on the body by a rubber/metal head bearing. The stabiliser is pivoted on the suspension strut via a pivoting plastic linkage. The rear axle of the vehicle is designed as a trailing arm rear axle and comprises a chassis sub-frame supporting a trailing arm, a single-tube gas-pressure shock absorber and a coil spring on each wheel side. A stabiliser is arranged between the trailing arms. In the direction of the body, four elastomer bearings are found in the chassis sub-frame and are used for vibration decoupling.

Front axle *Rear axle*

Fig. 3-10: Mercedes-Benz A-Class chassis

Fig. 3-11 and Fig. 3-12 show the cinematic points for the front and rear axle for the right-hand side of the vehicle for a right-turning system of coordinates on the level of the road surface in the middle of the front wheels.

Front axle	x [mm]	y [mm]	z [mm]
A-arm front inside	210	414	-89
A-arm rear inside	-100	434	-78
ball joint	5	725	-100
steering rod -> steering rack	138	392	7
steering rod -> wheel carrier	145	737	-10
wheel centre	0	746	0
roll centre	87		
steering column	138	250	7
steering wheel	-1100	350	520
transmission ratio steering	134 rad/m (i_{total} = 19.0 : 1)		
spring mount wheel carrier	5	725	-100
spring mount body	-26	568	523
damper mount wheel carrier	-3	626	65
damper mount body	-26	568	523
stabiliser body mount	250	440	50
stabi link -> stabiliser	50	530	50
stabi link -> wheel carrier	50	530	-100

Fig. 3-11: Kinematics points of the front axle of Mercedes-Benz A-Class

Rear axle	x [mm]	y [mm]	z [mm]
trailing arm outside	-2073	547	24
trailing arm inside	-2073	447	24
wheel centre	-2423	713	0
roll centre	0		
spring mount wheel carrier	-2393	555	-50
spring mount body	-2453	528	137
damper mount wheel carrier	-2156	540	-104
damper mount body	-2363	540	132
stabiliser body mount	-2170	400	50
stabi link -> stabiliser	-2370	490	50
stabi link -> wheel carrier	-2370	490	-100

Fig. 3-12: Kinematics points of the rear axle of Mercedes-Benz A-Class

- **BMW 330xi**

The front axle of the BMW 330xi is also a McPherson axle with a front-positioned rack-and-pinion steering and a stabiliser. It is connected with the body by a front-axle bracket. The wheel control is taken on by not only the suspension strut, but also an L-shaped cross-member forged of aluminium. For the wishbone, a non-elastic ball-and-socket joint at the connection to the front-axle bracket was selected, in order to ensure precise wheel control. The longitudinal suspension is done by the rubber bearing at the back with an adapted characteristic for the drive and the braking area. A hydraulic damping additionally integrated into the rubber bearing prevents transmissions of oscillations from the wheel area into the body. The wheel control joint integrated into the wishbone on the outside is designed elastically. This measure results, inter alia, in a harmonious pivoting property [HAR98]. The front axle has a lateral force compensation as a dive reduction. The steering stub is a weight-optimised forged steel part. The connection with the supporting tube of the suspension strut is done with a clamping lug. The entire front axle unit is portrayed in Fig. 3-13.

The rear axle of the test vehicle is a so-called central pivot spindle. It is connected with the body via a rear-axle bracket with four large-volume rubber bearings. The wheel forces and torques are absorbed by the trailing arm (integral cast part) and the two wishbones. The large longitudinal suspension important for the tyre comfort and noise quality is enabled by the specifically orientated bearing of the trailing arm, without undesired alterations of the steering angle resulting.

The arrangement of the wishbone has been selected in such a way that the toe-in practically does not alter in suspension. This is an important prerequisite for a comfort-emphasised spring and shock absorber coordination [HAR98]. The drive-off and anti-dive control ensures a low pitch angle and thus increases the drive comfort. A portrayal of the rear axles can also be seen in Fig. 3-13.

Front axle Rear axle

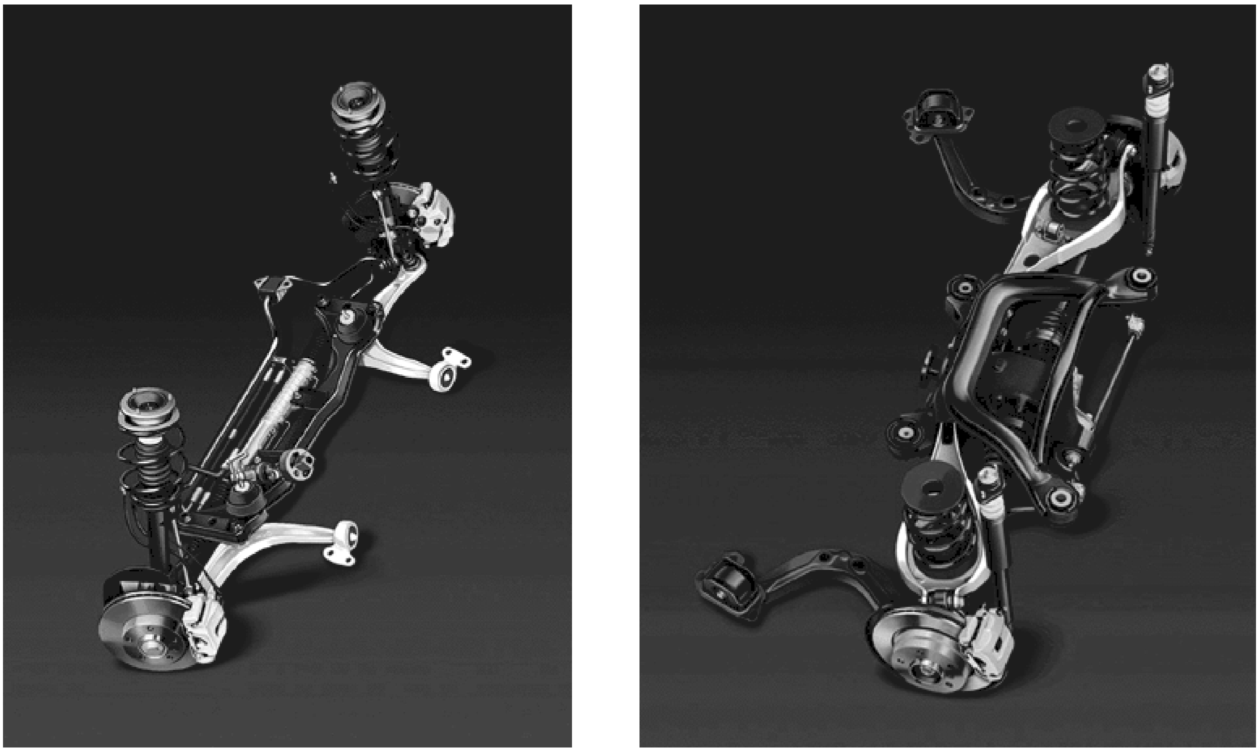

Fig. 3-13: Chassis of the BMW 330ix

The position of the cinematic points in question can be seen in Fig. 3-14 (front axle) and Fig. 3-15 and (rear axle). The values are based on a right-turning system of coordinates on the level of the road surface in the middle of the wheels.

The coordinate points of the front axle are those of the rear-wheel driven 330i version, as can be seen in Fig. 3-13 (no drive shafts). As the differences between the driven and the non-driven front axle are only very slight and the wheel lifting curves of the two-wheel drive version match those of the four-wheel drive version very well, the known front-axle cinematic of the BMW 330i is used for the simulation model. The rear axle is identical for both versions anyway.

Front axle	x [mm]	y [mm]	z [mm]
A-arm front inside	-35	330	-101
A-arm rear inside	-341	318	-92
ball joint	-1	654	-120
steering rod -> steering rack	57	306	-79
steering rod -> wheel carrier	123	667	-97
wheel centre	0	735.5	0
roll centre	93		
steering column	42	168	-79
steering wheel	-1124	330	560
transmission ratio steering	129.625 rad/m (i_{total} = 15.5 : 1)		
spring mount wheel carrier	-31	551	311
spring mount body	-42	507	448
damper mount wheel carrier	11	585	77
damper mount body	-31	551	311
stabiliser body mount	167	366	-3
stabi link -> stabiliser	-13	509	-10
stabi link -> wheel carrier	-12	510	-77

Fig. 3-14: Kinematics points of the front axle of the BMW 330xi

Rear axle	x [mm]	y [mm]	z [mm]
trailing arm body	-2260	725	40
upper transverse link body	-2563	165	49
upper transverse link wheel carrier	-2718	679	107
lower transverse link body	-2563	165	-26
lower transverse link wheel carrier	-2743	682	-130
wheel centre	-2725	739	0
roll centre	131		
spring mount wheel carrier	-2674	512	45
spring mount body	-2652	503	185
damper mount wheel carrier	-2832	579	-96
damper mount body	-2844	529	414
stabiliser body mount	-2885	247	-4
stabi link -> stabiliser	-2642	412	-26
stabi link -> wheel carrier	-2638	415	69

Fig. 3-15: Kinematics points of the rear axle of the BMW 330xi

3.1.4 Tyre maps

The ika has a tyre test bench which is suited for the examination of car tyres and also motorbike tyres and permits almost all wheel/tyre combinations with a rim diameter between 13“ and 19“. The basis of the test bench is an outer drum surface driven by a DC motor with which traction speeds of up to 180 km/h can be achieved. The tyres to be tested are guided on this surface; during the test, the slip angle, camber angle, wheel load and interior tyre pressure can be varied independent of one another, Fig. 3-16.

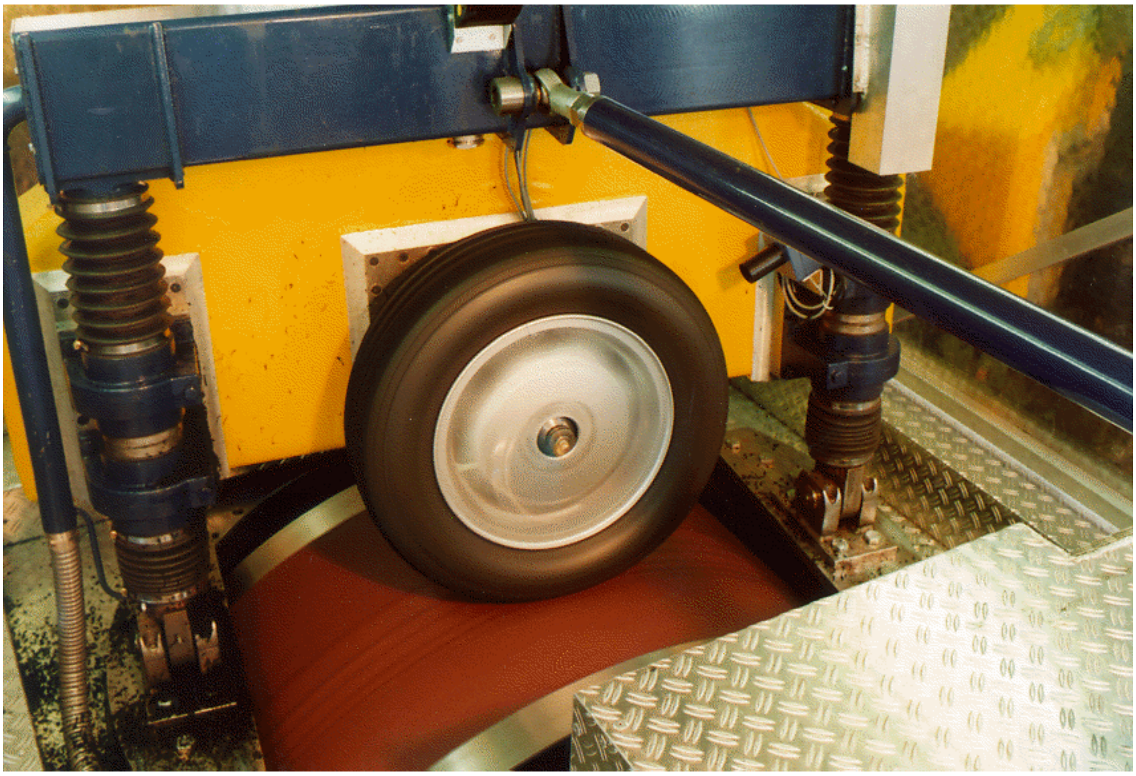

Fig. 3-16: Tyre test bench at ika

To detect the forces and torques occurring on the tyres, a 6-component dynamo hub with piezo-electric quartz force sensors has been installed. The detection of the measured data is supplemented by sensors for tyre pressure, slip and camber angle, wheel and drum speed as well as tyre temperature.

The measurement programme entails the examination of the quasi-stationary properties of the tyre in a longitudinal and lateral direction as well as combinations of the loads. From these examinations, parameters for the “Pacejka Magic Formula (SIMPACK’89)“ tyre model are found for the vehicle simulation computations, this formula acting as the tyre model for both vehicle simulation models. Fig. 3-17 to Fig. 3-22 show both individual measurement results from the tyre test bench as well as the parameters derived from them for the tyre model for the tyres of the Mercedes-Benz A Class and the BMW 330xi.

- **Mercedes-Benz A-Class**

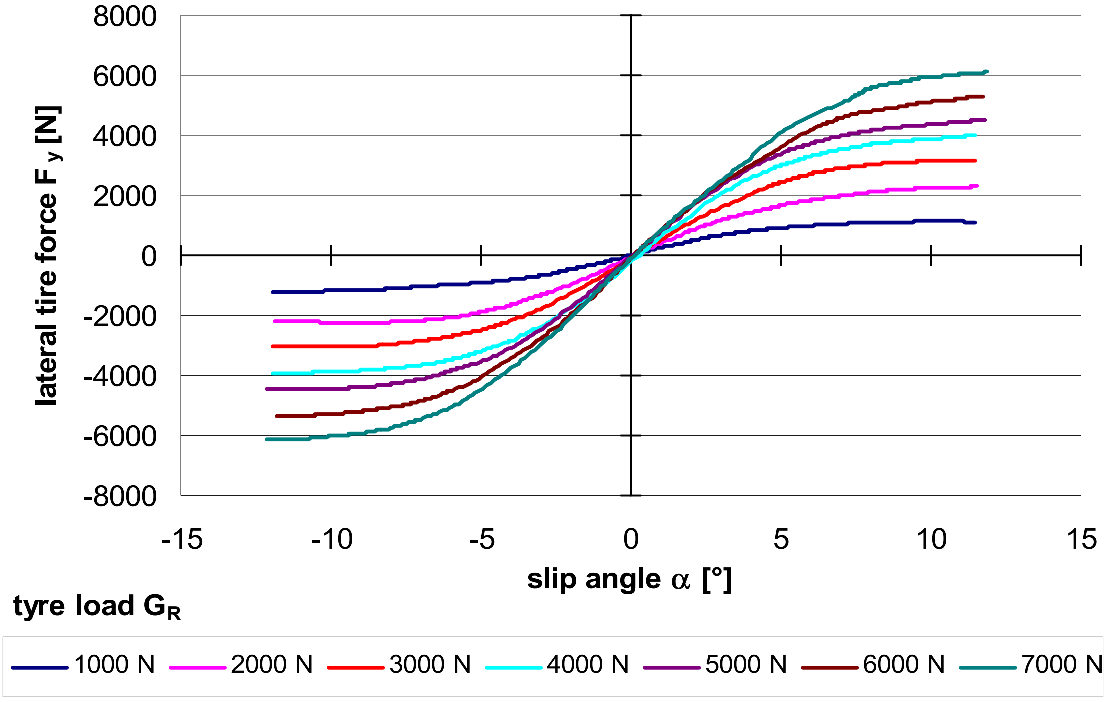

Fig. 3-17: Tyre performance map Mercedes-Benz A-Class, lateral force depending on slip angle

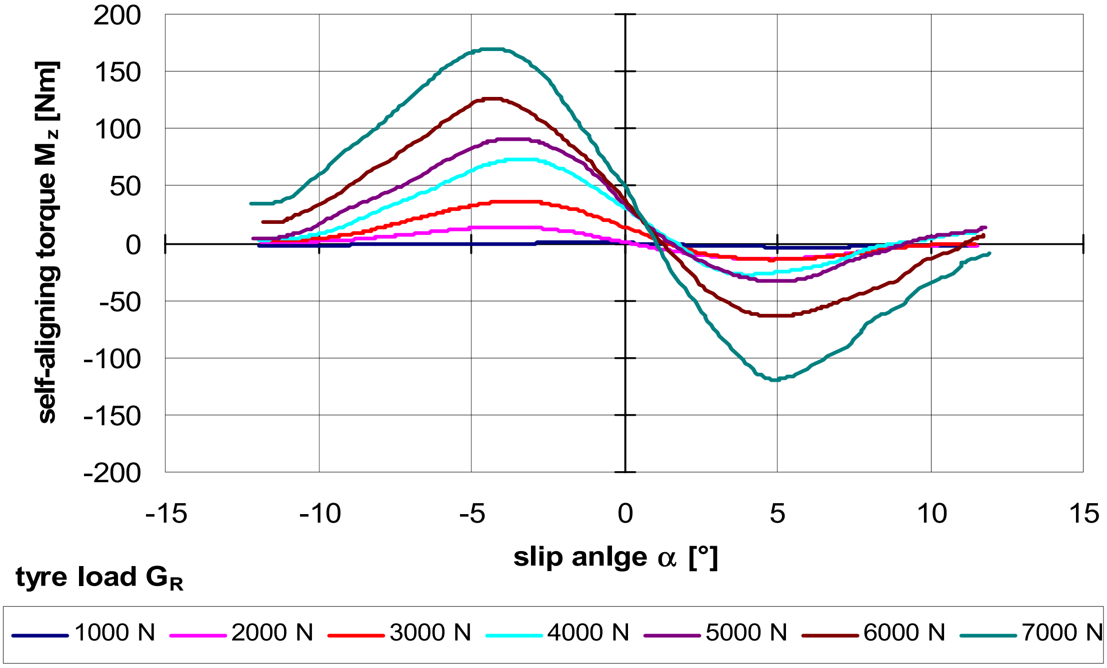

Fig. 3-18: Tyre performance map Mercedes-Benz A-Class, self-aligning torque depending on slip angle

Parameters of the tyre	
x01 Longitudinal Coefficient	-28.1983
x02 Longitudinal Coefficient	1124.52
x03 Longitudinal Coefficient	63.6611
x04 Longitudinal Coefficient	85.6943
x05 Longitudinal Coefficient	0.0740026
x06 Longitudinal Coefficient	-0.0717008
x07 Longitudinal Coefficient	0.7822
x08 Longitudinal Coefficient	-1.18694
y01 Lateral Coefficient	-43.6004
y02 Lateral Coefficient	1177.9
y03 Lateral Coefficient	965.218
y04 Lateral Coefficient	1.22727
y05 Lateral Coefficient	0.217334
y06 Lateral Coefficient	-0.0214168
y07 Lateral Coefficient	-0.0415905
y08 Lateral Coefficient	1.56328E-09
y09 Lateral Coefficient	0
y10 Lateral Coefficient	0
y11 Lateral Coefficient	0
y12 Lateral Coefficient	0
y13 Lateral Coefficient	0
g01 Aligning Coefficient	-3.62125
g02 Aligning Coefficient	-2.52245
g03 Aligning Coefficient	0.299796
g04 Aligning Coefficient	-2.34122
g05 Aligning Coefficient	-0.585279
g06 Aligning Coefficient	0.0421779
g07 Aligning Coefficient	-0.1
g08 Aligning Coefficient	-1
g09 Aligning Coefficient	0.04
g10 Aligning Coefficient	-0.117404
g11 Aligning Coefficient	-0.1
g12 Aligning Coefficient	0.00551318
g13 Aligning Coefficient	-1.5

Fig. 3-19: Parameters of the tyre Mercedes-Benz A-Class

- **BMW 330xi**

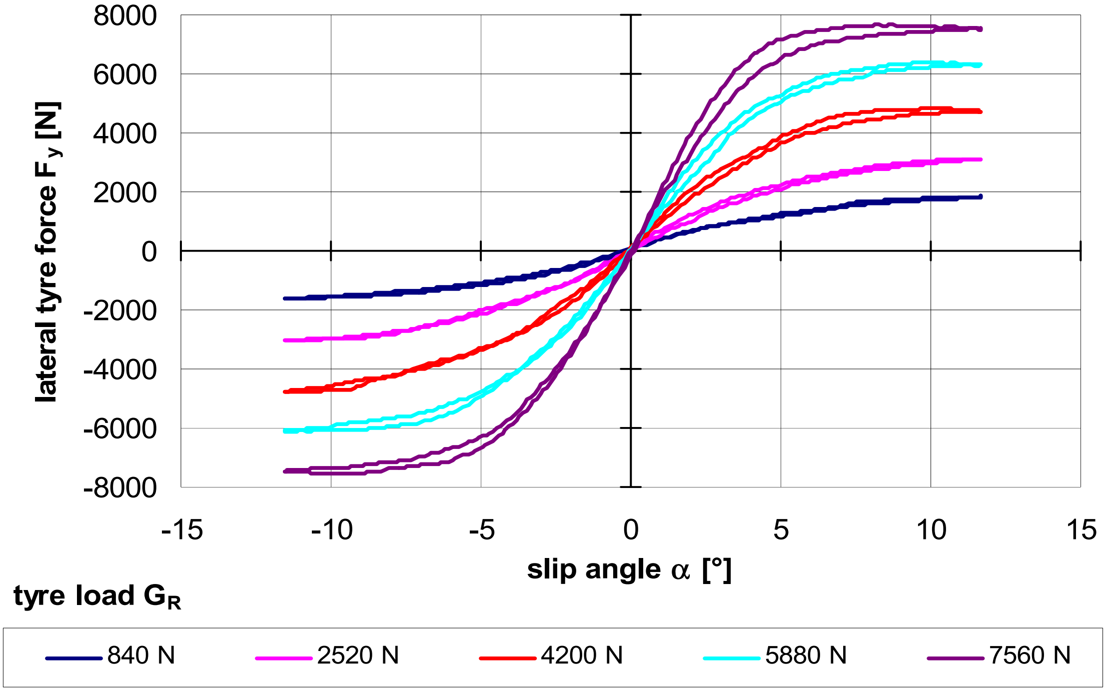

Fig. 3-20: Tyre performance map BMW 330xi, lateral tyre force depending on slip angle

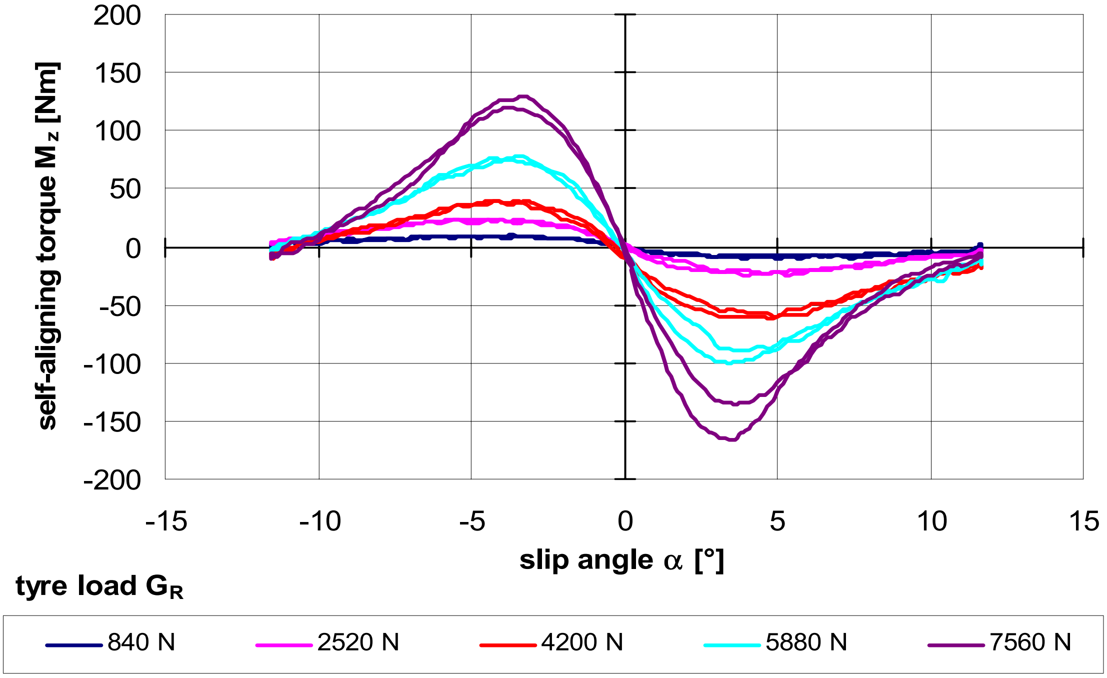

Fig. 3-21: Tyre performance map BMW 330xi, self-aligning torque depending on slip angle

Parameters of the tyre	
x01 Longitudinal Coefficient	-25.6375
x02 Longitudinal Coefficient	1295.69
x03 Longitudinal Coefficient	0.528598
x04 Longitudinal Coefficient	234.596
x05 Longitudinal Coefficient	0.0507029
x06 Longitudinal Coefficient	-0.00356828
x07 Longitudinal Coefficient	-0.0297997
x08 Longitudinal Coefficient	0.483149
y01 Lateral Coefficient	-37.6078
y02 Lateral Coefficient	1250.93
y03 Lateral Coefficient	84791.7
y04 Lateral Coefficient	1.31326
y05 Lateral Coefficient	0.00203523
y06 Lateral Coefficient	-0.029953
y07 Lateral Coefficient	0.0414868
y08 Lateral Coefficient	-0.17549
y09 Lateral Coefficient	0.0198274
y10 Lateral Coefficient	0
y11 Lateral Coefficient	-12.7869
y12 Lateral Coefficient	0.00812141
y13 Lateral Coefficient	0
g01 Aligning Coefficient	1.71083
g02 Aligning Coefficient	4.79826
g03 Aligning Coefficient	0.550648
g04 Aligning Coefficient	1.68363
g05 Aligning Coefficient	-0.0506931
g06 Aligning Coefficient	0.000901097
g07 Aligning Coefficient	-0.0509564
g08 Aligning Coefficient	-0.818663
g09 Aligning Coefficient	0.0111663
g10 Aligning Coefficient	-0.0291375
g11 Aligning Coefficient	0.976861
g12 Aligning Coefficient	0.0814416
g13 Aligning Coefficient	0.215077

Fig. 3-22: Parameters of tyres BMW 330xi

3.1.5 Spring characteristics

The ika wheel-alignment bench enables purposeful examination of the axle cinematics of individual axles or of entire vehicles. All compression positions imaginable can be imitated via four hydraulic units. With the help of universal wheel substitution systems, the loads to be simulated are initiated into the axle in a cinematically correct way.

As rigid support is of particular importance in cinematic examinations of vehicles due to the high forces occurring, a very rigid clamping system which is nevertheless easy to adapt to the vehicles to be measured is available. In Fig. 3-23 there is a portrayal of how one of the test vehicles is supported with the help of cross traverses via the side sill of the vehicle body relative to the environment.

Fig. 3-23: Kinematics and compliance test-bench with fixed vehicle

The operation of the total of twelve hydraulic axles is done with force or distance control with the help of an NC control device and a PC. Test routines which run automatically implement the complete measurement programme and determine all the relevant measured data such as compression travel, wheel loads, toe-in and camber angle, etc. Low-friction air bearings of the wheel substitution systems on the axles to be measured enable unfalsified application of forces into the axle. The applied or resulting forces are detected with the help of wire-strain gauge power sensors in all three coordinate directions.

Two cable potentiometers per measurement tower record the displacement of the wheel contact points on the xy level. The compression is measured with inductive distance sensors attached to the measurement tower. The alterations of the toe-in and camber angle are measured via an auto-collimator and a mirror integrated into the wheel substitution system, Fig. 3-24.

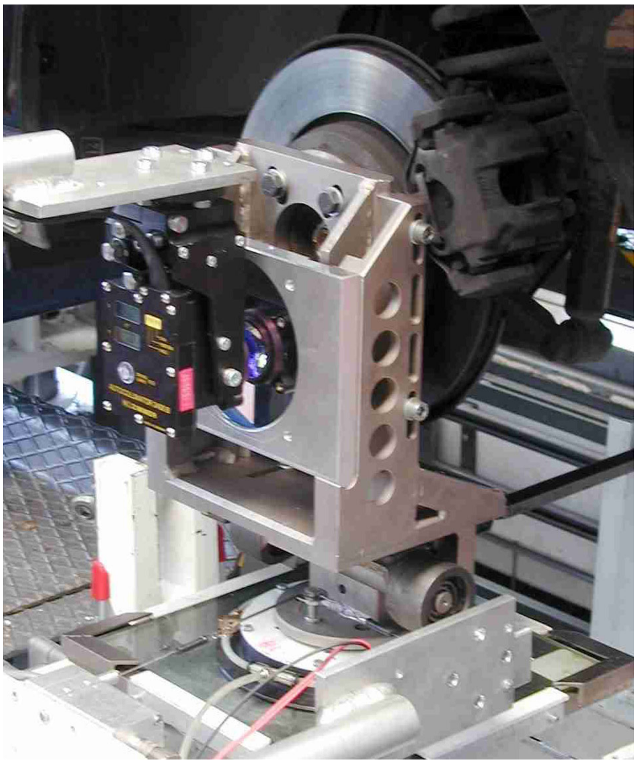

Fig. 3-24: Tyre replacement system with sensors

Fig. 3-24 gives an overview of the measurement technique used on each wheel. The wheel substitution system directly fitted to the wheel carrier is clearly visible. This system can be variably used to adjust the wheel radius, the wheel offset and the castor. The mirror of the optical measurement devices to detect the alteration of the toe-in and camber angle is directly attached to the wheel substitution system. On the bottom end of the wheel substitution system, there is a plate, which portrays the upper half of the pneumatic bearings with integrated small bores. Under it, there is a glass panel, on which the wheel substitution system moves in operation without friction. In order to realise vertical wheel movements, the complete measurement tower is moved up and down via an integrated hydraulic actuator. On the one hand, the sensor for detection of the movement distance, on the other hand a force measurement element to detect the wheel load have been integrated into this tower.

In the current paper, the axle measurement bench primarily serves to measure the body spring characteristics and the stabiliser spring characteristics. The kinematics of the axles are already known thanks to knowledge of the pivot points. In the measurements, both wheel carriers of an axle are moved evenly to start with in order to generate a pure movement suspension without load on the stabiliser. Afterwards, both wheel carriers are moved in the opposite direction, by which a roll suspension is simulated and the stabiliser contributes to the overall elastic force on a wheel carrier. The results of these measurements and the wheel-related spring characteristics derived from them are shown in Fig. 3-25 to Fig. 3-30.

- **Mercedes-Benz A-Class**

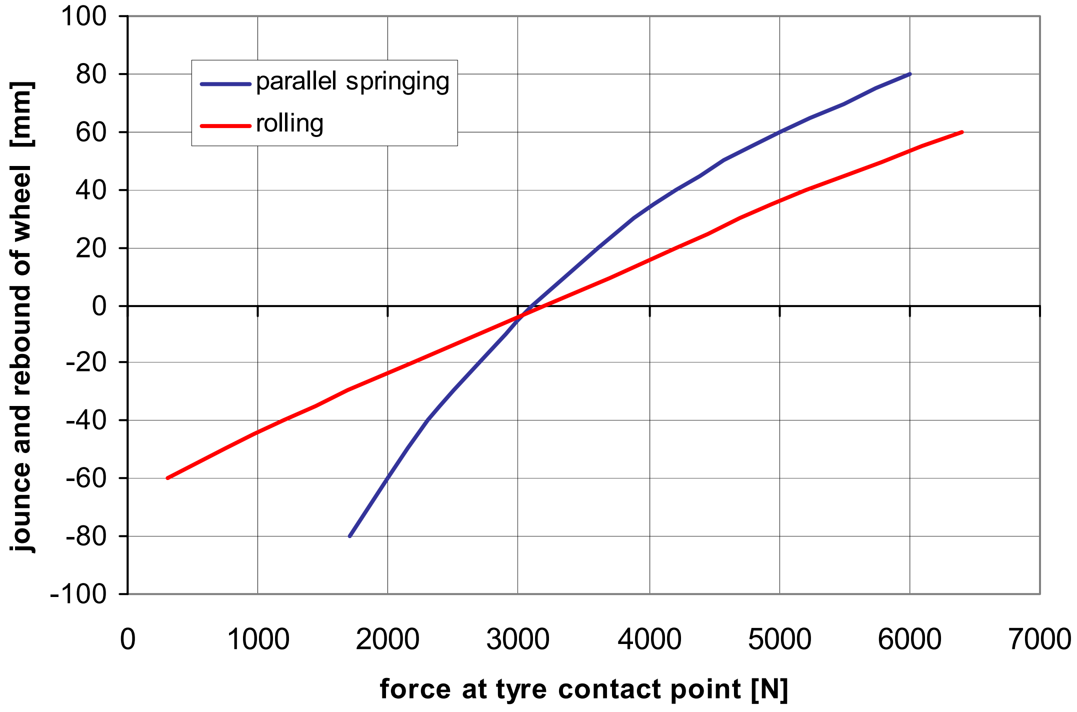

Fig. 3-25: Spring characteristic Mercedes-Benz A-Class, front axle

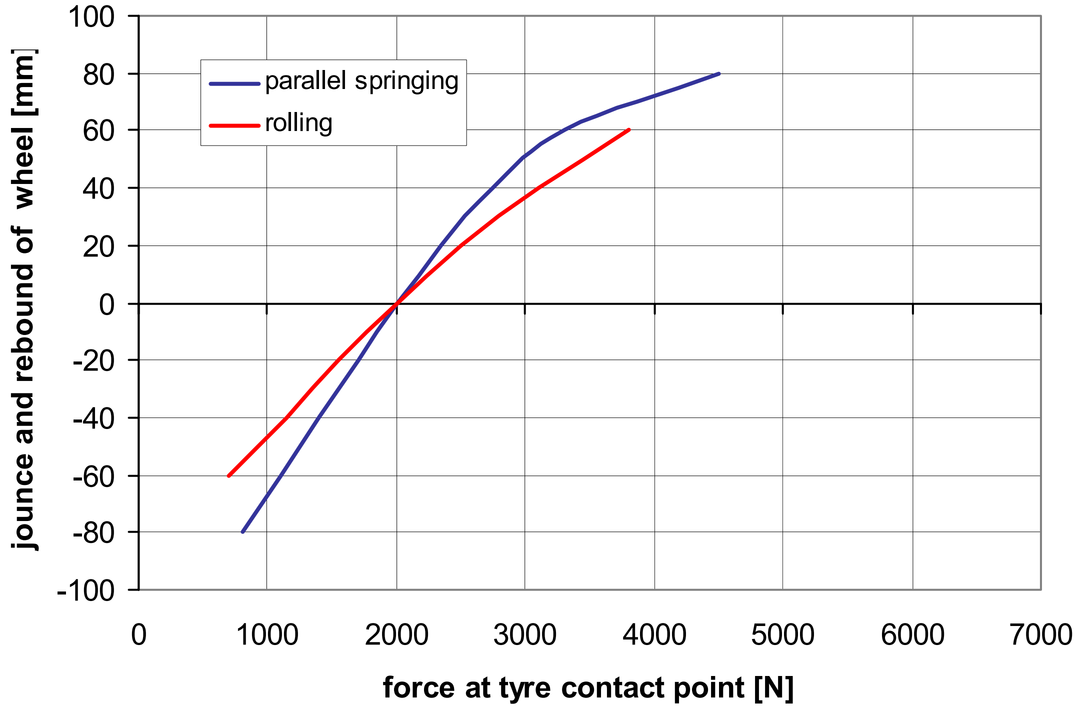

Fig. 3-26: Spring characteristic Mercedes-Benz A-Class, rear axle

	spring rate [N/mm]
tyre specific spring rate body's spring front axle	22.8
tyre specific spring rate stabiliser front axle	24.0
tyre specific spring rate body's spring rear axle	19.4
tyre specific spring rate stabiliser rear axle	4.8

Fig. 3-27: Tyre specific spring rates Mercedes-Benz A-Class

- **BMW 330xi**

For the movement and roll suspension measurements, differing spring travels are selected for the two test vehicles, as the wheel substitution system rises from the glass panel of the measurement tower in mutual suspension on the front axle from a rebound travel as low as about 60 mm (increased overall spring characteristic in roll suspension). In order to compute the share of spring force of the stabiliser, the course of the spring force of the movement suspension is subtracted from that of the roll suspension.

Although the spring characteristics are not exactly linear, they can nevertheless be portrayed well by differential lines in the area of the static wheel load. The gradients of the differential lines represent the wheel-relative spring characteristics for body springs and stabilisers.

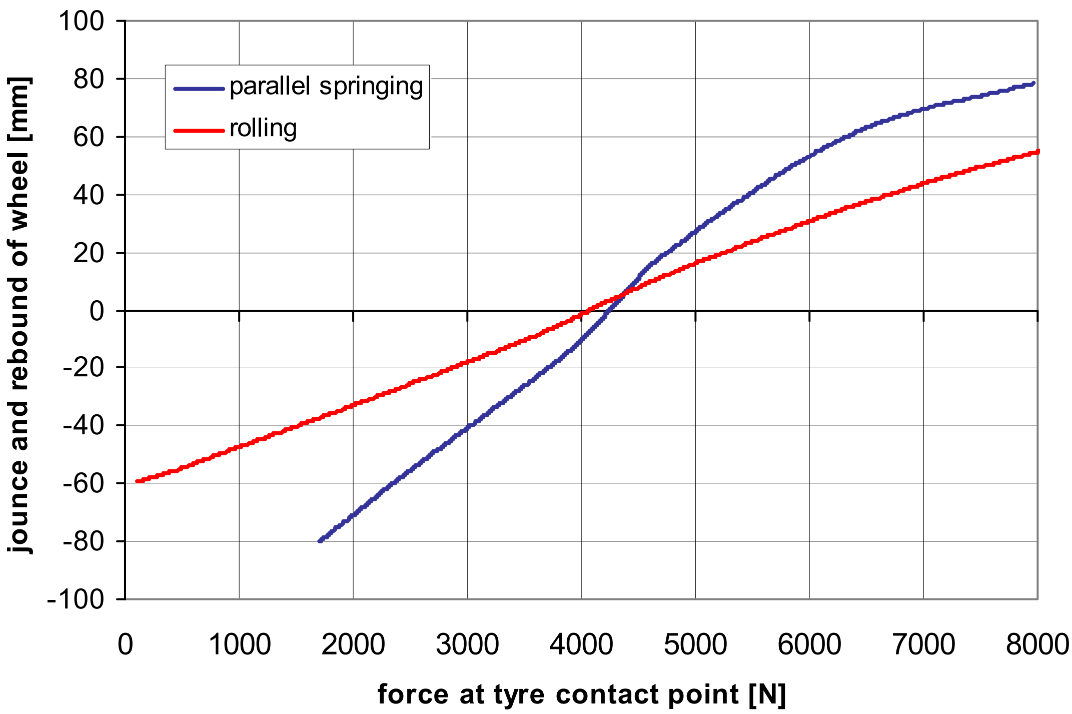

Fig. 3-28: Spring characteristic BMW 330xi, front axle

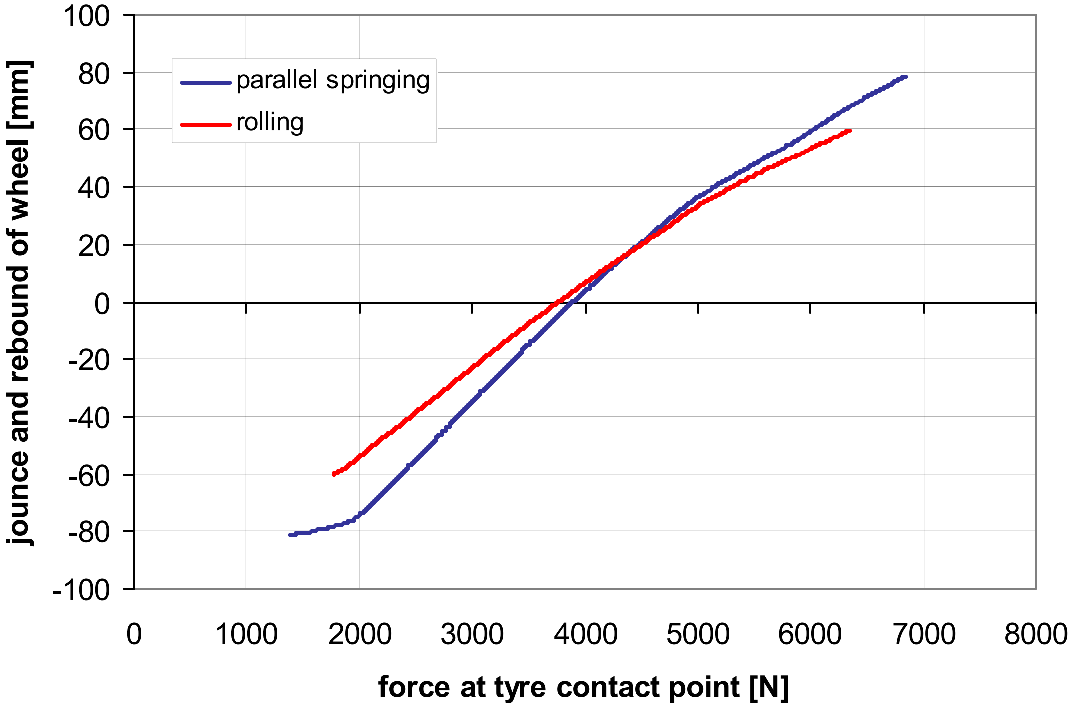

Fig. 3-29: Spring characteristic BMW 330xi, rear axle

	spring rate [N/mm]
tyre specific spring rate body's spring front axle	34.8
tyre specific spring rate stabiliser front axle	38.0
tyre specific spring rate body's spring rear axle	30.9
tyre specific spring rate stabiliser rear axle	8.3

Fig. 3-30: Tyre specific spring rates

3.1.6 Damper characteristics

The damper characteristics of the front and rear axle damper of the two test vehicles are measured on the servo-hydraulic test bench at ika. The individual dampers are clamped in a tension test bench and excited with differing sinus-shaped distance signals of the same amplitude, but varying frequency. The excitation frequency and amplitude can be used to determine the piston speed at zero run and the force measured corresponds to the damper force. The results of the measurements are shown in Fig. 3-31 and Fig. 3-32. In particular, the rear axle damper of the A Class manifests extremely high damping forces as a result of its prone installation position.

- **Mercedes-Benz A-Class**

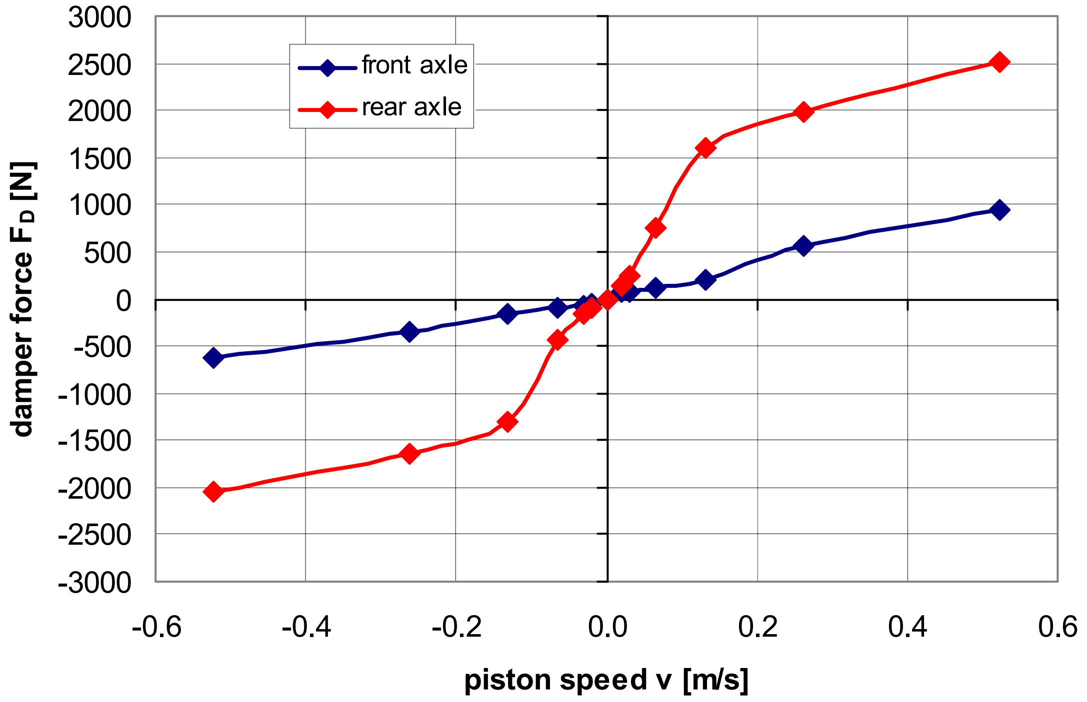

Fig. 3-31: Damper characteristic Mercedes-Benz A-Class

- **BMW 330iX**

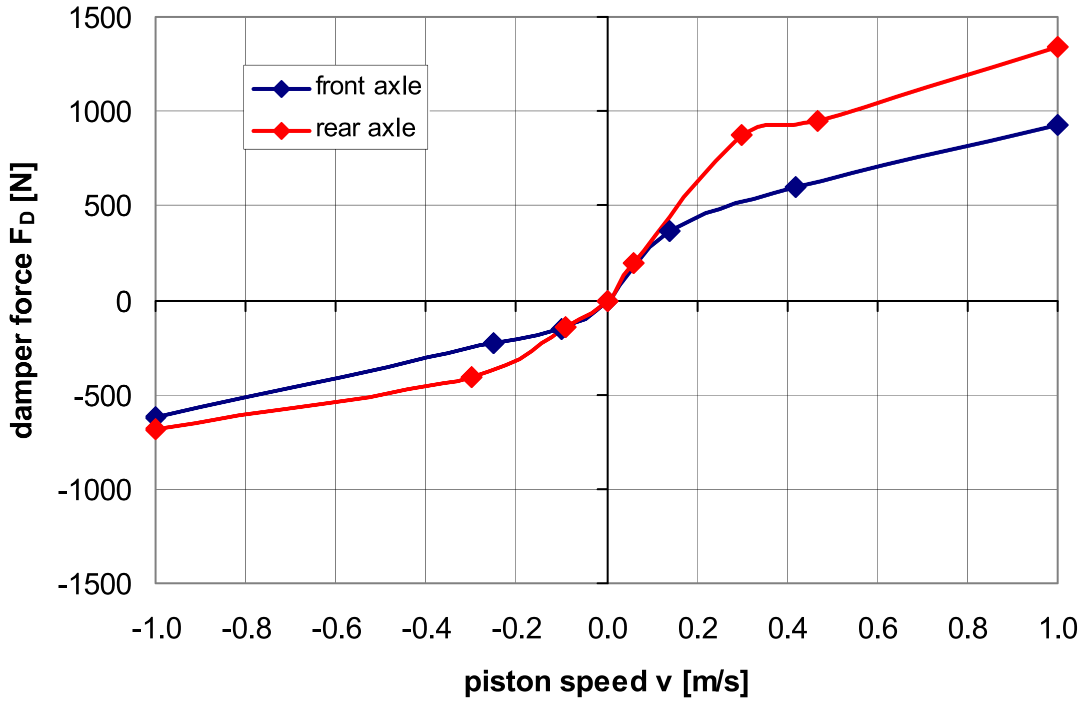

Fig. 3-32: Damper characterstic BMW 330xi

3.1.7 Brake force distribution

In the course of this study, the connection between brake pressure applied by the hydraulic unit of the brake and the resulting brake power on the wheel must be determined. During the driving tests held at a later point in time, there can be a deduction of the brake power actually existing on the wheels with the help of this ratio. The pressure sensors and their installation are described in more detail in Chap. 3.2.

These measurements are done on the “ABS test bench” of the ika. The ABS test bench has four sets of rollers driven independently of one another onto which the vehicle is placed. Thanks to a movable frame for the rollers for the rear axle, the test bench can be adjusted to various wheel bases. All four wheels are driven evenly via the rollers with a speed corresponding to a traction of 6.5 kph. The reaction torque and thus the effective brake power up to a maximum of 5 kN are measured by a force transmitter interposed between the drive unit support and the frame. A detection roller measures the actual wheel speed in order to switch the test bench off automatically in the event of excessive slip between the rollers and the wheel. A principal diagram of the ABS test bench is shown in Fig. 3-33.

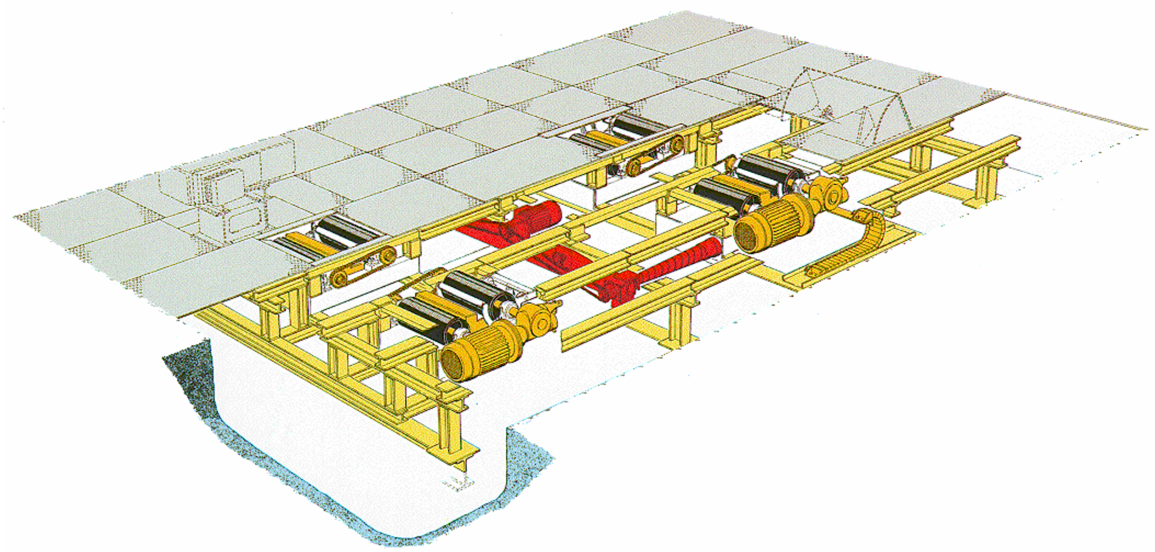

Fig. 3-33: ABS test-bench

While the test is being held, the ABS test bench drives all four wheels evenly to start with. Thanks to a continuous operation of the brake pedal, the brake power on all the wheels is increased until the blocking of one axle results, by which the vehicle is lifted out of the contact rollers. During this process, the four wheel brake powers and the brake pressures are recorded, the two brake powers of one axle being identical.

- **Mercedes-Benz A-Class**

In Fig. 3-34 a brake power measurement for the Mercedes-Benz A Class is shown, in which the brake power of the front and rear axles are shown as mean values:

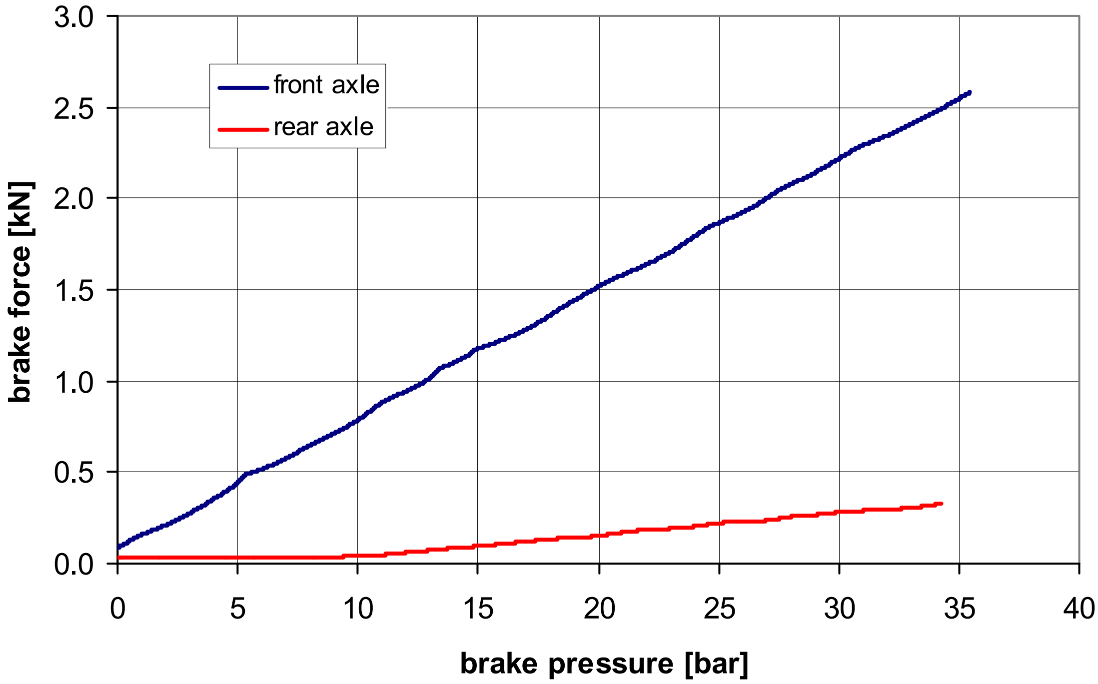

Fig. 3-34: Brake force distribution Mercedes-Benz A-Class

The variables recorded result in the following connections for brake power and brake pressure for the front and the rear axle:

$$F_{B,FA} = 0{,}075 \frac{kN}{bar} \cdot p_{FA} \qquad \text{Eq. 3-5}$$

$$F_{B,RA} = 0{,}013 \frac{kN}{bar} \cdot p_{RA} \qquad \text{Eq. 3-6}$$

From these connections, the brake force distribution of the test vehicle can also be determined by the gradient of the brake-power lines of the front axle being related to the rear axle:

$$\frac{F_{B,FA}}{F_{B,RA}} = \frac{0{,}075}{0{,}013} = \frac{5{,}77}{1} \approx \frac{85}{15} \qquad \text{Eq. 3-7}$$

In this way, a figure of about 85% to 15% results for the brake proportioning device, i.e. in braking, 85% of the brake power is produced by the front axle, with the rear axle contributing about 15% of the brake power.

- **BMW 330iX**

The braking system of the BMW 330xi can be measured with an analogous mode of procedure, Fig. 3-35.

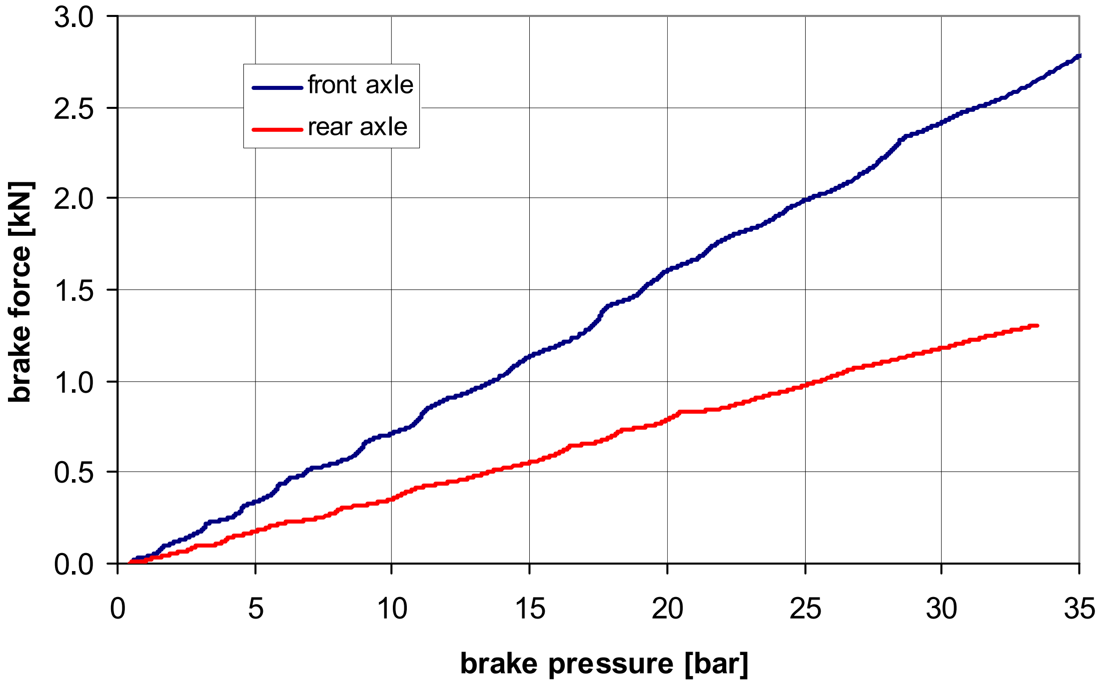

Fig. 3-35: Brake force distribution BMW 330xi

Here, the following connections result for brake power and brake pressure:

$$F_{B,FA} = 0{,}0787 \frac{kN}{bar} \cdot p_{FA} \qquad \text{Eq. 3-8}$$

$$F_{B,RA} = 0{,}0389 \frac{kN}{bar} \cdot p_{RA} \qquad \text{Eq. 3-9}$$

Here too, the brake proportioning of the test vehicle can be determined by the gradients of the brake-power lines being related to one another:

$$\frac{F_{B,FA}}{F_{B,RA}} = \frac{0{,}0787}{0{,}0389} = \frac{2{,}023}{1} \approx \frac{2}{1} \qquad \text{Eq. 3-10}$$

In the BMW, 2/3 of the brake power are produced by the front axle, with the rear axle contributing 1/3 of the brake power.

3.2 Driving tests

In order to be able to hold the driving tests to examine the test vehicles and specifically the vehicle dynamics controller, the vehicles are equipped with extensive measurement technique. All the measurement devices used and the measurement variables recorded by them are listed in Fig. 3-36.

measuring device	measured variables
measuring steering wheel	steering angle
	steering torque
gyroscopic sensor	yaw, roll and pitch velocity
	yaw, roll und pitch angle
	vertical, lateral und longitudinal acceleration
Correvit	longitudinal velocity
	lateral velocity
pressure sensor	brake pressure front left
	brake pressure front right
	brake pressure rear left
	brake pressure rear right
measuring computer	control of the measuring devices
	digitising
	storage

Fig. 3-36: Applied measuring devices

The variables needed for the assessment and evaluation of the driving tests are the longitudinal velocity, the steering wheel angle, the yaw velocity, the roll angle, the lateral acceleration, the sideslip angle as well as the four braking forces of the individual wheels. As not all of these variables can be determined directly, but partly only indirectly using other measurement variables, reference is made below individually to the various measurement devices and the measurement variables required.

- Measurement steering wheel

  The standard steering wheel is replaced by a measurement steering wheel in each case. In this way, the steering torque and steering angle variables can be measured, with only the steering angle being of interest for the following examinations. It is measured with two TTL impulses phase-offset by 90°. The zero point adjustment is done by a switch on the steering wheel [DAT98].

Alongside pure detection of the steering angle, the measurement steering wheel additionally has an adjustable steering angle stop, with the help of which reproducible driving tests can be done by means of a constant steering angle. The measurement steering wheel installed in the Mercedes-Benz A Class is portrayed in Fig. 3-37.

Fig. 3-37: Measurement steering wheel

- <u>Gyroscopic Sensor</u>

The gyroscopic sensor used is in a position to determine all the vehicle angles, angular velocities and vehicle accelerations in the direction of the three main axes. The foundation for the determination of the angular variables is the property of a centrifuge always to maintain its rotary axis in space. The gyroscopic sensor can detect accelerations of ±1.2 g with a resolution of 0.001g. With regard to the angle measurements, a range of ±60° applies for the pitch and roll angle with a resolution of 0.01°, whereas yaw angles of ±180° with a resolution of 0.03° can be detected. The measurement range for the rotation characteristics is a standard of ±60°/s.

Not all the measurement variables output by the gyroscopic sensor are needed for the driving tests held. For this reason, only the pitch and roll angle, the yaw velocity as well as the three vehicle accelerations in the direction of the main axes are recorded.

In an ideal case, the gyroscopic sensor is attached precisely on the level of the centre of gravity of the vehicle. As this cannot be realised for the test vehicles used, the gyroscopic sensor is placed as close as possible to the centre of gravity, by which no inadmissible deviations of the measured values from the variables at the centre of gravity of the vehicle occur. The gyroscopic sensor used in the Mercedes-Benz A Class is portrayed in Fig. 3-38.

Fig. 3-38: Gyroscopic sensor

- <u>Correvit</u>

  To determine the vehicle's longitudinal and lateral velocity at its centre of gravity, a CORREVIT S-CE sensor is used, Fig. 3-39. This is a non-contact velocity measurement system which can determine both the longitudinal and also the lateral velocity of the vehicle. With the help of a lamp, a spot of light is projected onto the road surface. The reflected light manifests a statistical distribution of light and dark spots of the road surface structure. As a result of the movement of the vehicle across the surface, the light/dark contract spots are modulated in such a way that a velocity-proportional frequency can be measured in the sensor [WAL96].

  As assembly of the Correvit sensor precisely at the centre of gravity of the vehicle is not possible, it is attached to the vehicle tail. The longitudinal velocity of the vehicle at the centre of gravity is measured well without alterations, but the lateral velocity no longer corresponds to that at the centre of gravity of the vehicle, as there is a superposition of lateral vehicle movement and vehicle yaws at the rear. For this reason, the amount of lateral velocity resulting from yaw velocity and overall lever arm (distance of the rear axle from the centre of gravity of the vehicle l_r + distance of the Correvit from the rear axle l_c)

must be subtracted in order to compute the lateral velocity at the centre of gravity of the vehicle:

$$v_{lateral,CoG} = v_{lateral,C} - \dot{\psi} \cdot (l_r + l_C) \quad \text{Eq. 3-11}$$

A further measurement variable to be determined indirectly and of interest for the evaluation and assessment of the driving tests is the sideslip angle β. The sideslip angle is defined as the angle between the real longitudinal velocity of the vehicle v_{long} and the resultant velocity at the centre of gravity of the vehicle v_{res}. It can thus be determined from longitudinal velocity v_{long} and lateral velocity at the centre of gravity $v_{lateral,CoG}$ according to Eq. 3-12:

$$\tan(\beta) = \frac{v_{lateral,CoG}}{v_{long}} \Leftrightarrow \beta = \arctan\left(\frac{v_{lateral,CoG}}{v_{long}}\right) \quad \text{Eq. 3-12}$$

Fig. 3-39: Correvit

- <u>Pressure sensors</u>

In order to assess the function of the vehcle dynamics controller, knowledge of the brake power on the individual wheels is of decisive importance. Chap. **Error! Reference source not found.** has already described how deductions of the brake powers on the wheels can be made from the brake pressures. For this reason, pressure sensors with a measurement range of 0 bar to 210 bar are fitted in all four wheel brake lines. These sensors work with wire-strain gauges switched to a full bridge, which are attached to a metal membrane. Evaluation electronics inside the sensor convert the signals from the bridge circuit into an analog output voltage between 0 V and 10 V. The four pressure sensors are fitted on the outlet of the brake hydraulic unit, as can easily be seen in Fig. 3-40.

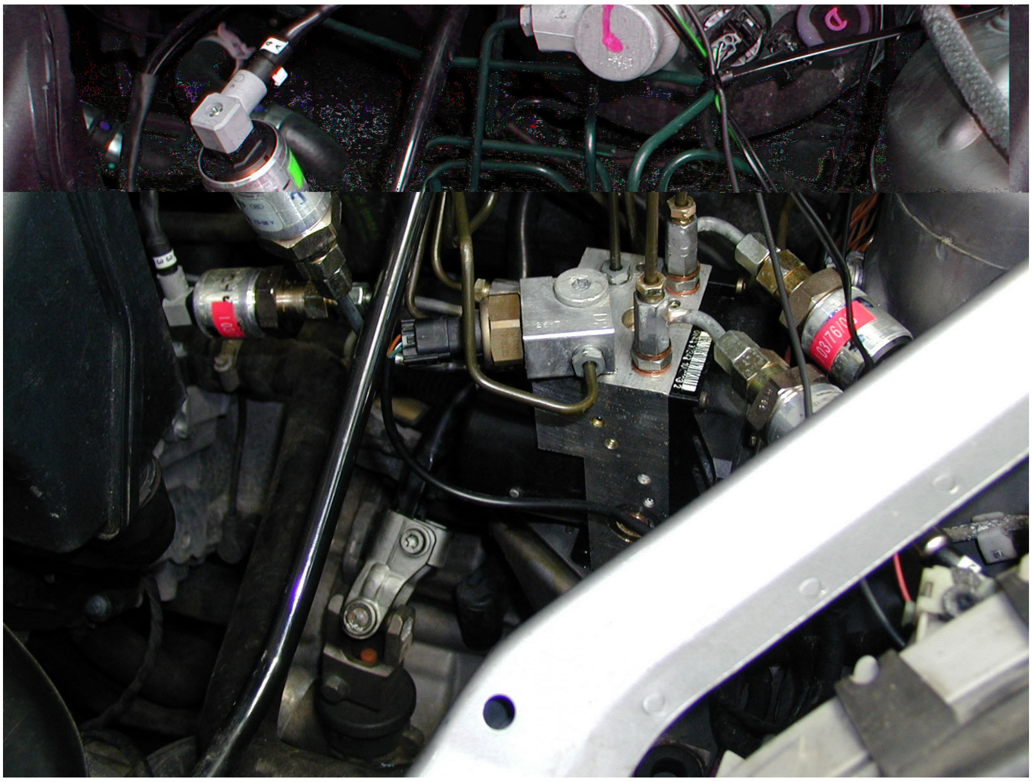

Fig. 3-40: Pressure sensors

- Measurement computer

The analog voltage signals provided by the measurement devices described are fed into a portable measurement computer of the firm of DEWETRON, which digitalises and records them with a resolution of 12 bit. The measurement software used is again DIAdem, which not only has a suitable scaling and visualisation, but also the possibility of computing indirect measurement variables by online computation.

In order to be able to read the measurement variables displayed on the monitor or to operate the computer by the driver during driving manoeuvres, the computer is firmly fitted on a measurement rack instead of the passenger's seat. The measurement rack also contains further components of the measurement technique, such as the evaluation unit of the gyroscopic sensor, Fig. 3-41.

Fig. 3-41: Measuring computer

Supply of voltage to the measurement computer and all the other measurement devices is guaranteed by the 12 V electric system voltage of the car battery, to which a second battery is connected in parallel as a buffer.

In the course of the driving tests, three various standard manoeuvres are done on the test run of the ika. Alongside the measurement of the pure driving performance of the vehicle, the intervention behaviour of the vehicle dynamics controller is examined by driving tests being done with and without the vehicle dynamics controller being activated. In addition, the manoeuvres are done partly on a wet, partly on a dry road surface.

- <u>Steady state cornering</u>

  Steady state cornering primarily serves to measure the self-steering properties of the vehicles. On a circle with a radius of R = 40 m, the circular movements are started at 30 km/h and increased to 50 km/h in steps of 5 km/h. From 50 km/h upwards, the measurements are increased in steps of 2 km/h up to the maximum possible speed. All the steady state cornering is done on a dry road surface and without the vehicle dynamics controller.

- <u>Step steer input</u>

  The step steer input is used to examine the vehicle's reaction to a leap in the increase of the steering wheel angle. The tests are always done at 70 kkm/h for three differing steering wheel angles. The three steering wheel angles are selected in such a way that constant lateral accelerations of 4, 6 and 8 m/s² result on a dry surface following a process of entering the bend. For the implementation of the tests, the steering angle stop of the measurement steering wheel is set before the measurement in question in such a way that the required steering wheel angles are complied with. The step steer inputs are done both on dry and also on wet road surfaces. ESP or DSC control interventions did not take place.

- <u>ISO-double lane change</u>

  The double lane change (elk test) is a manoeuvre to assess the dynamic driving properties of a motor vehicle. It portrays a swerve in front of an obstacle suddenly appearing, with a quick steering back to the original lane taking place. In Fig. 3-42 the dimensions for the set-up of the lines of the double change of lane are shown. The overall length is 61m, the widths of the various lanes are calculated on the basis of the width of the vehicle.

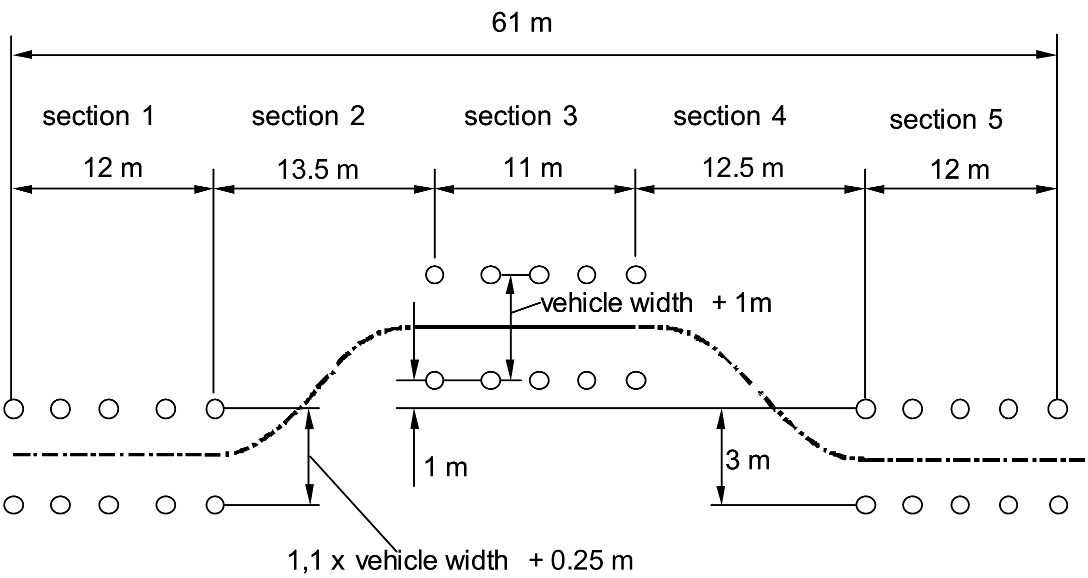

Fig. 3-42: Double lane change according to ISO

The tests are hold on both a dry and a wet surface, with and without vehicle dynamics controller. In order the eliminate any influences of the engine management, such as a reduction of the motor torque, the vehicle is accelerated on approaching the first line until the required velocity is achieved. Directly before entry into the first line, the gear is disengaged on the basis of the ISO norm so that no motor torques are effective any more during the test. Only the brake power applied by the vehicle dynamics controller is applied during the test, none by the driver. The initial velocity of the series of tests is selected at 45 km/h and then increased in steps of 5 km/h until safe driving of the double lane change is no longer possible (without knocking the pylons over).

The two Fig. 3-43 and Fig. 3-44 are the final portrayal of the tests held for the two test vehicles. The results of the driving manoeuvres are portrayed in the following chapters together with the simulation results.

- **Mercedes-Benz A-Klasse**

driving test	**variation**	**with ESP**		**without ESP**	
		dry	**wet**	**dry**	**wet**
steady-state cornering	v = 30 to 60 km/h			√	
step steer input	a_y = 4, 6, 8 m/s²			√	√
double lane change	v = 45 to 65 km/h	√	√ (1)	√	√ (1)

(1) up to 60 km/h

Fig. 3-43: Performed driving tests Mercedes-Benz A-Class

- **BMW 330iX**

driving test	**variation**	**with DSC**		**without DSC**	
		dry	**wet**	**dry**	**wet**
steady-state cornering	v = 30 to 64 km/h			√	
step steer input	a_y = 4, 6, 8 m/s²			√	√
double lane change	v = 45 to 70 km/h	√	√ (1)	√	√ (1)

(1) up to 65 km/h

Fig. 3-44: Performed driving tests BMW 330xi

4 Simulation models

The simulations are done with the MATLAB /Simulink software tool. MATLAB (matrix laboratory) from the firm of MathWorks Inc. integrates numerical analysis, matrix calculation, signal processing and graphic portrayal in one single package of programmes. It is based on fundamentals of matrix calculation. In the industrial area, MATLAB is frequently used in research and development for solving practical mathematical and mechanical problems.

MATLAB becomes particularly user-friendly through the numerous module libraries, the so-called tool boxes, and the matching Simulink extension. By putting various modules together, Simulink enables the production of complex, dynamic models as well as simulation and the parameter variation, also during the sequence of the simulation. For modelling, Simulink provides a graphical user interface (GUI), which makes the set-up of models as block diagrams by simple click-and-drag mouse operations possible. Simulink can analyse systems which can be defined by continuous differential equations and discreet differential equations, i.e. it can produce time-discreet and time-continuous systems. Large complex models can be divided into sub-systems, which means that the models remain easy to understand and also structural conditions of the system to be portrayed can be reproduced.

Fig. 4-1 shows the entire simulation model.

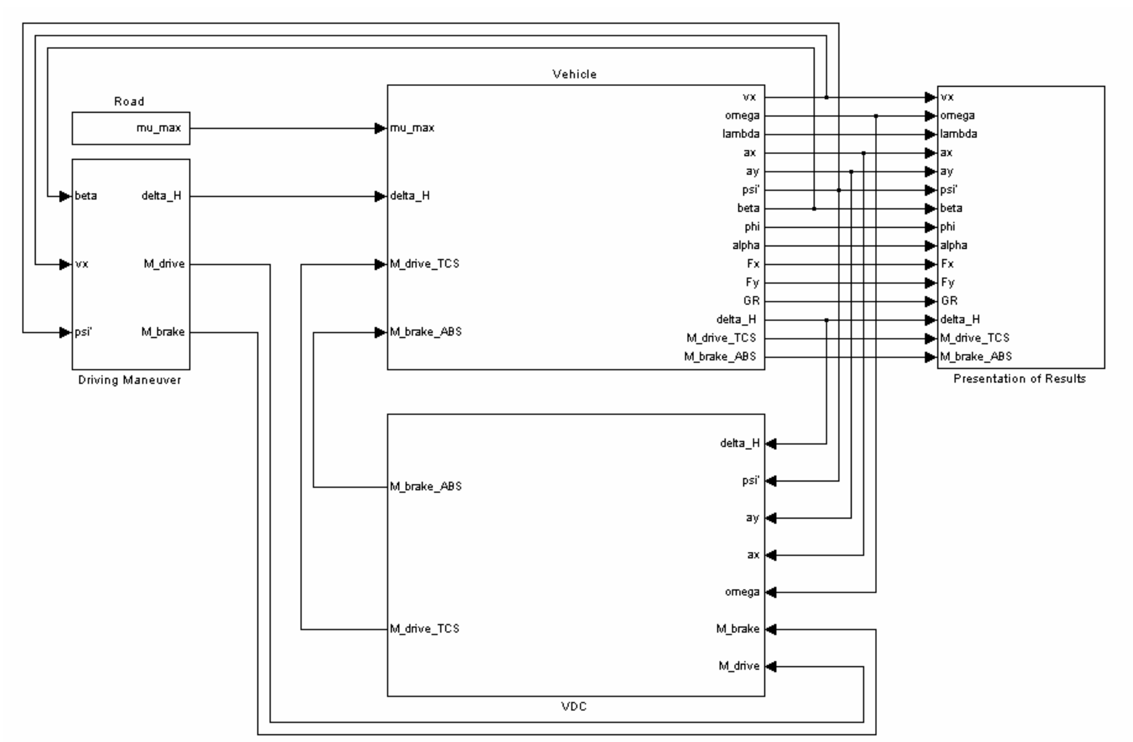

Fig. 4-1: Entire simulation model

The central upper block portrays the vehicle model. Under it, as an equally large block, there is the model of the vehicle dynamics controller, which possesses the most important lateral dynamic figures as input variables and can for its part have an influence on the vehicle via alterations of brake and drive torque. Both the vehicle and the vehicle dynamics controller model are explained in detail in the following chapters.

With the help of a drive manoeuvre generator, the nominal figures for a certain manoeuvre are generated and forwarded to the vehicle model by the two left-hand blocks. The manoeuvre generator has a graphical user interface (Fig. 4-2), via which the user can select the peripheral data of all customary manoeuvres. The block on the extreme right in Fig. 4-1 is only used to portray the result.

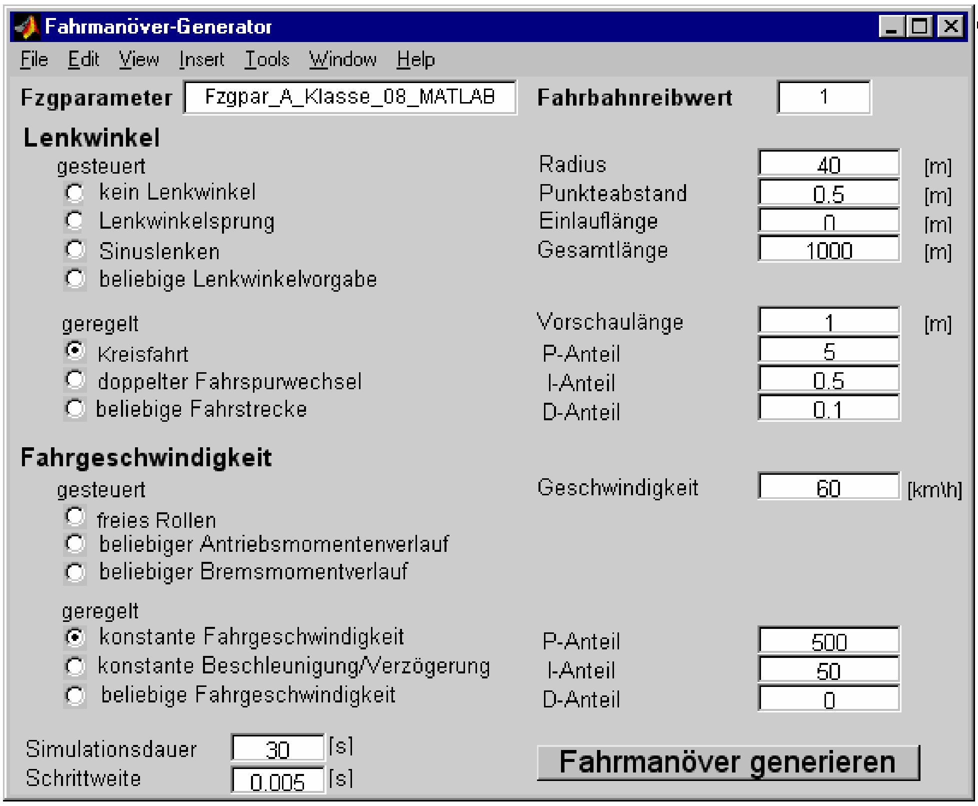

Fig. 4-2: User interface for generating the driving maneuvers

4.1 Vehicle models

The two vehicle models are not constructed as MATLAB / Simulink models, but as multi-body systems in the SIMPACK software tool. In the multi-body mode of observation, the object to be simulated is put together as a few, absolutely rigid bodies and used to form complex structures with springs, dampers, joints etc., these then being called multi-body systems. Such systems can be described with a few mathematical, numerically solvable equations. For the model set-up, the user has a catalogue of elementary components and power laws at his disposal.

The connection of the SIMPACK vehicle models to the remaining MATLAB / Simulink simulation environment is done by a so-called co-simulation. In this, the SIMPACK integrator solves the equations of the mechanical system set up in SIMPACK and the MATLAB integrator solves the equations of the control engineering system set up in MATLAB. After the expiry of a certain stipulated output step, the two programmes exchange their results and calculate the next integration step on the basis of the new data.

For the set-up of the vehicle models, all the data from Chap. 3.1 are processed. In addition, plausible approximation values are used for variables difficult to determine, such as the moments of inertia of small components (e.g. the tie rods). Both vehicle models are pure cinematic models without elasto-cinematic elements.

- **Mercedes-Benz A-Klasse**

Fig. 4-3 shows the vehicle model of the Mercedes-Benz A Class. Fig. 4-4 to Fig. 4-14 show how well the results of the driving tests could be simulated with it. In them, the simulation results are compared with the driving tests without ESP. In steady state cornering and step steer input, the steering angles are generated by the manoeuvre generator. For the simulation of the double lane change, the courses of the steering angle measured in the driving test are used.

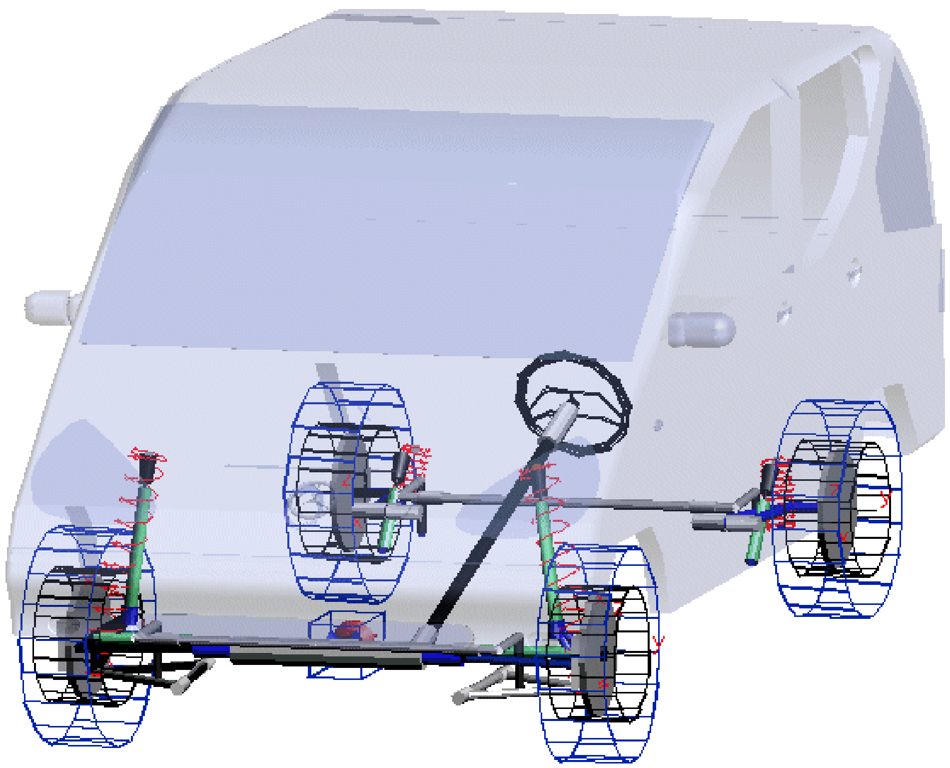

Fig. 4-3: Mercedes-Benz A-Class simulation model

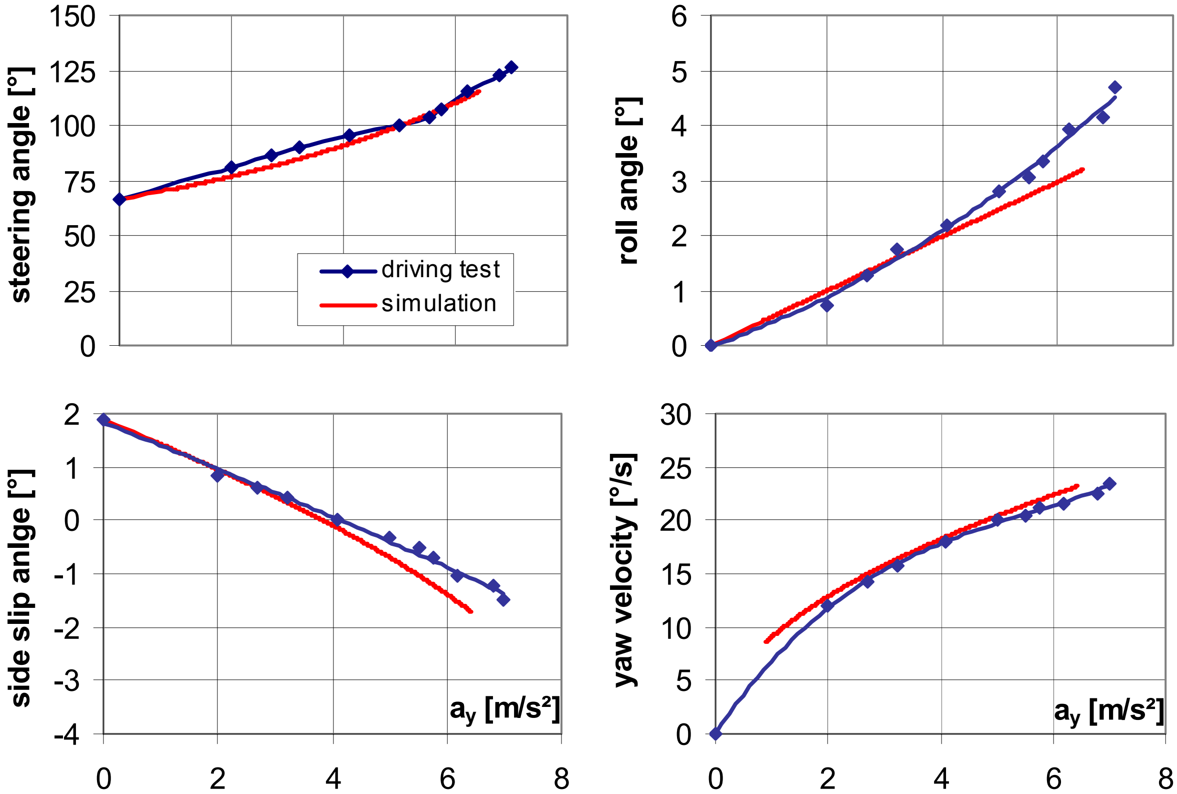

Fig. 4-4: Steady state cornering

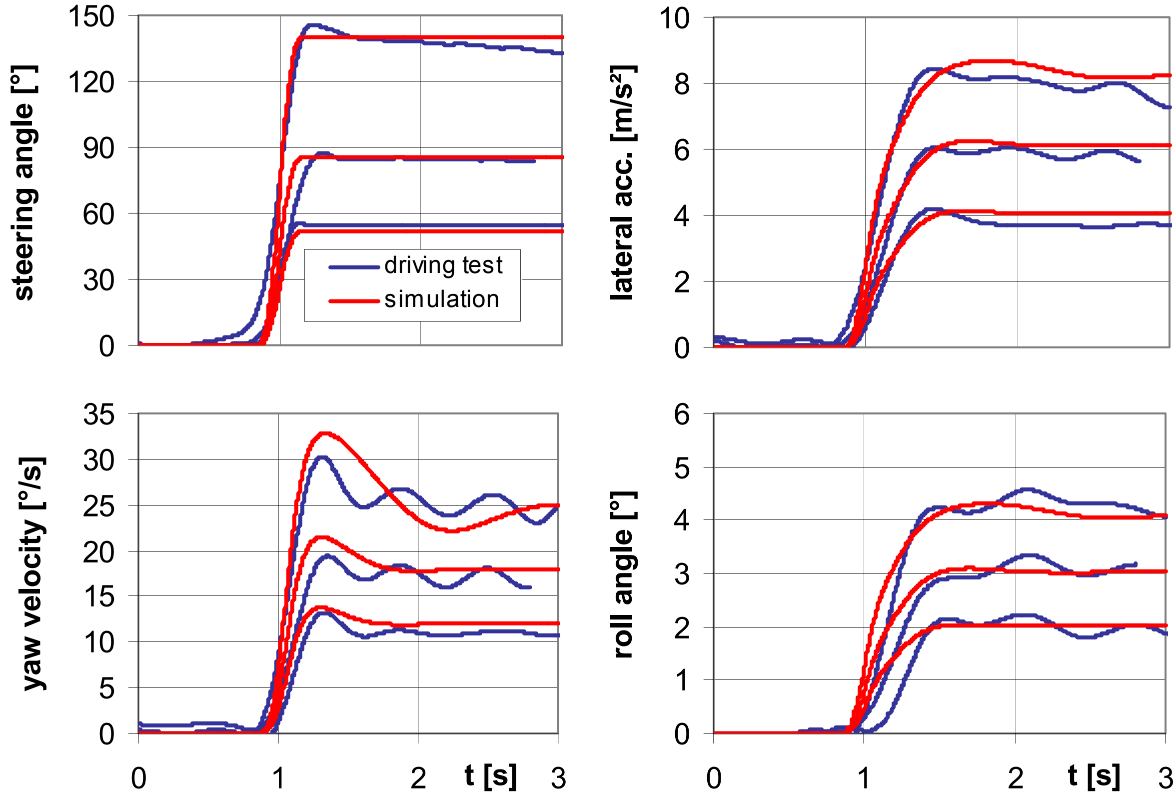

Fig. 4-5: Step steer input, dry asphalt

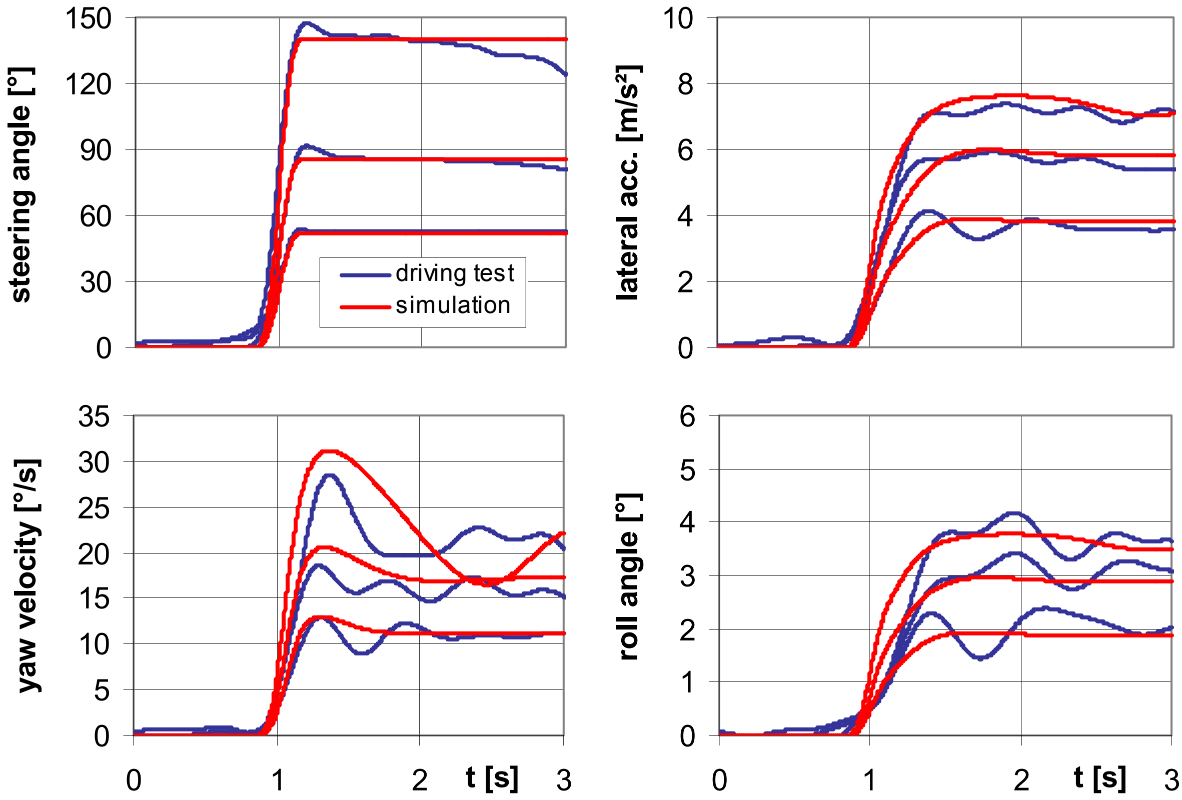

Fig. 4-6: Step steer input, wet asphalt

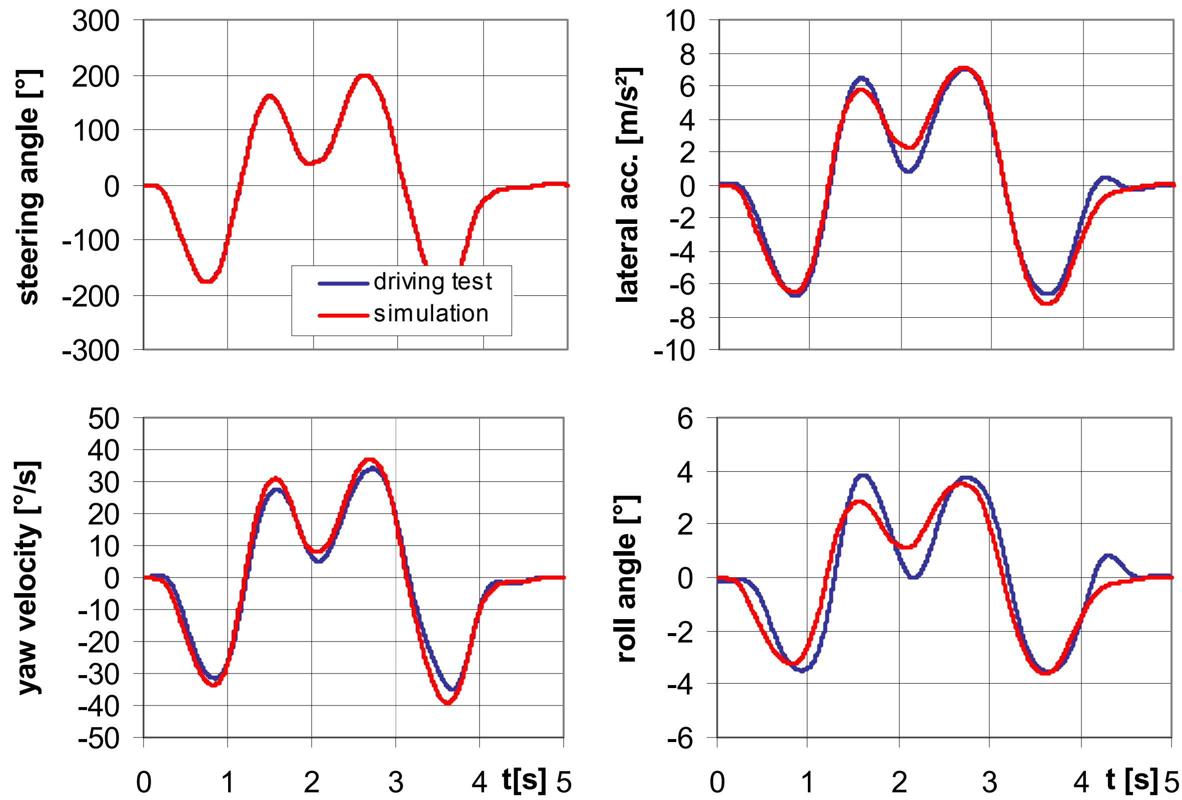

Fig. 4-7: Double lane change, 45 km/h, dry asphalt

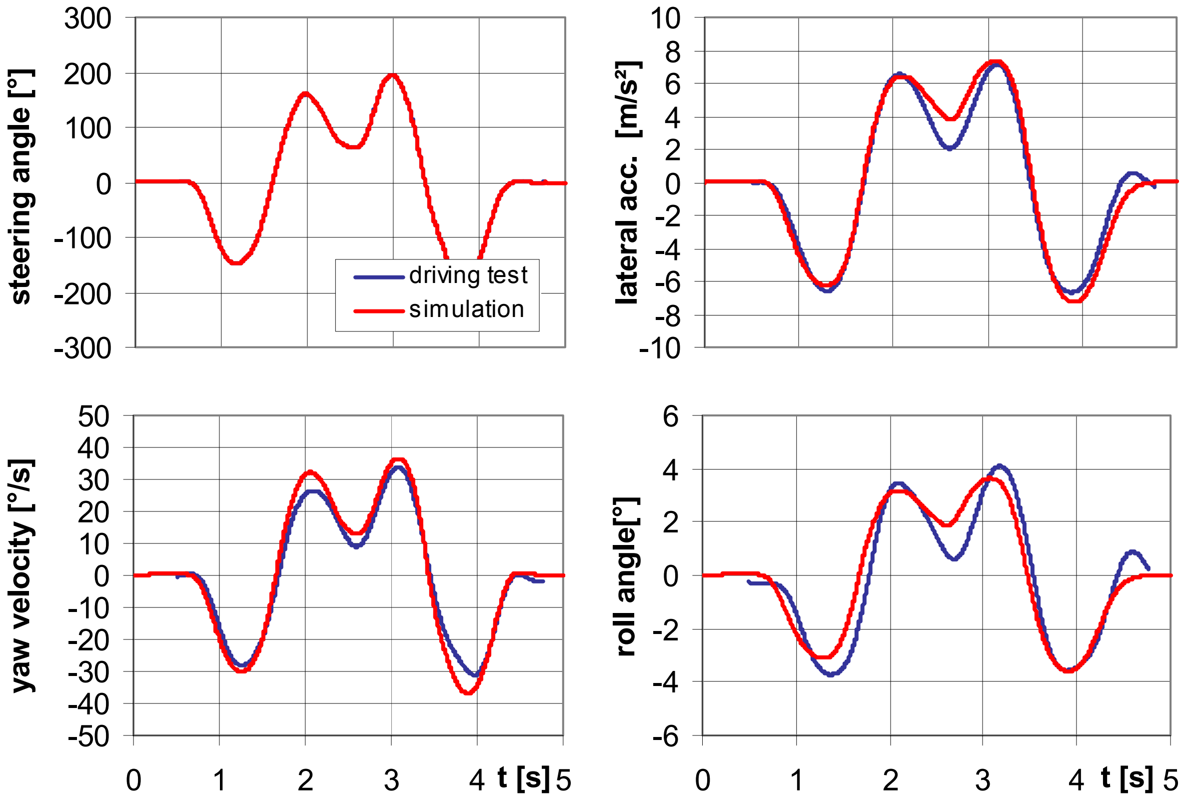

Fig. 4-8: Double lane change, 50 km/h, dry asphalt

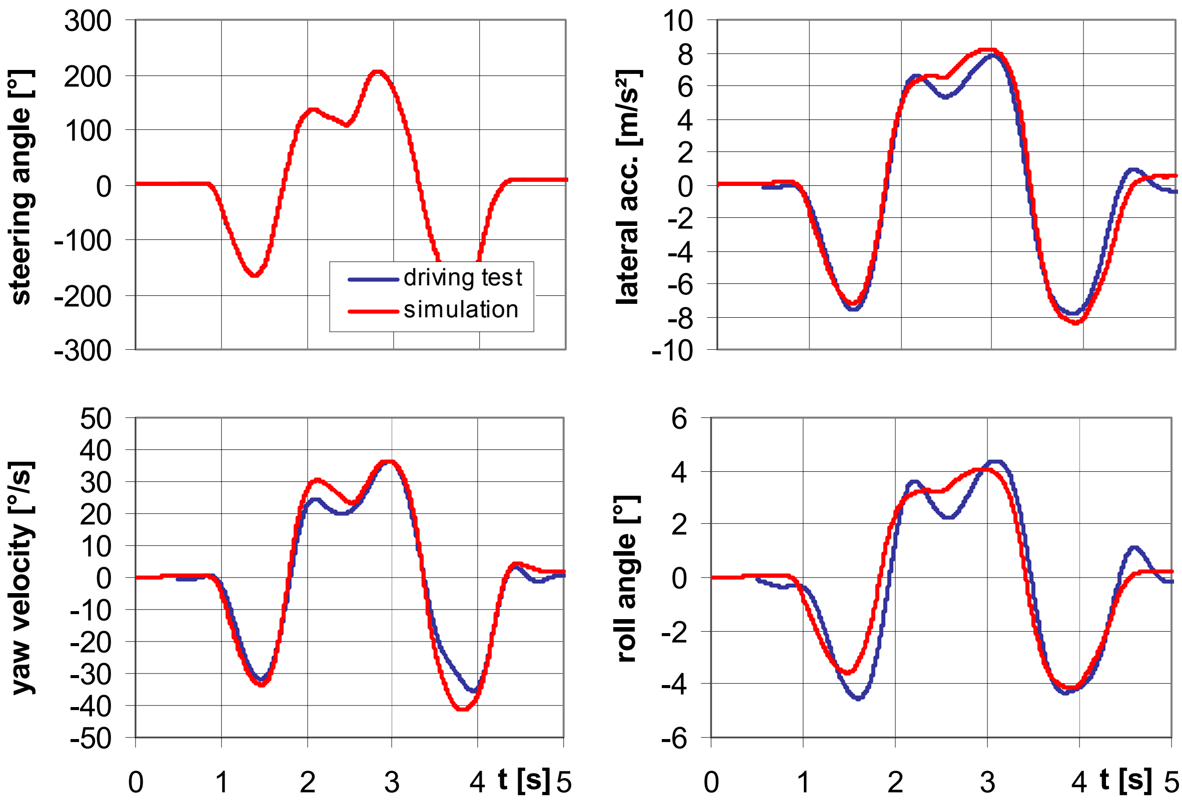

Fig. 4-9: Double lane change, 55 km/h, dry asphalt

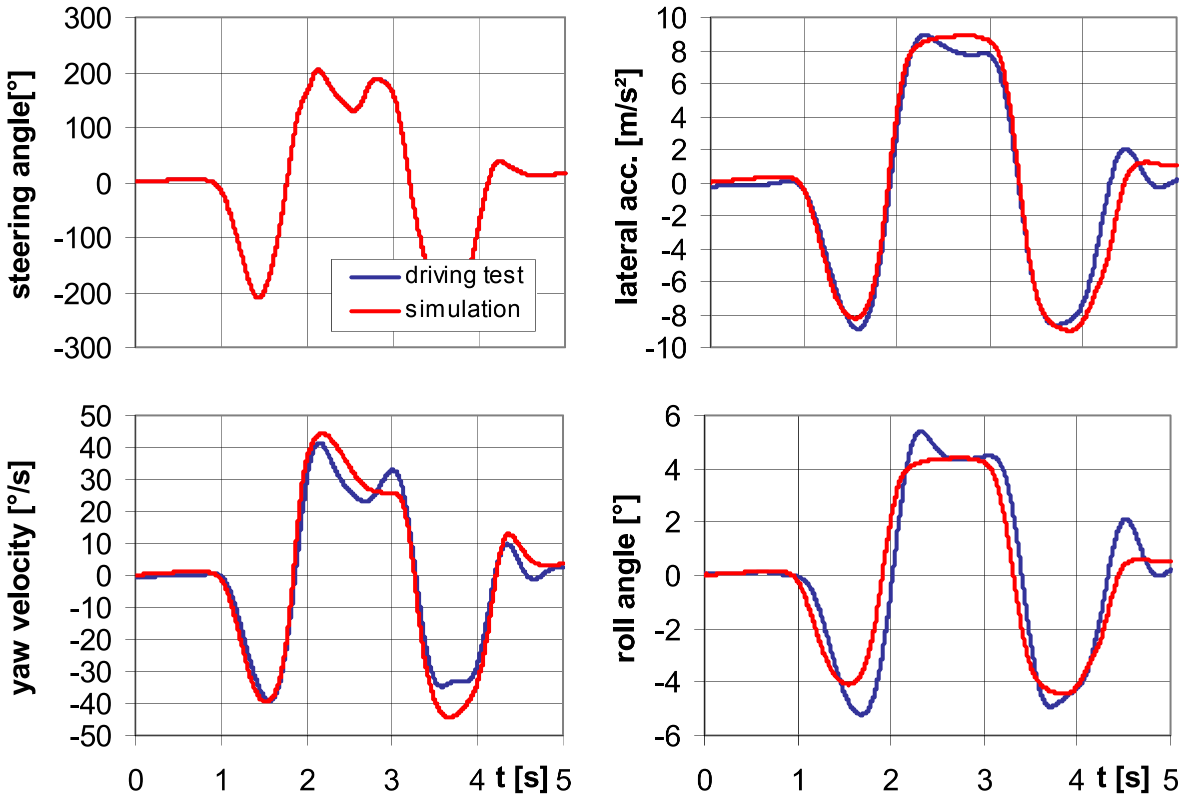

Fig. 4-10: Double lane change, 60 km/h, dry asphalt

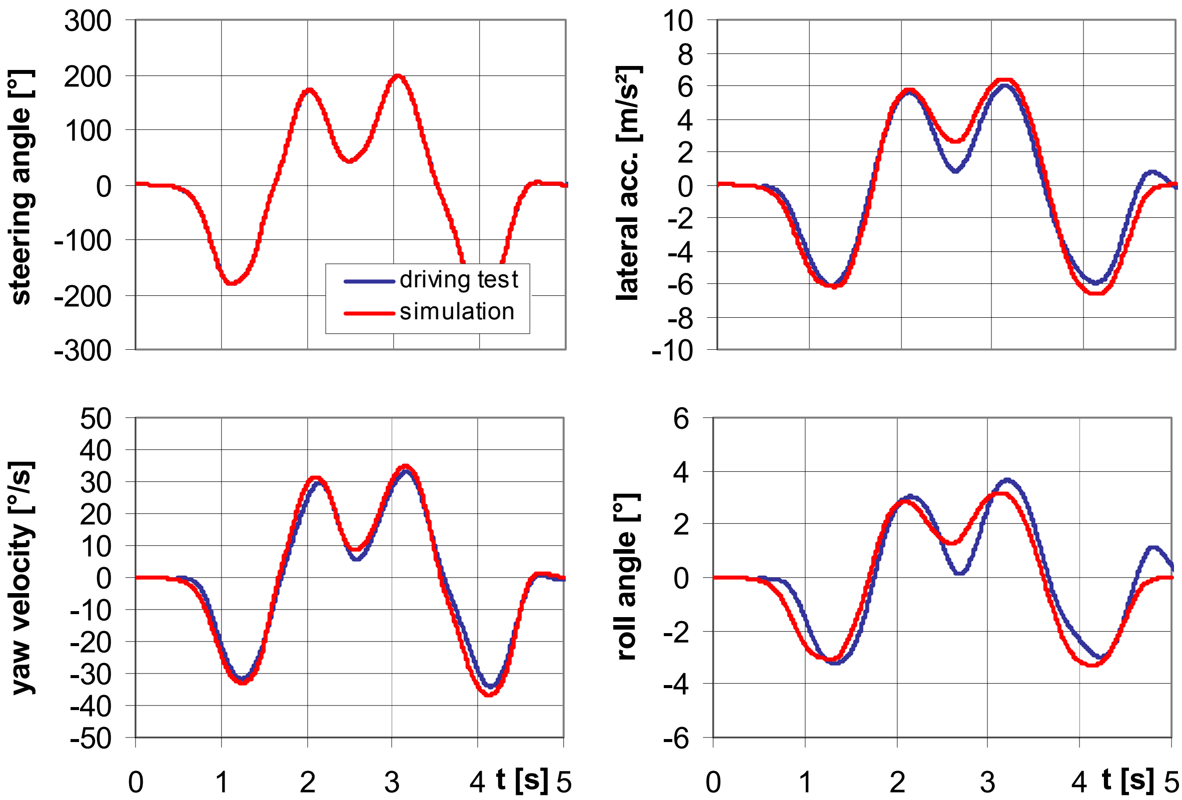

Fig. 4-11: Double lane change, 45 km/h, wet asphalt

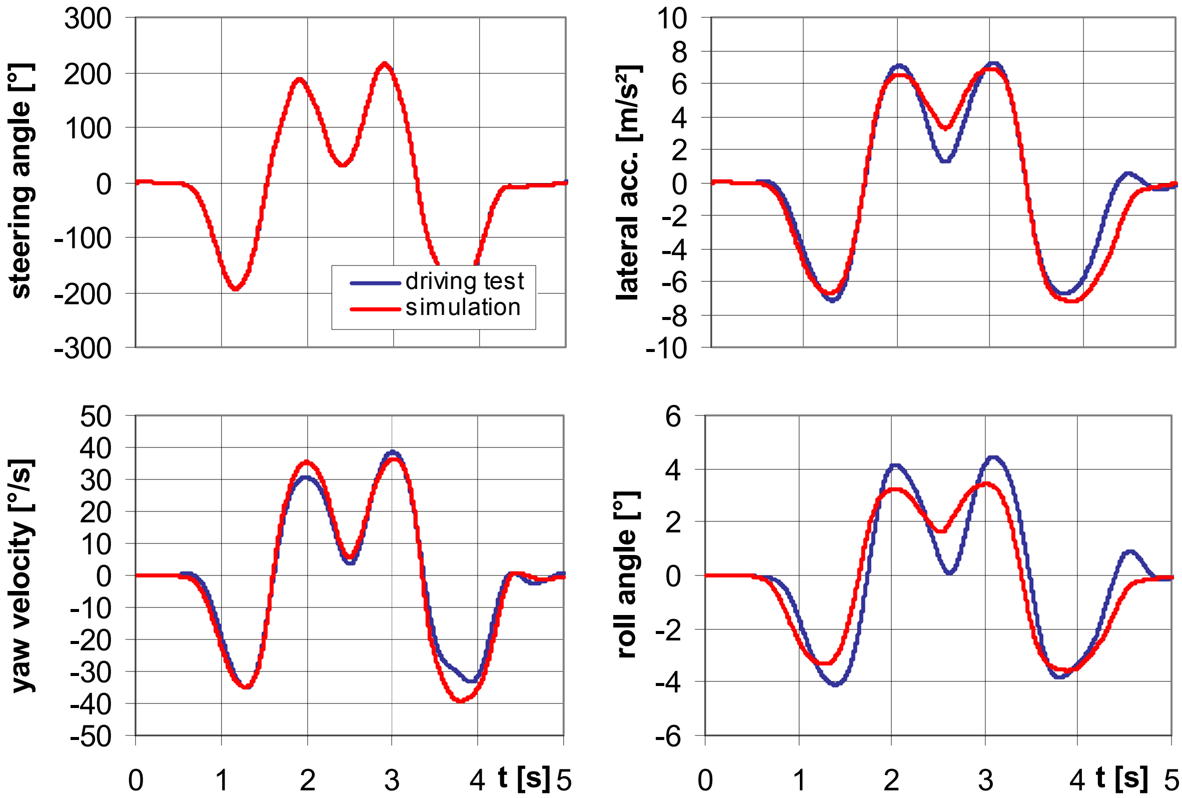

Fig. 4-12: Double lane change, 50 km/h, wet asphalt

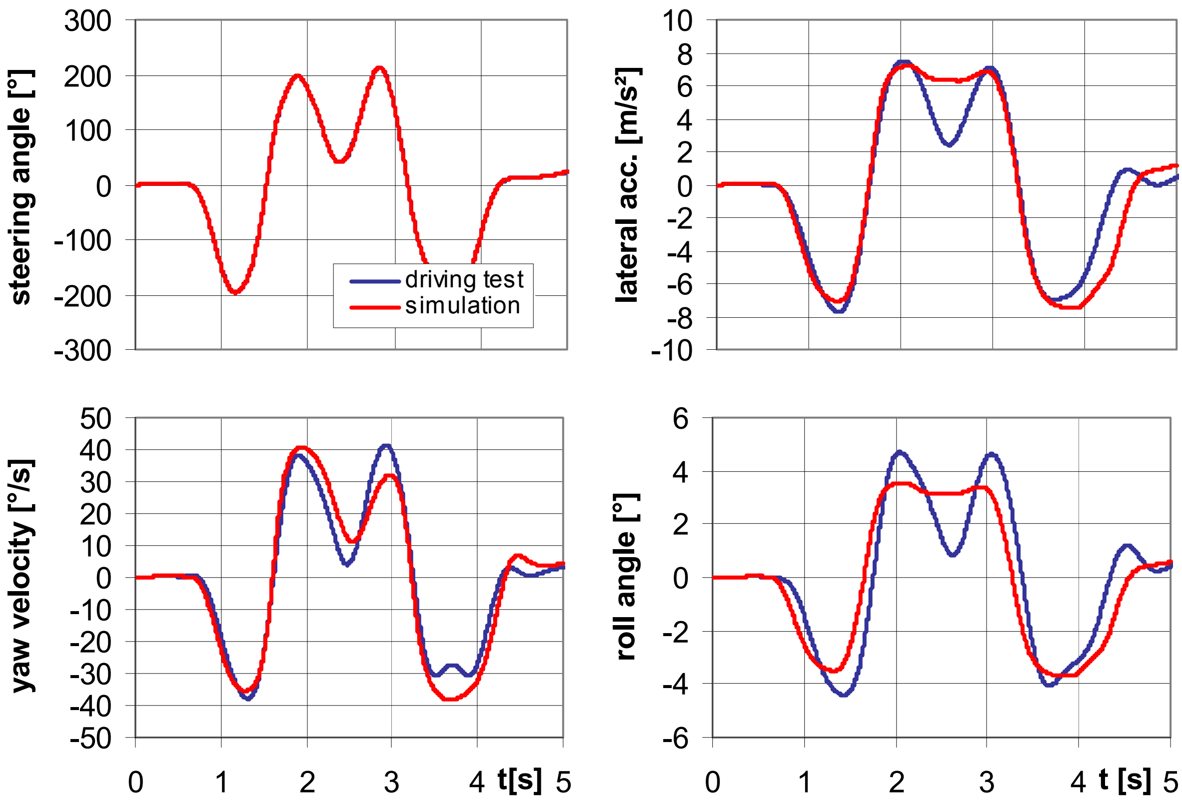

Fig. 4-13: Double lane change, 55 km/h, wet asphalt

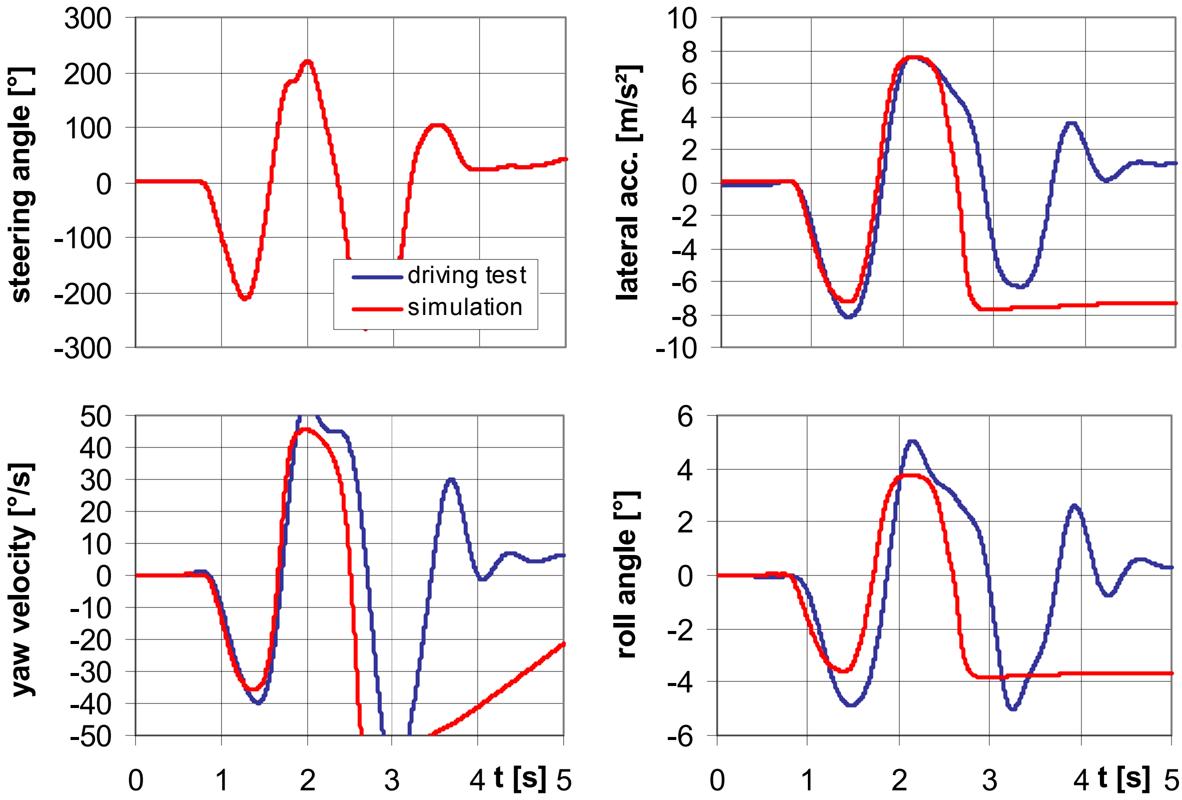

Fig. 4-14: Double lane change, 60 km/h, wet asphalt

All the portrayals show a good correspondence between the driving test and the simulation. Only in the last portrayal (Fig. 4-14) does the vehicle model lose its stability, whereas the real vehicle can be compensated. The sequence of all the movement variables (in particular the steering angle) however does show that the real vehicle was moved in the absolute borderline area here and accordingly the simulation can very easily show a highly deviating behaviour as a result of minimally differing peripheral conditions.

- **BMW 330iX**

The set-up of the BMW vehicle model is analogous to that of the A Class model, Fig. 4-15. Here too, the vehicle-specific parameters enable a good approximation to the results of the driving test without DSC, as Fig. 4-16 to Fig. 4-26 prove. As the BMW is more of a rear-dominated vehicle despite its four-wheel drive, it is shown as a rear-driven vehicle in the simulations. Apart from the steady state cornering, only slight drive torques become active, the distribution of the drive torques does not play any role anyway, as a freely rolling vehicle is always simulated.

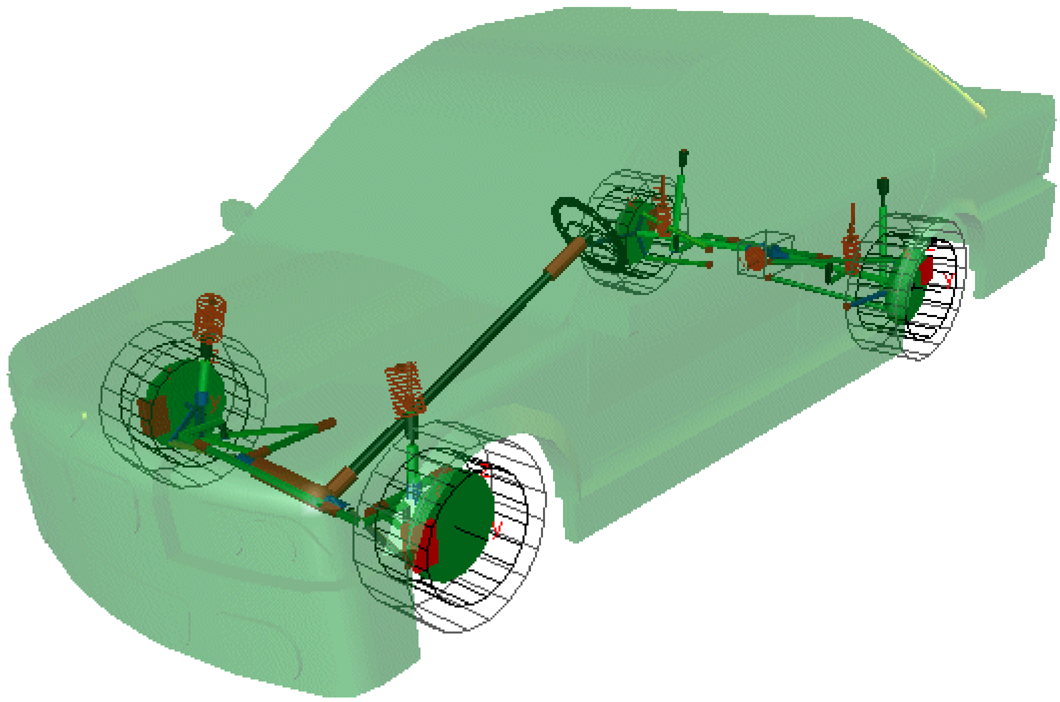

Fig. 4-15: BMW 330xi simulation model

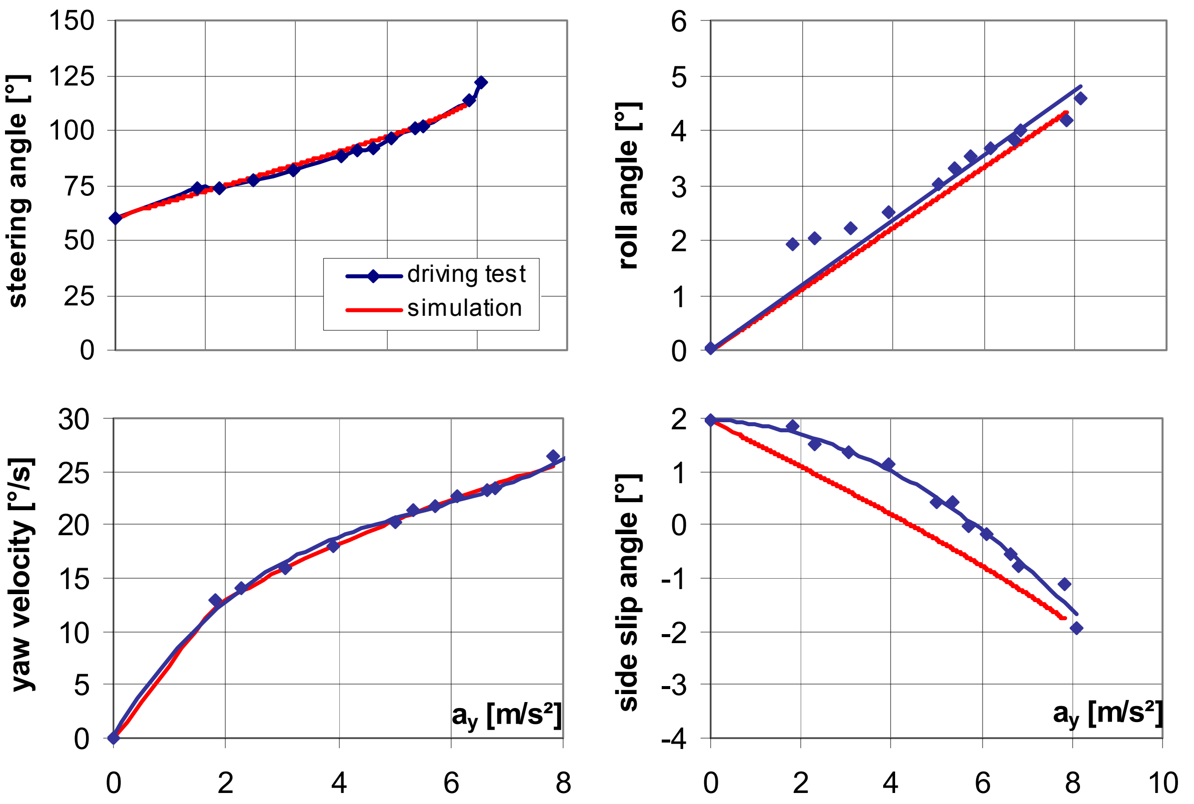

Fig. 4-16: Steady state cornering

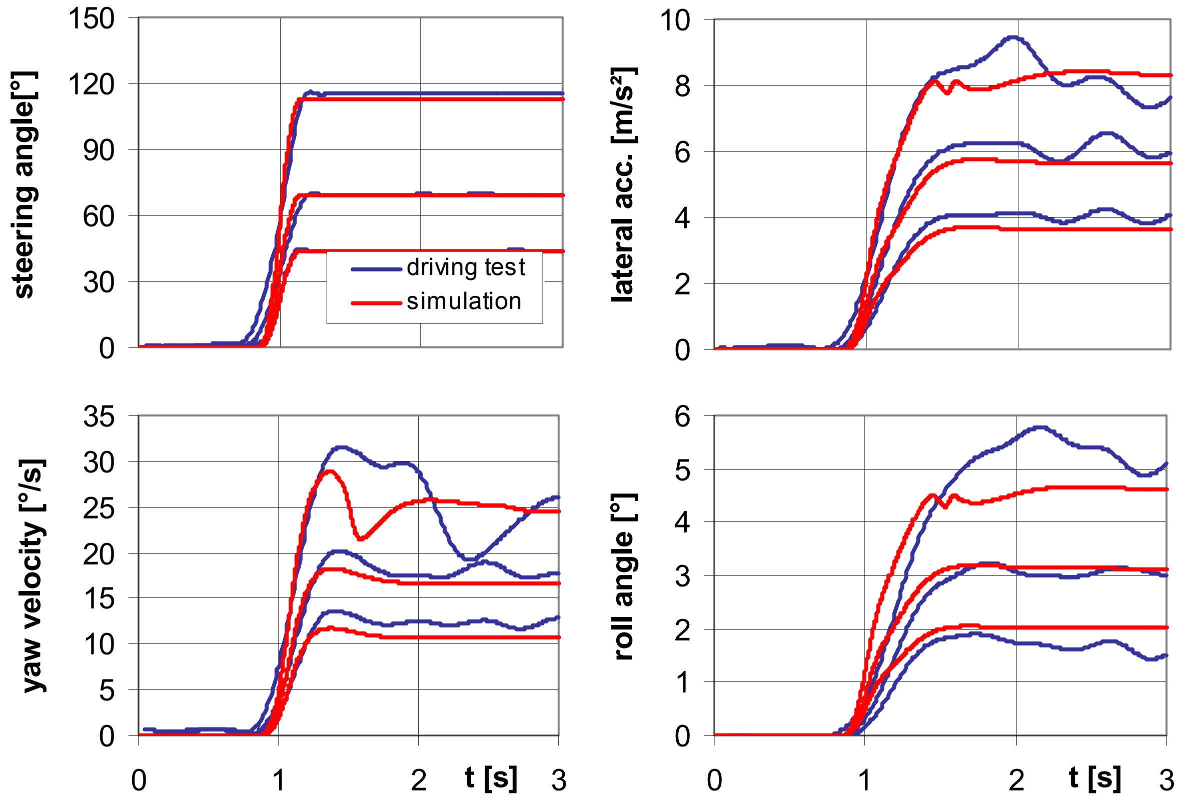

Fig. 4-17: Step steer input, dry asphalt

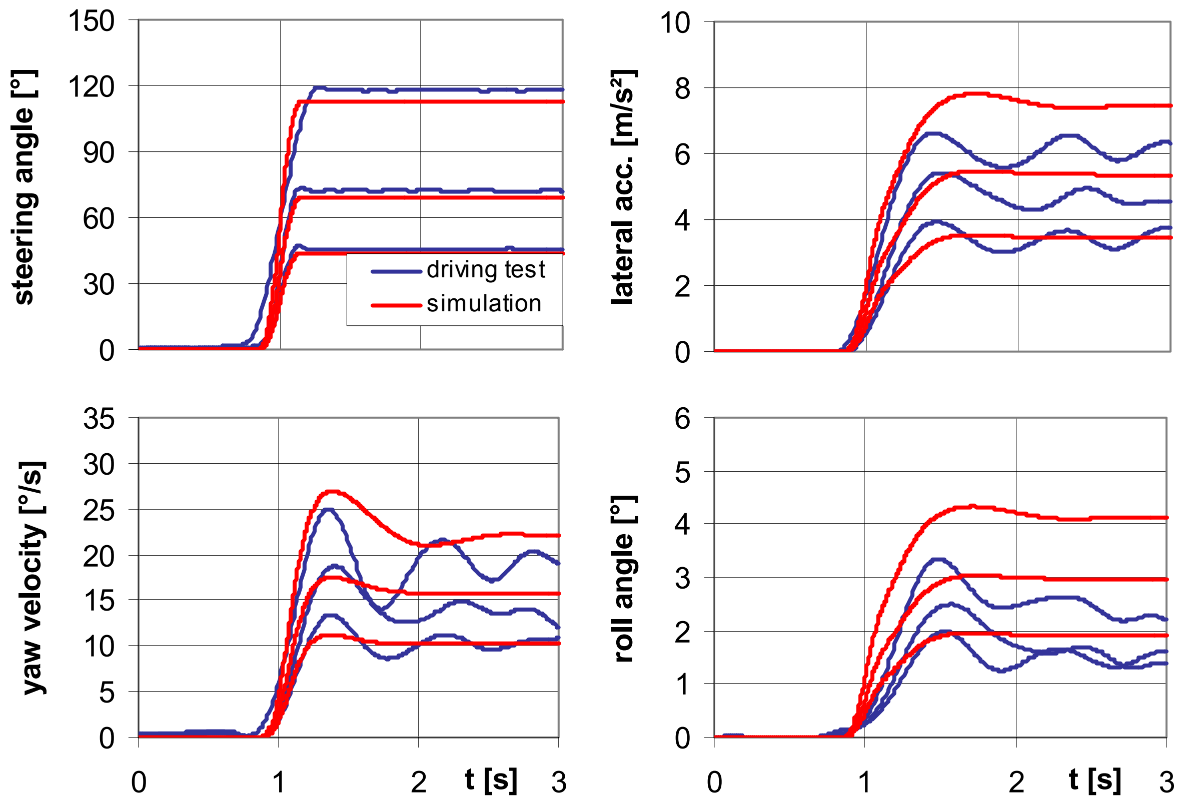

Fig. 4-18: Step steer input, wet asphalt

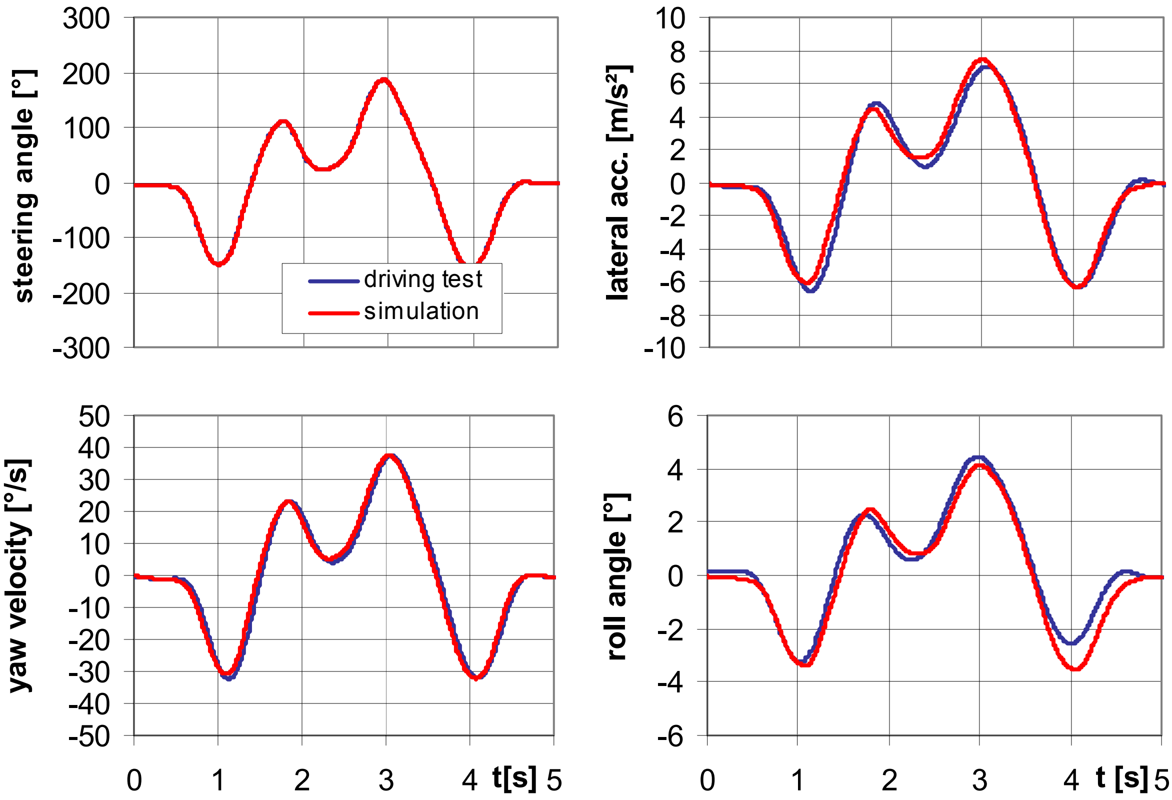

Fig. 4-19: Double lane change, 45 km/h, dry asphalt

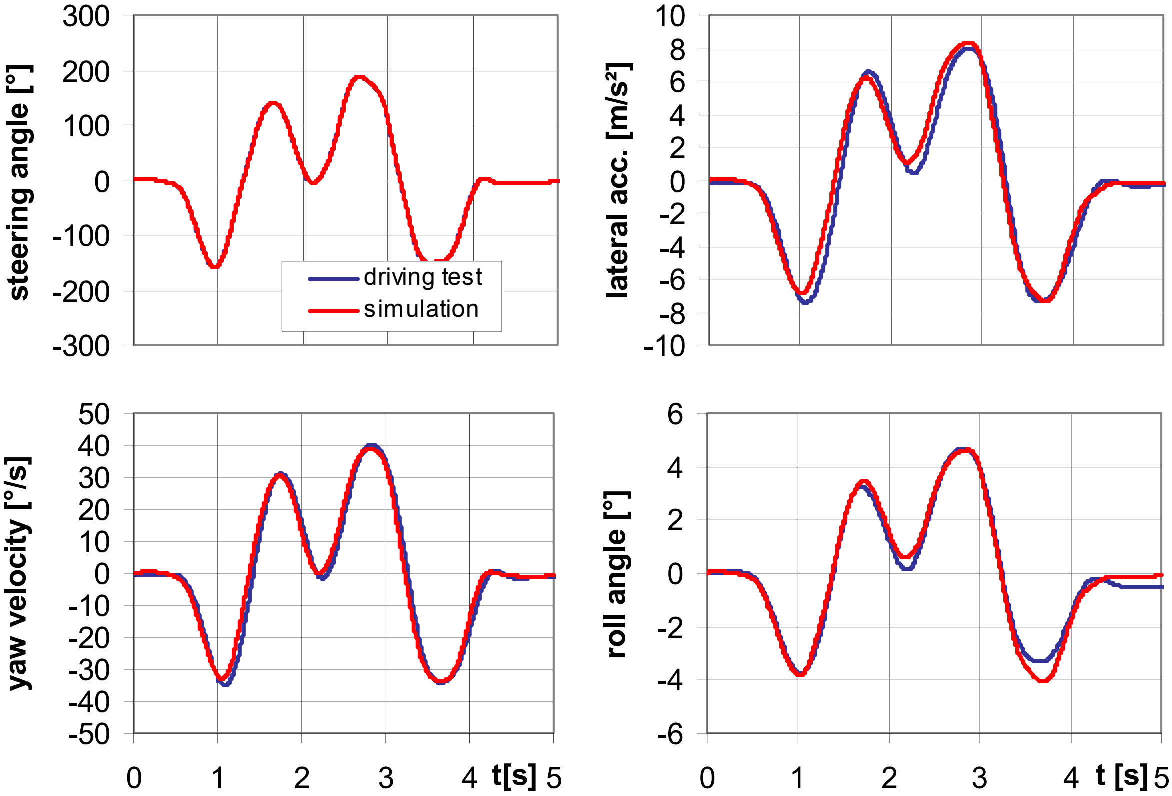

Fig. 4-20: Double lane change, 50 km/h, dry asphalt

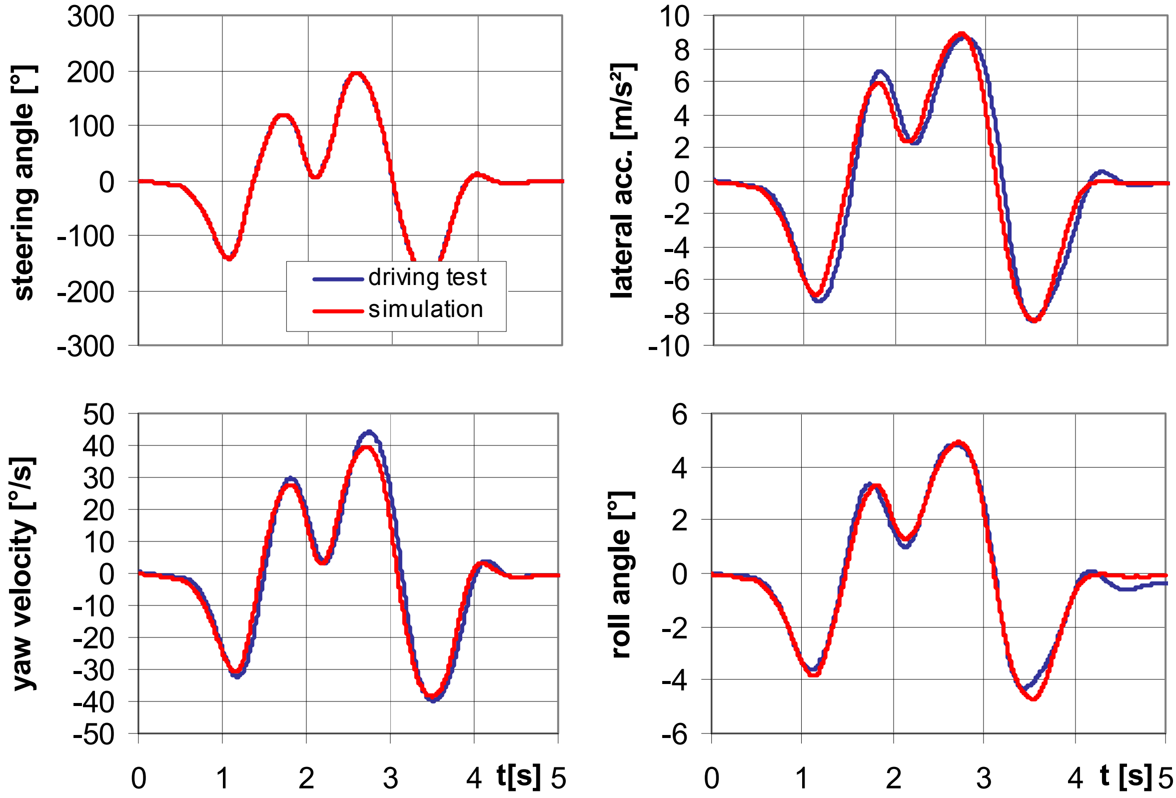

Fig. 4-21: Double lane change, 55 km/h, dry asphalt

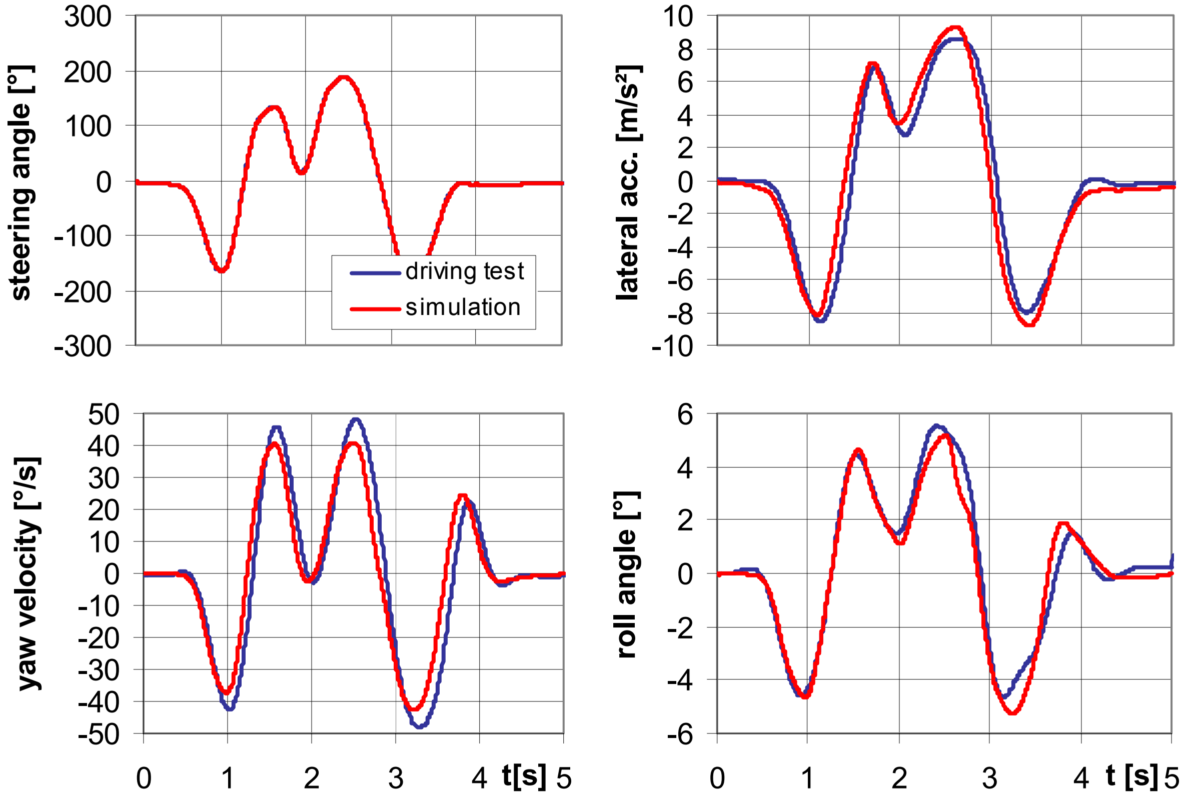

Fig. 4-22: Double lane change, 60 km/h, dry asphalt

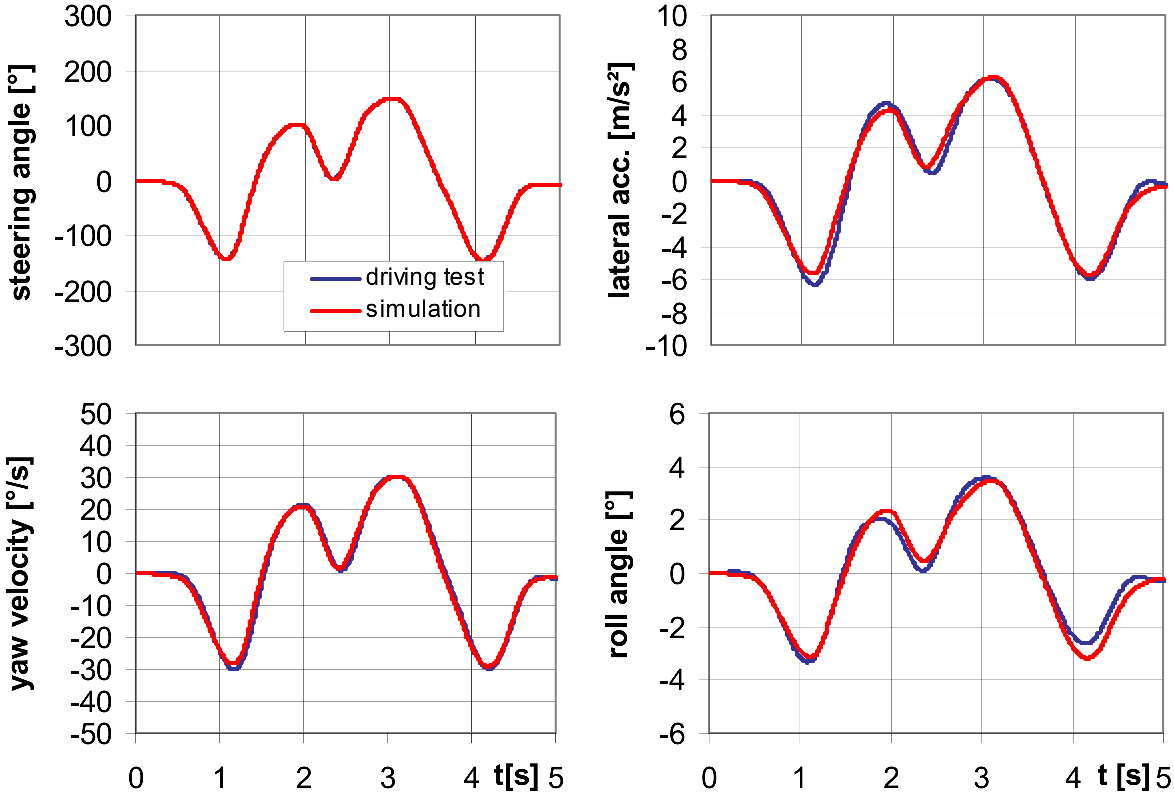

Fig. 4-23: Double lane change, 45 km/h, wet asphalt

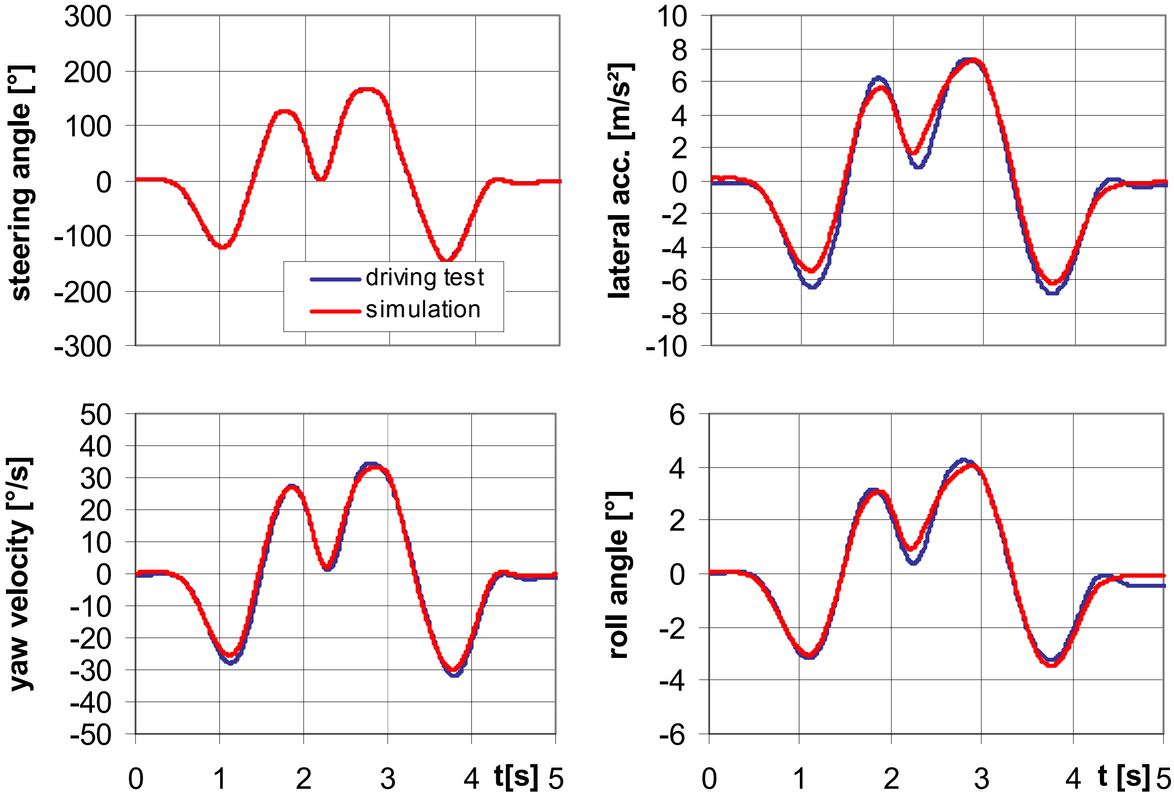

Fig. 4-24: Double lane change, 50 km/h, wet asphalt

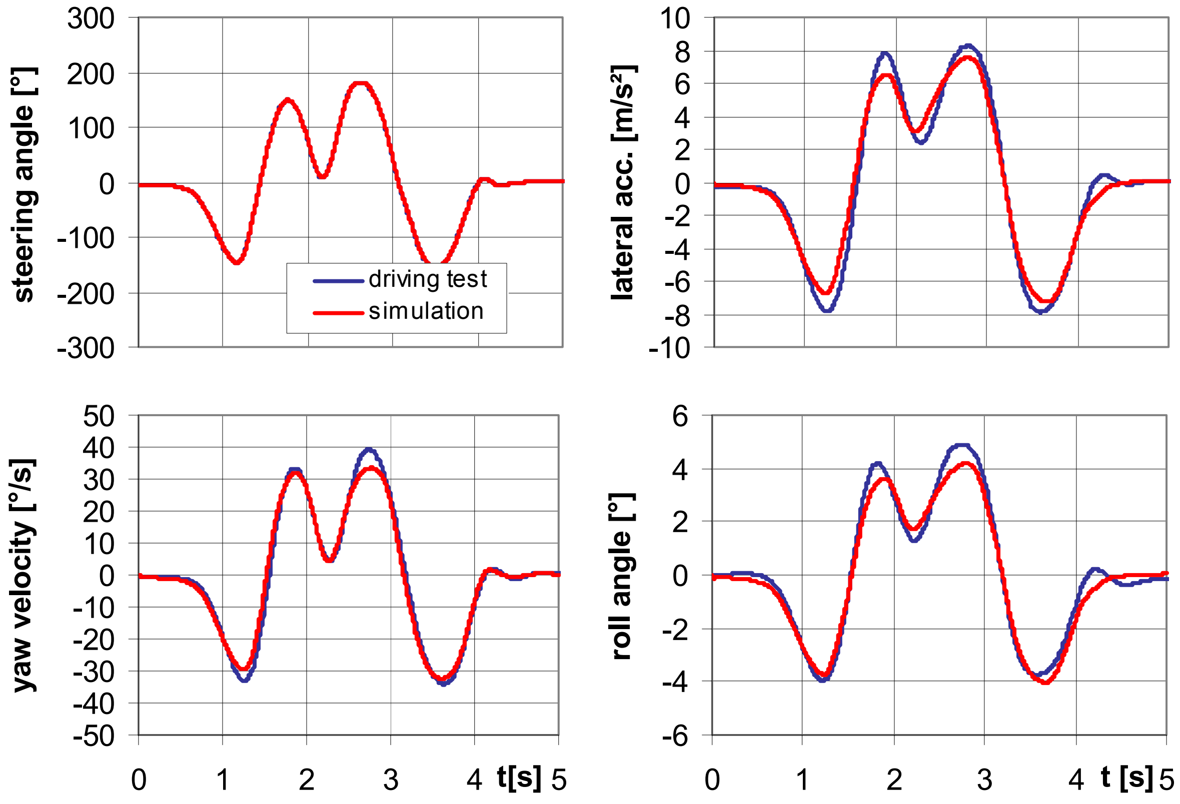

Fig. 4-25: Double lane change, 55 km/h, wet asphalt

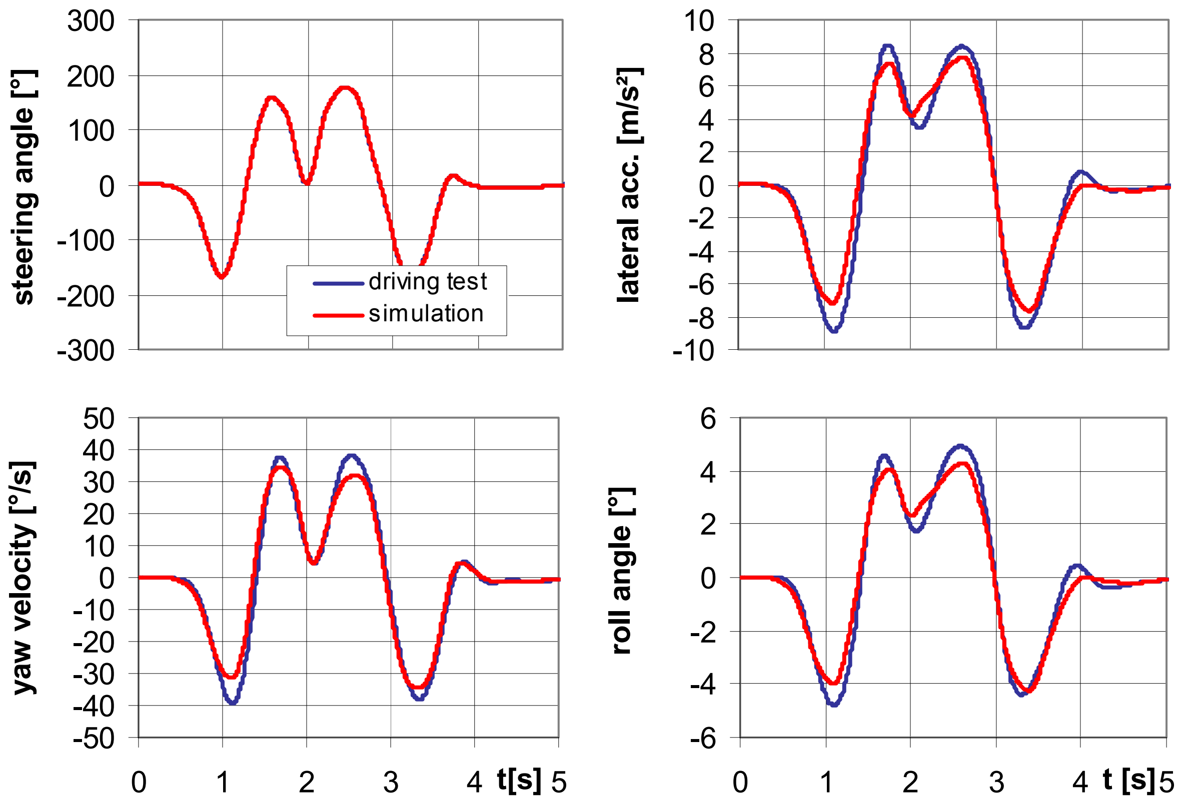

Fig. 4-26: Double lane change, 60 km/h, wet asphalt

4.2 Vehicle dynamics controller model

The vehicle dynamics controller models for the two vehicles examined have an identical basic structure. But they do differ through different parameters and threshold figures as well as a series of details, which result, for example, from the vehicle-specific drive concepts. For this reason, the driving-dynamics control models for the Mercedes Benz A Class and the BMW 330xi are explained together below and the differences occurring are shown and explained separately.

The vehicle dynamics controller comprises four blocks: sensors, controller, actuators and plausibility checks and an error switch, Fig. 4-27. It has seven input channels, by which the steering wheel angle, yaw velocity, longitudinal and lateral acceleration, wheel speeds and the brake and drive torques applied by the driver are provided. The two output channels of the vehicle dynamics controller supply the drive torque and the brake torques to be applied to the four wheels. In addition, Fig. 4-27 contains an error storage display, which displays a possible occurrence of an error.

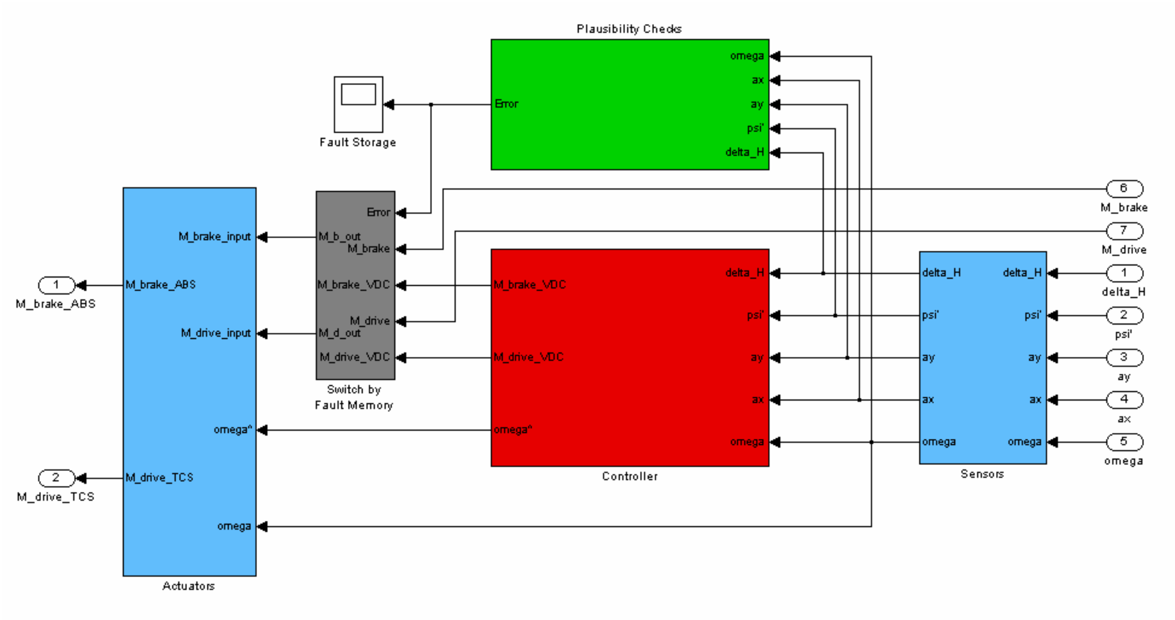

Fig. 4-27: Setup of the vehicle dynamics controller

The function of the error switch entails putting the vehicle dynamics controller out of operation if a malfunction occurs in it and thus only permitting the brake torques and drive torques applied by the driver. If there is no malfunction, the error switch forwards the brake and drive torques stated by the driver and the vehicle dynamics controller to the following actuators in a suitable way. With regard to the brake torque, it compares the signals of all four wheels of the vehicle incoming from the driver and from the vehicle dynamics controller individually and forwards the larger of the two torques to the output. The drive moment stated by the driver is multiplied by a reduction factor output by the vehicle dynamics controller within the error switch. In uncritical driving situations, this factor is 1, which means that there is no alteration of the drive torque. Only if the vehicle dynamics controller makes an intervention into the engine management due to a critical driving condition is the reduction factor reduced accordingly, as a result of which the output drive torque is reduced. Further reference is made to the function of the other four blocks and their way of working below.

4.2.1 Sensors

The "Sensors" sub-system provides the vehicle dynamics controller with the variables measurable in a real vehicle: steering wheel angle, yaw velocity, longitudinal and lateral acceleration as well as the four wheel speeds. All these variables are needed in order both to recognise the current driving state and also to estimate a vehicle reaction intended by the driver. In order to be able to examine the fail-safe behaviour of the vehicle dynamics controller, it is possible to lock an error on to any sensor variable at any point in time within the sensor block, Fig. 4-28. With the "Lock-on Error" sub-systems, various forms of error can be selected, Fig. 4-29. The individual forms of error are imitations of real malfunctions of sensors which can actually happen and entail in detail:

- Total failure (signal size equal to zero)
- Inversion of the measurement signal (signal size with negative sign in front)
- Offset (signal size multiplied by defined factor)
- Signal noise (signal size multiplied by stochastic factor)
- Long wavelength drifting (signal size multiplied by low frequency sinus signal)

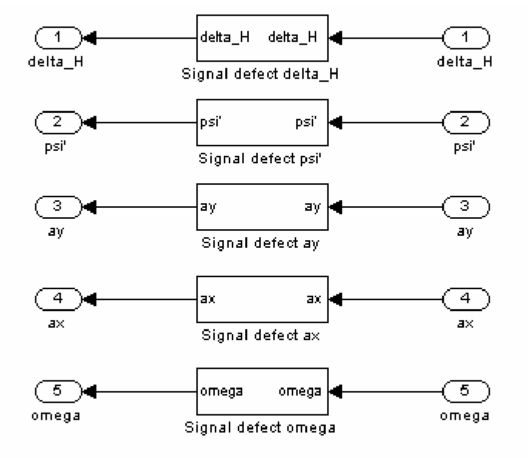

Fig. 4-28: Signal defect application

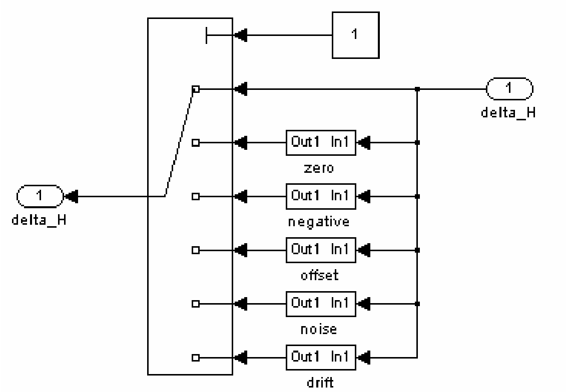

Fig. 4-29: Possible signal defects

The sensor signals used and their locked-on errors are identical for both vehicles.

4.2.2 Controller

The "Controller" system is the module of the vehicle dynamics controller which results in active brake interventions and reductions of engine torque. It comprises the three observer, control algorithm and control strategy sub-systems, Fig. 4-30. This principal set-up is identical for both test vehicles. Below, the three sub-systems of the controls are explained in detail and the differences between the two test vehicles demonstrated.

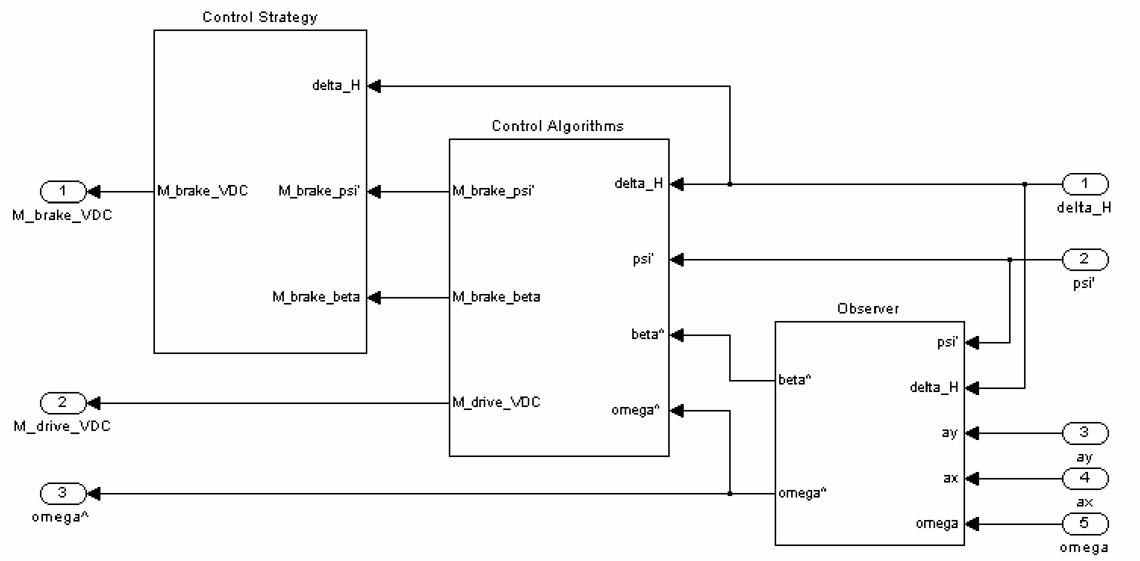

Fig. 4-30: Structure of the controller

4.2.2.1 Observer

The observer makes use of the directly measurable variables of wheel speeds, longitudinal and lateral acceleration, yaw velocity and steering wheel angle provided by the sensors in order to estimate the vehicle variables of longitudinal velocity and sideslip angle. In a real vehicle, these variables cannot be measured or can only be measured with a disproportionately great effort. Therefore, they are estimated in the sub-systems of the observer existing for this purpose, Fig. 4-31.

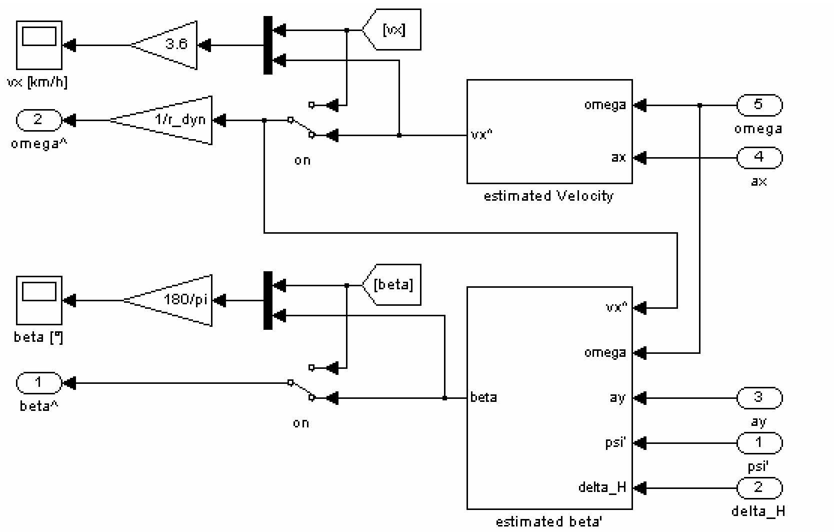

Fig. 4-31: Observer setup

The longitudinal velocity of the vehicle calculated is converted to a wheel speed by division by the dynamic wheel radius of the vehicle tyres. Together with the calculated sideslip angle, this wheel velocity forms the output variables of the observer. As can be seen in Fig. 4-31, the observer contains two displays in which both the estimated longitudinal velocity of the vehicle as well as the estimated sideslip angle can be compared with the vehicle variables occurring in the simulation model. (In a simulation model, the actual velocity and the actual sideslip angle are naturally available all the time.) With the help of the displays, the quality of the variables calculated can be verified. If need be, two switches can be used to have recourse to the variables supplied directly by the vehicle model for the further processes. The calculation of longitudinal vehicle velocity and the sideslip angle are explained below separately.

i) Estimation of the velocity

The estimation of the vehicle velocity is done in two different ways. On the one hand, an arithmetic averaging from three wheel speeds is done in the "Velocity only from wheel speeds" sub-system, Fig. 4-32. For this, the two wheel speeds of the non-driven axles and the wheel speed of the driven axle are used, the latter currently being the smaller of the two speeds. With the use of only one driven wheel, a realistic value is achieved for the mean wheel speed, this value being converted to the estimated vehicle velocity by multiplication with the dynamic wheel radius of the wheel tyres [REI93].

Alongside the calculation of an arithmetic mean of the wheel speeds, the "Velocity only from wheel speeds" sub-system permanently checks the deviation of all four wheel speeds from the calculated mean. For each wheel, the absolute value of the deviation is related to the estimated wheel speed. If one of the four wheel speed deviations exceeds a relative deviation of 5%, the "Switch" outlet of the sub-system jumps from 1 to 0, which signalises to the velocity estimator that the estimated value from the wheel speeds is possibly no longer precise enough.

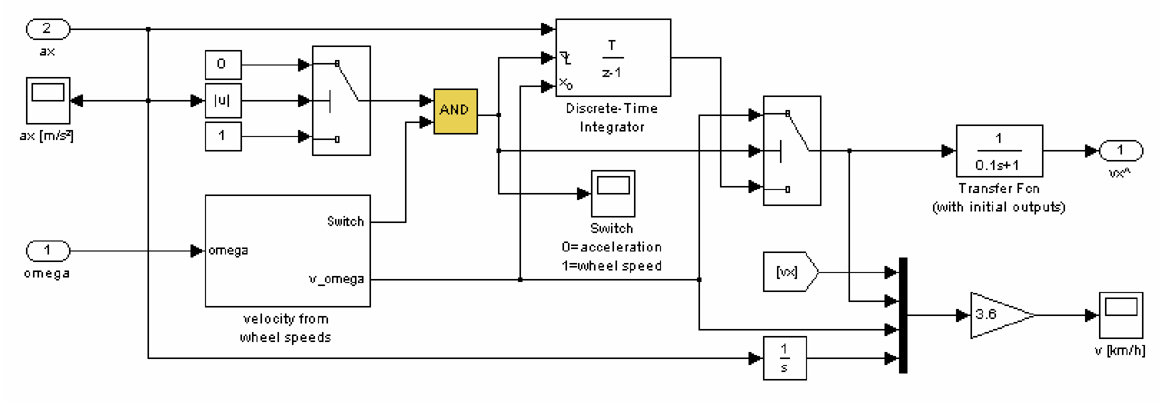

Fig. 4-32: Estimation of the longitudinal velocity

In this case, the velocity is no longer estimated by the mean wheel speeds, but by an integration of the longitudinal acceleration. In addition, the variable of the longitudinal acceleration itself is involved in the assessment of the driving condition. If its absolute figure exceeds a threshold value of 0.5 m/s^2, there is also a switch-over to integration. In this, the integration starts at the last “valid” figure from the wheel speeds in each case.

A permanent integration of the longitudinal acceleration to determine the longitudinal velocity is not possible as the speed signal would drift away from the real figure after some time. For this reason, there is only integration in the estimation process during dynamic driving processes, with the starting figure being provided by the stationary estimation.

The transmission function contained in Fig. 4-32 ensures a harmonious transition of the longitudinal velocity between the two estimation procedures. In addition, there are again a number of displays contained in the sub-system in order, on the one hand, to make switches between the two estimation processes clear and, on the other, to check the calculated longitudinal velocity against the actual velocity of the vehicle model.

The quality of the observation of the velocity is made clear by a comparison between the actual (yellow) and estimated (red) variables in a double lane change at 60 km/h, Fig. 4-33. Despite massive brake interventions by the vehicle dynamics controller (middle picture) and as a result higher slip figures of individual wheels, both sequences of velocity (left picture) are practically identical as a result of the strategy described above (right-hand picture).

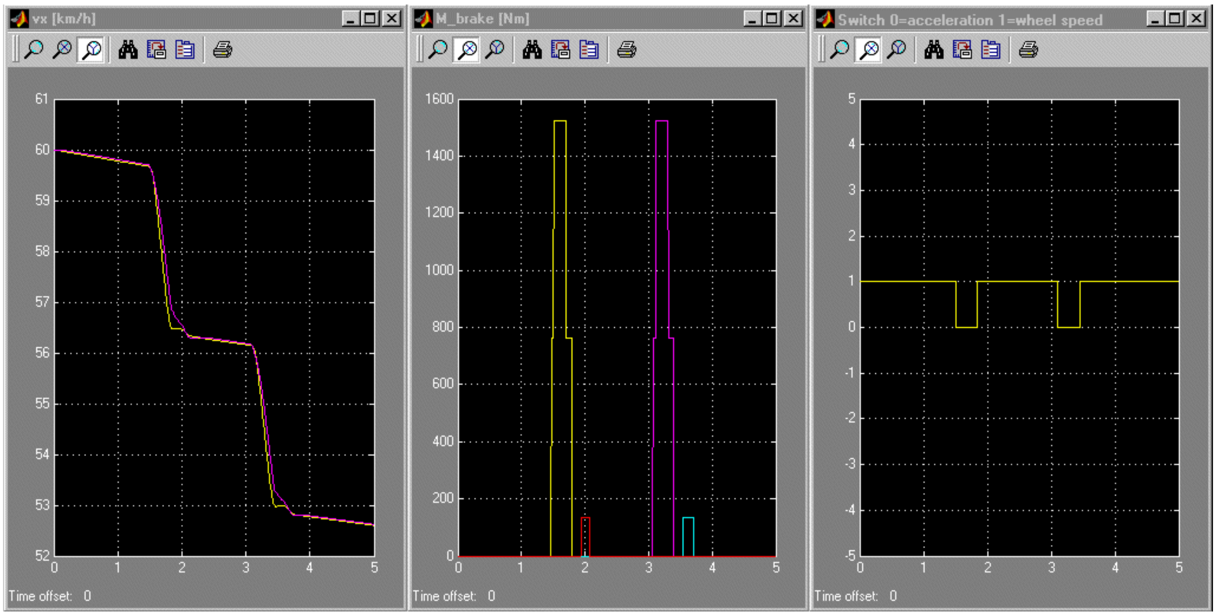

Fig. 4-33: Actual and estimated velocity

The reference angular wheel velocity determined in this way is used below for the brake slip and drive slip control as well as for the calculation of the nominal yaw velocity.

ii) Estimation of the sideslip angle

In the estimation of the sideslip angle, similar to the estimation of velocity, the observer makes a distinction between a stationary and a dynamic driving condition. The assessment of the driving condition is done by the “Switch” sub-system, which is marked in yellow in Fig. 4-34.

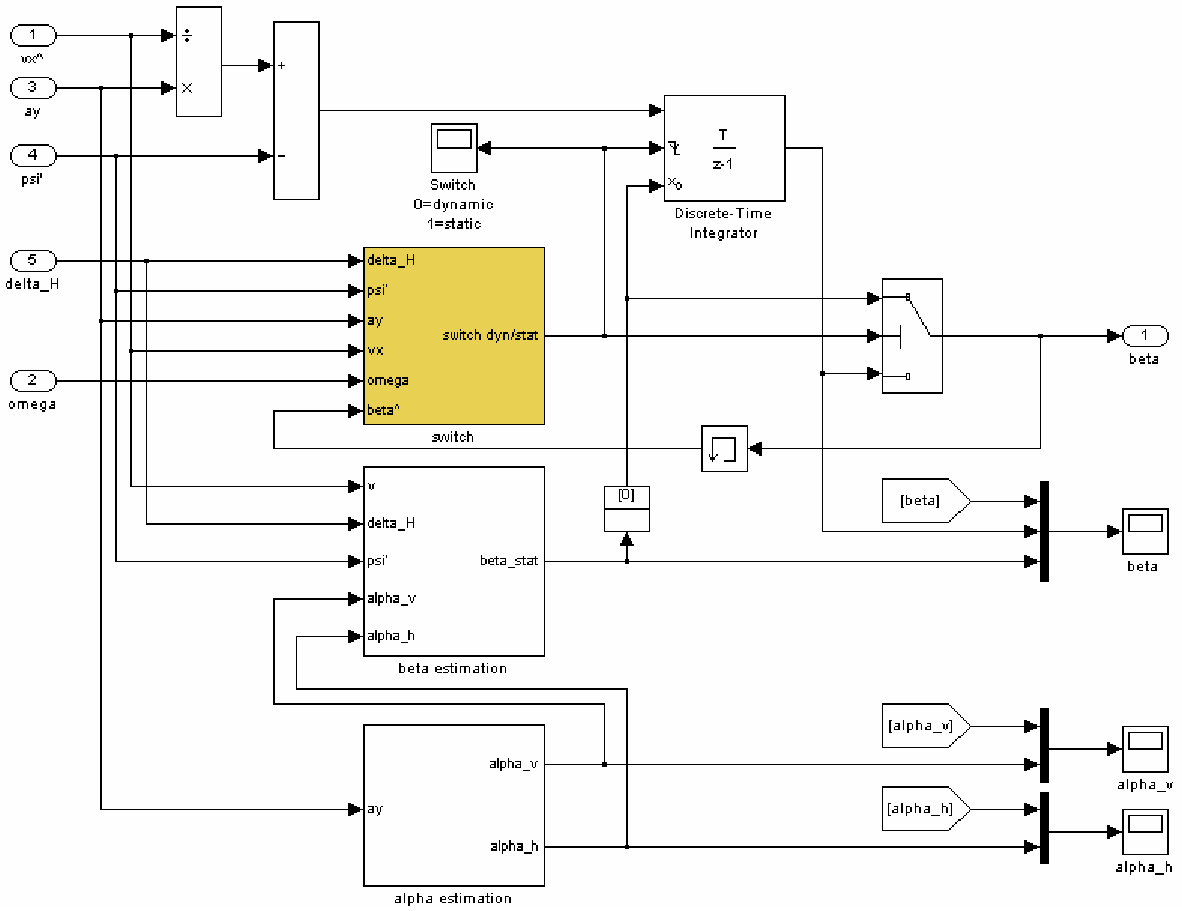

Fig. 4-34: Sideslip angle estimation

The “Switch” sub-system monitors the five input variables of the sideslip angle calculation, i.e. the longitudinal velocity vx^, the lateral acceleration ay, the yaw velocity psi’, the steering wheel angle delta_H and the wheel speeds omega of all four wheels, already estimated, and also the output variable of the system itself: the sideslip angle beta. With these variables, the system provides a total of six criteria which define either a stationary or a dynamic driving condition.

From the estimated longitudinal vehicle velocity and the four wheel speeds, the longitudinal slip of the individual wheels is calculated. The steering wheel angle, yaw velocity and lateral acceleration variables are derived according to time. In this way, their alteration is registered. With regard to the sideslip angle, the system observes its absolute value. It is only if all five criteria are below certain thresholds for more than 1.5 seconds or, as a sixth criterion, the longitudinal velocity is lower than 8 m/s that the system recognises the driving condition as being stationary. If one or more of the criteria exceed(s) the threshold value at a longitudinal velocity above 8 m/s, a dynamic driving condition is detected, as a result of which the output of the system jumps from 1 to 0 again. The thresholds of the six criteria result from extensive simulations and have the following values in detail:

- d(delta_H)/dt $\leq 0{,}5\ ^{1}/_{s}$
- d(psi')/dt $\leq 0{,}03\ ^{1}/_{s}$
- d(ay)/dt $\leq 0{,}3$ m/s
- Schlupf $\leq 0{,}5\%$
- beta $\leq 6°$
- vx ≤ 8 m/s

If the observer assesses the driving condition as being dynamic, an integration is done as for the velocity estimation. The variable to be integrated is the sideslip angle velocity, which is calculated from the longitudinal velocity, lateral acceleration and yaw velocity input variables according to Eq. 4-1:

$$\dot{\beta} = \frac{a_y}{v_x} - \dot{\Psi} \qquad \text{Eq. 4-1}$$

The integration of the sideslip angle velocity thus provides the sideslip angle of the vehicle during dynamic manoeuvres.

If the criteria for a stationary handling performance have been fulfilled, the initial value of the integrator is reset, with the result that it can start with the last valid value of the stationary calculation for a new integration. For stationary behaviour, the sideslip angle is determined in a different way. On the basis of a bicycle vehicle model, it can be determined from the slip angle α of the front axle or the rear axle. The formula connections provided by the bicycle vehicle model are stated below:

$$\alpha_f = \delta - \beta - \frac{l_f \cdot \dot{\Psi}}{v} \qquad \Leftrightarrow \beta = \delta - \alpha_f - \frac{l_f \cdot \dot{\Psi}}{v} \qquad \text{Eq. 4-2}$$

$$\alpha_r = -\beta + \frac{l_r \cdot \dot{\Psi}}{v} \qquad \Leftrightarrow \beta = \frac{l_r \cdot \dot{\Psi}}{v} - \alpha_r \qquad \text{Eq. 4-3}$$

Alongside the known geometrical vehicle variables l_f and l_r as well as the yaw velocity, longitudinal velocity and steering angle input variables, calculated from the steering wheel angle via the steering step-up in question, the slip angle represents variables unknown as yet. For this reason, they must be generated in the „alpha estimation“ sub-system.

Here, a slip angle is calculated from a side force by means of an inverse tyre model. A tyre model which is, on the one hand, designed simply enough in order to permit a reversal, but, on the other hand, provides sufficiently precise results, is the HSRI tyre model [WIE74], [CHE87]. The function of this model is briefly portrayed schematically below:

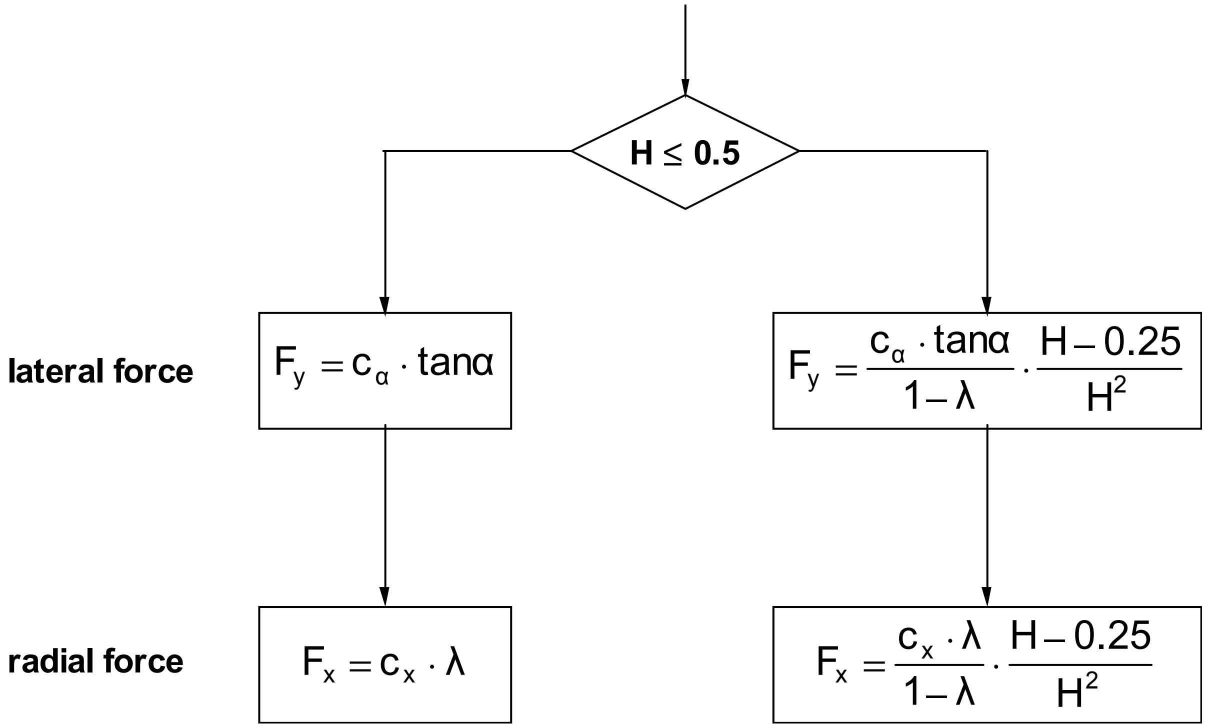

Fig. 4-35: HSRI tyre model

Alongside the slip rigidity c_α, slip angle α, peripheral force rigidity c_x, and longitudinal slip λ variables, the HSRI model contains a variable H, which is used inter alia for a case distinction. This variable is calculated as follows:

$$H = \frac{\sqrt{(c_x \cdot \lambda)^2 + (c_\alpha \cdot \tan\alpha)^2}}{\mu \cdot G_R \cdot (1-\lambda)} \qquad \text{Eq. 4-4}$$

As, according to Eq. 4-2 and Eq. 4-3, the sideslip angle can equally be calculated from the slip angles of the front and rear axle, the non-driven vehicle axle is used within the estimation of the sideslip angle in order to simplify the HSRI tyre model. As practically no longitudinal slip λ can be seen on the non-driven wheels in a stationary vehicle and $\tan(\alpha)=\alpha$ holds for small slip angles, the HSRI tyre model can be simplified with regard to the lateral tyre forces as follows:

$$H \leq 0{,}5 \Rightarrow F_y = c_\alpha \cdot \alpha \qquad \text{Eq. 4-5}$$

$$H > 0{,}5 \Rightarrow F_y = c_\alpha \cdot \alpha \cdot \frac{H-0{,}25}{H^2} \qquad \text{Eq. 4-6}$$

Factor H is thus also considerably simplified with a coefficient of friction of μ = 1:

$$H = \frac{c_\alpha \cdot \alpha}{\mu \cdot G_R} \qquad \text{Eq. 4-7}$$

Now, the two side force equations of the tyre model can be converted according to the slip angle:

$$H \leq 0{,}5 \Rightarrow \alpha = \frac{F_y}{c_\alpha} \quad \text{Eq. 4-8}$$

$$H > 0{,}5 \Rightarrow \alpha = \frac{(\mu \cdot G_R)^2}{4 \cdot c_\alpha \cdot (\mu \cdot G_R - F_y)} \quad \text{Eq. 4-9}$$

The side forces F_y of the axle in question contained in the equations can be determined from the mass of the vehicle, the location of centre of gravity and the lateral acceleration at the centre of gravity:

$$F_{y,FA} = m \cdot a_y \cdot \frac{l_r}{l} \quad \text{Eq. 4-10}$$

$$F_{y,RA} = m \cdot a_y \cdot \frac{l_f}{l} \quad \text{Eq. 4-11}$$

The slip rigidities still needed for the calculation of the slip angle for the front and rear axle are available as constants. In this way, all the variables needed for the inverse tyre model are known. The HSRI model is implemented in the “alpha estimate” sub-system and supplies the slip angles alpha_v and alpha_h as output variables. These are then used in the “beta estimate“ sub-system in order to determine the sideslip angle of the vehicle.

Again, there are a number of displays within the sub-system in order to be able to check the quality of the sideslip angle estimate, the slip angle estimate and the assessment of stationary/dynamic behaviour. The sideslip angle is provided to further systems by the observer.

The quality of the estimate is also to be portrayed for the observer on the basis of the double lane change at 60 km/h. As the double lane change represents a highly dynamic manoeuvre, there is always dynamic calculation during the passing of the lines (right-hand picture). There is only a change to static calculation some time after the last line has been left (about 6.7s). In this way, the observed sideslip angle (red), which has already slightly drifted away, is again corrected to the actual value (yellow) (left-hand picture).

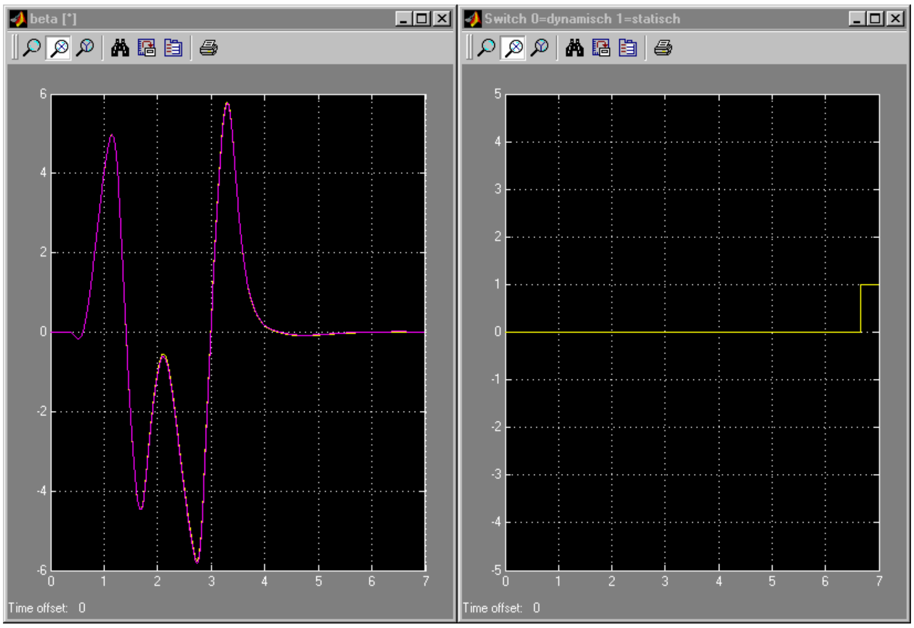

Fig. 4-36: Actual and estimated sideslip angle

4.2.2.2 Yaw velocity control and sideslip angle limitation

The “Control algorithm” sub-system is the part of the controller in which the active brake interventions and interventions into engine management are generated. This is done by the two controls which work in parallel: “Sideslip angle limitation” and “Yaw velocity control“, which are shown in Fig. 4-37. Both controls provide four brake pressures for the individual vehicle wheels as output variables. If certain thresholds are exceeded, the controls apply fixed required brake levels, which are defined within the vehicle parameters. In reality, there are mathematically much more sophisticated algorithms in order to compensate the difference between nominal and actual yaw velocity. However, it is seen that a very good adaptation to the real systems can be achieved by the relatively simple requirements of fixed brake pressure levels.

The brake pressures, which are generated equally by the two control blocks for front and rear axle, are reduced on the rear axle by a brake proportioning deposited in the vehicle parameters. In order to cope with the period of time needed in a real vehicle to build up the brake pressures, a delay is provided between the reaction of the vehicle dynamics controller and the brake pressure outlets. This is achieved by the “Build-up time” blocks contained in Fig. 4-37, in which there is no difference in size, but a delay between the input variable and the output variable. The “Yaw velocity control” block also has an “Engine torque” output variable which allows it to make interventions into the engine management.

Together with the two main control blocks, the “Control Algorithm” system also has a sub-system for calculation of the nominal yaw velocity required on the basis of the driver’s requirements, two switches and again a number of displays for visualisation of the output variable. The two switches make it possible to activate or deactivate the two controls individually. This results in the possibility of using the vehicle with or without the control algorithms in question. The calculation of a nominal yaw velocity is necessary for the yaw velocity control, to which detailed attention will be paid in the following sub-point.

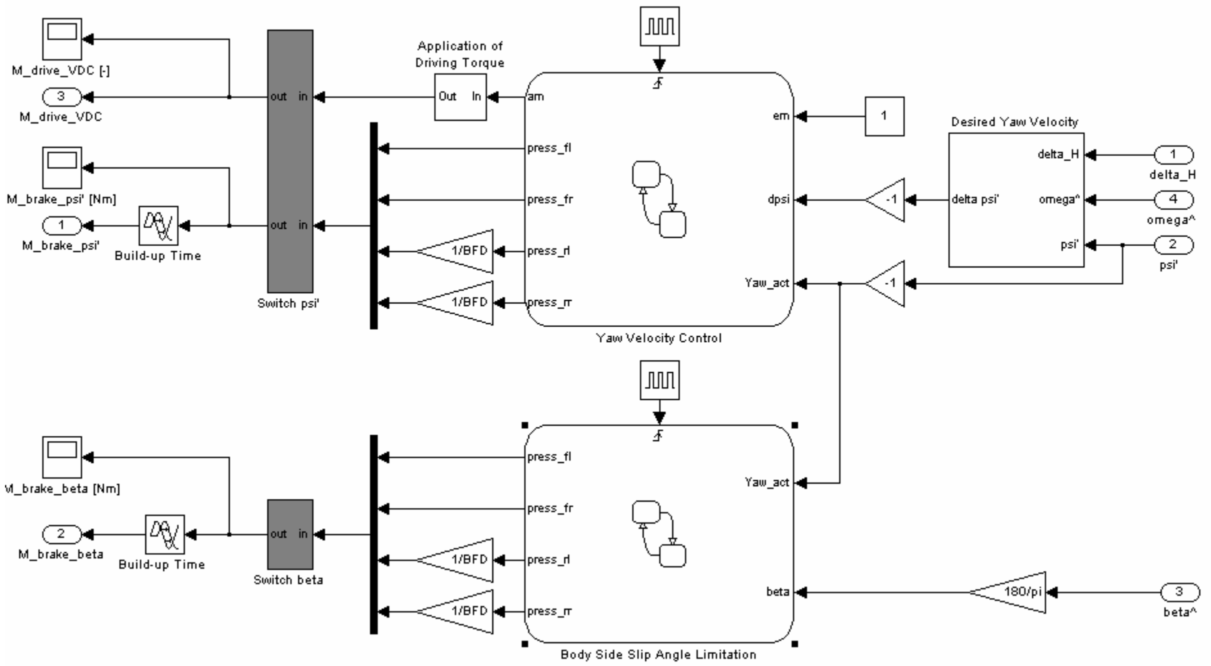

Fig. 4-37: Set-up of the control algorithm

i) Yaw velocity control

The yaw velocity control compares the current yaw velocity of the vehicle with a calculated nominal yaw velocity resulting from the driver's requirements. If excessive deviations occur in this, the control recognises oversteering or understeering of the vehicle and starts a contrary brake reaction. The yaw velocity control comprises the "Desired yaw velocity" system, which generates the nominal yaw velocity and calculates the difference to the actual yaw velocity, and the "Yaw velocity control", which purposefully makes engine torque and brake interventions if certain thresholds are exceeded; these exist in Fig. 4-37. The precise mode of function of the two systems is explained below.

The set-up of the "Desired yaw velocity" sub-system is portrayed in Fig. 4-38. Using the two reference wheel speed and steering wheel angle input variables, the system determines the nominal yaw velocity. For this, the wheel speed is converted to a reference speed by multiplication with a dynamic wheel radius. The "Delay" sub-system converts the steering wheel angle into a steering angle by means of the steering step-up. In order to take the phase delay between the steering wheel angle provided by the driver and the yaw velocity reaction into account, it forwards the steering angle with a certain delay in time. This means that the measured vehicle yaw velocity and the calculated nominal yaw velocity are practically phase-identical. The filter used is an all-pass filter with an angular frequency of 20 Hz for the Mercedes Benz A Class and 23.25 Hz for the BMW330xi.

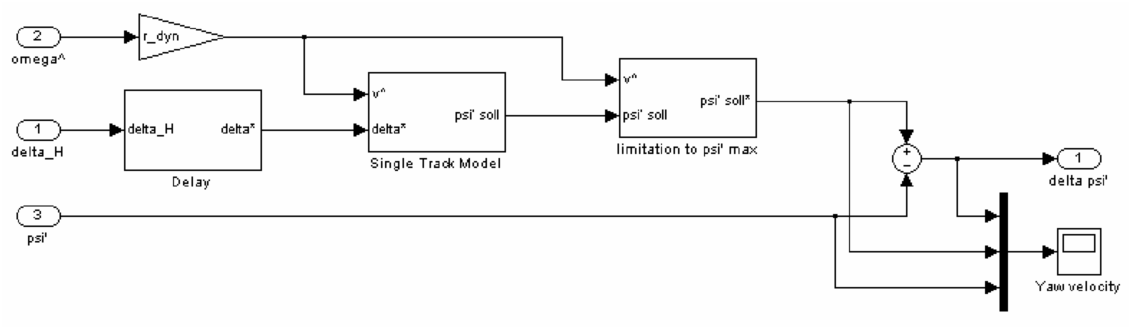

Fig. 4-38: Calculation of nominal yaw velocity and yaw velocity difference

The variables provided in this way, reference velocity v^ and steering angle delta*, are converted into the nominal yaw velocity in the “bicycle model“ sub-system from Fig. 4-38. In this, the system uses Eq. 4-12, which is derived from a bicycle vehicle model (cf. Eq. 2-2).

$$\dot{\psi}_{nominal} = \delta_{wheel} \cdot \frac{v}{l \cdot \left(1 + \frac{v^2}{v_{char}^2}\right)} \qquad \text{Eq. 4-12}$$

The characteristic velocity v_{char} occurring in the equation is a constant vehicle variable which can be determined experimentally in tests. The nominal yaw velocity now determined can be above the maximum possible yaw velocity limited by the coefficient of friction of the road surface. The maximum yaw velocity results from Eq. 4-13 as follows:

$$\dot{\psi}_{max} = \frac{g \cdot \mu}{v} \qquad \text{Eq. 4-13}$$

If the calculated nominal yaw velocity is above the maximum figure stated in Eq. 4-13, it is limited to the highest possible figure by the “Limitation to psi’ max.” sub-system, with μ = 1 always being presupposed, as the coefficient of friction is not estimated in the model when set up.

Fig. 4-39 shows how the hand steering angle in a double lane change at 60 km/h is firstly delayed as a function of the frequency (yellow line, left picture) and the nominal yaw velocity calculated from it then limited to the maximum figure (yellow line, right picture).

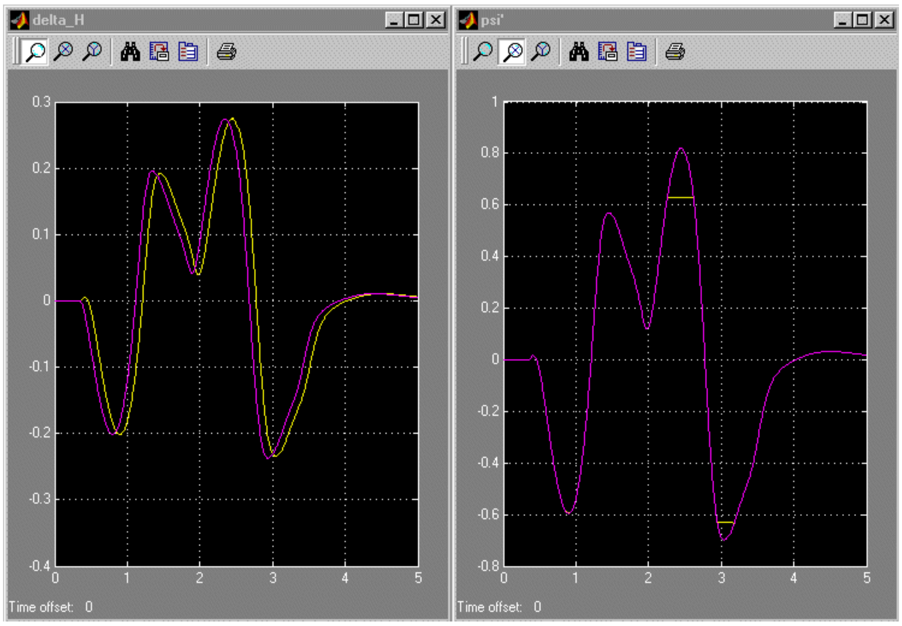

Fig. 4-39: Nominal yaw velocity calculation

The third input variable, the measured vehicle yaw velocity, is now subtracted from the nominal yaw velocity available, in order to obtain the “delta yaw” output variable of the sub-system. This yaw velocity difference is used as an input variable in the following “yaw velocity control“.

The “yaw velocity control“ sub-system is implemented as a state flow object. A state flow object defines various states which result in distinct reactions via various threshold values on the basis of its input variables. As the vehicle dynamics controller of the Mercedes Benz A Class and the BMW 330xi are designed differently, the state flow diagrams of the yaw velocity controls in question have an identical basic scheme, but also distinct differences. As the thresholds stored also differ from one another, the state flow diagrams of the individual test vehicles are described separately.

- **Mercedes-Benz A-Klasse**

The state flow diagram for the Mercedes-Benz A Class is shown in Fig. 4-40. The actual yaw velocity, the yaw velocity difference and a factor for the engine torque are used as input variables. The actual engine torque is not required within the state flow object, as it is merely to be between the engine torque provided by the driver and one quarter of this engine torque. A further input variable is the pulse generator. It provides the state flow object with the detection rate of the control, which has been selected at 25 Hz. In this way, the detection rate corresponds with that of real systems.

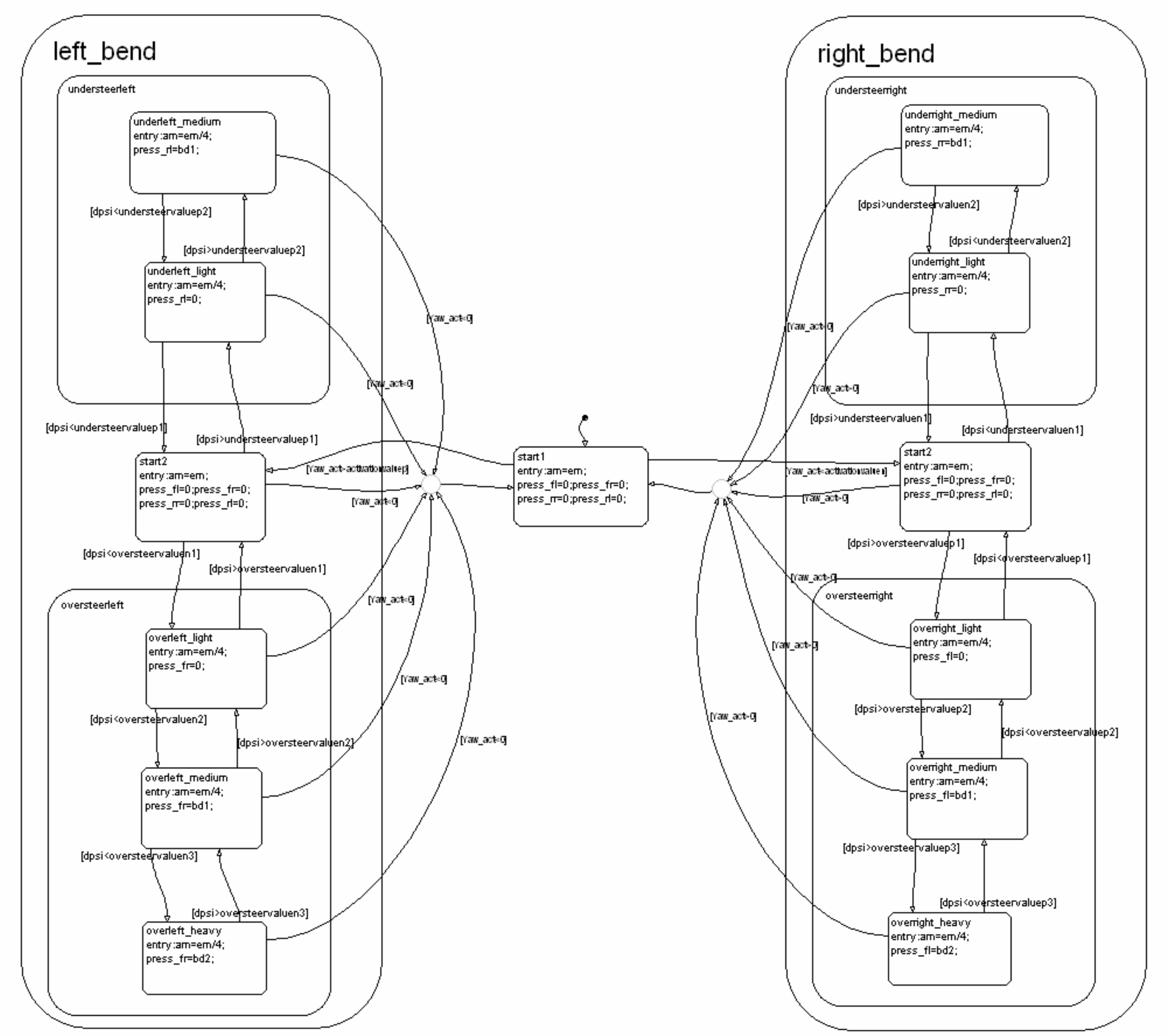

Fig. 4-40: Stateflow diagram of the MB A-Class yaw velocity control

Each of the small blocks in Fig. 4-40 represents a certain state. The block in the centre of the overall arrangement represents the starting condition, in which there is no taking of bends and thus no interventions in engine management or the brake system. If the actual yaw velocity exceeds the “activation figure”, a left or right bend is recognised depending on the sign in front of the yaw velocity. All the threshold figures of the state flow diagram for taking a left or right bend, as the case may be, such as the “activation figure”, are equally high as regards their amount. They merely differ by the sign in front of them, which the result that they are designated with a p ending for positive and an n ending for negative figures (e.g. “Aktivierungswertp“ and “Aktivierungswertn“).

If the actual yaw velocity exceeds the “activation figure”, a condition for a transition to another state has been fulfilled. These transitions are shown on the state flow diagrams as arrows and their fulfilment criteria are added in square brackets. The transition arrows lead the current position over into another state if a fulfilment criterion exists. So if the yaw velocity exceeds the “Aktivierungswertp“, the initial state “start2“ of the left bend is activated. In this state, merely a left-hand bend is detected. Interventions with regard to the engine torque or brake pressures are not done. On the basis of this neutral left-hand bend, the possible cases of understeering and oversteering are to be explained below for the yaw velocity control.

If the vehicle shows understeering properties, the nominal yaw velocity is larger than the actual yaw velocity. If this difference becomes larger than the “Untersteuerwertp1“ threshold stated by the vehicle parameters, the system jumps into the “Unterlinks_leicht“ state. In this state, there is no brake intervention, but the engine torque is reduced to ¼ of the engine torque available at the driver’s request. If the yaw velocity difference drops below “Untersteuerwertp1“, the system returns to the original state of the left-hand bend. The engine torque is not increased to its originally value immediately, as an “Application of the drive torque” sub-system in Fig. 4-37 only permits this if no reduction of the engine torque is recognised for at least 2 s. This limitation is to prevent, for example, a recognition of no bends between the steering stops and thus a high engine torque becoming effective, which would ensure unstable vehicle properties, in quick swerves with a steering to the left and then quickly to the right. If the “Application of the drive torque” system allows the entire engine torque again, the factor does not leap to 1, but is increased to 1 at a suitable speed by a filter with an angular frequency of 5 Hz.

If the yaw velocity difference increases again, with the result that the next threshold “Untersteuerwertp2“ is exceeded, the system leaps from block “Unterlinks_leicht“ to the block “Unterlinks_mittel“. In this case, the engine torque is still kept at ¼ of the input variable, but a brake reaction is now also initiated. As the vehicle is in a left-hand bend, the left-hand rear wheel is braked, in order to generate a torque around the vertical axis of the vehicle which ensures turning into the bend. For this, the „Unterlinks_mittel“ state applies the brake pressure “bd1” defined in the vehicle parameters on the left-hand rear wheel of the vehicle, leading to a corresponding brake power after the reduction by the brake proportioning. As there is no hydraulic stepping-up provided either in the control model or within the vehicle model, the controlled variable “bd1” is not actually a hydraulic brake pressure, but a brake torque which becomes active on the wheel. In order to cope with the transmission behaviour between brake pressure and brake power in a real vehicle, the “build-up time” block in Fig. 4-37 ensures a dead time of the brake system (see above).

The “Unterlinks_mittel“ state is the strongest control reply to an understeering behaviour of the vehicle, with the result that brake pressure “bd1“ is maintained on the rear left-hand wheel of the vehicle until a condition resulting in a change to a different state is reached. On the one hand, such a condition is fulfilled if the yaw velocity difference drops below the threshold figure “Untersteuerwertp2“. In this case, the system changes back into the “Unterlinks_leicht“ state in which it had been before. This corresponds to a sequential switching between the individual states. On the other hand, there is the possibility for each state block to jump directly back into the “start1” neutral starting position within the state flow diagram. The condition resulting in this is a reversal of the sign in front of the yaw angle velocity, i.e. a change from a left-hand bend to a right-hand bend. This condition becomes necessary because there can be a slight phase delay between the estimated nominal yaw velocity and the actual yaw velocity, despite all-pass filtering of the steering angle. In this way, a yaw velocity difference above a threshold can remain, although the vehicle is turning in the opposite direction in the meantime. Without the additional possibility of changing, this would mean that no alteration of state is recognised and a brake pressure is maintained. As this is not desired, there is an automatic switch to the “start1” neutral starting state in a change of bend.

The function of the control in the event of an oversteering reaction of the vehicle is principally very similar to that of understeering. The starting state is formed by the neutral position in a left-hand bend, which is recognised on the basis of the yaw angle velocity. If the vehicle starts to oversteer, the actual yaw velocity is above the nominal yaw velocity. This again results in a yaw velocity difference, which has an opposite sign to that of the difference for understeering in the vehicle, i.e. a negative sign for a left-hand bend. If the yaw velocity difference drops so far that it falls below the “Uebersteuerwertn1“ threshold, the “Ueberlinks_leicht“ state become active. In this state, the engine torque is reduced, as in slight understeering, but no brake intervention done. When the next highest threshold value “Uebersteuerwertn2“ is exceeded, the system changes to the “Ueberlinks_mittel“ state, in which there is no change in the reduced engine torque, but a brake reaction is also provided. As the vehicle oversteers in a left-hand bend, i.e. turns too strongly into the curve, the brake pressure “bd1” is applied to the right-hand front wheel and generates a brake power resulting in an effect stabilising the vehicle without a reduction by the brake proportioning, albeit with a delay in time as a result of the threshold duration. Unlike the understeering control, there is a further “Ueberlinks_stark“ state for an oversteering vehicle property, which comes into effect when the threshold figure “Uebersteuerwertn3“ is exceeded. Again, the engine torque is maintained without a change, whereas the brake pressure of the front right-hand wheel is increased to “bd2”. This is the highest possible brake pressure which the yaw velocity control can apply. As is also the case for understeering, the previous state is activated in the event of the amount of the yaw velocity difference dropping below a threshold value, by which the initiated reactions are withdrawn step by step.

The yaw velocity control during a right-hand bend functions exactly the same as for a left-hand bend, but with different signs in front. All the positive thresholds of the control for the Mercedes Benz A Class are listed below:

bd1	= 762500 Nmm
bd2	= 1525000 Nmm
build-up time	= 0,15s
v_char	= 14,5 m/s
Aktivierungswertp	= 0,05
Uebersteuerwertp1	= 0,07
Uebersteuerwertp2	= 0,19
Uebersteuerwertp3	= 0,28
Untersteuerwertp1	= 0,07
Untersteuerwertp2	= 0,10

- **BMW 330iX**

The yaw velocity control for the BMW 330xi not only has different brake power levels, threshold and activation figures, but also a different set-up compared with the Mercedes Benz A Class, Fig. 4-41.

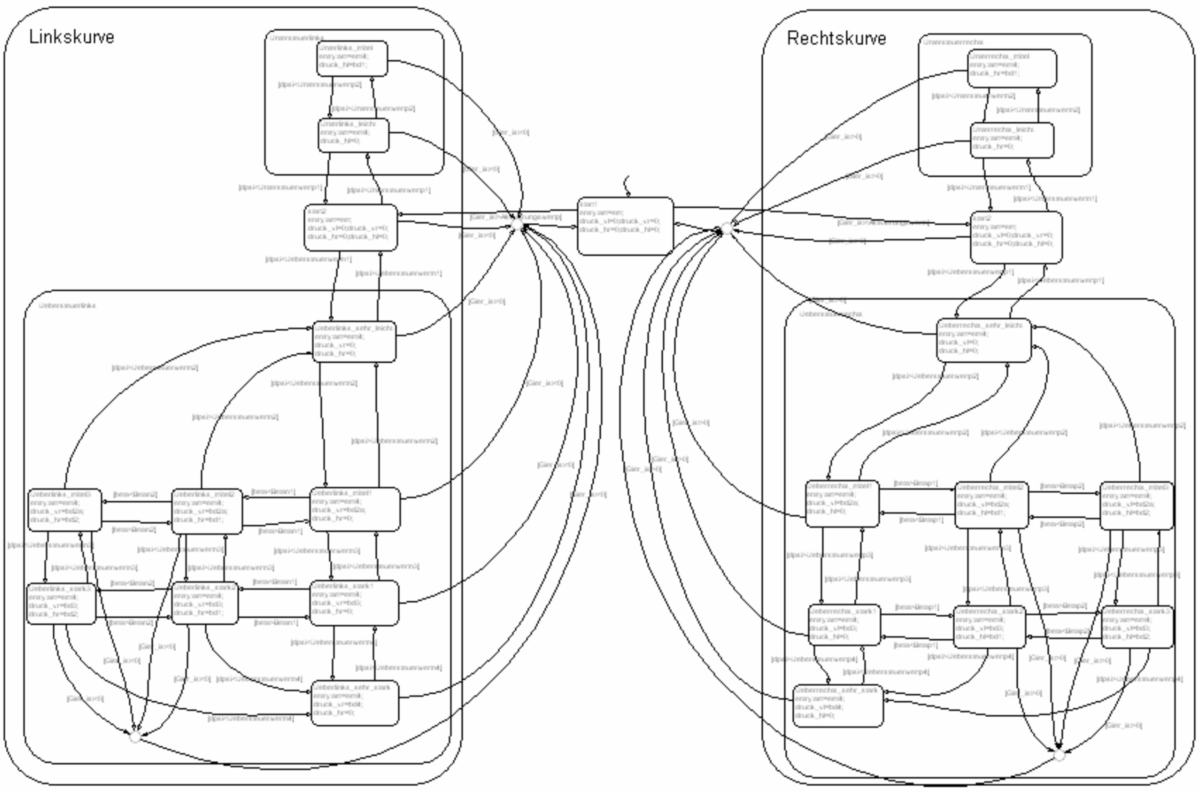

Fig. 4-41: Stateflow diagram of the BMW 330xi yaw velocity

The principal set-up of the state flow diagram is similar to that of the A Class. With a neutral starting state, “start1“, a left or right-hand bend is recognised on the basis of the yaw velocity when the “activation figure” is exceeded. If the yaw velocity difference exceeds threshold figures, which are called “Untersteuerwertp1“, “Uebersteuerwertp1“, etc., as for the A Class, the state changes to “Unterlinks_leicht“ or “Ueberlinks_leicht“. These two states, just like the entire understeering control, are identical to those of the Mercedes. There are two principal differences between the BMW and the Mercedes:

Unlike the A Class, three, and not two different levels of brake power are applied to the front axle in the BMW 330xi during an oversteering of the vehicle. This is accounted for by the state flow diagram being extended in the vertical by a further state, “Ueberlinks_sehr_stark“, which comes into effect if the threshold figure “Uebersteuerwertn4“ is exceeded. This state generates a further, increased brake torque on the front wheels.

The second difference is that brake power can be built up additionally on the rear wheels if the vehicle oversteers as a function of the size of the sideslip angle. As two different brake power levels exist on the rear axle, this results in two new threshold figures “Betap1“ and “Betap2“ as well the matching negative thresholds. In order to activate these two brake power levels, the state flow diagram for the “Ueberlinks_mittel1“ and “Ueberlinks_stark1“ states extends further in the horizontal, with the result that brake torques become active on the corresponding rear wheel with the same brake torque on the front axle if the beta threshold figures are exceeded, Fig. 4-41.

In the event of a yaw velocity difference being exceeded or fallen below without an alteration of the sideslip angle, the state can be changed, keeping the brake power on the rear axle, by which there is only a change of brake torque on the front axle. For a change of bends, it is possible to change into the “start1” neutral starting state in any state for the reasons described above.

As in the control for the Mercedes Benz A Class, the arrangement of the right-hand bend is identical with the left-hand bend. To close, all the parameters necessary for the yaw velocity control of the BMW are listed:

bd1	= 600000 Nmm
bd2a	= 900000 Nmm
bd2	= 1200000 Nmm
bd3	= 1800000 Nmm
bd4	= 2400000 Nmm
build-up time	= 0,05s
v_char	= 16,67 m/s
Aktivierungswertp	= 0,05

Uebersteuerwertp1	= 0,07
Uebersteuerwertp2	= 0,098
Uebersteuerwertp3	= 0,115
Uebersteuerwertp4	= 0,15
Untersteuerwertp1	= 0,07
Untersteuerwertp2	= 0,10
Betap1	= 1,8
Betap2	= 2,4

i) Sideslip angle limitation

Alongside the yaw velocity control, the control algorithm also contains a sideslip angle limitation, which becomes active if excessively large sideslip angles result from the yaw velocity control. This particularly becomes necessary on smooth road surfaces, as the yaw velocity control can result in lateral traction of the automobile due to its efforts to turn the vehicle into the bend, e.g. in understeering, see Chap. 2.1.1. As such driving states are not reasonable for the passengers, their occurrence is recognised in the form of an excessive sideslip angle and avoided by the sideslip angle limitation. The set-up of the sideslip angle limitation, which is identical for both test vehicles used with the exception of the vehicle parameters, is shown in Fig. 4-42. It is again a state flow diagram with the actual yaw velocity, detection rate and the calculated vehicle sideslip angle input variables. The function of the sideslip angle limitation is described below.

Like the yaw velocity control, the sideslip angle control has a neutral starting state, “start1“, in which no bend is recognised. The transition into a left or right-hand bend, initiated by exceeding of the joint yaw velocity threshold “Activation figure”, is also identical. With the transition into a bend, the neutral state “start2” of a bend is activated, in which no kind of intervention is done. Like the yaw velocity regulation, the example of a left-hand bend is to be used to described the attitude angle control below.

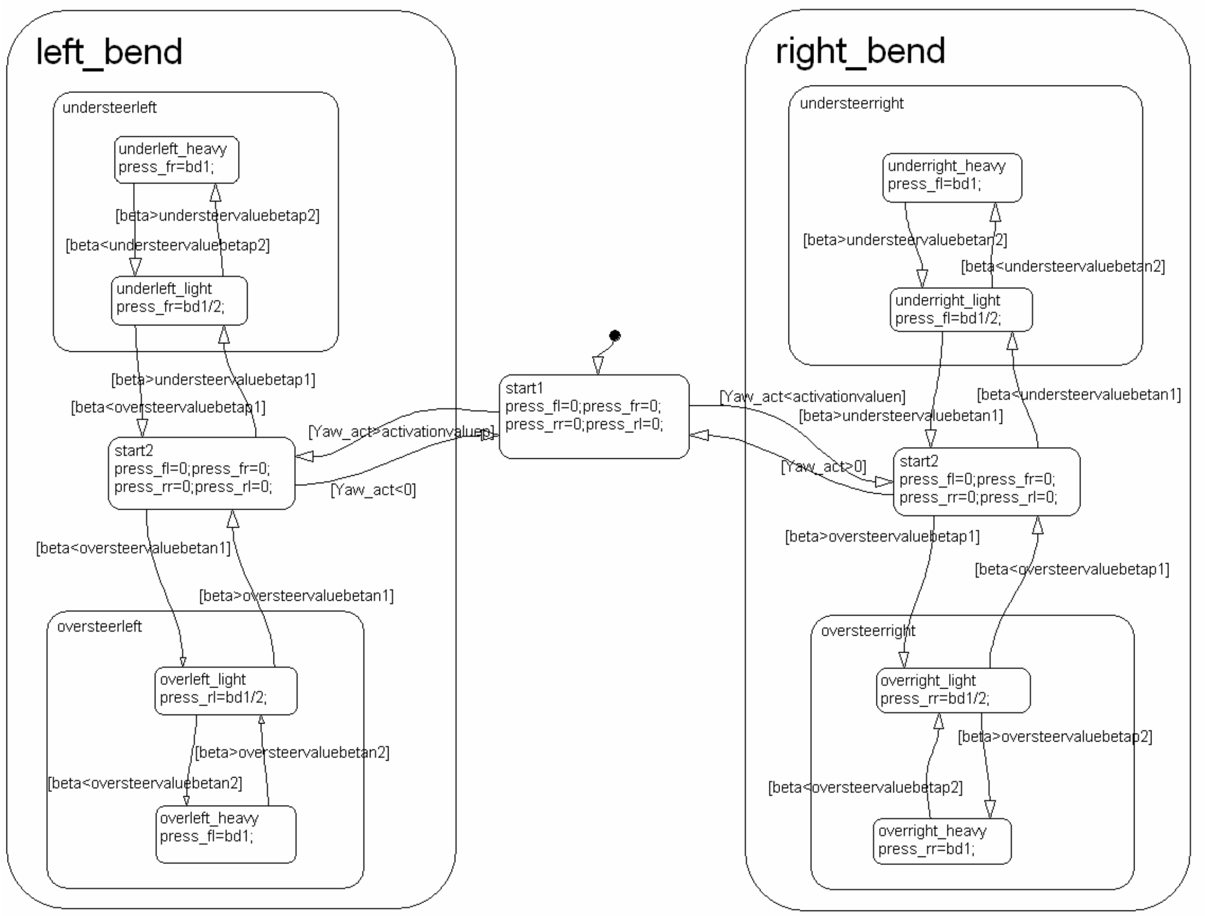

Fig. 4-42: Stateflow diagram of the side slip angle limitation

If, in a left-hand bend, the vehicle shows understeering, the yaw velocity control brakes the left-hand side of the vehicle, in order to generate a turn into the bend. On low coefficients of friction of the surface, e.g. black ice, this can lead to a strong turning of the vehicle and thus a very high sideslip angle without the vehicle reaching the required nominal yaw velocity, as the latter is above the maximum possible yaw velocity. In order to avoid this undesired driving state, the sideslip angle limitation counteracts it by opposing brake interventions. If the threshold figure “Untersteuerwertbetap1“ is exceeded, the “Unterlinks_leicht“ state is activated and the right-hand front wheel is given the brake power “bd1“. In this way, the vehicle is steered back against the original direction of rotation. If the sideslip angle occurring is larger than the threshold figure “Untersteuerwertbetap2“, the state flow diagram changes into the “Unterlinks_stark“ state and increases the brake pressure on the front right-hand wheel to “bd1“.

The brake interventions initiated and the reduction of the sideslip angle connected with them result in a reversal of the current yaw velocity. For the yaw velocity control, this state results in recognition of a change of bend, which is why a transition from any control state to the “start1” neutral starting state, Fig. 4-40 and Fig. 4-41, is provided for in the control. Within the sideslip angle limitation, the reversal of the yaw velocity is however an intended reaction, in order to reduce the sideslip angle. This is why the transitions to the neutral state “start1“ known from the yaw velocity control are not contained in the state flow diagram of the attitude angle control. In this way, the brake pressure “bd1“ or “bd1“/2 is maintained until the threshold figures in question, “Untersteuerwertbetap1“ and “Untersteuerwertbetap2“ have been fallen below and the state “start2“ of the neutral left-hand bend has occurred. On the basis of this state, there is a change to the starting state “start 1” at a yaw velocity which is lower than the “Aktivierungswertp“.

The function of the sideslip angle limitation in oversteering vehicles is similar to that of understeering. On the basis of the brake intervention initiated in oversteering by the yaw velocity control, the sideslip angle can increase greatly on smooth road surfaces. The sign in front of the sideslip angle is opposite to that in understeering, with the result that the first threshold figure is designated as “Uebersteuerwertbetan1“. If this threshold figure is fallen short of, the “Ueberlinks_leicht“ state is active. In this case too, half the brake pressure “bd1“ is applied, albeit to the left-hand rear wheel. If the attitude angle drops so far that it falls below the threshold figure “Uebersteuerwertbetan2“, the brake pressure is increased to “bd1“. As it is a rear wheel in the brake intervention, the brake pressure is subsequently reduced accordingly by the brake proportioning. As a result of the brake interventions, the amount of the sideslip angle is reduced until the sideslip angle limitation has returned to the neutral bend state “start2“.

The set-up of the sideslip angle limitation for taking a right-hand bend is exactly the same way as for the yaw velocity control, as a mirror-image of the left-hand bend. This means that the signs in front of the threshold figures are inverted and the opposite side of the vehicle is braked. The amount of the threshold figures and the size of the brake torques applied are identical with those of the left-hand bend control.

Just as in the yaw velocity control, a realistic build-up of brake power is achieved with the sideslip angle control by means of a time delay in the form of a threshold duration. The threshold duration corresponds to that of the yaw velocity control. To close, all the vehicle parameters affecting the sideslip angle limitation for both test vehicles are listed:

Uebersteuerwertbetap1 = 10°

Uebersteuerwertbetap2 = 12°

Untersteuerwertbetap1 = 10°

Untersteuerwertbetap2 = 12°

4.2.2.3 Control strategy

Since the vehicle reaction resulting from control of the yaw velocity and limitation of the angle of deviation are directly opposed, it makes no sense to activate both regulation algorithms at the same time. When responses to both types of control are present, the control algorithms must be deliberately switched on and off, in order to obtain the desired road performance. This function is assumed by the "control strategy" subsystem from Fig. 4-30. The creation of this subsystem is identical for both test vehicles, Fig. 4-43.

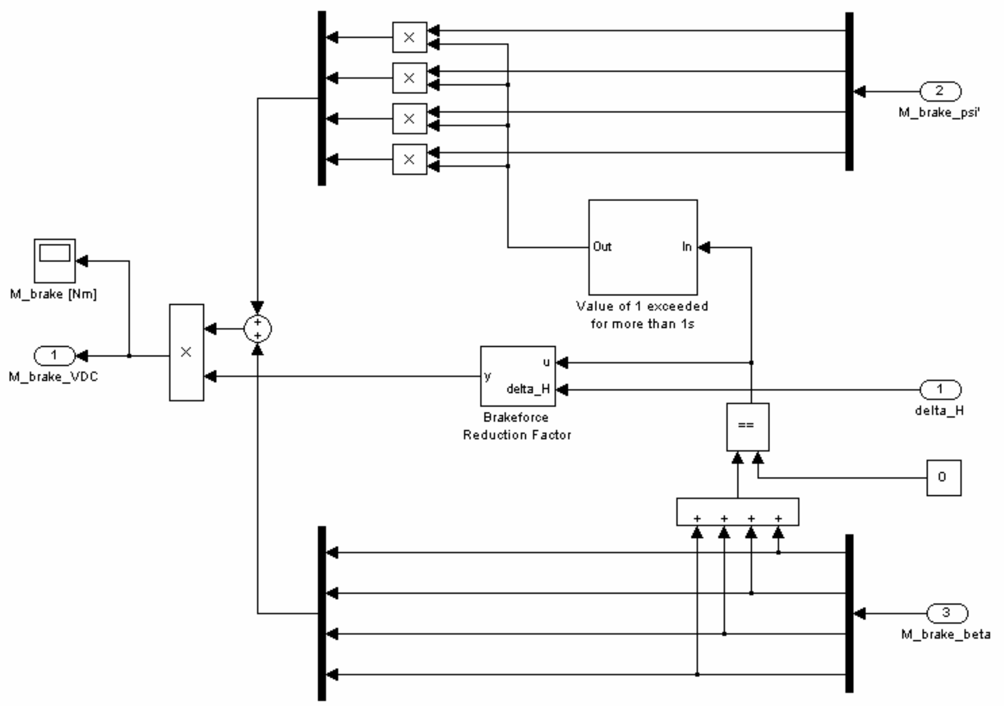

Fig. 4-43: Structure of the control strategy

System input is provided by the yaw velocity control and slip angle - each working independently - together with the steering wheel angle. The control strategy normally transfers to the subsequent systems the braking torque that is generated by limiting the yaw velocity. As soon as the slip angle limitation exerts a braking force, however, the braking momentum of the yaw velocity regulation is disregarded, and the braking actions generated by the slip angle regulation are transferred unchanged to the output "M_brake_VDC". In practical terms, this procedure corresponds to switching from yaw velocity regulation to slip angle limitation. The yaw velocity regulation is restored only when the slip angle limitation stops creating braking torque for more than 1s.

Simply switching between yaw velocity regulation and slip angle limitation would result in continuously alternating braking interventions by the two controls when cornering on a slippery road. This would then cause a yawing oscillation around the high axis. Since this situation is undesirable, a mechanism is incorporated in the 'control strategy' to prevent this.

A multiplier is applied to the control strategy braking moments prior to output. At first this factor has the value of 1, so that all braking moment outputs remain unchanged. After the first braking interventions from the slip angle limitation, this factor is reduced from 1 to 0.6, when the yaw velocity regulation is reactivated. All braking momentum generated from then on is multiplied by the reduced factor 0.6, thus reducing the response of the vehicle. If the reactions once again lead to a response from the slip angle limitation, then the braking momentum they generate also reduces these appropriately. When switching back again to yaw velocity regulation, the 0.6 factor is multiplied once more by 0.6, so that the reduction factor is now held at 0.36, which further reduces the influence of the driving dynamics control systems.

These procedures may be repeated a number of times, each time leading to a multiplication of the reduction factor by 0.6. By reducing the braking momentum, the vehicle is allowed to reach a stable driving state without the yaw velocity regulation having to be deactivated. Due to the frictional resistance of the road, this leads to a yaw velocity below the yaw rate desired by the driver. As soon as the driver returns the steering wheel to the straight-ahead position, the reduction factor is set back to 1, to permit reaction to the new driving situation with active braking unimpaired.

4.2.3 Actuators

The changes in braking and drive momentum cannot be transferred directly from the driving dynamics controller to the wheels of the vehicle. The high braking torque in particularly can cause a single wheel to lock up very easily. Since a locked wheel cannot transfer lateral forces, a driving dynamics controller without appropriate wheel slippage regulation would have a negative impact on the stability of the vehicle. The models shown below are based on [REI93].

4.2.3.1 Antilock braking system (ABS)

The **a**ntilock **b**raking **s**ystem (ABS) has the task of stopping the wheels from locking when the brakes are applied. The locking of a wheel (brake slippage λ_B=1) not only leads to a reduction of the available braking power relative to frictional conditions – leading to reduced braking – but, more importantly, to a considerable reduction in lateral forces. If excessive braking is applied to the front axle, steering control suffers; if the rear axle locks, there is an increased likelihood of skidding [WAL95]. In Fig. 4-44 the progress of the effective braking force F_B and the maximum permissible lateral force F_α via the ABS λ_B are plotted.

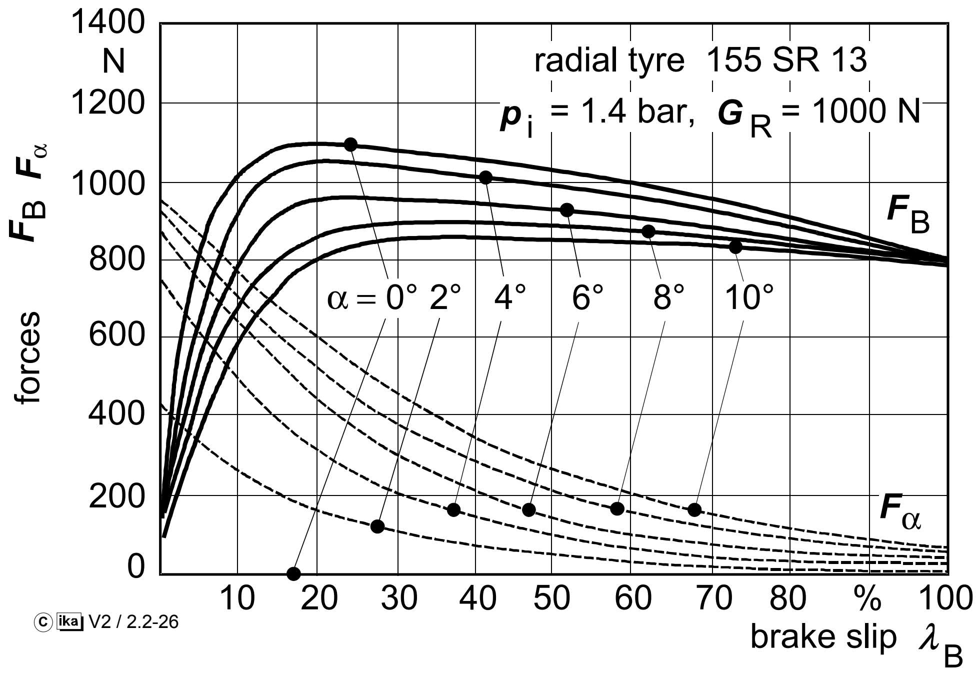

Fig. 4-44: Longitudinal and lateral force depending on brake slip λ_B [WAL96b]

The ABS regulates the braking pressure, limiting brake slippage to values between 10% and 30%, and so achieving high deceleration combined with good lateral force. The frictional coefficient between tyres and road surface, and thus the available braking force, depends on type of tyres, the slip angle, and also to a large degree on the nature of the road surface.

Since there are more or less distinctive friction resistance maxima at roughly the same braking slippage, this would be an ideal control variable for the ABS system. The slippage between road and tyre is not ascertainable directly, however. Other suitable control variables must be found.

Looking at the sum of the moments at a braked wheel produces the following equation:

$$M_B = \mu \cdot F_z \cdot r_{dyn} - \Theta_{red} \cdot \ddot{\varphi}_R \qquad \text{Eq. 4-14}$$

mit: M_B Braking momentum
μ Frictional resistance between tyre and road
F_Z Wheel load
r_{dyn} Dynamic wheel radius
Θ_{red} Reduced moment of inertia
$\ddot{\varphi}_R$ Angular acceleration of the wheel

From a specific threshold, a high braking momentum can no longer be $\mu \cdot F_z$ applied as peripheral power to the tyre contact area. Braking momentum therefore leads to deceleration at the wheel once maximum grip has been exceeded. As a result of the high sensitivity due to the different factor sizes $F_z \cdot r_{dyn}$ and Θ_{red}, high wheel decelerations can be induced, which are a suitable control variable for automatic anti-lock systems.

The ABS determines the wheel angle acceleration by differentiating between the signals provided by the revolution counters at the wheel. However, precise control of the deceleration process requires additional variables, since a slight wheel acceleration over a longer period can also lead to wheel locking.

"Relative slip" is frequently used as a second control variable. With the help of logical associations, a reference speed is derived from the speeds of several wheels, which approximates the ideal wheel speed for optimum grip at the time of observation. Comparison of the actual wheel speed with the reference speed provides the respective 'relative' slip sizes.

The operation of a control cycle is in principle the same for all automatic anti-lock devices controlled by wheel deceleration. Excessive braking pressure applied by the driver is compensated for setting wheel deceleration between an upper and lower limit. The methods for creating reliable adherence (as independent as possible of external disturbance variables) to the limits necessary for optimum braking vary by ABS system type.

Im folgenden soll der Ablauf eines Regelvorgangs einer ABS-Regelung betrachtet werden, die die Regelgrößen Raddrehzahlverzögerung und relativen Schlupf verwendet,

In the following, we shall examine the operation of a control procedure for an ABS system using the controlled variables of rotational wheel deceleration and relative slip, Fig. 4-45.

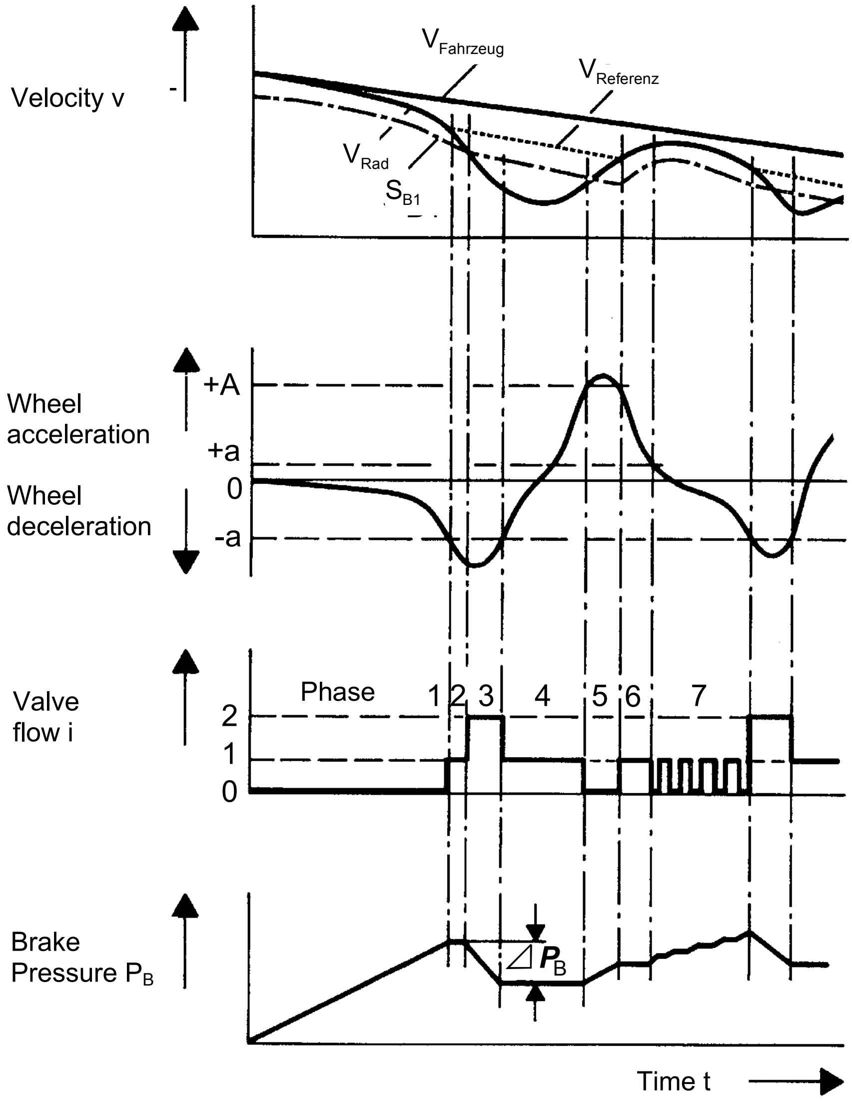

Fig. 4-45: Control process of an ABS-control (Bosch)

Due to an increase in the braking pressure by the driver, the wheel's peripheral speed slows more quickly than the vehicle's speed. If the wheel deceleration is below that required to reach the characteristic "-a" threshold of maximum grip, braking pressure is maintained at the current value. If wheel speed is below the slip-switching threshold s_{B1}, braking pressure is reduced until the "-a" threshold is reached again. If rotational wheel acceleration in this phase of constant braking pressure exceeds the upper acceleration limit "+A", the braking pressure is increased once again. Between the "+A" and "+a" acceleration signal, braking pressure is held, then slowly increased until the "-a" wheel deceleration is reached again. Here, a new control cycle begins, initiated this time, however, by a reduction in pressure.

Even when braking is done carefully, the wheel can lock due to a slow build up of pressure in the wheel brake cylinder, or due to large moments of inertia and small adhesion coefficients - without reaching the deceleration threshold value "-a". Relative slip is therefore added as a second control variable. Reaching a specific slip value then induces a reduction in braking pressure.

On the basis of the characteristics of an ABS controller described above, a realistic, mathematical ABS model was developed and constructed for the simulations in this paper in MATLAB/SIMULINK as well as the special MATLAB application, SIMULINK/Stateflow.

The simulated ABS controller works on the principle of single wheel regulation (individual regulation), i.e., maximum possible adhesion is gained for each, individual wheel, providing maximum possible retardation of the vehicle. Each individual wheel must consequently be fitted with a sensor for the control variable (wheel velocity) and its own brake pressure circuit. The brake pressure is therefore controlled separately, independent of the behaviour of the other wheels.

Processing of the input parameters, braking momentum (M_brake), reference the reference wheel angle speed (omega^), and the wheel speed of the individual wheels (omega) can be seen in Fig. 4-46. The output variable is the regulated braking momentum for each, individual wheel (M_brake_ABS).

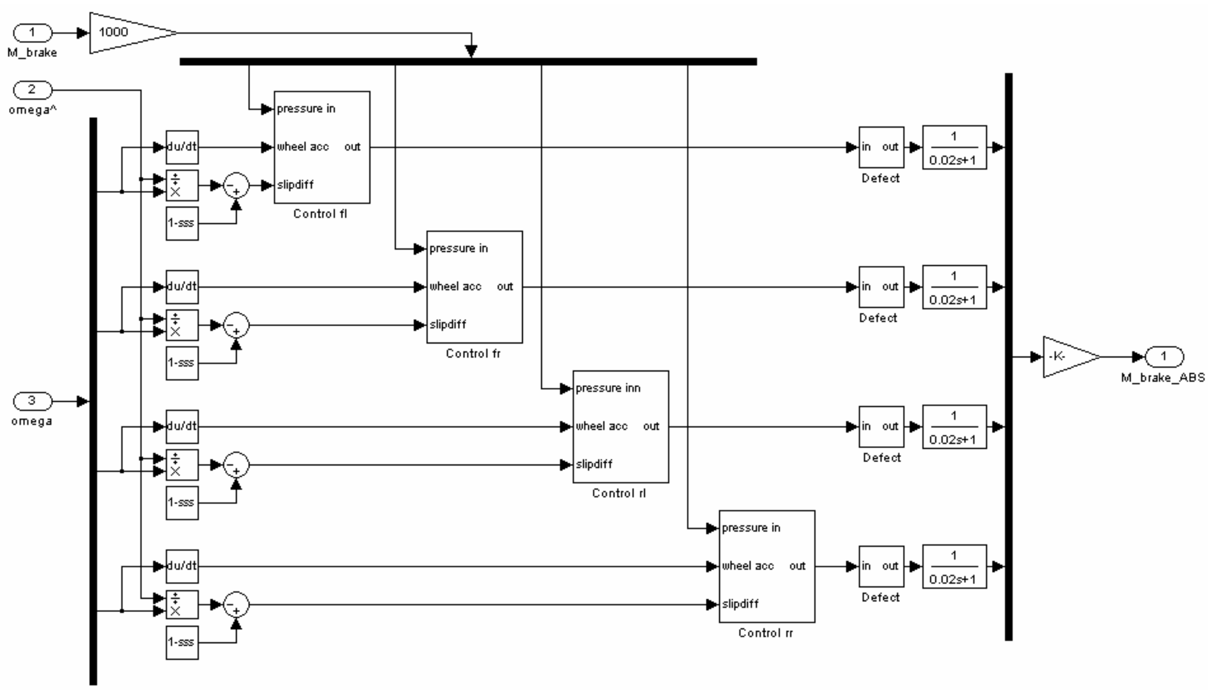

Fig. 4-46: Structure of the ABS-block

First, the input vectors of the wheel speeds and the braking pressures are split up again. With the aid of the reference rotational speed, the values for relative slip λ_B are calculated for each wheel.

$$\lambda_B = 1 - \frac{\omega_r}{\omega_{ref}} \qquad \text{Eq. 4-15}$$

To make it possible to recognise when a specific predetermined slip has been exceeded (slip-switching threshold "sss" is stored in the vehicle parameters) the difference between the slip-switching threshold and relative slip is calculated. In addition, wheel accelerations are calculated via differentiation links.

The three parameters, wheel acceleration (wheel acc), desired braking pressure (pressure in) and difference between relative slip and slip-switching threshold (slip diff) are then used as inputs for four subsystems. Output from these subsystems is the respective braking momentum, which is delayed by PT_1 links with a cut-off frequency of 50 Hz, in order to smooth out the abrupt build-up and release of pressure. For later simulations only the "error actuation" block is connected (Fig. 4-47). From here it is possible to simulate the failure of a valve to open or a delay in pressure generation by a sticking valve.

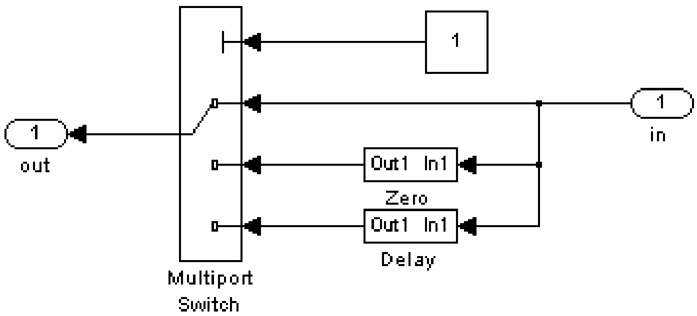

Fig. 4-47: Defect application

The structure of the "Control vl" subsystem is shown in Fig. 4-48. The Stateflow block "controller" is the central control unit. As well as the three input variable already mentioned, the derivation of the wheel acceleration (radbeschlp) and seven other events (events) are calculated. These can trigger different actions in the Stateflow model, or transitions from one state to another, such as exceeding or falling short of the wheel acceleration switching thresholds already described above "+A", "+a" and "-a". As zero points have to be defined In order to create events in Stateflow, is it necessary to calculate the respective differences between the switching thresholds and the wheel acceleration. Moreover, a trigger signal is generated (pulse generator) to make available an event that occurs regularly after a specified, fixed time-step. The trigger signal specifies the working frequency of the ABS controller, which is 25 Hz. If the braking pressure must now be reduced at a particular wheel, then this happens every 0.04 seconds at a constant, predefined pressure difference.

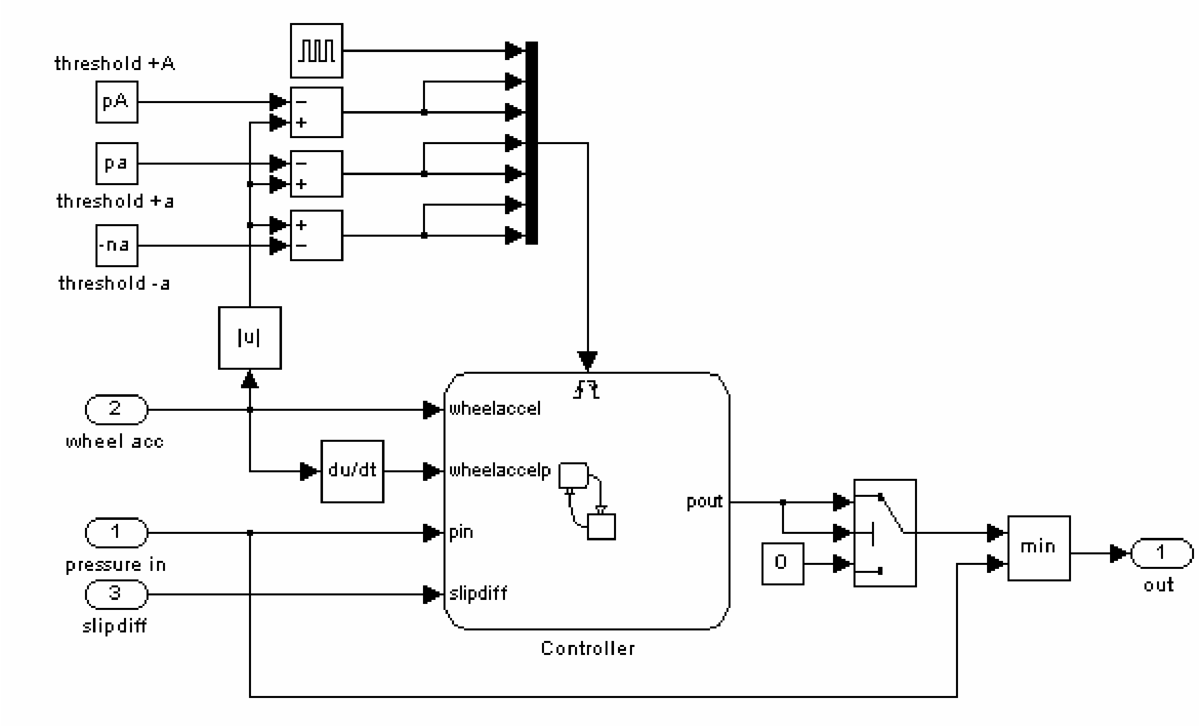

Fig. 4-48: ABS subsystem “Control front left”

Since this braking pressure is adjusted by lowering or increasing fixed braking pressure values, negative braking pressures or braking pressures larger than the input pressures may be temporarily transmitted by the Stateflow block. A switch prevents the transmission of negative pressures, so that these are not passed on to the wheel.

How the Stateflow model then uses the input information to calculate a modified output braking pressure into relation to the predefined input braking pressure in order to avoid locking the wheels, is illustrated by Fig. 4-49.

At the beginning of the regulation process, the 'start' state is active. The output pressure is set to 0 here. The introduction of a braking intervention (requirement: [pin>0]) causes the transition to the 'braking' state. As long as this state is activated, the output variable "pressure" follows the braking pressure "pin" (during: pout=pin) required by the driver/driving dynamics controller. The ABS controller is therefore not active. If the adhesion of tyre to road is exceeded by too high a brake pressure setting, the anti-lock braking system cuts in. This can happen in two different ways. On the one hand, it is possible for wheel acceleration to exceed the maximum permissible threshold value of "-a". The control is then activated by the wheel acceleration (state: wheel acceleration) by a transition ([radbeschl < na & pin > 1]) pointing directly to the substate "state5" where the braking pressure is reduced (during: pout-=PBnn).

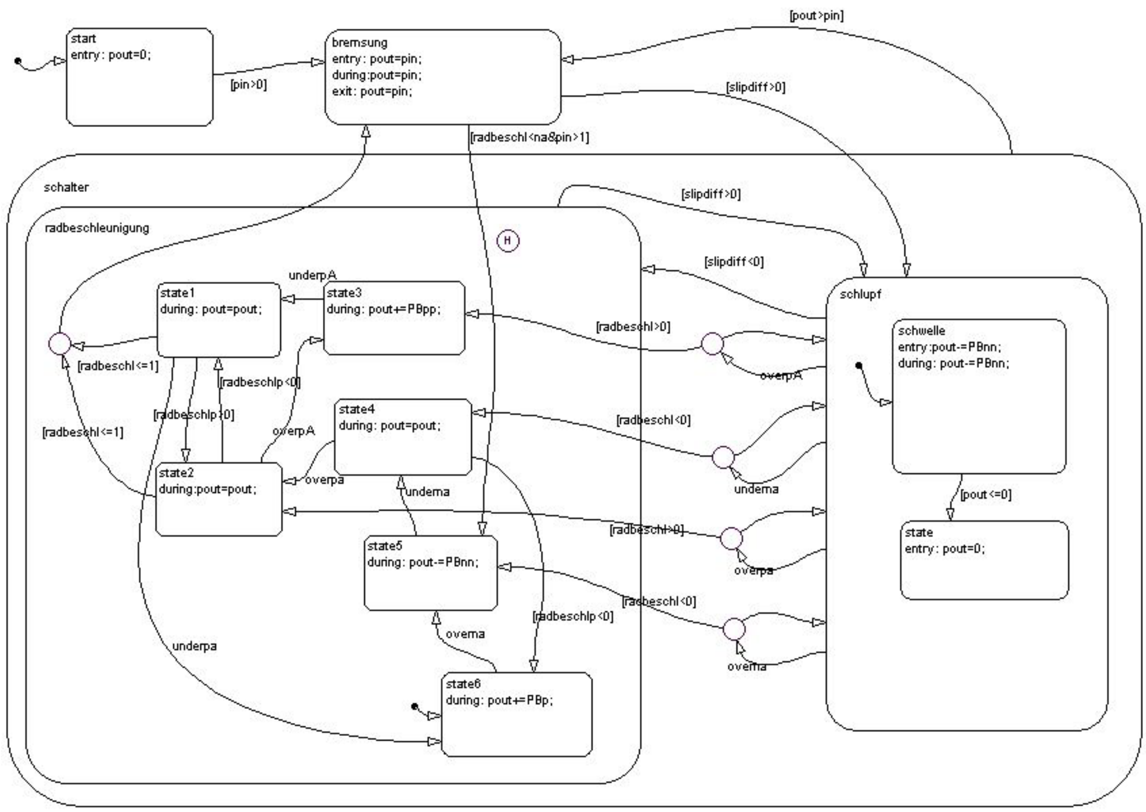

Fig. 4-49: Stateflow model of the ABS controller

On the other hand, the relative slip of a wheel may exceed a specific, predefined slip threshold ([slpidoff > 0]) thus activating the slip control (condition: slip). This control involves reducing the braking pressure in the sub-state "threshold" (during: pout-=PBnn).

Pressure is reduced by the command "pressure = PBnn“. Here, PBnn is the predefined pressure difference by which the braking pressure is reduced once only during the 'entry' action or at every triggering during the 'during' action. The commands for slow (pressure+ = PBp) and fast pressure increase (pressure+= PBpp) work in the same way. These pressure differences are stored in the vehicle parameters.

The following is a brief explanation of control via wheel acceleration in a control cycle. The wheel acceleration control is activated by state5 when the maximum wheel deceleration "a" is exceeded, i.e. via condition [wheel acc < na & pin > 1]. When entering state5, the braking pressure is reduced by PBnn and, as long as this state is active, it continues to be reduced to slow down wheel deceleration. When wheel deceleration subsequently falls below "-a" and the related "underna" events begin, the activity is transferred to state4, in which the pressure is held. There are now two further paths. Modification of the wheel acceleration changes its indicator ([wheel acc < 0]) and state6 is entered, whereupon braking pressure is slowly increased slowly (: pout+ = PBp). Or the wheel acceleration increases further and exceeds the threshold value for "+a" (event "overpa"), which activates state2.

In state2 the braking pressure remains constant (during: pout=pout) and the wheel acceleration assumes values between "+a" and "+A". If the wheel acceleration should suddenly fall again here e.g. due to modification of the friction conditions between the road and tyre, the indicator ([wheel acc < 0]) changes and a transition leads to state1. If, however, wheel acceleration further increases, it will exceed the threshold value "+A" (event "overpA") and the braking pressure will quickly be increased in state3. As a result of the activation of state1, wheel acceleration will quickly drop below "+A" (event "underpA"). Here, the pressure is held. Wheel acceleration lies between "+A“ and "+a“ and falls.

Once again there are two paths from state1. If wheel acceleration increases again (wheel acc >0), this leads back to state2. If wheel acceleration falls further, it falls below the threshold value "+a" (event "underpa") and the pressure is slowly increased by the activation of state6 (during: pout+=PBp). Wheel acceleration/ deceleration is located between "+a" and "-a". If deceleration increases further, the threshold value "-a" is exceeded (event "overna"), whereupon the wheel acceleration control cycle in state5 closes.

A transition in the control of slip can take place at every time, if the wheel slip exceeds the slip-switching threshold. Here, the transition linked to the condition "[slipdiff > 0]" is executed and the "slip" state is activated. Wheel acceleration control is resumed if one of the events "overpa", "underpa" or "overna" occurs, whereby the correct wheel acceleration indicator must still be checked or, if the slippage has once again fallen below the slip threshold value ([slipdiff < 0]). During the event-controlled transition from slip control to wheel acceleration control, the substates matching the event are selected directly. If a movement below the slip-switching threshold initiates the transition, only the upper state "wheel acceleration" is activated. For this reason, a history junction must be activated in addition to the sub-state which last was active, in order to obtain the control rhythm.

The upper state "switch" is responsible, with the aid of the condition "[pout > pin]" for switching off ABS control when the desired braking pressure is reached. Then the Stateflow model is put on hold again, the "braking" state is active and the output braking pressure of the ABS controller follows the desired braking pressure until the wheel deceleration or slip switching threshold is exceeded again.

To achieve good results with the ABS controller, this process must be precisely tuned. This tuning involves the wheel acceleration switching thresholds, the slip-switching thresholds, and the constants for reducing braking pressure and increasing braking pressure slowly and quickly. Numerous simulations have shown good results for all driving manoeuvres with the following ABS control system settings:

sss	= 0,2	slip-switching threshold	[-]
na	= -330	wheel acceleration switching threshold (-a)	[rad/s²]
pa	= 83	wheel acceleration switching threshold (+a)	[rad/s²]
pA	= 100	wheel acceleration switching threshold (+a)	[rad/s²]
PBpp	= 65000	rapid increase in pressure	[Nmm]
PBp	= 55000	slow increase in pressure	[Nmm]
PBnn	= 200000	pressure reduction	[Nmm]

Fig. 4-50 to Fig. 4-52 serve to clarify the mode of operation of the controller, which was recorded with a target deceleration of 3 m/s ², an initial speed of 70 km/H and with a road surface frictional resistance value of μ=0.2.

In Fig. 4-50 it is clear that braking without ABS (red curve) causes the wheels to start locking immediately (slip = -100%). When ABS is switched on however, slip is held between 10% and 30%, which represents optimum exploitation of available adhesion.

The next illustration (Fig. 4-51) clarifies this based on wheel velocity. While braking without ABS reduces wheel velocity almost immediately to zero, wheel locking is prevented by the intervention of the regulator during the entire braking procedure.

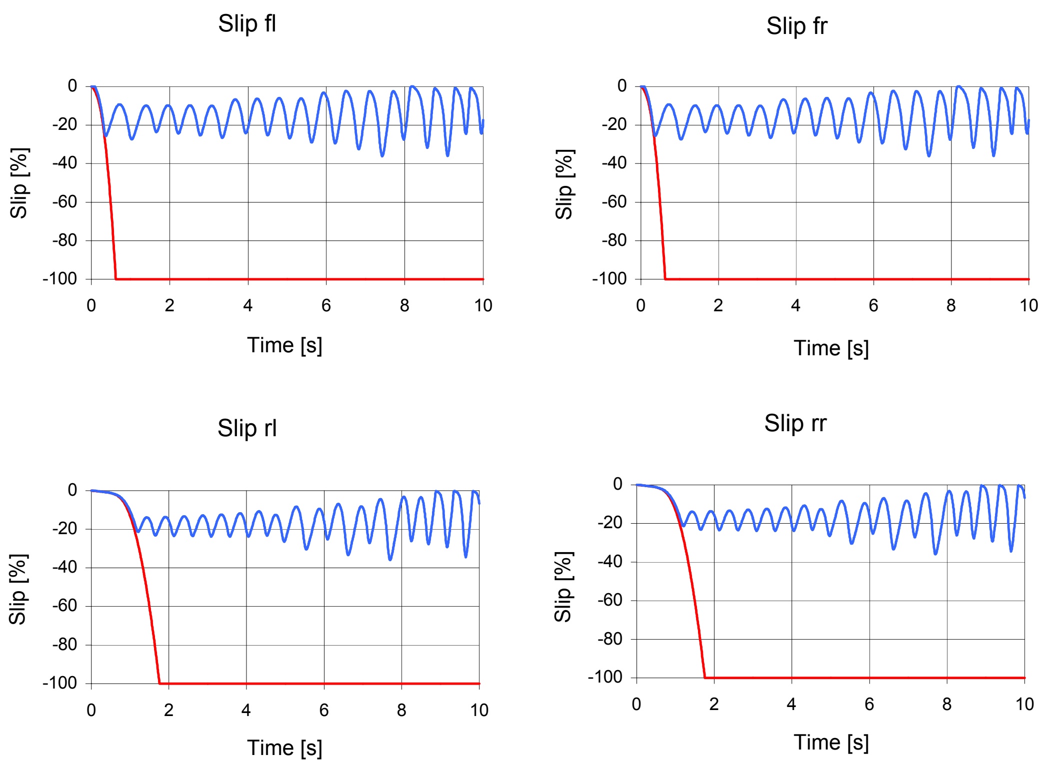

Fig. 4-50: Brake slip with and without ABS

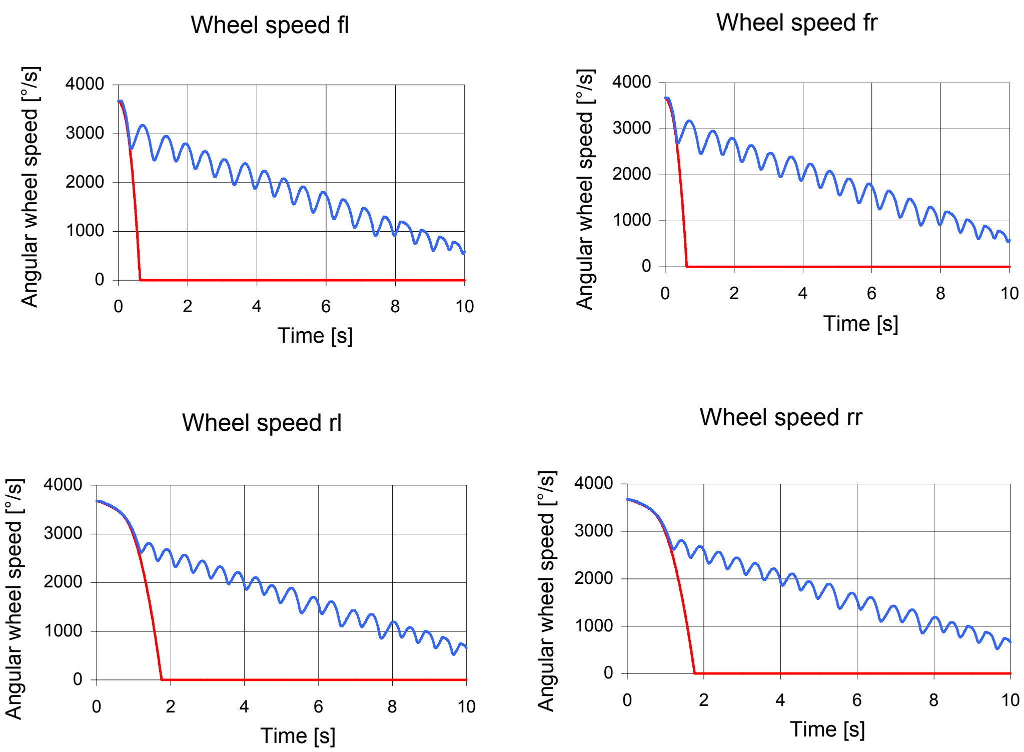

Fig. 4-51: Wheel speed while braking with and without ABS

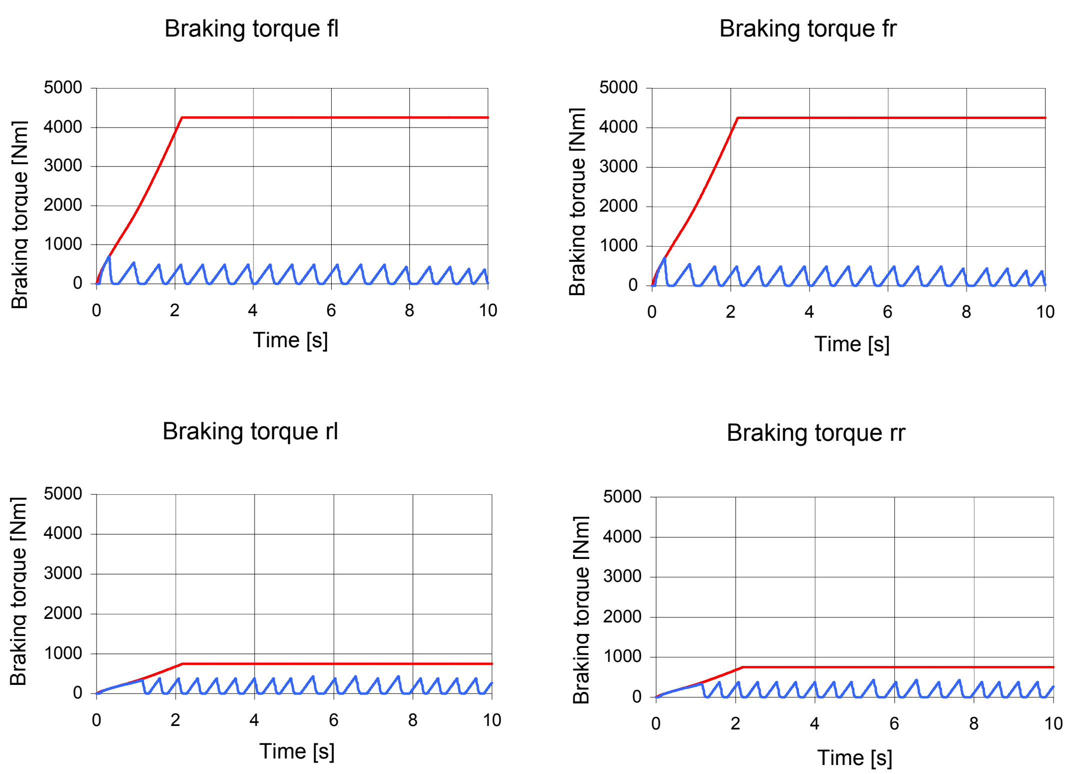

Fig. 4-52: Brake torques while braking with and without ABS

4.2.3.2 Traction Control System (TCS)

The traction control system prevents the wheels spinning when accelerating, cornering or driving on slippery roads, and provides increased traction and greater lateral force.

There are optimum adhesion coefficients both for acceleration and lateral force (see illustrations of the ABS system). To ensure driving safety and stability, certain slip limits must therefore not be exceeded. This is achieved by a targeted reduction of driving torque.

Unlike the anti-lock braking system where the individual wheel speeds are compared to the reference speed and relative slip serves as a control variable, an TCS only compares the speed of one wheel with the other.

In principle, there are three evaluation methods available for calculating speed differences between driven and non-driven wheels, which then serve to activate a specific control strategy:

1. Comparison the driven and the non-driven wheels of one side of a vehicle (side comparison)

2. Comparison of the driven and the diagonally opposed non-driven wheel (diagonal comparison)

3. Comparison of the average wheel speeds of the driven and non-driven axle (average comparison)

The performance of so-called 'average' comparison method stands out [REI93] and is therefore the preferred method for creating the differential speed.

A distinction is generally made between two operating modes. If the vehicle has a speed of under 38 km/H and one wheel only starts to slip, the so-called becomes "Select high" control mode is used (the faster wheel is adjusted). At a speed of over 38 km/H, or when both wheels threaten to spin at the same time, the so-called "Select-Low" control (adjustment of the slower wheel) is applied. To distinguish between the two operational modes, the reference speed is used to calculate of the actual speed of the vehicle.

In addition, three application areas are recognised according to [REI93].

- When the vehicle is **driving off**, the speed of the non-driven wheels is less than 10 km/h.
- The criterion for the **acceleration of the vehicle in a straight line** is maximum acceleration of a driven wheel of more than 2 *g (corresponding to 1.962 m/s²) and a speed difference on the non-driven wheels of less than 1 km/h.
- When the above conditions do not apply, it is assumed that the vehicle is driving on a slippery **road or round a curve**.

Starting off is not taken into account by this TCS model, since it is not simulated.

The control strategy compares the speed difference with variable limits. If the speed difference dv is larger than the upper limit, the driving torque is reduced a step at a time, held between the limits and then gradually increased again. According to [REI93] these limits look like this:

Select-high-Mode:	Acceleration range:	upper limit:	dv=6+0,04*v
		lower limit:	dv=5+0,02*v
	Cornerring:	upper limit:	dv=4+0,04*v
		lower limit:	dv=3+0,02*v
Select-low-mode:	Acceleration range:	upper limit:	dv=3+0,04*v
		lower limit:	dv=2,5+0,02*v
	Cornerring:	upper limit:	dv=1+0,04*v
		lower limit:	dv=0.5+0,02*v

With help of the relationships described above, a drive/slip control mechanism is created in the Matlab/Simulink.

As shown in Fig. 4-53 the control mechanism, which works at a frequency of 25 Hz as in reality, requires the angular velocities of the wheels (omega), the reference angular velocity (omega ^) and the driving torque (M_drive) as input parameters. The output variable is the modified driving torque (M__drive_TCS).

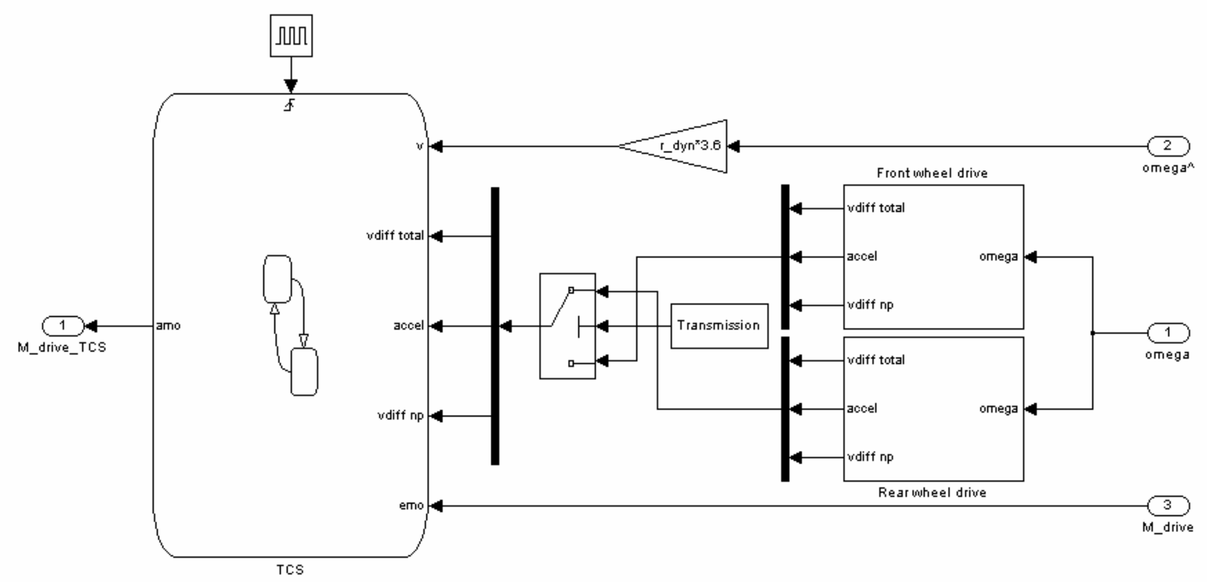

Fig. 4-53: Set-up of the TCS-block

First, the actual speed of the vehicle (V) is calculated by multiplying the reference angular velocity by the dynamic wheel radius (r_dyn).

As the LSD should be suitable for both front and rear-wheel drive, the parameters that depend on the type of drive type are calculated at the same time in the appropriate subsystems. The choice is made automatically via the vehicle parameters (for front-wheel drive: drive = 0).

Individually, these are:

vdiff total [km/h]	Difference between the average speeds of the driven wheels and the non-driven wheels
accel [m/s²]	Maximum acceleration of the wheels
vdiff np [km/h]	Difference between the speeds of the non-driven wheels to the amount

The following is an explanation of the calculation for front-wheel drive (Fig. 4-54).

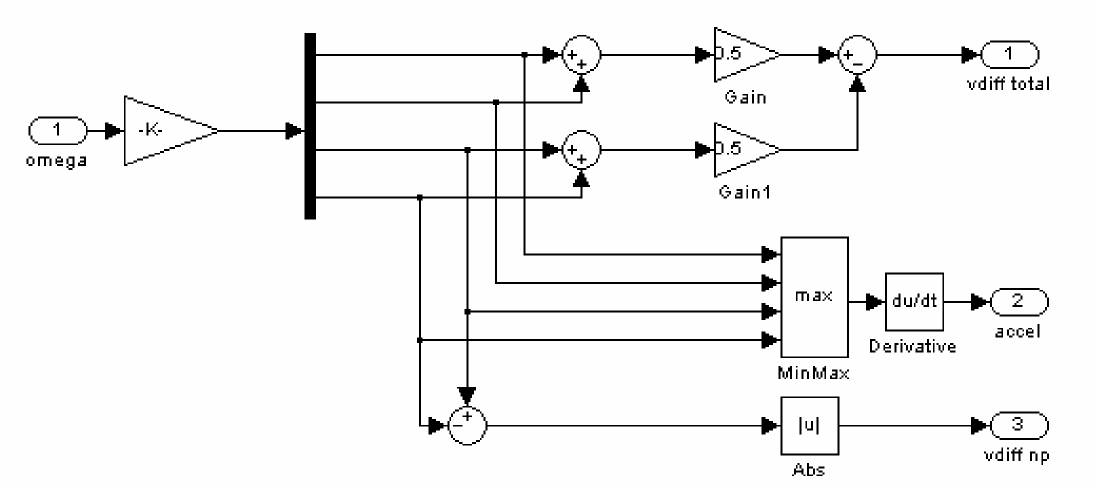

Fig. 4-54: Subsystem „Front wheel drive“

Here the average angular velocities are converted to wheel speeds (K=r_dyn*3,6) in each instance, the average speeds of the driven and the non-driven wheels are obtained and subtracted from each other (vdiff total). When calculating the maximum acceleration, speeds are initially converted into m/s, then analysed, and then finally the highest is sent to the controller. The final variable to be calculated is the speed difference between the non-driven wheels (vdiff np). The procedure is the same in the 'rear-wheel drive' subsystem.

As all the required variables are now available, we will now examine the controller (Fig. 4-55) in more detail.

As can be seen, the Stateflow model consists of two large ranges, corresponding to the two operational modes (select-high and select-low). These are both subdivided into the two application areas: acceleration and cornering.

To explain of the Stateflow model a possible control situation, we will describe by way of example a typical control situation in the select-low control range.

At beginning of the simulation the "start" state is active and the input momentum is passed on unchanged to the output momentum (amo = emo). The reference speed "v" is immediately checked in the first work cycle. Since in the example this should lie above 38 km/h, the state "sl" is activated by the arrow "[v > 38]" in select-low, in which the same actions are still carried out as in the initial state. If the conditions for the acceleration range are fulfilled in the following ([vdiff np < 1 && accel > 1.962 && vdiff total > 3+0.04*v], the state "Moru3" is activated. There, the driving torque is reduced per work cycle at 1/100 of the input momentum produced by the driver.

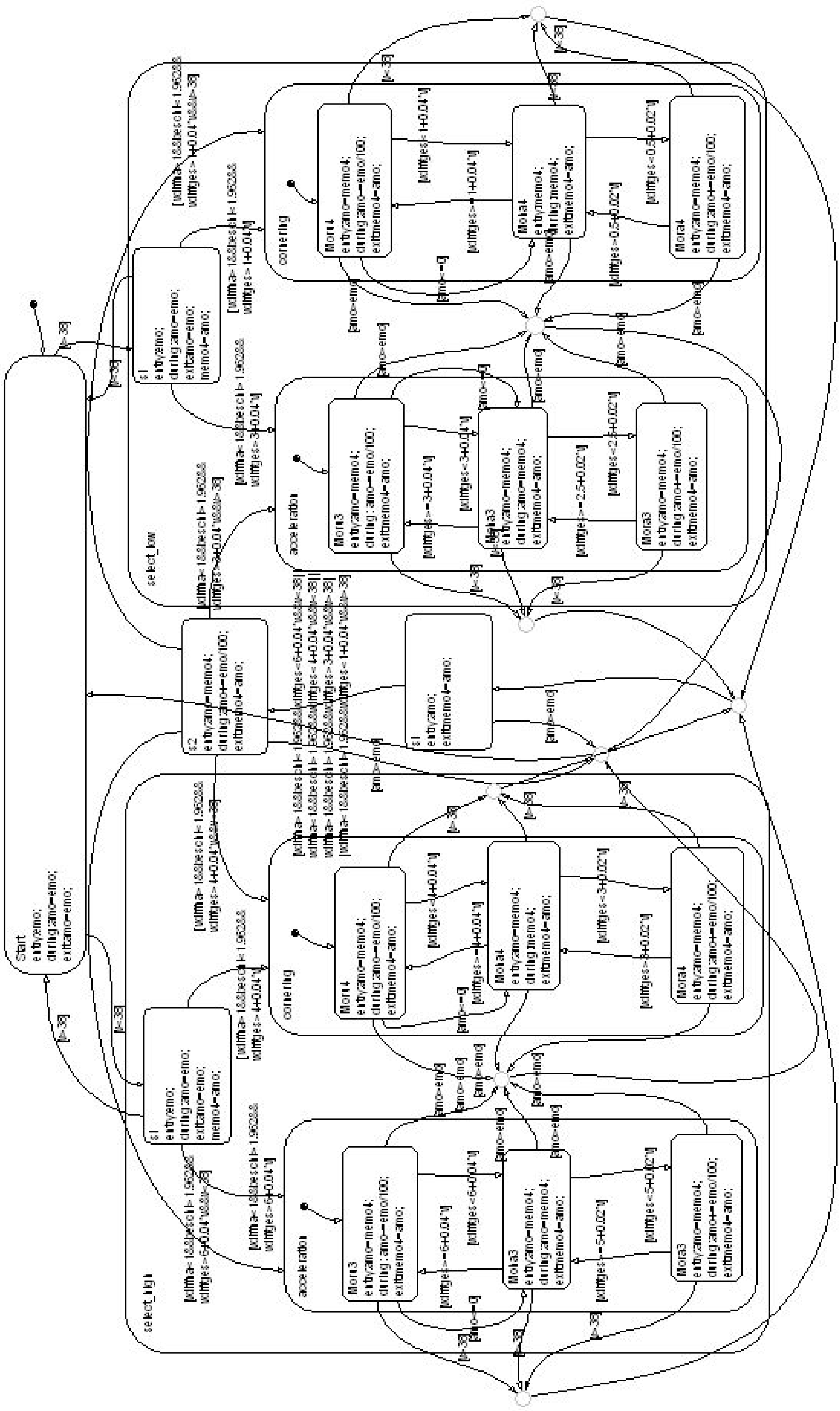

Fig. 4-55: Stateflow model of the TCS

If the value for vdiff total falls to between the values v_1 and v_2 ([vdiff total<3+0.04*v]) the current momentum is held. If vdiff total in the following also falls below the value v_2 ([vdiff total < 2.5+0.02*v]), the driving torque is again slowly increased (amo += emo/100) until the output momentum is equal to the input momentum (activation "start") or the condition for select-low control is no longer fulfilled (v < 38). Then the state "sl" in which the driving torque is held is activated. As soon as the driving conditions are no longer critical, it is gradually increased in state "s2" until it is larger than the input momentum (amo>emo, skip to the start state) or the driving conditions become critical once again.

The following illustrations serve to clarify the operation of the controller. They were recorded during a trip at 40 km/h, an acceleration of $1\ m/s^2$ and a road surface frictional resistance value of $\mu = 0.2$.

In Fig. 4-56 it is clear that the slip increases very quickly to 90% when accelerating without LSD (red curve). If the regulator intervenes, however, slip is reduced to about 8% (blue curve).

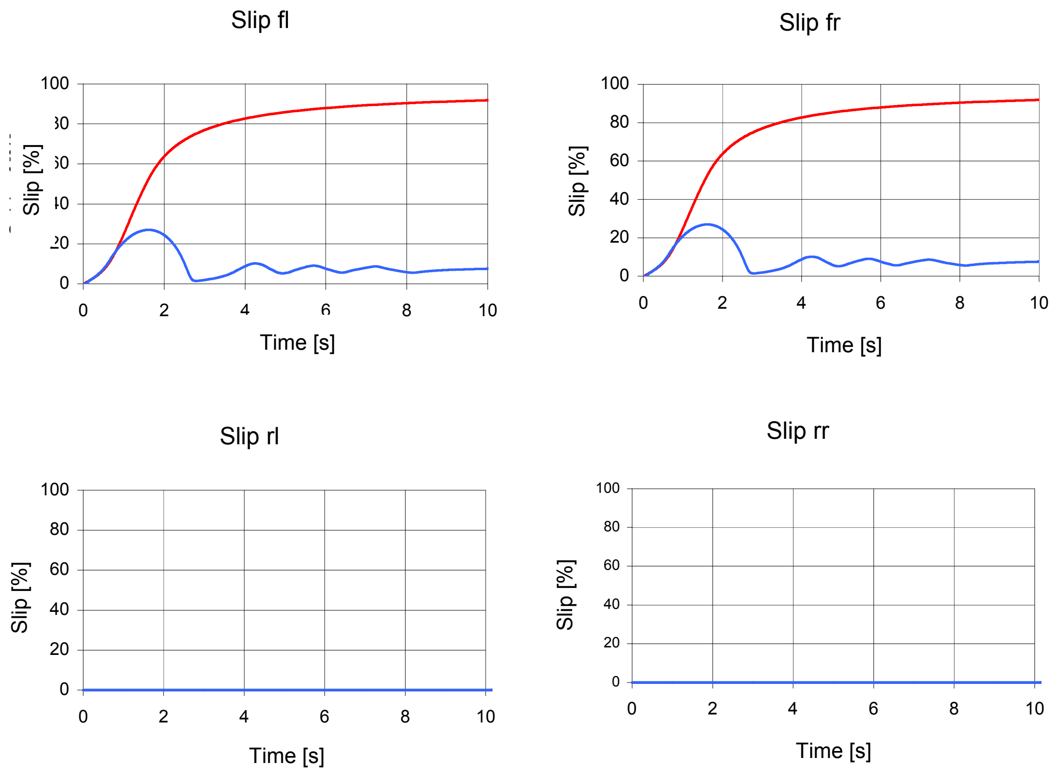

Fig. 4-56: Wheel slip with an without TCS

The following illustration (Fig. 4-57) shows the angular velocities of the individual wheels. The operation of the TCS is clear to see.

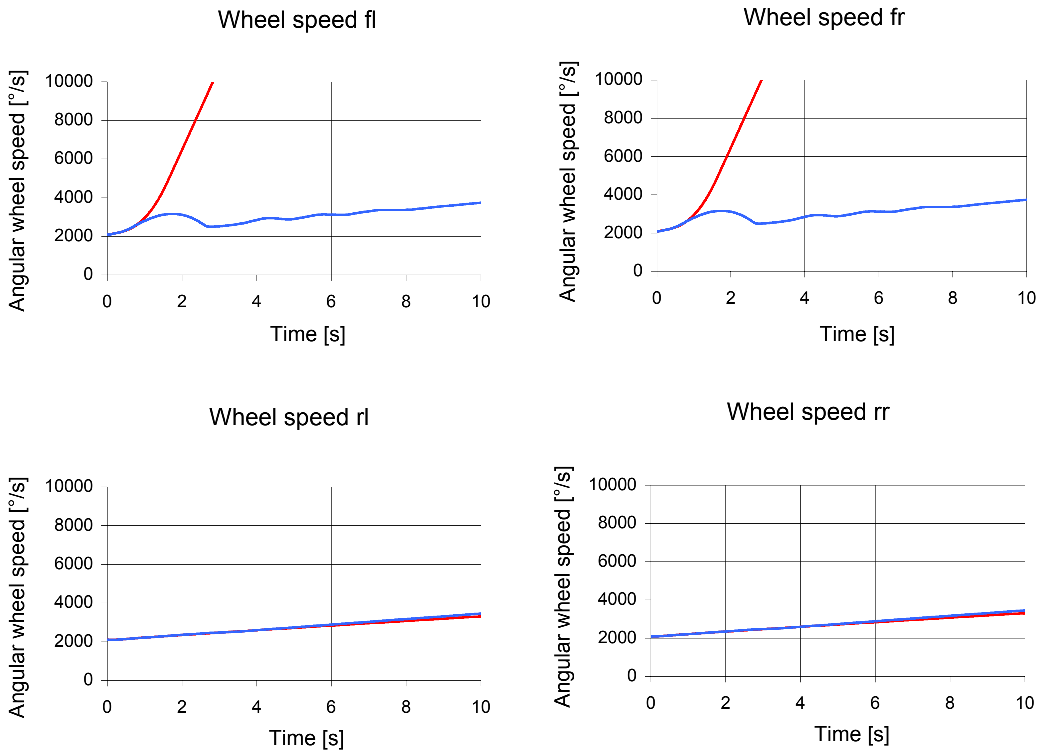

Fig. 4-57: Wheel speed of the wheels with and without TCS

The last figure (Fig. 4-58) shows the driving torque curve with and without regulation. The step-by-step reduction and subsequent increase can be seen quite clearly.

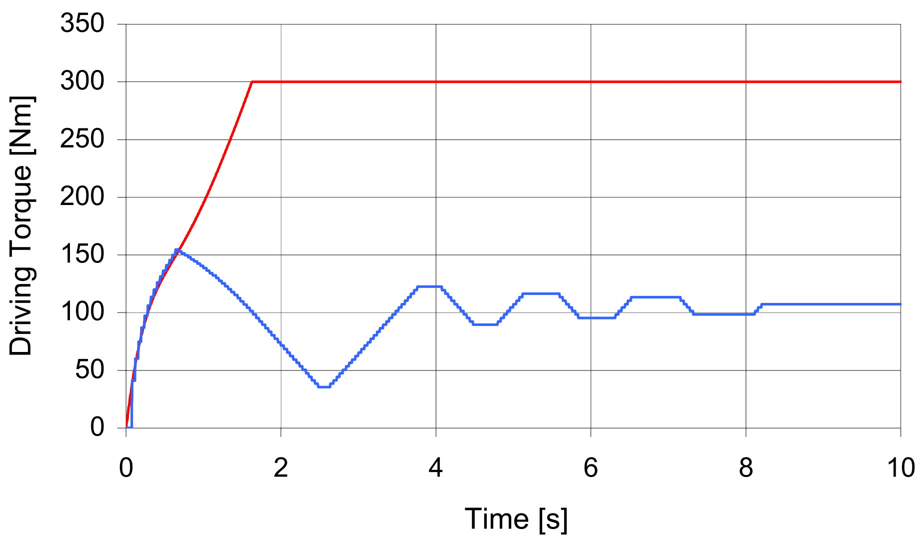

Fig. 4-58: Driving torque with and without TCS

4.2.4 Self diagnosis

The increased safety levels provided by modern wheel slip controllers is dependent to a great degree on the quality of the signals provided by the sensor. Defects or malfunctions in the sensors, particularly the yaw rates or the steering angle sensor, can have serious consequences on the correct operation of the driving dynamics controller. In extreme cases, interventions by the driving dynamics controller under normal, safe driving conditions can create critical situations over which the driver has no control. To avoid such a risk, the sensor signals must constantly be crosschecked for plausibility. In the event of an incorrect signal, the driving dynamics controller must be deactivated to avoid critical malfunctioning.

For the following observation, it has been assumed that only one fault will appears at any one time. The following possible faults that may occur during the operation are considered:

- The failure of a sensor or its wiring, i.e. the signal from the sensor is zero.
- A reversed sensor signal indicator, which can occur as a result of incorrect installation, for example.
- An offset as fault signal, i.e. a constant value added to the signal.
- A noise that masks the sensor signal.
- A drifting signal, i.e. a low frequency vibration is superimposed on the sensor signal.

It is task of the fault analysis to correctly recognize each of these faults in every driving situation as quick as possible. Incorrect activation of the error analysis must be prevented. As soon as the error analysis recognizes a fault, an error message must be sent to deactivate the driving dynamics controller and to specify the fault, so that this can be entered in the driving dynamics controller's error log for the purpose of diagnosis.

The error analysis structure is shown in Fig. 4-59. Error analysis consists of three main parts:

1. The estimator module generates a reference signal on the basis of the available sensor signals for each variable. As input, this block needs the sensor information for the four wheel velocities, the longitudinal acceleration, the transversal acceleration, the yaw rate, as well as the steering angle at the steering wheel.

2. The error detection carries out a comparison between the sensor signals and the reference signals. If fixed error thresholds are exceeded, the error detection sends an error message.

3. Error evaluation processes the error messages and sends a coded error signal with details the type of fault to the driving dynamics controller.

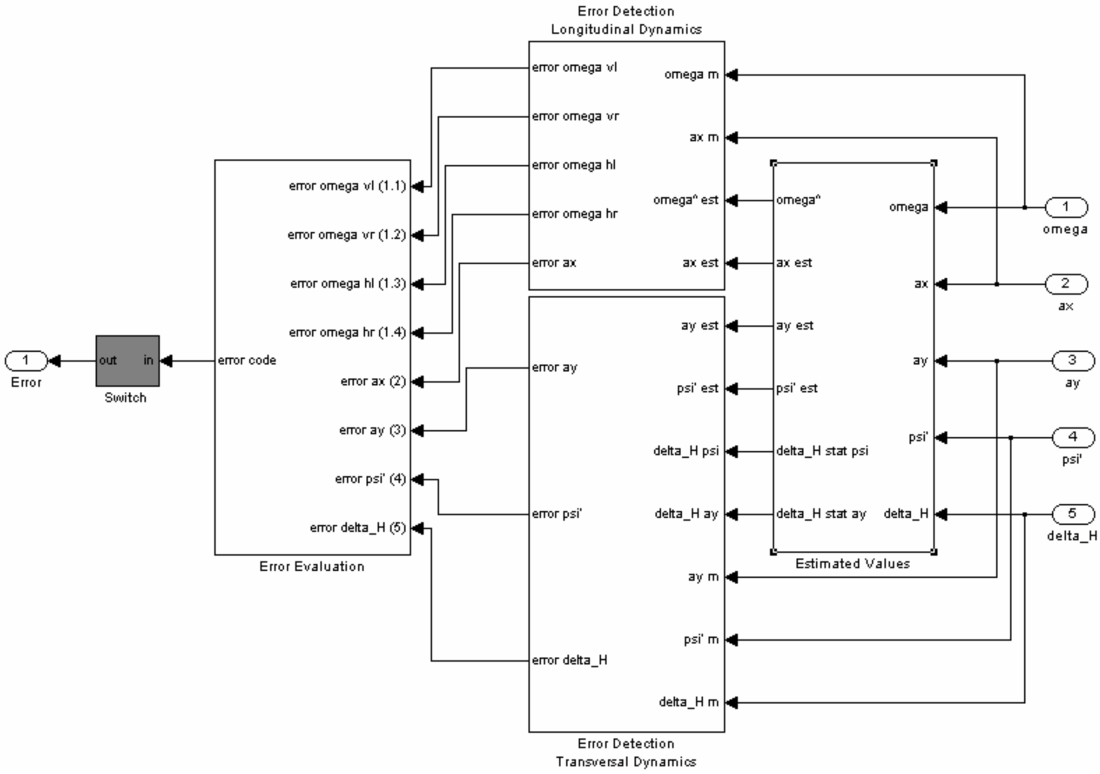

Fig. 4-59: Structure of the defect analysis

4.2.4.1 Calculating the reference values

The reference sizes for the error detector are calculated by the estimator module "Estimated Values" (Fig. 4-60). For this check to be meaningful, a comparison size, the so-called reference size, must be estimated from remaining signals available. The sensor signal of the checked variable must not affect the reference signal. The following reference variables are calculated to check signal plausibility:

- wheel velocity $\hat{\omega}$
- longitudinal acceleration a_x
- lateral acceleration a_y
- yaw velocity $\dot{\psi}$
- Steering angle at the steering wheel δ_H

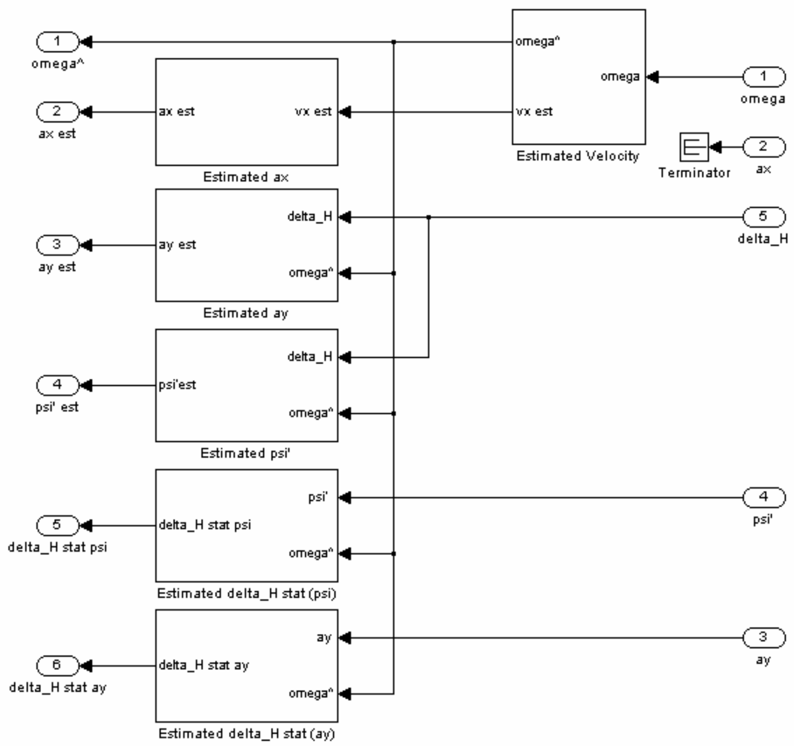

Fig. 4-60: Set-up of the subsystem „Estimated Values“

- **Longitudinal dynamics**

The longitudinal variables reference wheel velocity ω_{ref} and reference longitudinal acceleration $a_{x,ref}$ are directly connected, as a_x the derivation of the driving speed over time is

$$a_{x,ref} = \frac{d}{dt} v_{ref} \qquad \text{Eq. 4-16}$$

and the driving speed is calculated from the wheel velocity ω and the dynamic wheel radius r_{dyn}.

$$v_{ref} = r_{dyn} \cdot \omega_{ref} \qquad \text{Eq. 4-17}$$

This means that the calculation of a reference wheel velocity ω_{ref} must be the main component of the estimator for longitudinal dynamic variables.

The approach used by the vehicle model to determine the reference speed cannot be used here, as the longitudinal acceleration will at times be added to the calculation. An error in the acceleration signal also would distort the reference speed.

In the "estimated velocity“ block (Fig. 4-61), the reference speed is therefore determined exclusively from the wheel velocity. In addition to the wheel signal variables, there are four independently measured variables available. The fact that voltage variations on a real control unit can affect all velocity signals simultaneously is ignored here.

The four wheel velocities are basically very similar in nearly all driving situations. If a sensor signal is faulty, the signal is identified accordingly, so that it will stand out from the other signals. An average value is calculated from the three most compatible wheel velocities and this is used as the reference velocity. In addition, the associated reference speed is still calculated and sent to the parent "Estimated Values" system by multiplication with the dynamic wheel radius.

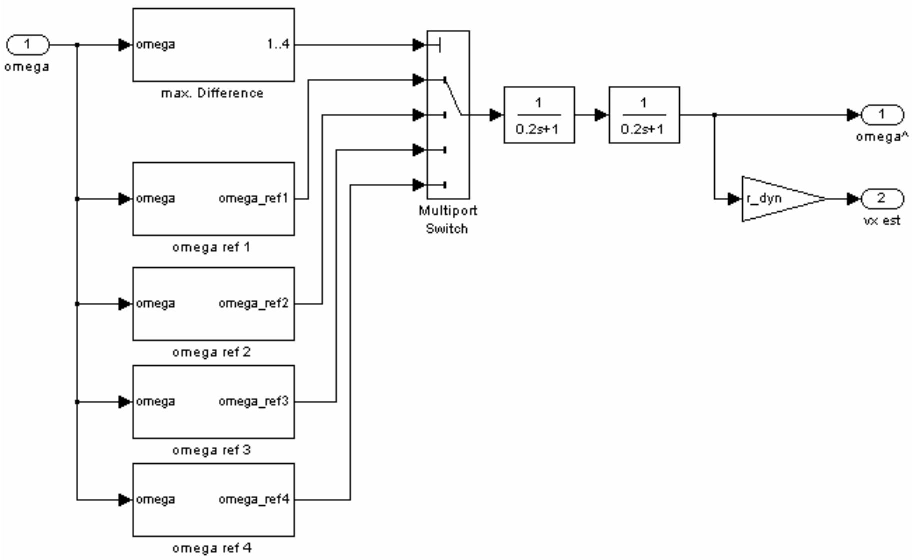

Fig. 4-61: Subsystem „Estimated Velocity“

First, the "max. difference" subsystem determines the wheel velocity value that shows the greatest deviation, i.e. the signal most likely to be the cause of the error. The number of this particular wheel whose velocity deviates most is used as the output signal, Fig. 4-62.

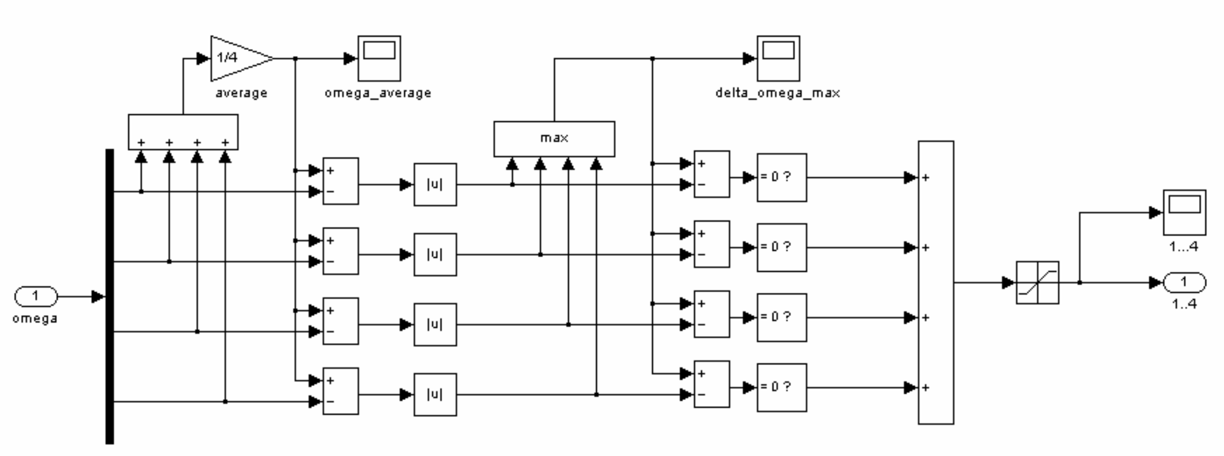

Fig. 4-62: Structure of the subsystem „max. difference“

All velocities are added and then divided by four, giving the "omega_average" wheel velocity. The difference between each individual wheel velocity and this average velocity is calculated. The wheel with the greatest "delta_omega" difference "delta_omega" is the one we are looking for. The velocity of this wheel shows the greatest deviation from the others. In the "delta_omega_max" model, the largest of the four values is deducted from the "delta_omega" of each wheel. The result of this calculation must now be exactly zero for the wheel showing the greatest deviation, since the following applies to this wheel: delta_omega = delta_omega_max.

The following blocks form a logical query as to whether the input signal is exactly zero. If the input is non-zero, they output zero; if the input is zero, they output the number of the particular wheel. These output signals are added and limited to the range one to four, in order to avoid errors that could occur when, for example, all wheel velocities are identical. The "max. difference" block provides the reference number of the wheel whose velocity is to be excluded from the reference velocity calculation.

The average of the three wheel velocities is calculated in the "omega ref 1" to "omega ref 4" in Fig. 4-61. The reference velocity that does not contain the divergent velocity signal is selected in the multiport switch on the basis of the "max.Difference" output signal. To smooth the sudden transition between different reference velocities, two transfer functions are inserted as filters after the Multiport switch output.

The resultant reference velocity "omega ^" and the resultant reference speed "vx_est", calculated by multiplication with the dynamic wheel radius "r_dyn", are output from the "estimated velocity “block ".

Now the speed signal vx_est is derived and the longitudinal acceleration ax_est is output from the "estimated ax" block in Fig. 4-60.

- **Lateral dynamics**

When calculating the lateral dynamic reference variables a_y, δ and $\dot{\psi}$, one of the variables should be estimated from the other variables. The equations of the bicycle model (Eq. 4-18 to Eq. 4-21) are available, illustrating a relatively simple relationship between these variables:

$$\delta_{stat} = \frac{\dot{\psi}}{v_{est}} \cdot l \cdot \left(1 + \frac{v_{est}^2}{v_{char}^2}\right) \qquad \text{Eq. 4-18}$$

$$\dot{\psi}_{stat} = \frac{v_{est}}{l \cdot \left(1 + \frac{v_{est}^2}{v_{char}^2}\right)} \cdot \delta \qquad \text{Eq. 4-19}$$

$$a_{y,stat} = v \cdot \left(\dot{\psi}_{stat} - \dot{\beta}\right) \qquad \text{Eq. 4-20}$$

To simplify the calculations, $\dot{\beta} = 0$ ($\dot{\beta}$ is normally small in comparison with $\dot{\psi}$). The steering angle δ is connected via the steering ratio i_L with the manual steering angle δ_H according to Eq. 4-21:

$$\delta_H = \delta \cdot i_L \qquad \text{Eq. 4-21}$$

Only stationary driving conditions can be described using these equations. Vehicle behaviour during dynamic driving manoeuvres also depends on the steering frequency and the driving speed and should be accounted for when determining the yaw velocity and lateral acceleration by the inclusion of additional transfer components. This dependency on variables a_y and $\dot{\psi}$ can be determined experimentally using simulations. The procedure for obtaining the yaw angle speed is illustrated here by way of example.

Simulations show that the transfer behaviour of the yaw angle speed can be shown very precisely with a transfer element in the form

$$F(s) = \frac{K_{12}s^2 + K_{11}s + K_{10}}{K_{23}s^3 + K_{22}s^2 + K_{21}s + K_{20}} = \frac{\dot{\psi}_{est}}{\dot{\psi}_{stat}} \qquad \text{Eq. 4-22}$$

However, the transfer behaviour is strongly dependent on the driving speed. This indicates that coefficients K_{ij} in Eq. 4-22 change with the driving speed.

The follwing may be written for the speed-dependent transfer behaviour:

$$\dot{\psi}_{est} = \dot{\psi}_{stat} \cdot \frac{K_{12}(v) \cdot s^2 + K_{11}(v) \cdot s + K_{10}(v)}{K_{23}(v) \cdot s^3 + K_{22}(v) \cdot s^2 + K_{21}(v) \cdot s + K_{20}} \qquad \text{Eq. 4-23}$$

These coefficients are determined with the aid of the MATLAB function "tfe" (transfer function estimate) by calculating the transfer function from $\dot{\psi}$ to $\dot{\psi}_{stat}$. The coefficients in the transfer element are adjusted so that the transfer behaviour of Eq. 4-23 corresponds to that of the vehicle model. The coefficients can therefore no longer be linked to the physical parameters of the vehicle.

This procedure is undertaken for driving speeds from 10 km/h to 150 km/h in steps of 10 km/h and the speed-dependent parameters K_{ij} (V) are determined. The following table (Tab. 4-1) shows the coefficients for the transfer function. The parameters are standardized so that a constant value is always obtained for K_{20}.

v [km/h]	**K_{12}**	**K_{11}**	**K_{10}**	**K_{23}**	**K_{22}**	**K_{21}**	**K_{20}**
10	0.323	1.19	1.088	0.0045	0.34	1.19	1.11
20	0.18525	1.2445	1.216	0.0075	0.22	1.19	1.11
30	0.19125	1.33	1.3125	0.0095	0.225	1.19	1.11
40	0.182	1.43	1.3975	0.0095	0.21	1.19	1.11
50	0.1888	1.568	1.536	0.0103	0.2	1.19	1.11
60	0.201	1.7	1.664	0.0111	0.19	1.19	1.11
70	0.229	1.83	1.77	0.013	0.186	1.19	1.11
80	0.32085	1.9182	1.7802	0.017	0.21	1.19	1.11
90	0.4015	2.1024	1.8615	0.02	0.222	1.22	1.11
100	0.49665	2.2715	1.8865	0.0233	0.232	1.25	1.11
110	0.608	2.419	1.968	0.0262	0.24	1.26	1.11
120	0.7308	2.523	2.001	0.03	0.25	1.27	1.11
130	0.98	2.62	1.43	0.036	0.285	1.35	1.11
140	1.15	2.65	1.1	0.047	0.295	1.4	1.11
150	1.7	2.7	0.7	0.06	0.37	1.6	1.11

Tab. 4-1: Coefficients of the transfer function for the yaw velocity

These coefficients are mapped according to speed in the MATLAB/Simulink subsystem that calculates the reference variable for $\dot{\psi}$ (Fig. 4-63). The performance maps interpolate the individual values of the coefficients K_{ij} (v) according to driving speed, which are then passed on to the "psi" transfer block.

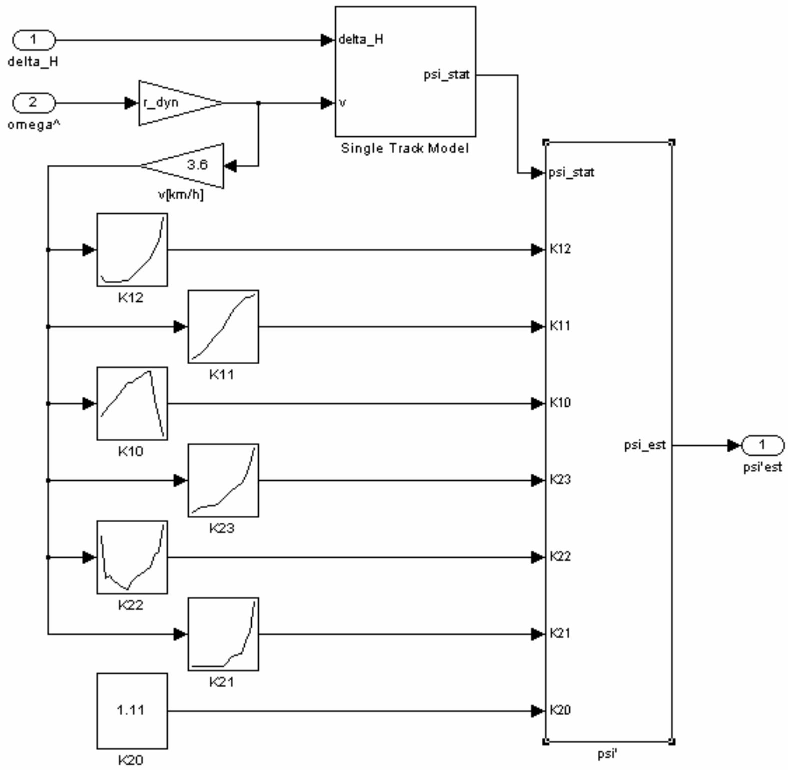

Fig. 4-63: Structure of the subsystem „Estimated psi' "

In the "psi" subsystem, the transfer function is modelled according to Eq. 4-23, in the form of control circuit elements. Values interpolated from the performance maps are processed in each stage of the calculation (Fig. 4-64).

A transfer function is shown with this structure that is both frequency and speed dependent. This can be illustrated in 3-D as an area. In Fig. 4-65 the transfer behaviour of the vehicle is represented as a blue area and that of the "estimated psi' estimator for the reference variable is represented $\dot{\psi}_{est}$ as red area. The frequency responses for driving speeds of 10 to 90 km/h are shown by way of illustration. The strong speed dependency of the transfer behaviour is easily recognisable, as is the marginal difference between the measured and the modelled characteristics.

The consistency of the transfer function is again reflected in the accuracy of the estimated reference variables for $\dot{\psi}$. This is shown in the following diagrams (Fig. 4-66 bis Fig. 4-68) for the double lane-change driving manoeuvre, sinusoidal steering and step steer input.

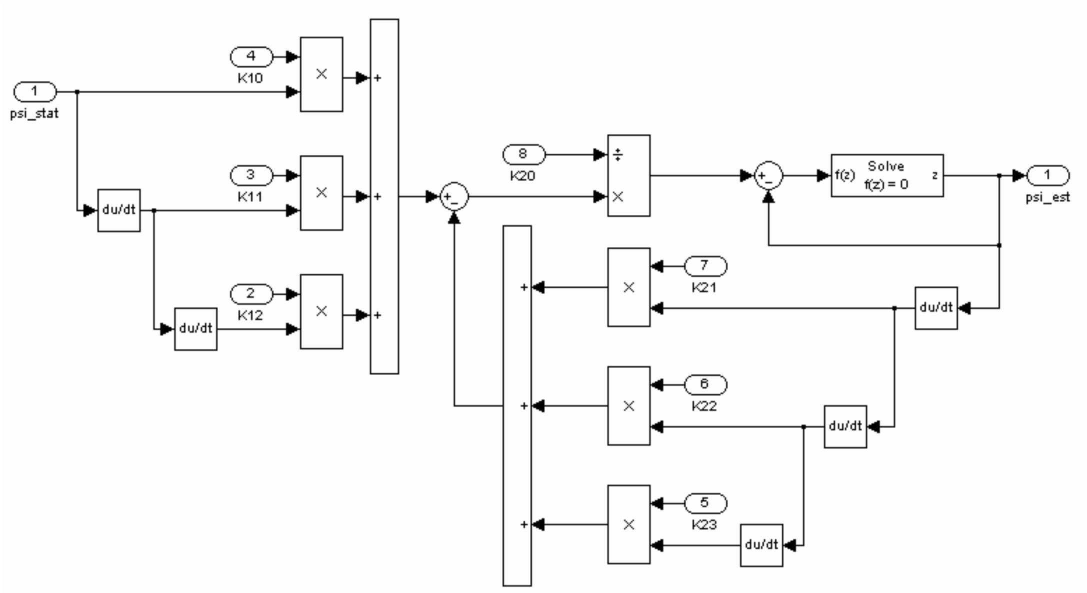

Fig. 4-64: Modelling of the transfer function for „psi' “

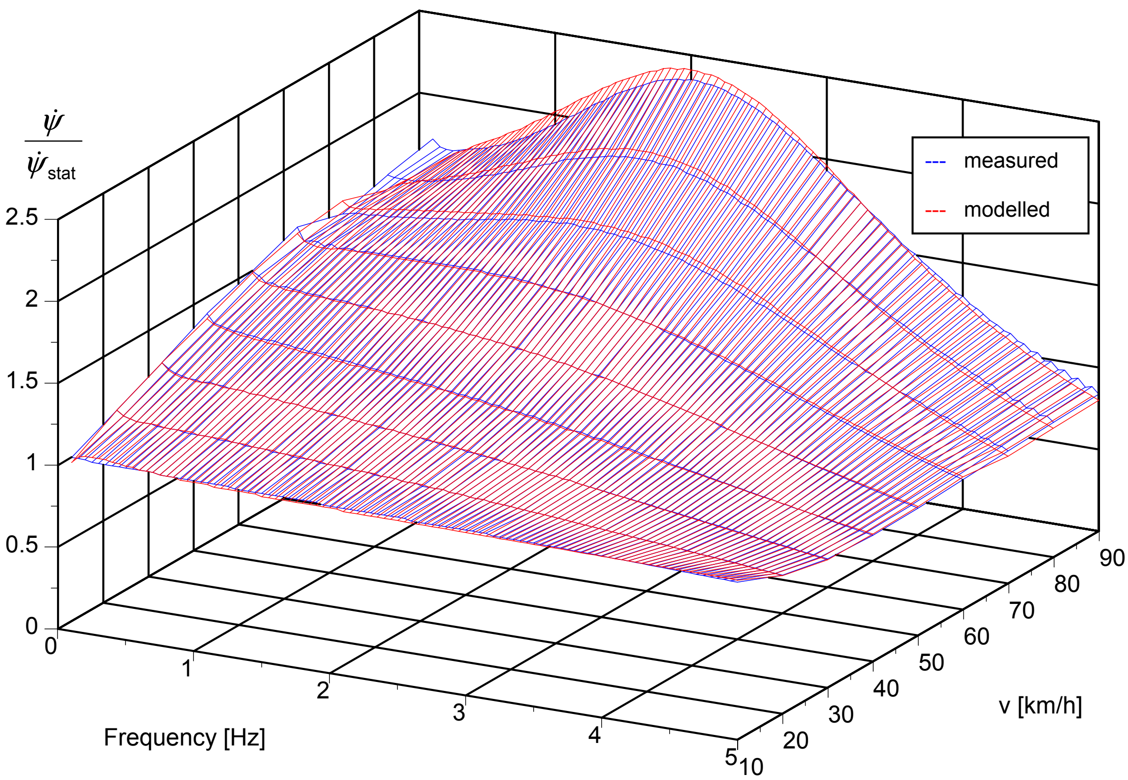

Fig. 4-65: Transfer characteristic of vehicle and model for the yaw velocity

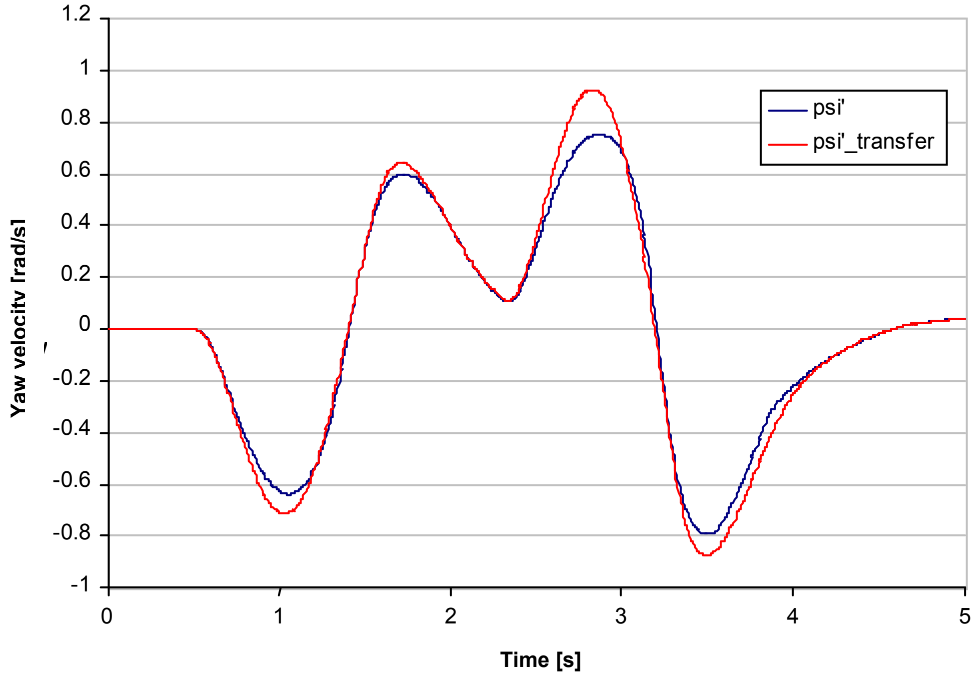

Fig. 4-66: Measured and estimated yaw velocity during double lane change with v=50 km/h

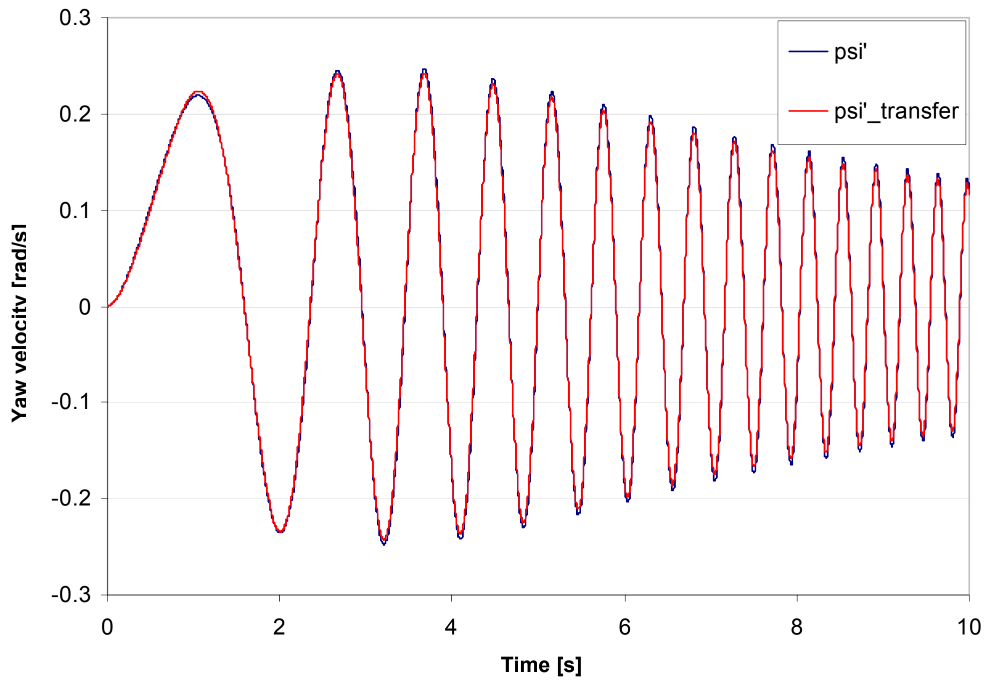

Fig. 4-67: Measured and estimated yaw velocity during sinusoidal steering input (0,1 to 3 Hz) with v=70 km/h

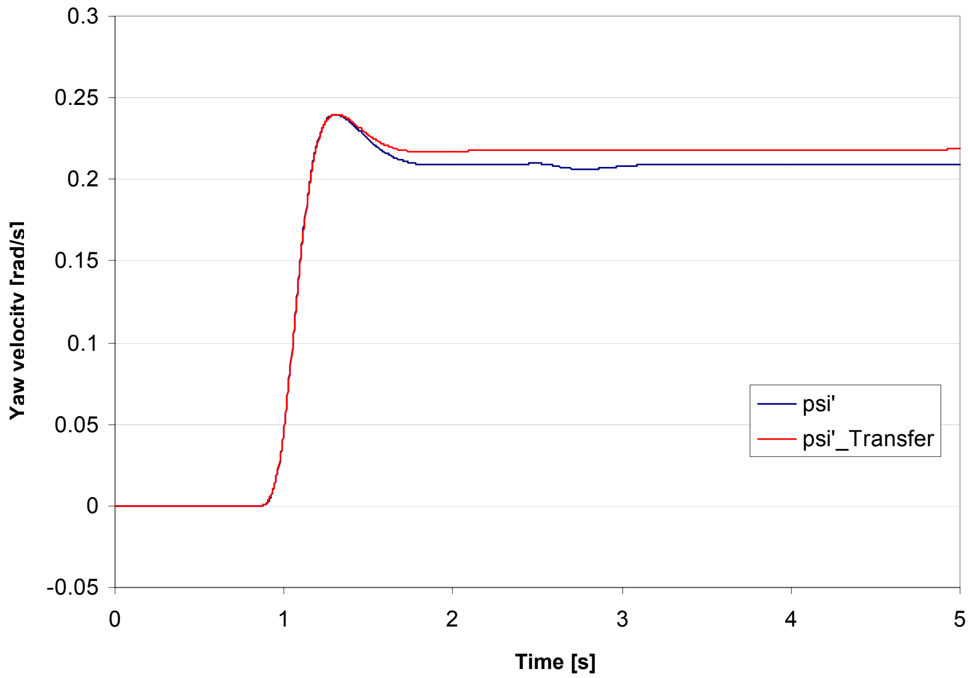

Fig. 4-68: Measured and estimated yaw velocity during a step steer input of 52° at v=70 km/h

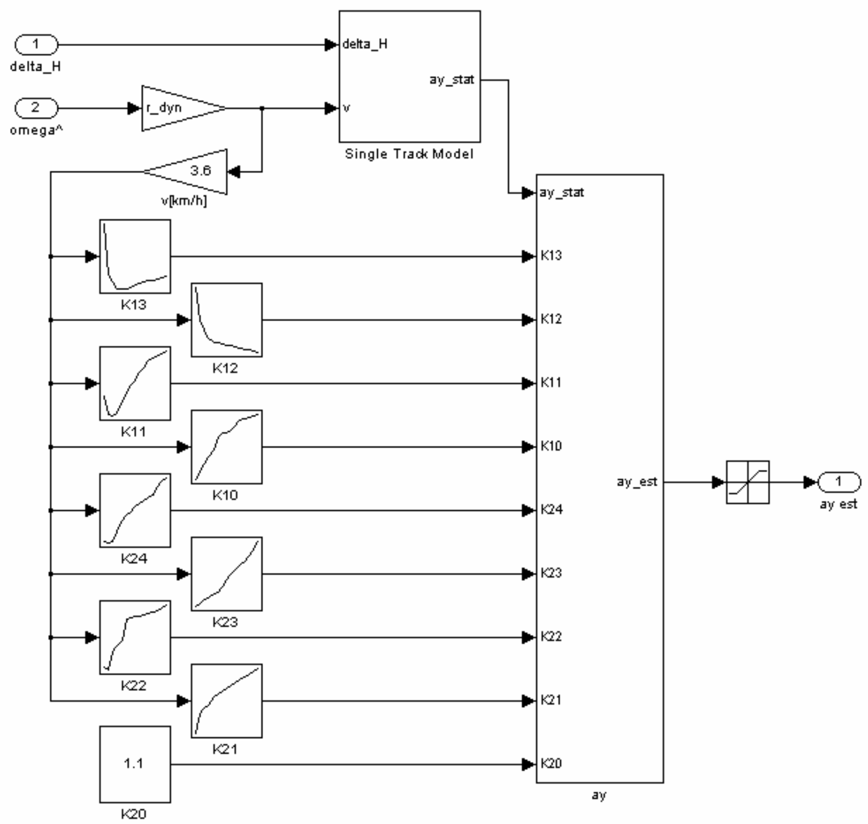

Fig. 4-69: Subsystem „Estimated ay“

Lateral acceleration is dealt with in the same way as the transfer function. Here too, $a_{y,stat}$ is calculated from the context of the bicycle model and, using the same procedure, shown as a speed-dependent transfer function. In this case, however, a transfer function in the form

$$a_{y,est} = a_{y,stat} \cdot \frac{K_{13}(v)\cdot s^3 + K_{12}(v)\cdot s^2 + K_{11}(v)\cdot s + K_{10}(v)}{K_{24}(v)\cdot s^4 + K_{23}(v)\cdot s^3 + K_{22}(v)\cdot s^2 + K_{21}(v)\cdot s + K_{20}} \qquad \text{Eq. 4-24}$$

has to be selected to produce a satisfactory representation of the frequency responses. The coefficients obtained are listed in Tab. 4-2. Two additional performance maps are therefore located in the block "estimated ay“ (Fig. 4-69) for the coefficients K_{13} and K_{24}. The transfer function in the block "ay" (Fig. 4-70) is more comprehensive by two derivations. To avoid malfunction, the maximum achievable lateral acceleration is restricted to 1 g.

V [km/h]	K_{13}	K_{12}	K_{11}	K_{10}	K_{24}	K_{23}	K_{22}	K_{21}	K_{20}
10	0.06	0.644	1.64	1.08	0.000025	0.0038	0.15	1.1	1.1
20	0.021	0.35	1.47	1.19	0.000019	0.005	0.145	1.17	1.1
30	0.015	0.251	1.46	1.31	0.000025	0.0074	0.172	1.19	1.1
40	0.0105	0.182	1.48	1.4	0.00006	0.0085	0.18	1.2	1.1
50	0.01	0.143	1.58	1.5	0.0001	0.0105	0.187	1.23	1.1
60	0.01	0.138	1.68	1.7	0.00012	0.012	0.218	1.24	1.1
70	0.011	0.123	1.74	1.75	0.00013	0.0146	0.219	1.25	1.1
80	0.013	0.118	1.78	1.76	0.00015	0.019	0.221	1.26	1.1
90	0.014	0.11	1.85	1.8	0.00016	0.022	0.222	1.27	1.1
100	0.015	0.1	1.89	1.85	0.00017	0.0245	0.224	1.28	1.1
110	0.016	0.09	1.95	1.93	0.00018	0.0265	0.226	1.29	1.1
120	0.017	0.078	1.98	1.95	0.00019	0.029	0.228	1.3	1.1
130	0.018	0.07	2	1.98	0.00022	0.032	0.23	1.31	1.1
140	0.019	0.06	2.02	2	0.00024	0.035	0.233	1.32	1.1
150	0.02	0.05	2.04	2.02	0.00025	0.04	0.238	1.33	1.1

Tab. 4-2: Coefficients of the transfer function for the lateral accelaration

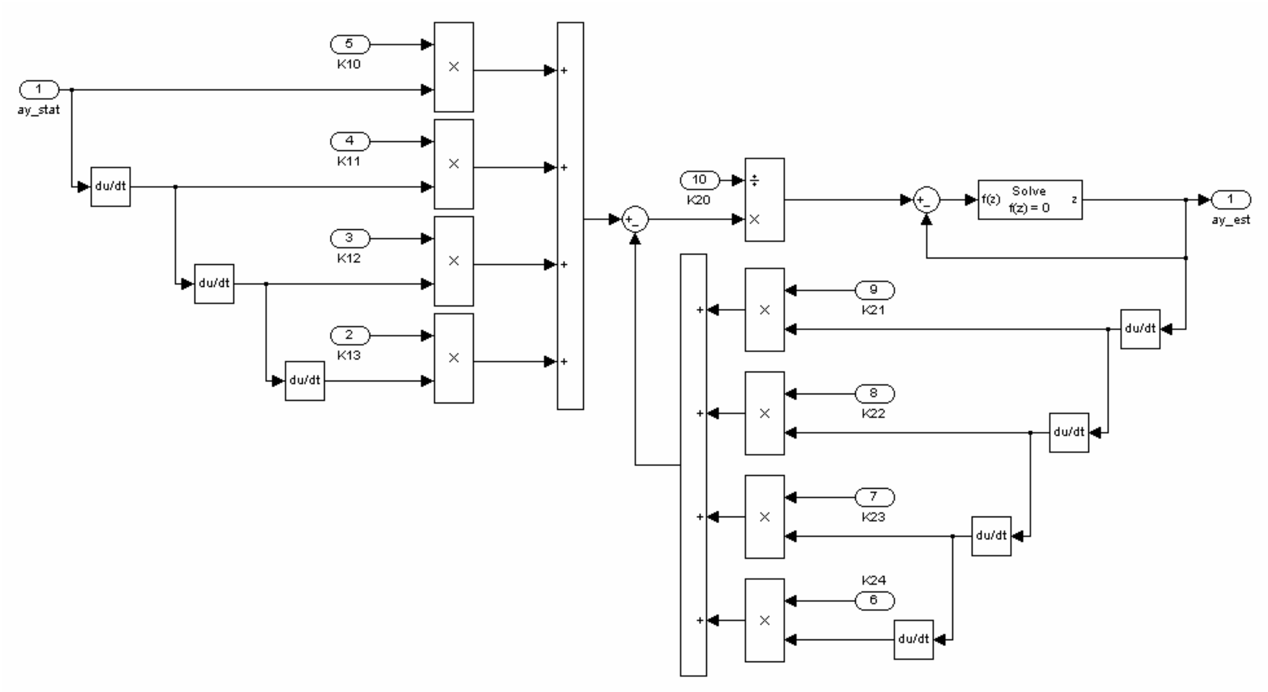

Fig. 4-70: Modelling of the transfer function in block „ay“

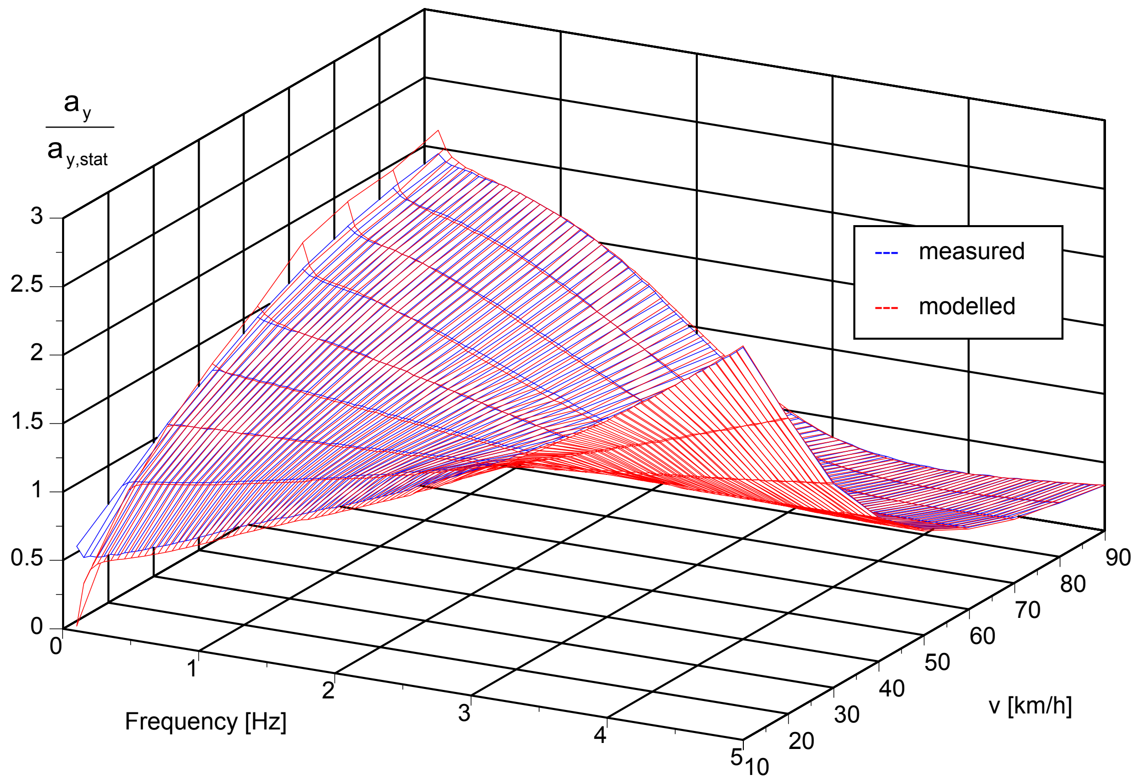

Fig. 4-71: Transfer characteristic of vehicle and model for the lateral acceleration

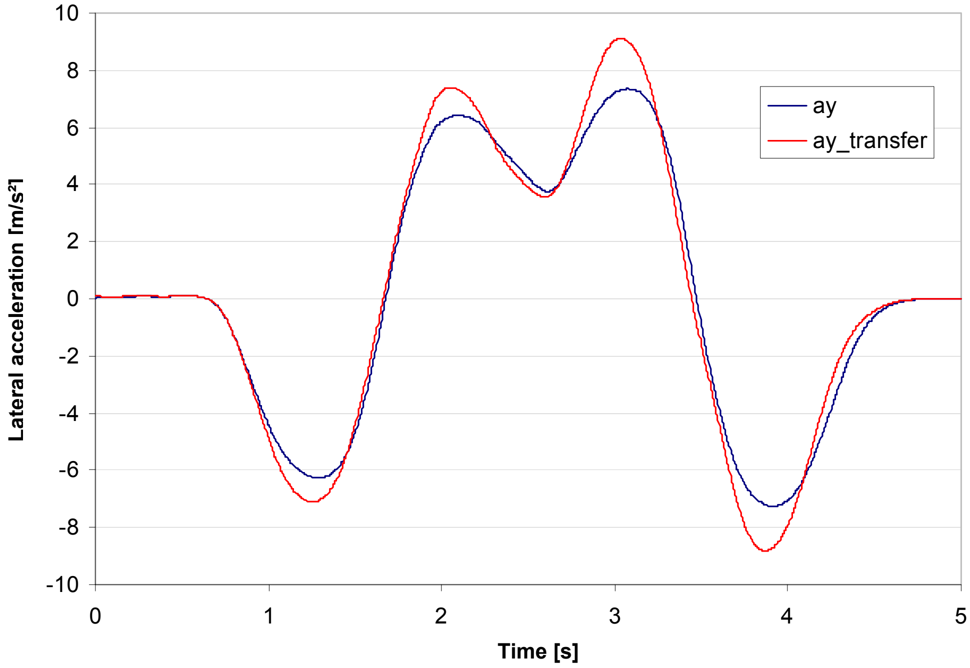

Fig. 4-72: Measured and estimated lateral acceleration during double lane change with v=50 km/h

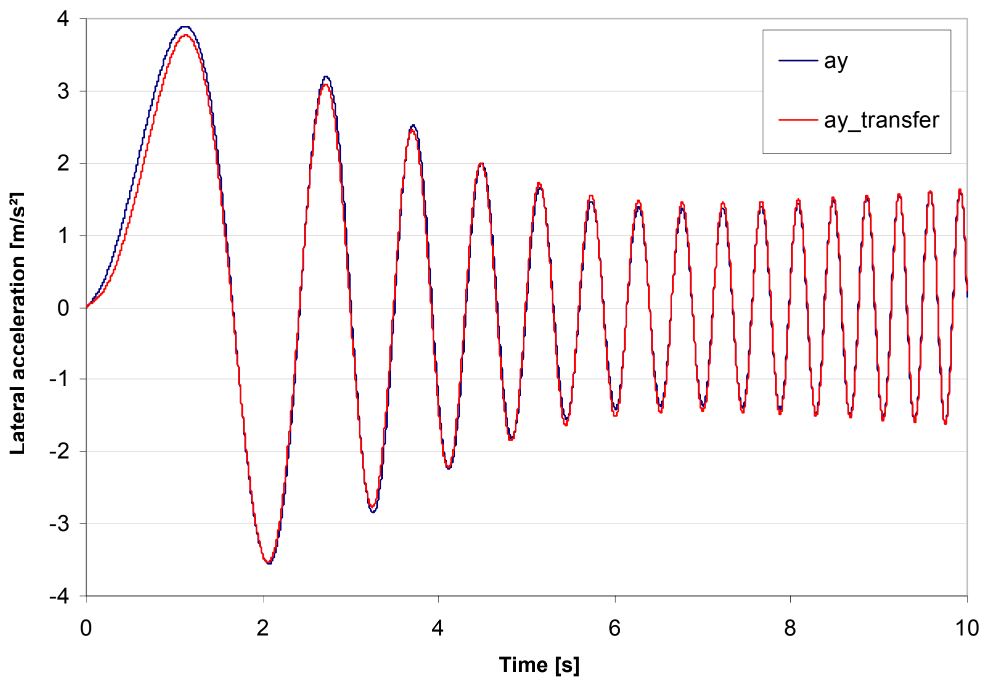

Fig. 4-73: Measured and estimated lateral acceleration during sinusoidal steering input (0.1 to 3 Hz) with v=70 km/h

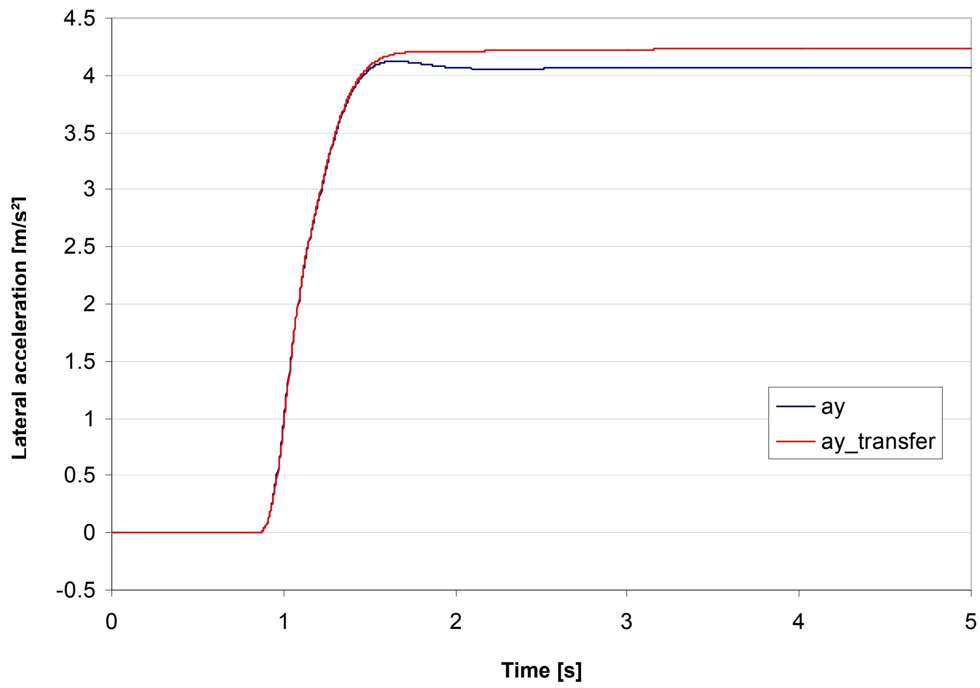

Fig. 4-74 Measured and estimated lateral acceleration during step steer input of 52° at v=70 km/h

The modelled and measured speed-dependent transfer function is shown as a 3D graphic in Fig. 4-71. The close agreement between the estimated reference variable for a_y with the output signal from the vehicle model is shown in diagrams (Fig. 4-72 to Fig. 4-74) for the various driving manoeuvres.

The simulation results for $\dot{\psi}$ and a_y show that the values estimated on the basis of the speed-dependent transfer functions are accurate enough to serve as reference variables for checking signal plausibility.

It requires only the inclusion of the steering angle to fully determine the transversal dynamic variables. There is a problem if we want to estimate the steering angle δ from the measured signals $\dot{\psi}$ and a_y. There is always a time delay between steering angle input and vehicle reaction. This is not a problem when estimating the vehicle responses from the steering angle, since the phase delay caused by the dynamic transfer functions is accounted for. Conversely, you can at best assume a time delayed steering angle input. If the vehicle is near stationary, this time delay will be near zero and the steering angle may be assessed accurately enough from the equation for the stationary yaw amplification factor (Eq. 4-18).

As with the transfer elements used for calculating the reference variables of $\dot{\psi}$ and a_y no satisfactory result can be achieved here, since such transfer elements mask the estimated signal with an additional phase delay.

Because of this uncertainty in estimating, two reference signals are calculated for the steering angle at the steering wheel δ_H for the stationary case. The variable "delta_H stat psi“ from the measured yaw angle speed

$$\delta_{H,stat,\dot{\psi}} = \frac{\dot{\psi}}{v_{est}} \cdot l \cdot \left(1 + \frac{v_{est}^{\;2}}{v_{char}^{\;2}}\right) \qquad \text{Eq. 4-25}$$

and „delta_H stat ay“ from the measured lateral acceleration, whereby the simplified version is used

$$a_y = \frac{\dot{\psi}}{v} \qquad \text{Eq. 4-26}$$

as it provides a sufficiently accurate relationship for stationary conditions:

$$\delta_{H,stat,a_y} = \frac{a_y}{v_{est}^{\;2}} \cdot l \cdot \left(1 + \frac{v_{est}^{\;2}}{v_{char}^{\;2}}\right) \qquad \text{Eq. 4-27}$$

Both reference variables for δ_H are passed on from the estimator module "estimated values" to the error detection.

4.2.4.2 Error detection

It is task of error detection to compare the reference sizes calculated in the subsystem "estimated values" with the sensor signals, and to issue an error signal as soon as the difference no longer lies within a plausible range between the two signals. The comparison procedures and the specification of these activation threshold values are described below.

As has already been explained with reference to the creation of reference variables, there are close relationships within the lateral dynamics variables and also between the transversal dynamic variables. Error detection is therefore divided into one section for the longitudinal dynamics: "error detection longitudinal dynamics“, and one section for transversal dynamics: "error detection transversal dynamics“ (Fig. 4-59).

The procedures for error detection are the same for every variable: The deviation of the sensor signal from the reference variable (relative of absolute) is calculated and then compared with specific threshold values. The reference variables are solely estimated values. Depending on the driving situation, extreme, short-term deviations may occur. This is the case particularly with large signal gradients, as a small phase delay here between the sensor signal and the reference signal can lead to a relatively large difference in both values. Error diagnosis must therefore allow for the error thresholds to be exceeded for brief periods. However, if this lasts for too long, it is an indication that there is an error.

Fig. 4-75 shows the structural principles of the evaluation process. First, the deviation is calculated (relative or absolute). If an error threshold is exceeded, then a constant value is output to the error memory. This is integrated up over time. As soon as the integrated signal reaches the value 1 in the error memory, the error signal is transmitted at the "error" output.

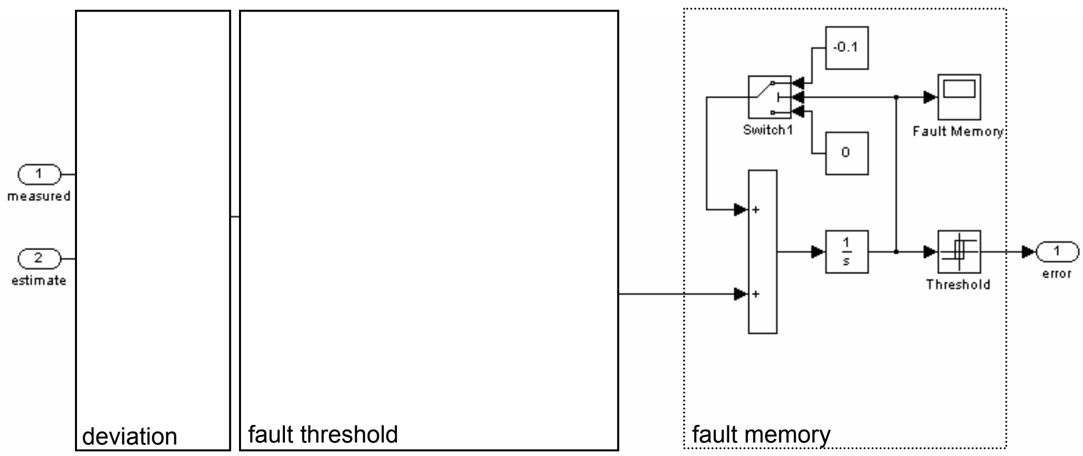

Fig. 4-75: Set-up of the failure detection

To prevent a brief deviation of the error threshold from triggering the error detection, a constant value is deducted from the error threshold signal in the error memory as soon as the content of the error memory exceeds zero. This causes the error memory to erase itself as long as the trigger threshold value 1 is not exceeded. A constant defines time period for erasure. Fig. 4-76 shows by way of example how a brief crossing of the error threshold of 0.1s effects signal transmission of the error threshold and the error memory during that time.

If the error threshold is exceeded for a longer time period, however, the error memory reaches the limit value of 1, an error is signalled and the driving dynamics controller deactivates. This can be seen in Fig. 4-77, where the error signal is activated approx. 1.2 s after reaching the error threshold of 1.

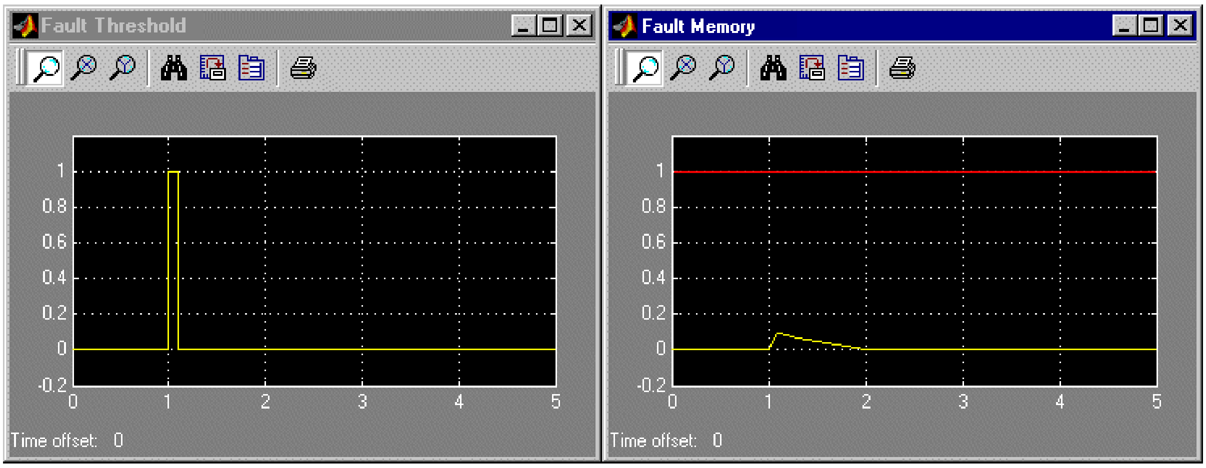

Fig. 4-76: Signal of fault threshold and fault memory for a short exceeding

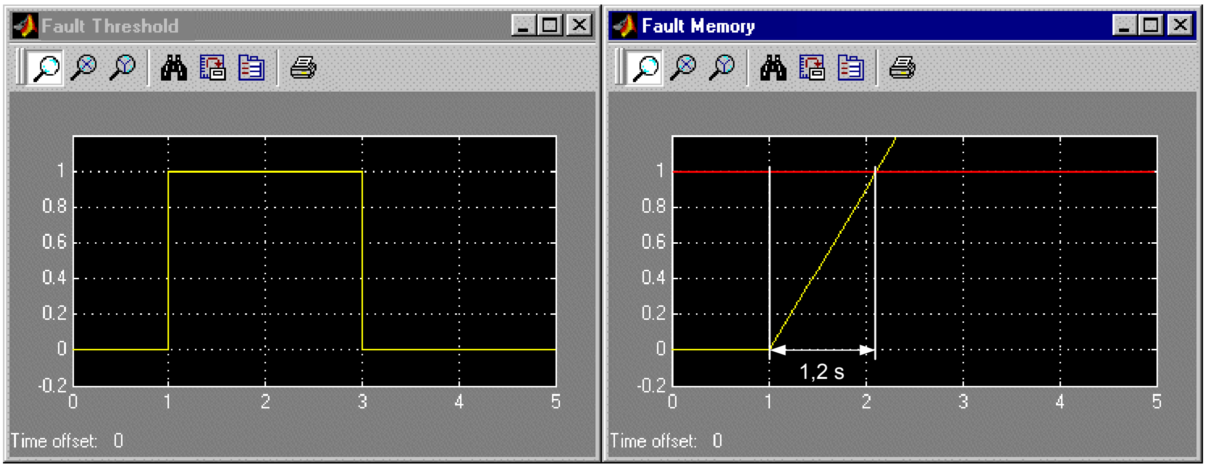

Fig. 4-77: Signal of fault threshold and fault memory for a long exceeding

The threshold for the start of error integration and the constant for deletion of error memory are defined on the basis of simulations of various driving manoeuvres, both with sensors intact, as well as with errors added to the sensor signals. The threshold values are adjusted so that the error detection reacts quickly and reliably when errors appear and does not deactivate driving dynamics during extreme driving manoeuvres when the sensor signals are appropriate. Threshold values and constants are defined for each error monitoring block in such a way that an error message is always sent when the error memory reaches the value 1. The error message is still output when the value of the error memory falls below 1.

The following describes how the error detection is adjusted for each sensor signal. Let us first examine the longitudinal dynamics.

- **Longitudinal dynamics**

In the "error detection longitudinal dynamics" block, the measured longitudinal acceleration is compared with the reference signal in Fig. 4-59 and the four wheel velocities are checked with the reference wheel velocities (Fig. 4-78).

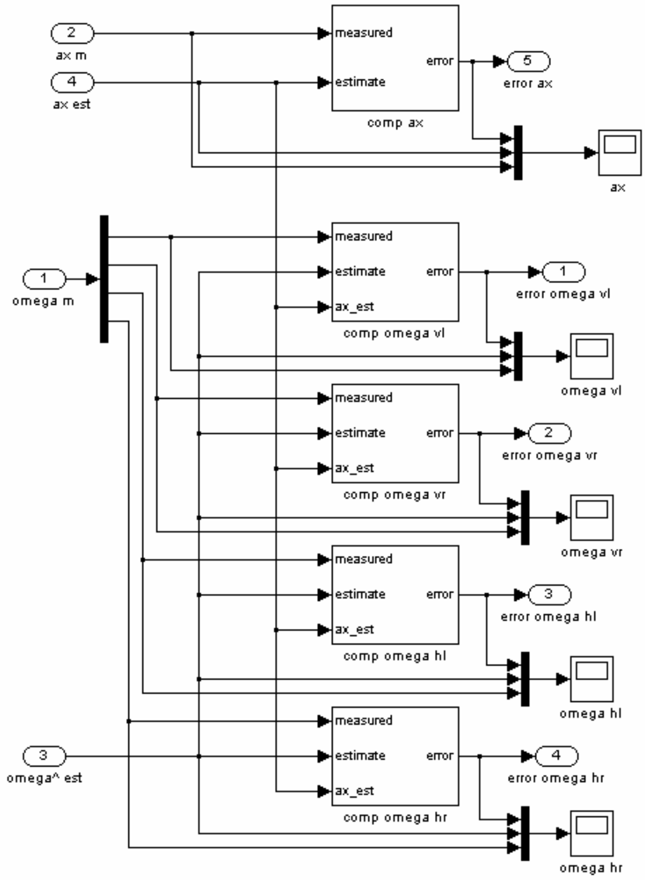

Fig. 4-78: Subsystem „Error Detection Longitudinal Dynamics“

As longitudinal acceleration changes its indicator when switching between braking and acceleration, the relative difference between the measured and estimated signal is very large in the zero point regions - even infinite at the zero point itself. The absolute difference between measured and estimated signal is therefore used here as the criterion for error detection. A difference of 1 m/s ² between the reference signal and the sensor signal is allowed as the error threshold. Since braking slip can cause the estimated signal to differ from the actual value of the longitudinal acceleration during strong braking interventions, the threshold value of 1.8 m/s ² is increased if there is a delay of than 0.5 m/s ². This distinction is created with two switches, which deactivate one of the two branches of the error threshold on the basis of the reference acceleration Fig. 4-79.

The constant signal of the error threshold has a value here of 1.2. 0.25 is used as the constant for deletion of the error memory.

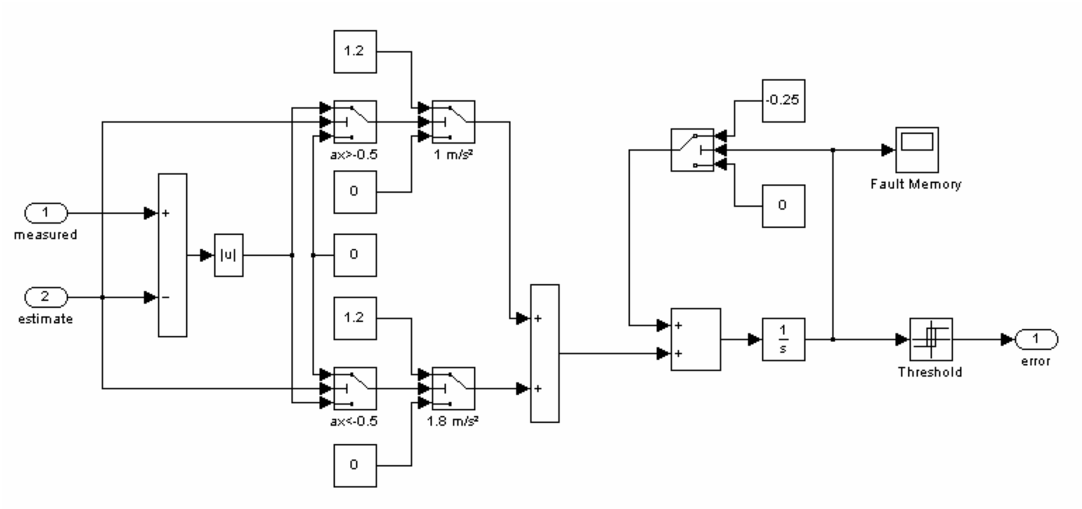

Fig. 4-79: Set-up of the subsystem „comp ax“

In Fig. 4-78 there are four blocks for monitoring the individual wheel velocities, "comp omega". Here, the wheel velocities are compared with the reference signal. As the structure of the four blocks is identical, their function is described using the front, left "comp omega fl" (Fig. 4-80) of the wheel velocity block.

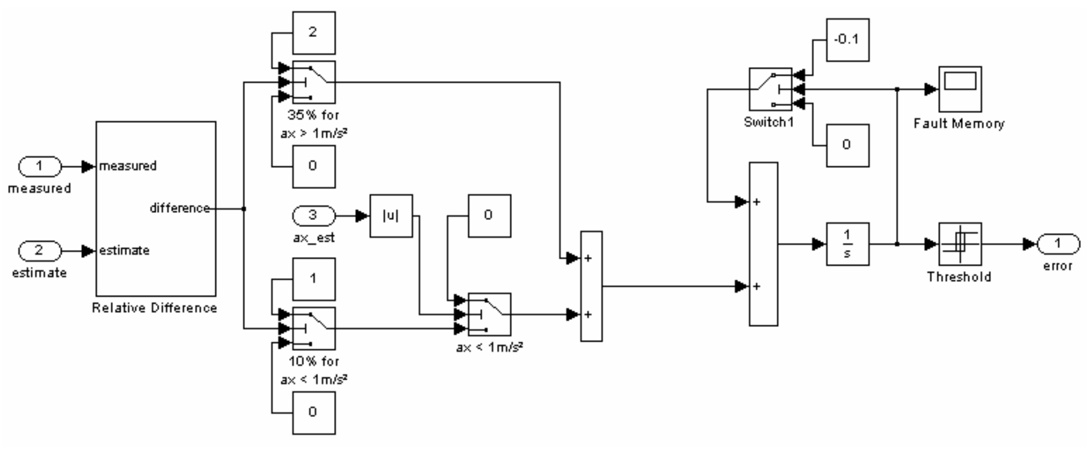

Fig. 4-80: Structure of the failure detection for the wheel speeds „comp omega fl“

Since the signal of the wheel velocities does not change its indicator like the other variables, there is no absolute difference here, but a relative deviation compared to the reference signal. There are two threshold values: If the deviation is more than 10% of the reference signal, then the value 1 is sent for integration into the error memory. If the measured signal deviated by around over 35%, which would be the case, for example, if the sensor failed completely, then the value 2 is integrated. This leads to a faster response to the error detection. Similarly, as in the longitudinal acceleration situation already described, when the ABS or the driving dynamics controller actuates, or during short-term spinning at the drive wheels, a relatively large difference may exist between the reference and measured variables without there being a fault. This is taken into account by the fact that the 10% threshold value for longitudinal accelerations or decelerations greater than 1 m/s ² is deactivated and replaced by a tolerance of 35%.

- **Lateral dynamics**

Lateral acceleration, yaw angle velocity and manual steering angle are monitored in the "error detection transversal dynamics" block (Fig. 4-81).

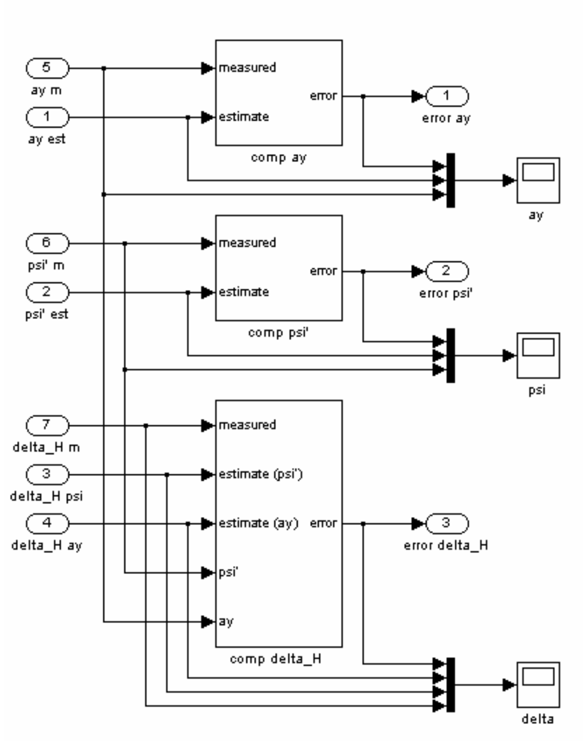

Fig. 4-81: Subsystem „Error Detection Transversal Dynamics“

The transversal acceleration sensor is monitored in the "comp ay" subsystem. (Fig. 4-82). Depending on the amount of reference lateral acceleration, there are four different threshold values for the absolute deviation of the estimated and measured signals. This enables the error detection to be sufficiently sensitive in the range of low lateral acceleration, while permitting larger tolerances in the area of higher lateral acceleration, where the estimated value can differ more strongly from the real value. The signal is checked in conjunction with the reference signal value, without having to compute a relative difference, which would be problematic in requiring a change of indicator. If the reference transversal acceleration is, for example, less than 0.1 m/s ² there is an increase in the error memory deviation of 0.3 m/s ². During very dynamic driving manoeuvres, where a_y is > 7 m/s², a deviation of 3 m/s² would be tolerated. If several threshold values are exceeded at the same time, a correspondingly higher vale is integrated into the error memory, leading to an earlier response to large deviations. For example, with an estimated lateral acceleration of 1 m/s ², a lateral acceleration deviation of around 2 m/s ² is measured. Both the threshold value of 1 m/s ² and the threshold value of 1.5 m/s ² respond, giving a value of 2 in each case. The value of 4 is integrated in the error memory, which halves response times to error conditions.

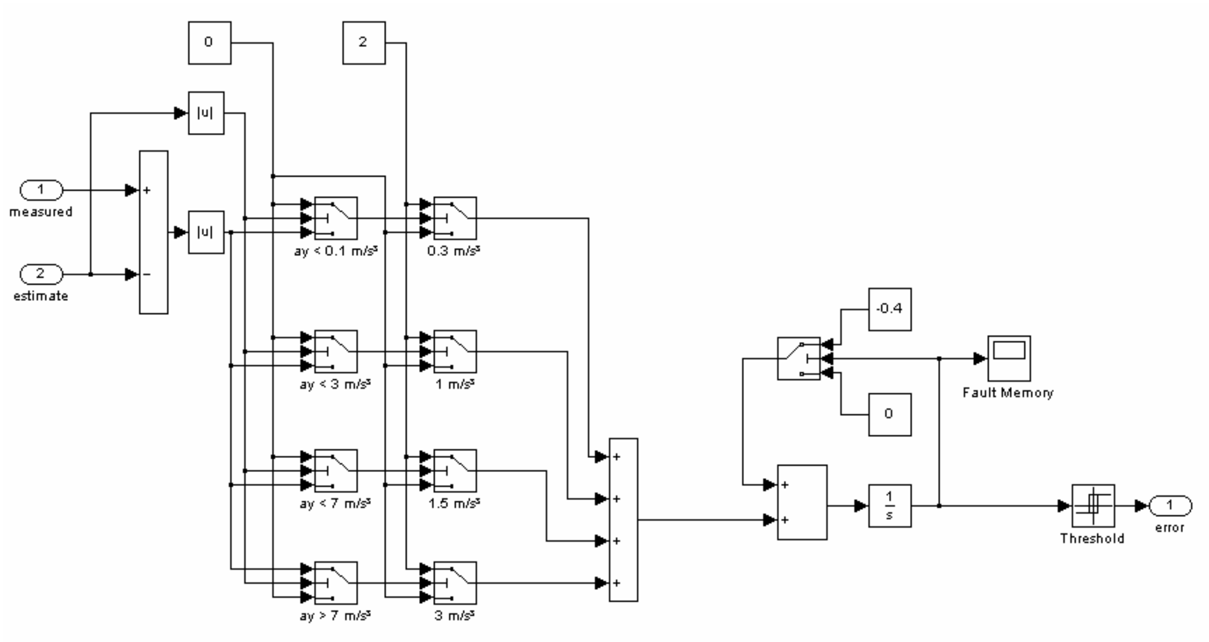

Fig. 4-82: Set-up of the subsystem „comp ay“

The error detection for the yaw angle speed is the same (Fig. 4-83), except that the error thresholds are adjusted appropriately.

The subsystem for monitoring the manual steering angle δ_H is rather more comprehensive. As described in Chapter 4.2.4.1, the system has two reference variables for the hand steering angle. In one, the reference variable is calculated from the measured lateral acceleration signal and in the other, from the yaw angle speed. Accordingly, there are two subsystems in the "comp delta_H" block, each of which monitors the steering angle using one of the reference variables.

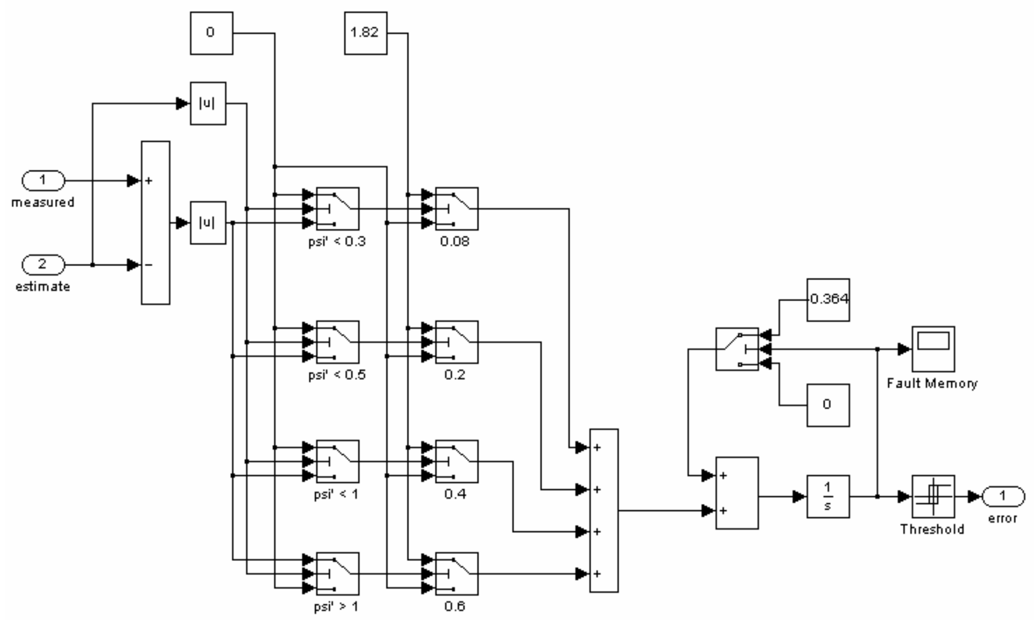

Fig. 4-83: Set-up of the subsystem „comp psi' "

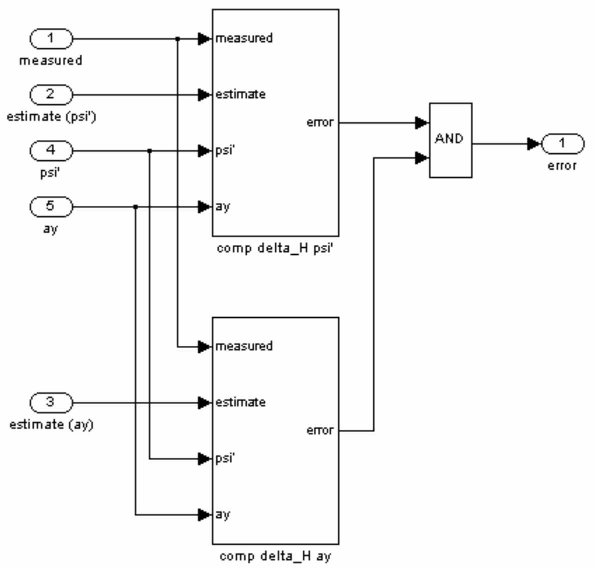

Fig. 4-84: Structure of the failure detection for the steering wheel angle δ_H

Both subsystems are identical in make-up, but each works with different input variables, that is, only one of the two reference signals. The structure of the subsystems is shown in Fig. 4-85.

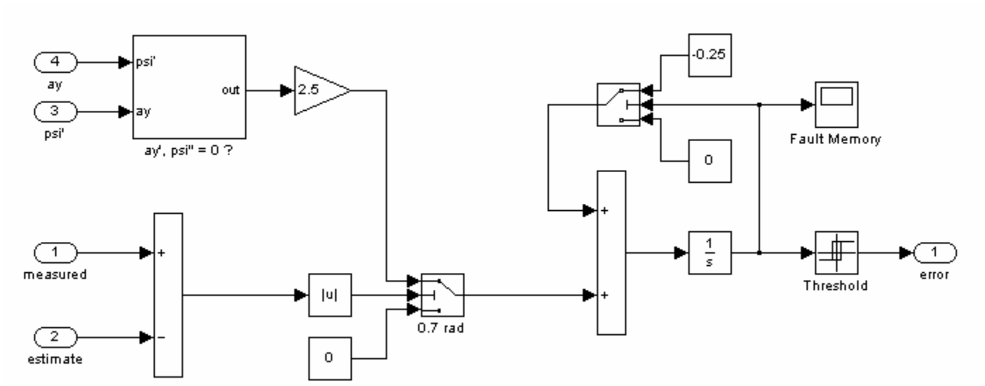

Fig. 4-85: Subsystem for monitoring the steering angle

As reference signal for the steering angle can only be satisfactorily estimated for a stationary vehicle, any reaction of the error detection must be prevented and the driving dynamics controller must be deactivated during dynamic manoeuvres. This function is provided, by sending a query to block „ay', psi'' =0 ?" as to whether the derivation of the variables a_y and $\dot{\psi}$ is equal to zero. This represents a satisfactory criterion for a stationary driving condition. In this kind of condition, the particular reference signal for the manual steering angle (from a_y or $\dot{\psi}$ is accurate enough. If the amounts of both derivations are sufficiently small, then the block outputs the value 1. If at least one derivation is too large, 0 will be output, preventing activation of error detection.

The AND unit in Fig. 4-84 which brings together the outputs of both subsystems, has the effect preventing error reporting unless both parts of the hand steering angle monitoring system recognize an error. This stops false alarms.

4.2.4.3 Error evaluation

There are eight error detection output channels each of which represents one error. These form the input variables of the error evaluation block - "error evaluation" in Fig. 4-59. Each of the eight channels can accept value 0 (for signal plausible) or the value 1 (signal error). When there is a signal error, it is task of error evaluation to send a signal to the driving dynamics controller indicating which sensor signal is faulty.

This task is made more difficult by the fact that, any error reported in one signal will quickly be followed by other error messages from other signals. The reason for this is that the reference variables will also be faulty and deviate from the measured signals, since these are derived from the faulty signal. After a certain time this can lead to the error thresholds being exceeded and to an error message. Error evaluation must also prevent such consequential errors from being stored in the error memory.

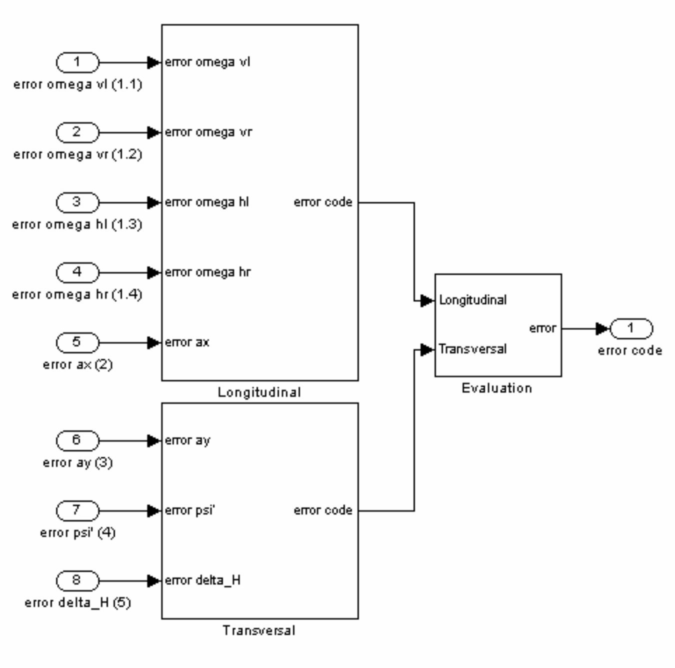

Fig. 4-86: Subsystem „Error Evaluation“

Error evaluation (Fig. 4-86), like error recognition, is divided in a section responsible for longitudinal dynamics (Longitudinal, Fig. 4-87) and a section responsible for lateral dynamics (Lateral, Fig. 4-88).

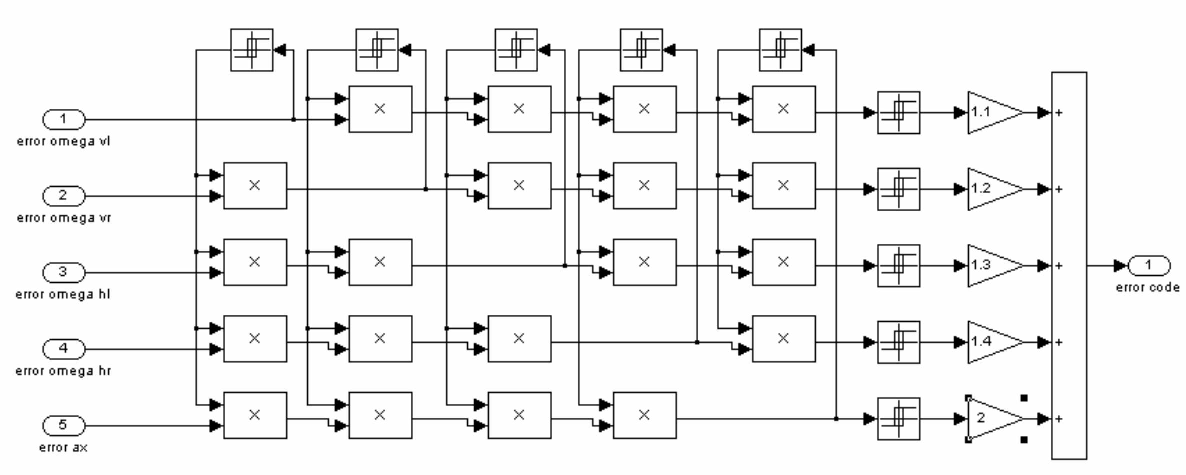

Fig. 4-87: Error evaluation for longitudinal dynamics

The longitudinal dynamics error evaluation creates a logical query as to which channel should report an error first. As long as the value of a channel jumps to 1, all other channels are set to zero. To prevent an error message from being deleted when a consequential occurs, the threshold block holds the signal at 1 once it has been activated. Finally, the error message is provided with the signal's code, which is then kept in the driving dynamics controller's error memory, allowing analysis of the error that has occurred.

The signal codes are organised as follows (Tab. 4-3):

longitudinal dynamics	
sensor	error code
ω_{vl}	1.1
ω_{vr}	1.2
ω_{hl}	1.3
ω_{hr}	1.4
a_x	2

lateral dynamics	
sensor	error code
a_y	3
$\dot{\psi}$	4
δ_H	5

Tab. 4-3: Assignment of the error codes

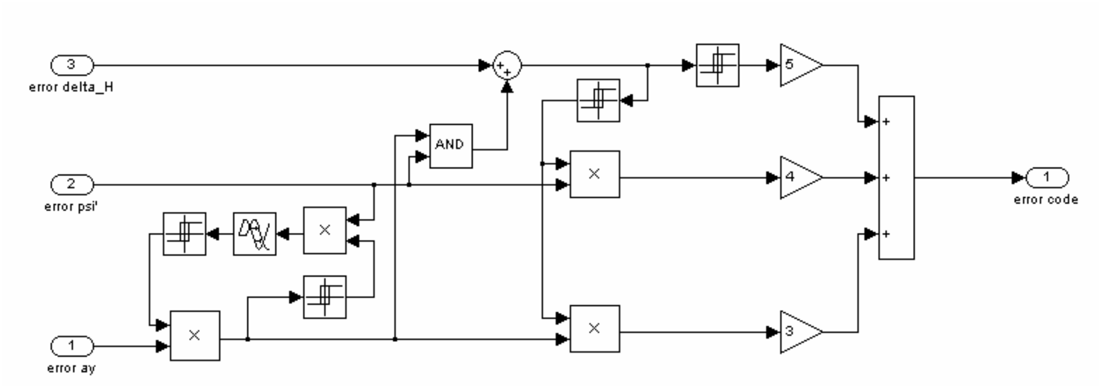

Fig. 4-88: Failure evaluation for lateral dynamics

For the lateral dynamics, the evaluation of the error signals is rather more complicated. As there is no reference signal for the manual steering angle in stationary situations, an error of the hand steering angle is recognized when an error is reported both for a_y and for $\dot{\psi}$.

According to simulations, the following logical rule is ideal:

- If an error is reported for δ_H, the two other channels are set to zero and error 5, the manual steering angle is output.

- If an error is reported for $\dot{\psi}$ error 4 (yaw angle speed) is output. If another error message is received for the manual steering angle, then the output is switched to error 5. The same applies for transversal acceleration, if the error signal for a_y arrives within 0.1 s. of the error signal for $\dot{\psi}$.

- If an error is reported for a_y, error 3 (lateral acceleration) is output. If another error message is received for δ_H or $\dot{\psi}$, the output is switched to error 5.

Finally, an evaluation is undertaken from the third block Fig. 4-86, designated "evaluation", to decide which part of the error evaluation ("longitudinal" or "transversal") should report an error first. This first error is passed to the outside, and any error message that may occur later in the other part, is ignored. Fig. 4-89 shows how the evaluation process is structured.

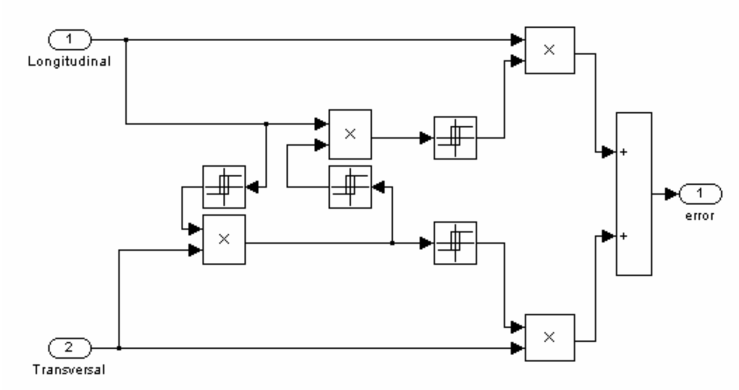

Fig. 4-89: Set-up of the evaluation between longitudinal and lateral dynamics

The function of the error analysis is checked with a total of 25 different driving manoeuvres, Tab. 4-4. There are 36 possible errors for each driving manoeuvres (Tab. 4-5) giving a total matrix of 900 combinations. The results of the simulations of driving manoeuvre no. 1 are listed in Tab. 4-6. The complete results of all simulations are listed in the appendix (Tab. 8-1 to Tab. 8-25). The numbers given stand for the time in seconds that has passed between the occurrence and the recognition of the error.

For the double lane changing driving manoeuvre, the error occurs at the beginning of the simulation. At the sinusoidal steering and straight-ahead driving it takes 5 s to settle down and produce comparable driving conditions; for the step steer input and steady state cornering it takes 30 s.

Some simulations with error occurrence in the lateral dynamics variables are entered as a combination in two times. This means that the error with the smaller time value is recognized first, which immediately results in the driving dynamics controller being switched off. Later, a further error is recognized and interpreted as an error in the steering angle. A hyphen "-" stands for a combination of error and driving manoeuvre, which cannot be recognized, e.g. a zero or negative error, when the corresponding variable is zero during the entire driving manoeuvre. An „x“ stands for an error that is not recognised by the error analysis.

Nr.	driving maneuver	parameters	results
1	**sinusoidal steering input**	0,1 Hz steering frequency	Tab. 8-1
2	v = 70 km/h	0,5 Hz steering frequency	Tab. 8-2
3	amplitude δ_H = 52°	1 Hz steering frequency	Tab. 8-3
4	**step steer input**	v = 40 km/h	Tab. 8-4
5	δ_H = 52°	v = 70 km/h	Tab. 8-5
6		v = 140 km/h	Tab. 8-6
7	**steady-state cornering**	v = 40 km/h, R = 60 m	Tab. 8-7
8		v = 70 km/h, R = 95 m	Tab. 8-8
9		v = 140 km/h, R = 250 m	Tab. 8-9
10	**double lane change (open-loop)**	v = 45 km/h	Tab. 8-10
11		v = 50 km/h	Tab. 8-11
12		v = 55 km/h	Tab. 8-12
13		v = 60 km/h	Tab. 8-13
14		v = 65 km/h	Tab. 8-14
15	**double lane change (closed-loop)**	v = 45 km/h	Tab. 8-15
16		v = 50 km/h	Tab. 8-16
17		v = 55 km/h	Tab. 8-17
18		v = 60 km/h	Tab. 8-18
19		v = 65 km/h	Tab. 8-19
20	**straight line driving (open-loop)**	v = 50 km/h	Tab. 8-20
21		v = 100 km/h	Tab. 8-21
22		v = 130 km/h	Tab. 8-22
23	**straight line driving (close-loop)**	v = 50 km/h	Tab. 8-23
24		v = 100 km/h	Tab. 8-24
25		v = 130 km/h	Tab. 8-25

Tab. 4-4: List of the driving maneuvers

Only the noise of the variance 30 rad/s at driving speeds above 100 km/h is not recognized in the simulations described. If we look at the signal path of the signal affected by noise, however, we notice that, in these simulations, the threshold value of 10% deviation is seldom exceeded and even then only for very short periods. A higher noise level would also be recognized in these driving situations. Moreover, the affected signal of the wheel velocity sensors does not cause any false intervention by the driving dynamics controller.

In a few combinations of double lane changing with errors in the lateral dynamic variables it is possible an error to be interpreted incorrectly. In driving manoeuvre no. 15 we see a situation where error messages for lateral acceleration followed by error messages for yaw angle speed are interpreted as an error in the yaw rate sensor. In driving manoeuvres 14 and 19 respectively double lane changing at 65 km/h, is recognized eight times as an error in the steering angle sensor instead of in lateral acceleration. Common to all these cases, however, is the fact that the driving dynamics controller was deactivated in good time.

Nr.	sonsor	failure	
1	**wheel speed front left**	zero	
2		offset	30 rad/s
3		noise	30 rad/s (variance)
4		drift 0,2 Hz	30 rad/s (amplitude)
5	**wheel speed front right**	zero	
6		offset	30 rad/s
7		noise	30 rad/s (variance)
8		drift 0,2 Hz	30 rad/s (amplitude)
9	**wheel speed rear left**	zero	
10		offset	30 rad/s
11		noise	30 rad/s (variance)
12		drift 0,2 Hz	30 rad/s (amplitude)
13	**wheel speed rear right**	zero	
14		offset	30 rad/s
15		noise	30 rad/s (variance)
16		drift 0,2 Hz	30 rad/s (amplitude)
17	**longitudinal acceleration**	zero	
18		negative	
19		offset	2 m/s²
20		noise	2 m/s² (variance)
21		drift 0,2 Hz	2 m/s² (amplitude)
22	**lateral acceleration**	zero	
23		negative	
24		offset	2 m/s²
25		noise	2 m/s² (variance)
26		drift 0,2 Hz	2 m/s² (amplitude)
27	**yaw velocity**	zero	
28		negative	
29		offset	0,25 rad/s
30		noise	0,25 rad/s (variance)
31		drift 0,2 Hz	0,25 rad/s (amplitude)
32	**steering angle**	zero	
33		negative	
34		offset	π
35		noise	π (variance)
36		drift 0,2 Hz	π (amplitude)

Tab. 4-5: Possible defects in the sensor signals

Overall, this indicates that an error was not recognized in 16 of the 900 simulations, which corresponds to 1.78%. In 8 cases (0.89%) the error was promptly recognized and the driving dynamics controller duly switched off, but an incorrect error message was sent to the error memory. In 97.33% of the simulated situations, the error analysis worked perfectly.

Sinusoidal steering 70 km/h

0,1 Hz			omega fl	omega fr	omega rl	omega rr	ax	ay	psi'	delta_H
omega fl	Zero		0.34							
	Offset	30 rad/s	0.34							
	Noise	30 rad/s	6.7							
	Drift	30 rad/s	1.38							
omega fr	Zero			0.34						
	Offset	30 rad/s		0.34						
	Noise	30 rad/s		6.7						
	Drift	30 rad/s		1.38						
omega rl	Zero				0.34					
	Offset	30 rad/s			0.34					
	Noise	30 rad/s			6.7					
	Drift	30 rad/s			1.38					
omega rr	Zero					0.34				
	Offset	30 rad/s				0.34				
	Noise	30 rad/s				6.7				
	Drift	30 rad/s				1.38				
ax	Zero						-			
	negative						-			
	Offset	2 m/s²					1			
	Noise	2 m/s²					2.69			
	Drift	2 m/s²					1.85			
ay	Zero							0.82		
	negative							0.6		
	Offset	2 m/s²						0.25		
	Noise	2 m/s²						0.42		
	Drift	2 m/s²						1.1		
psi'	Zero								1.48	
	negative								0.92	
	Offset	0,25 rad/s							0.3	
	Noise	0,25 rad/s							0.25	
	Drift	0,25 rad/s							1.78	
delta_H	Zero							0.6		1.4
	negative							0.6		0.9
	Offset	pi						0.62		0.65
	Noise	pi						0.45		10
	Drift	pi						0.64		0.88

Tab. 4-6: Simulation results of maneuver no. 1

4.2.5 Verification of the simulation results

The threshold values mentioned in the preceded chapter ensure that the intervention behaviour of the driving dynamics controller is comparable with a real system. Tuning is carried out with double lane changing on a dry and wet road. Both for the ESP of the Mercedes-Benz A Class (Fig. 4-90 to Fig. 4-95), and for the DSC of the BMW 3-Series (Fig. 4-96 to Fig. 4-101) there is a close correlation between driving test and simulation. The steering angle used for the simulations derives directly from the driving tests.

- **Mercedes-Benz A-Klasse**

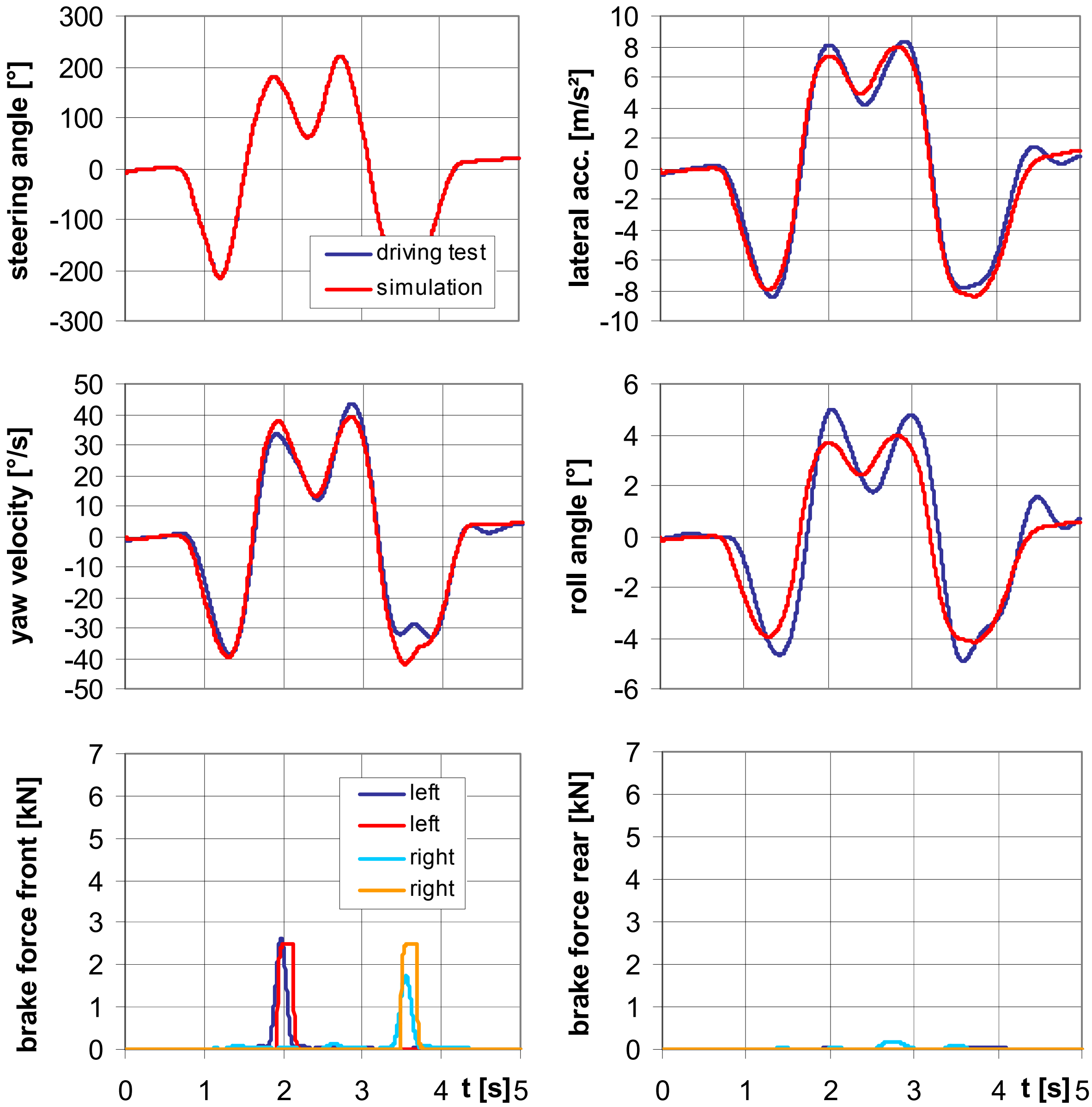

Fig. 4-90: Double lane change, 55 km/h, dry asphalt

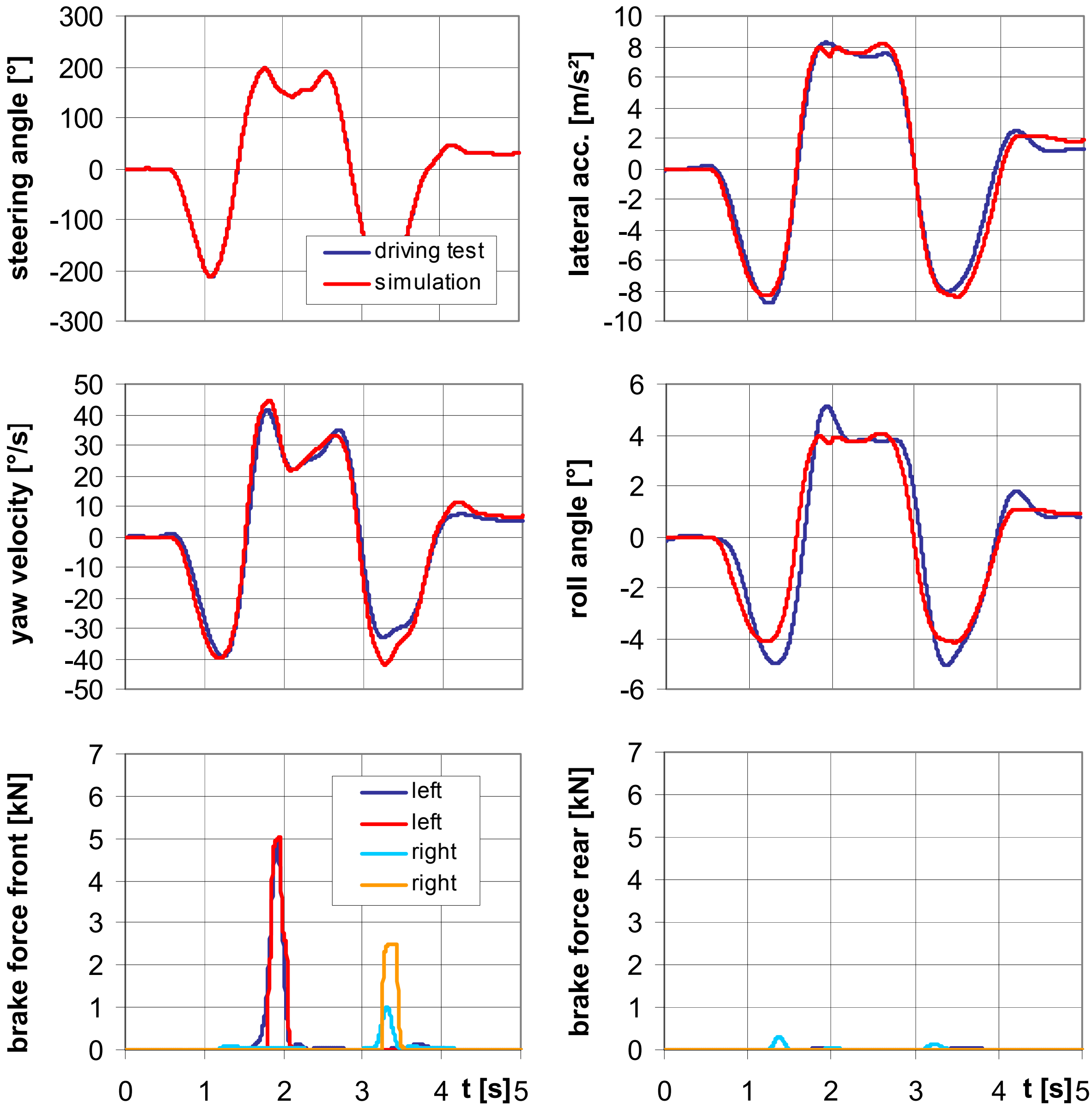

Fig. 4-91: Double lane change, 60 km/h, dry asphalt

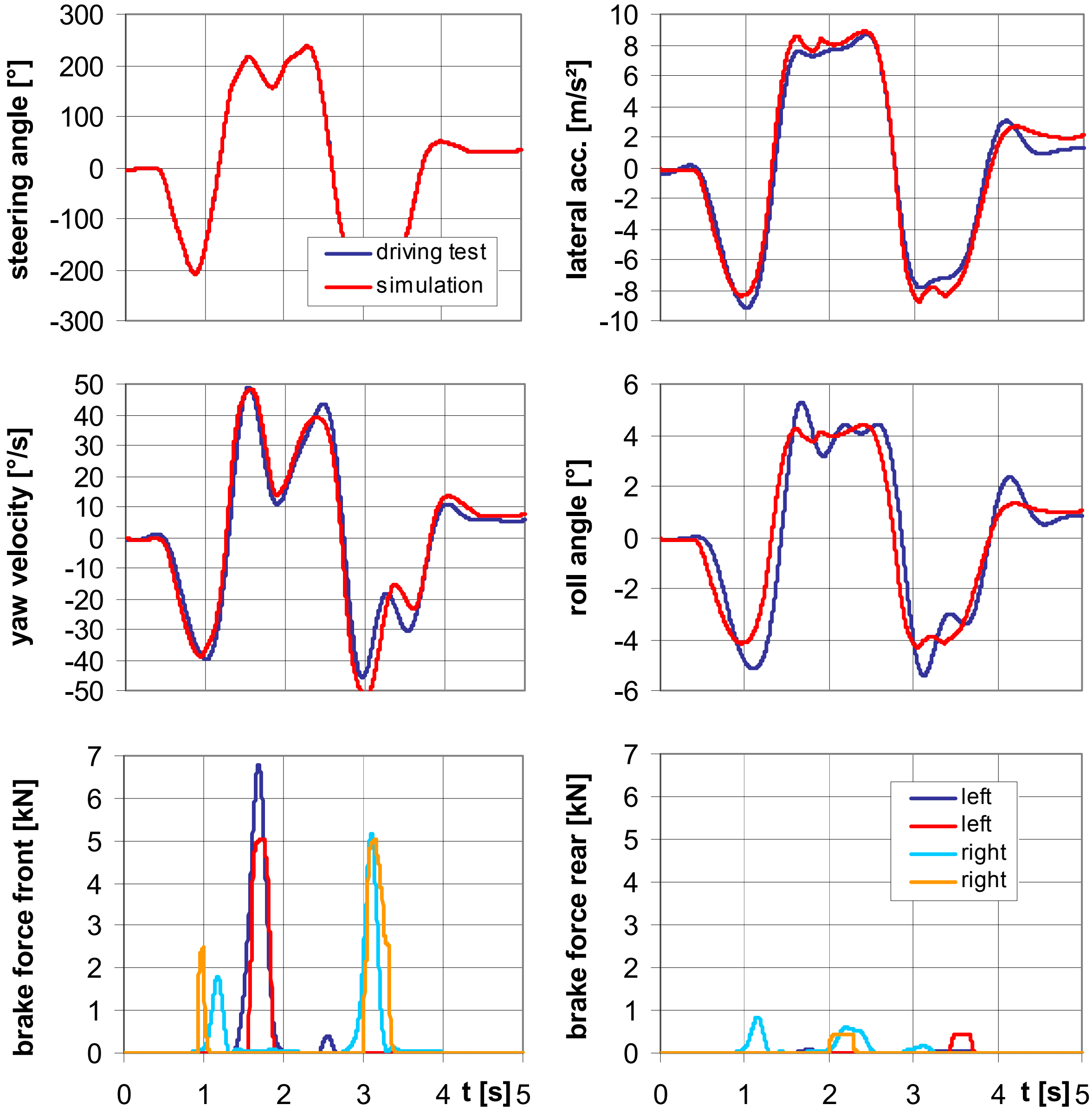

Fig. 4-92: Double lane change, 65 km/h, dry asphalt

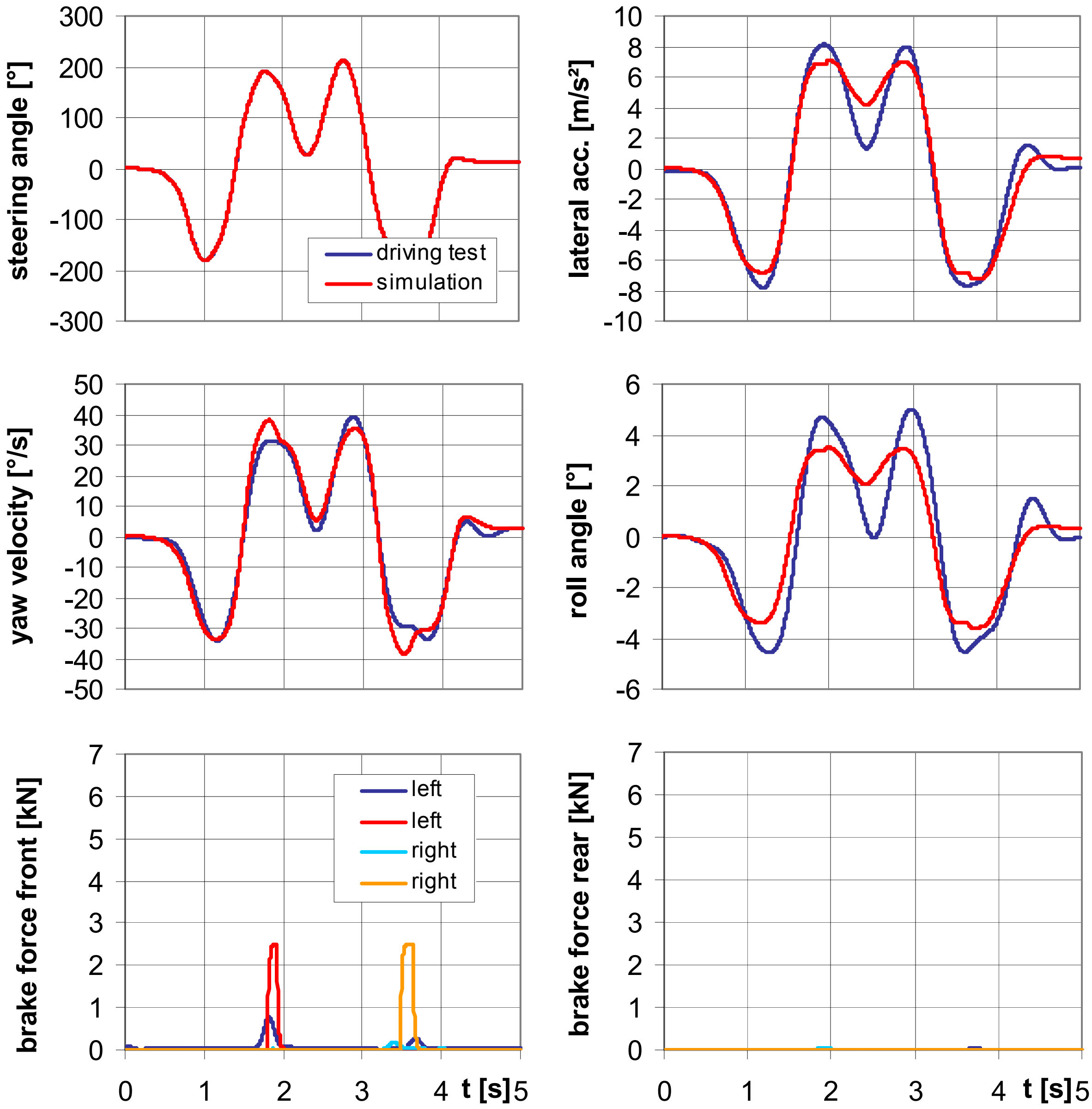

Fig. 4-93: Double lane change, 55 km/h, wet asphalt

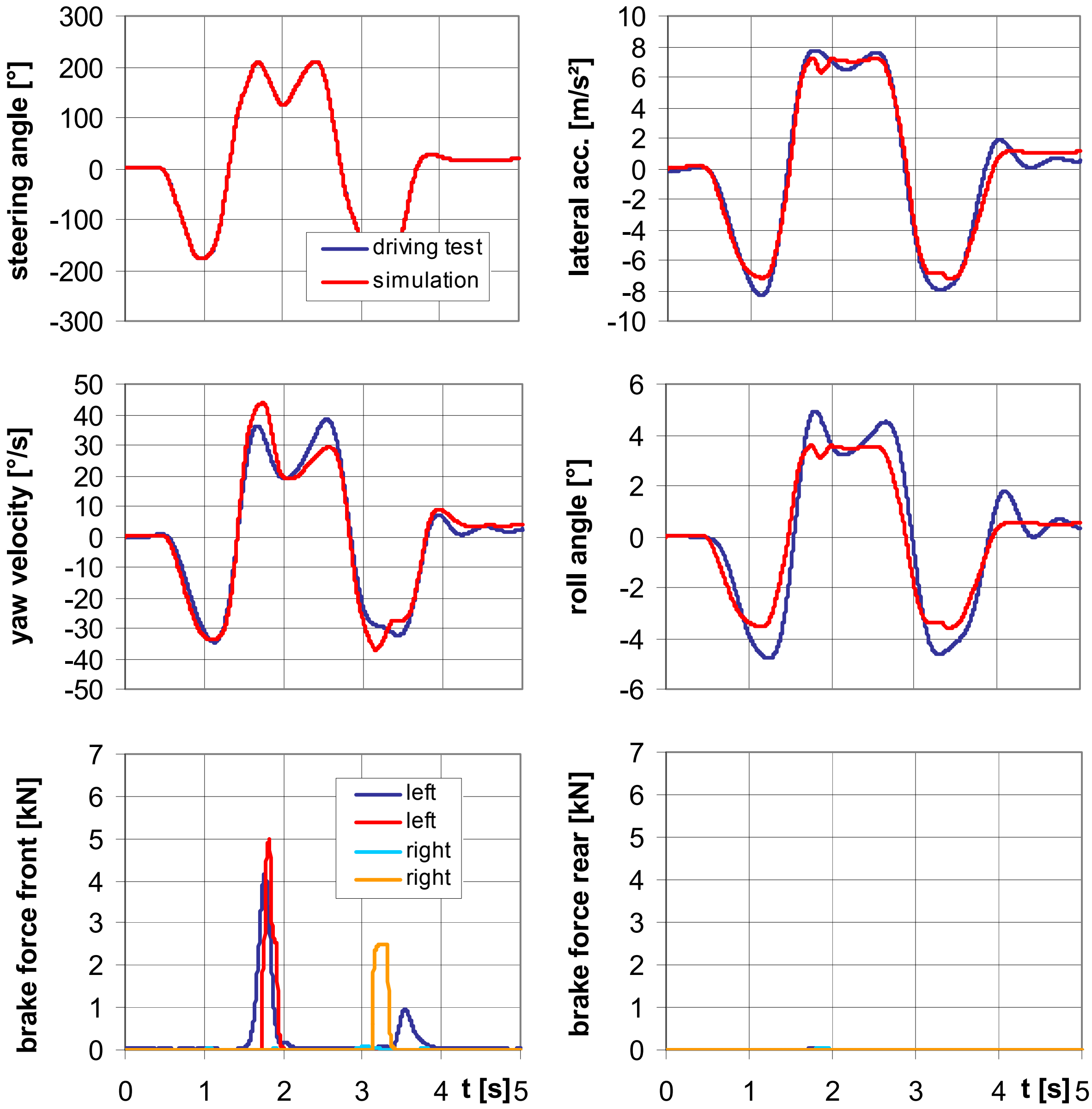

Fig. 4-94: Double lane change, 60 km/h, wet asphalt

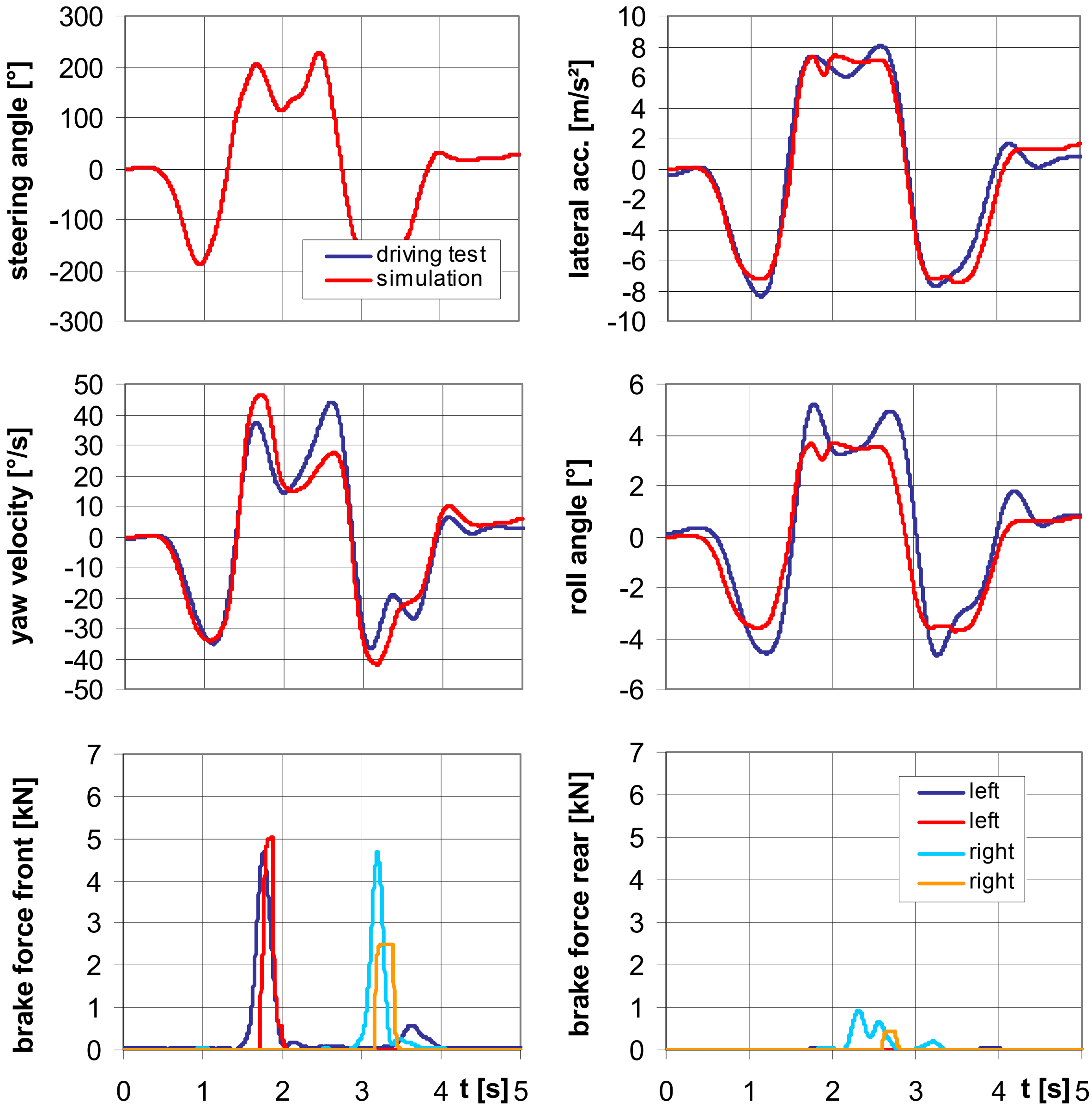

Fig. 4-95: Double lane change, 65 km/h, wet asphalt

- **BMW 330iX**

The BMW controller also can be very closely simulated with the controller model. In particular, the close agreement between the movement variables of yaw velocity and lateral acceleration shows that the controller model accurately simulates the timing and variables for the required braking interventions.

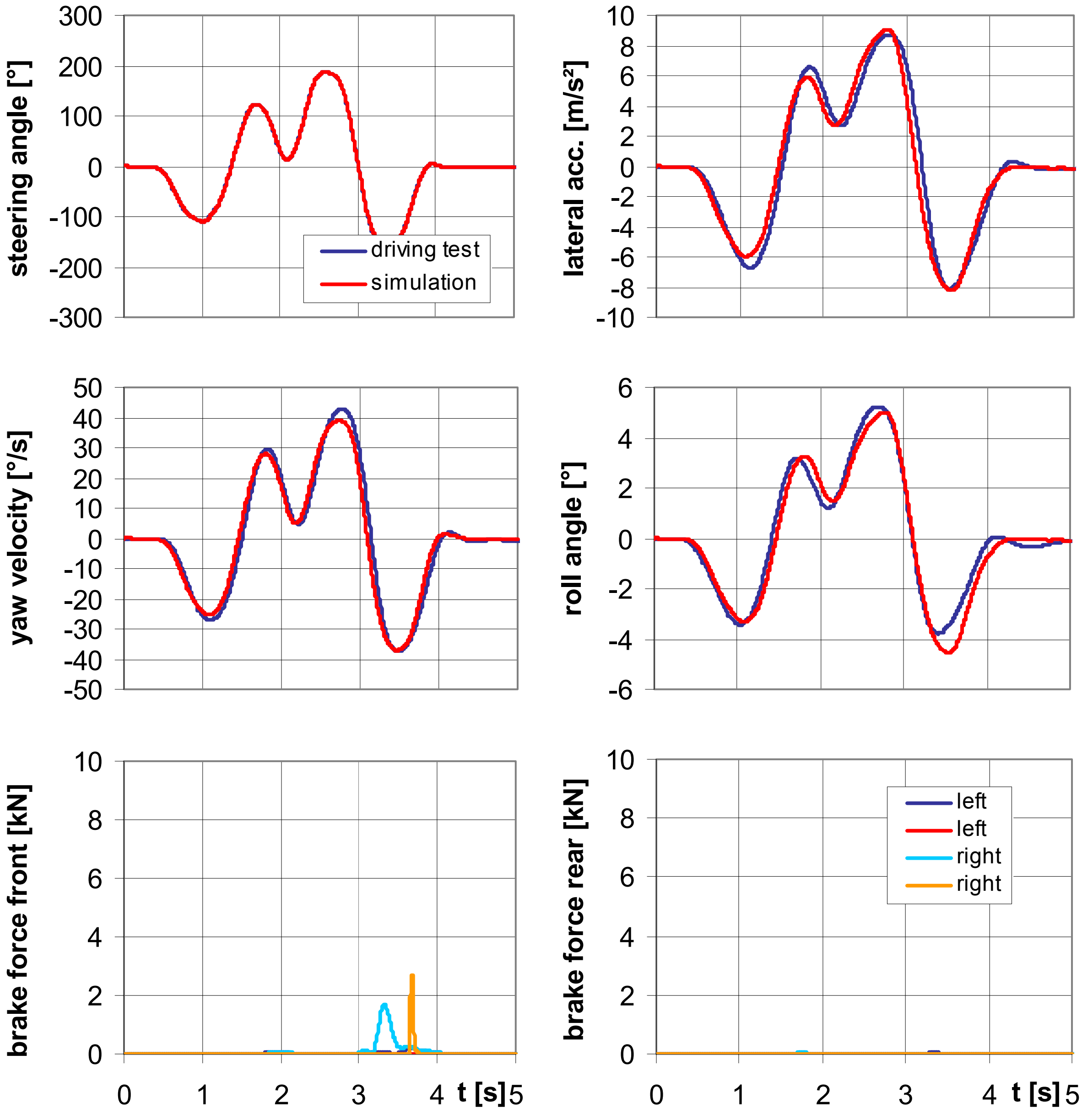

Fig. 4-96: Double lane change, 55 km/h, dry asphalt

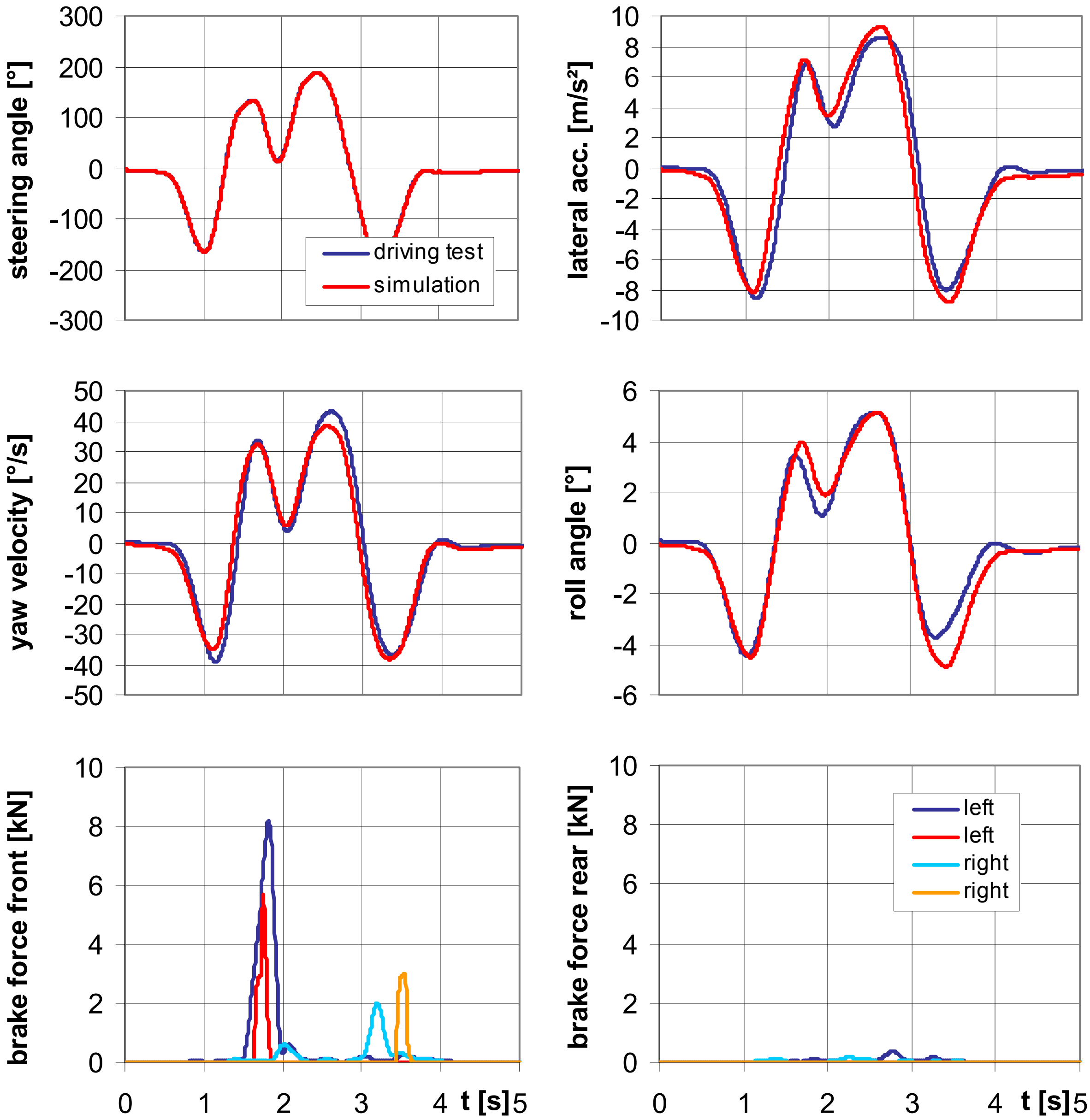

Fig. 4-97: Double lane change, 60 km/h, dry asphalt

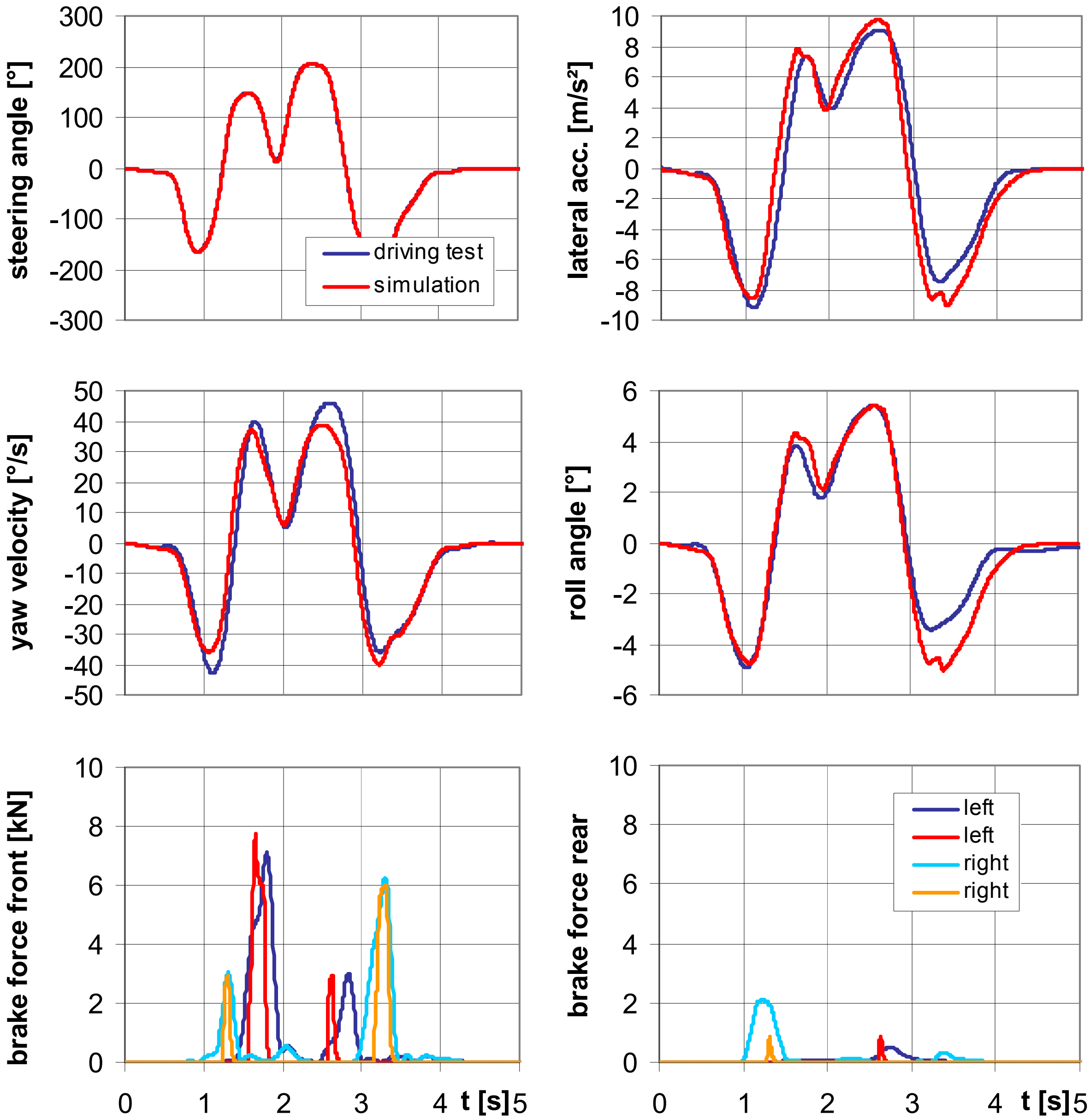

Fig. 4-98: Double lane change, 65 km/h, dry asphalt

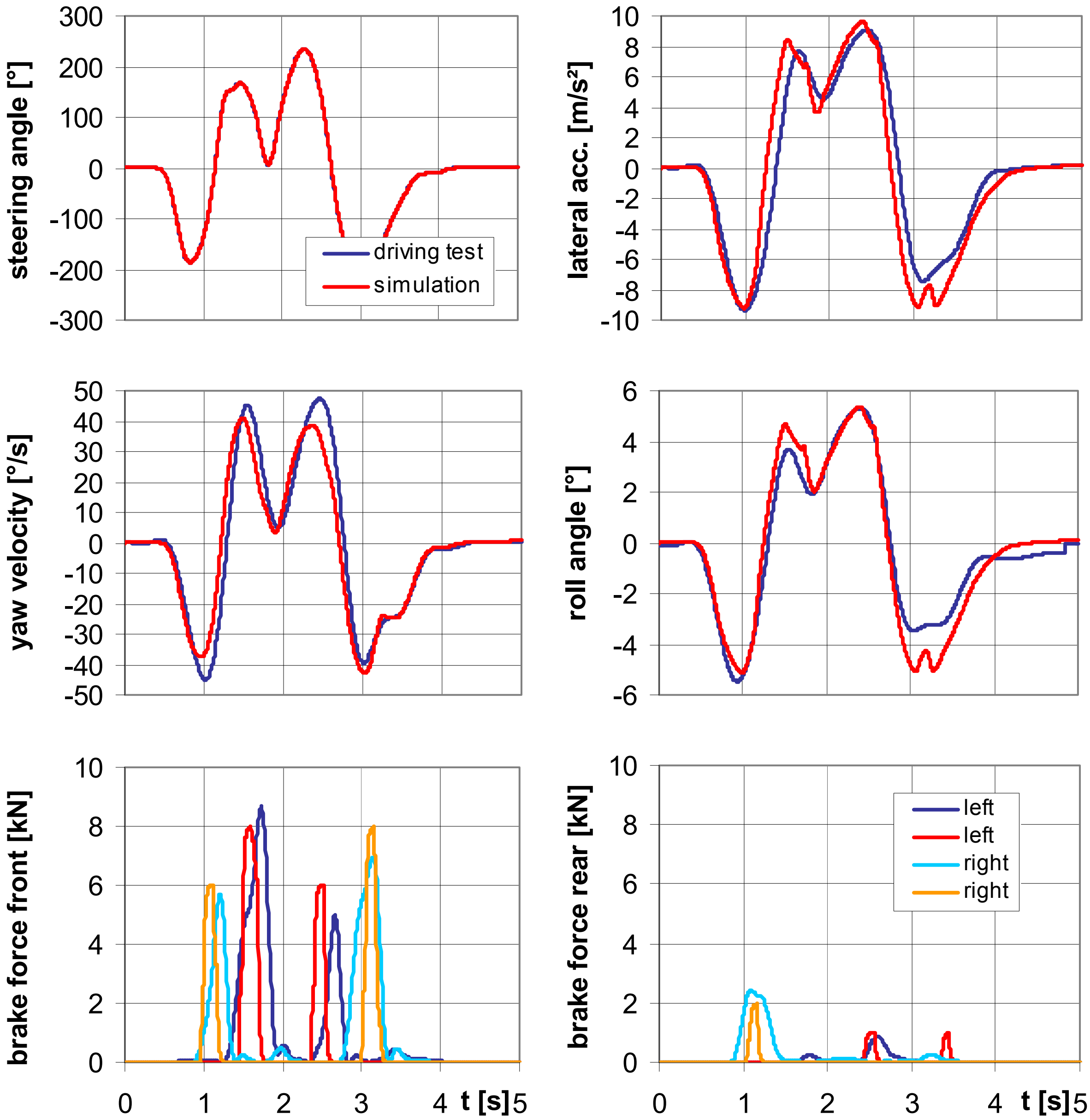

Fig. 4-99: Double lane change, 70 km/h, dry asphalt

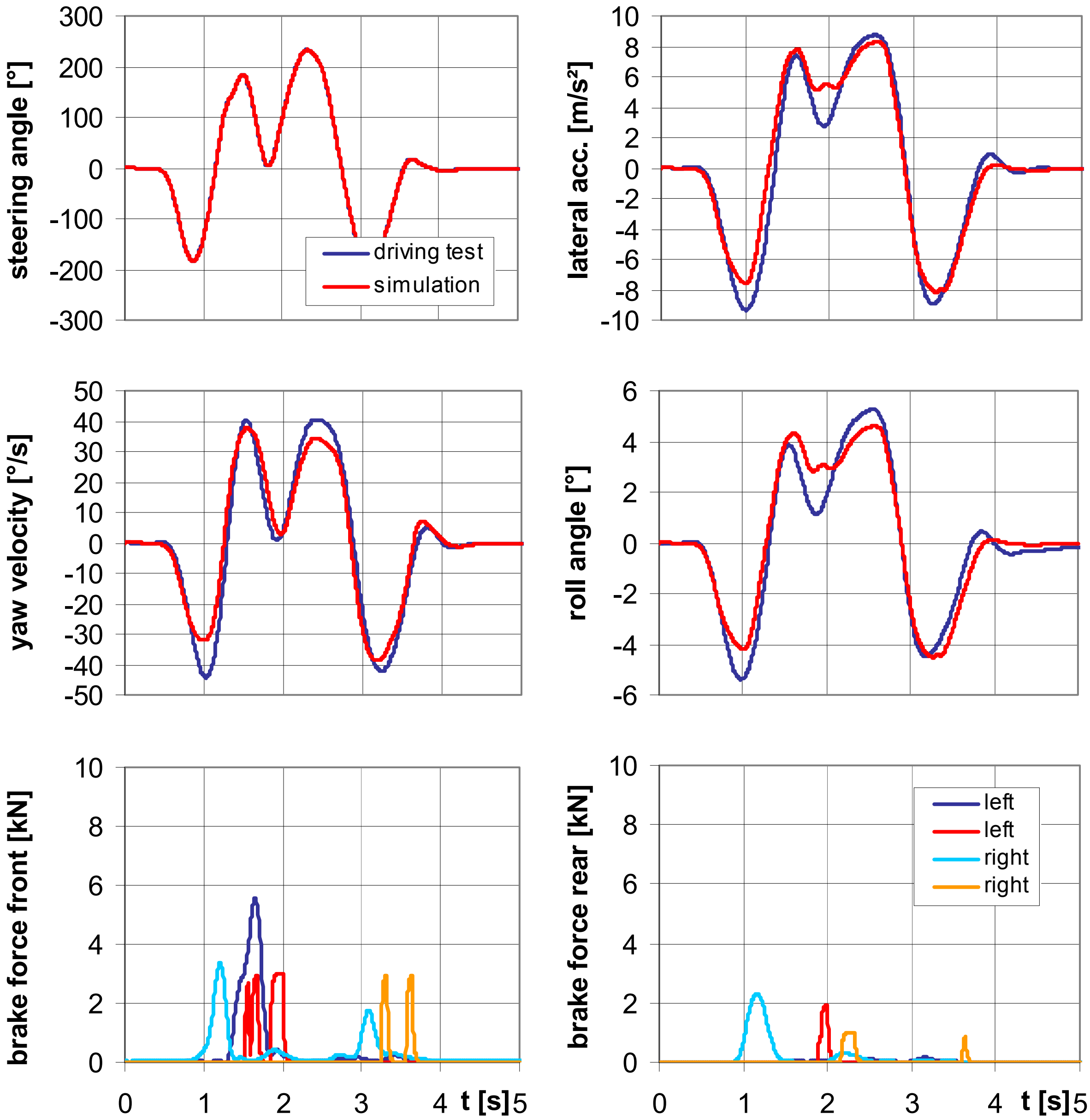

Fig. 4-100: Double lane change, 60 km/h, wet asphalt

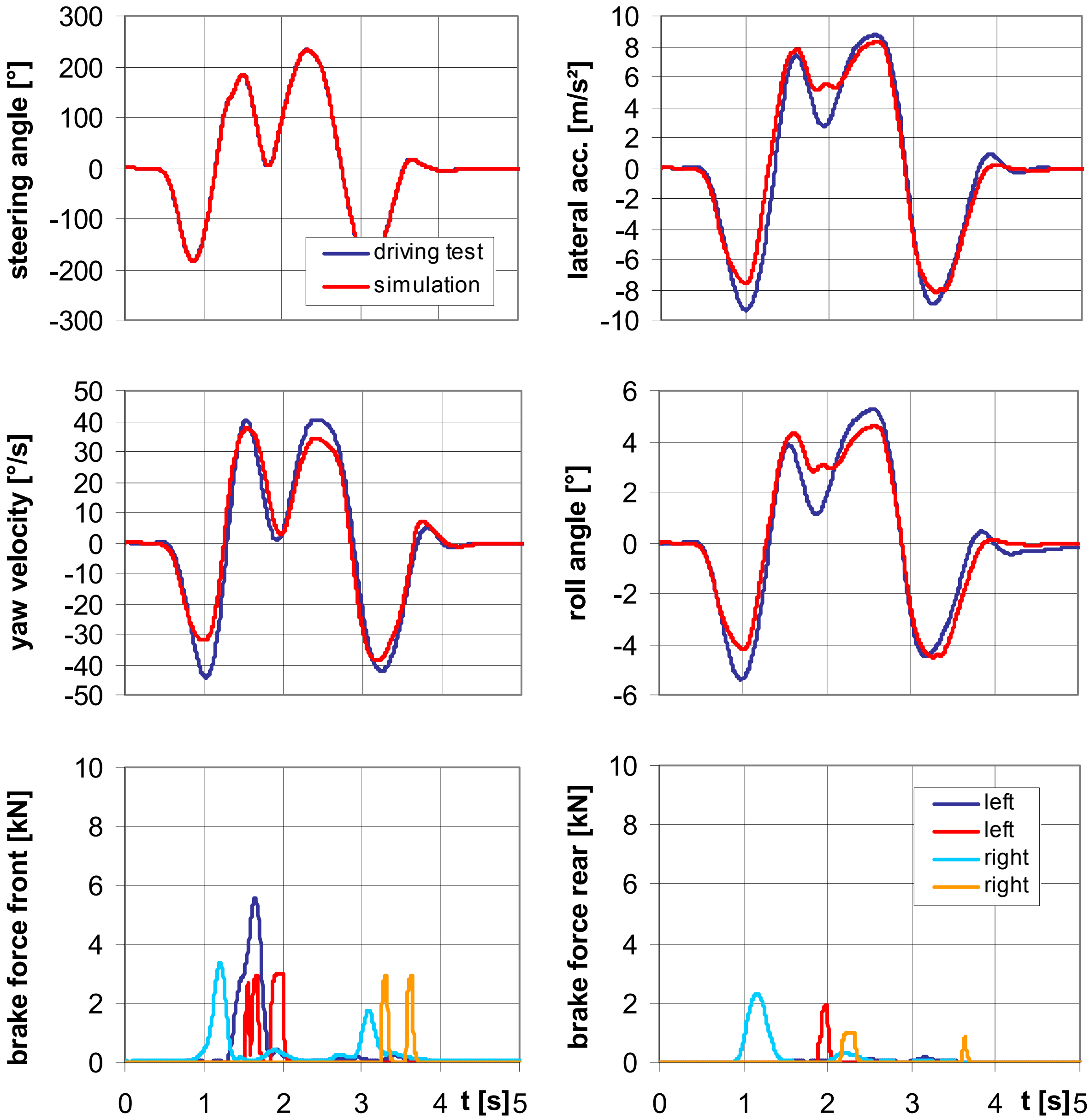

Fig. 4-101: Double lane change, 65 km/h, wet asphalt

5 Test procedure

Thanks to their built-in diagnosis routines, the electronically controlled systems in today's motor vehicles are monitored constantly. These routines monitor the correct functioning of hardware as well as the system peripherals (battery voltage, cable continuity etc. ...). In addition, sensor signals are cross-checked for plausibility and physical accuracy. If errors are diagnosed in the system, entry is logged in the system's error memory, and depending on severity of the error, the system is deactivated partly or completely. The driver is made aware of system deactivation either through illumination of the MIL (Malfunction Indication Light) or on a text message display.

The possibilities for the recognition of malfunctions within the system are limited, however. Self-diagnosis routines only cover about 70-80 % of the possible errors from [TRW01] for all electronically controlled systems.

In addition, problems can only be recognised, when they reach a certain degree of severity, Fig. 5-1. A "grey area" therefore exists between the functioning of all components within normal parameters (green) and the recognition of an error by self-diagnosis (red). In this "grey area", we would include the deterioration of certain system characteristics (wear and tear, corrosion, dirt, etc. ...) which the self-diagnosis system is unaware of, even though they influence the quality of the control system itself. This is confirmed both by tests on an ABS system, where electrical resistances were increased [IKA99], as well as through the simulation results which follow.

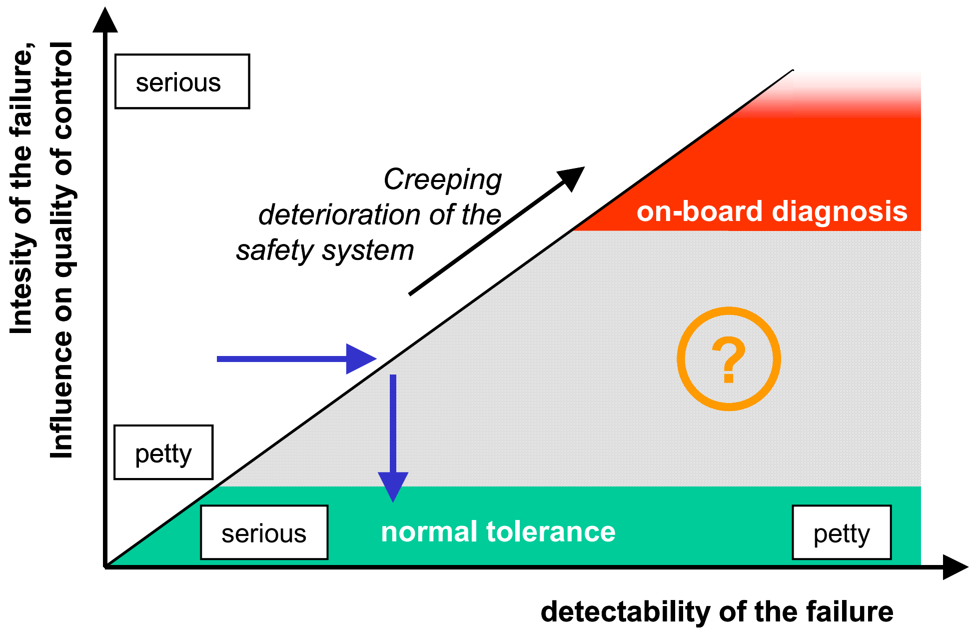

Fig. 5-1: Coherence between intensity of the failure and its detectability

For a vehicle test to be useful to the vehicle owner, it should assess both of these aspects:

1) There are limited options for self-diagnosis.
2) Creeping system deterioration is only recognized late in the day.

Also, vehicle manufacturers and suppliers are not happy using MIL as their only source of information. For quality testing purposes, suppliers carry out signal tests, in which it is necessary to peer "deep" into the system electronics in order to accurately assess the state of the control unit. [KLU99] Vehicle manufacturers test control units as they are delivered, in addition to testing on the production line (see Fig. 2-8). An extension of the test rig strategy described in Chapt. 2.2 is certainly conceivable, in which the vehicle would be subjected to an appropriate critical driving situation. The braking power occasioned by the dynamic movement of the rolling road could then be measured directly at the wheel Fig. 5-2.

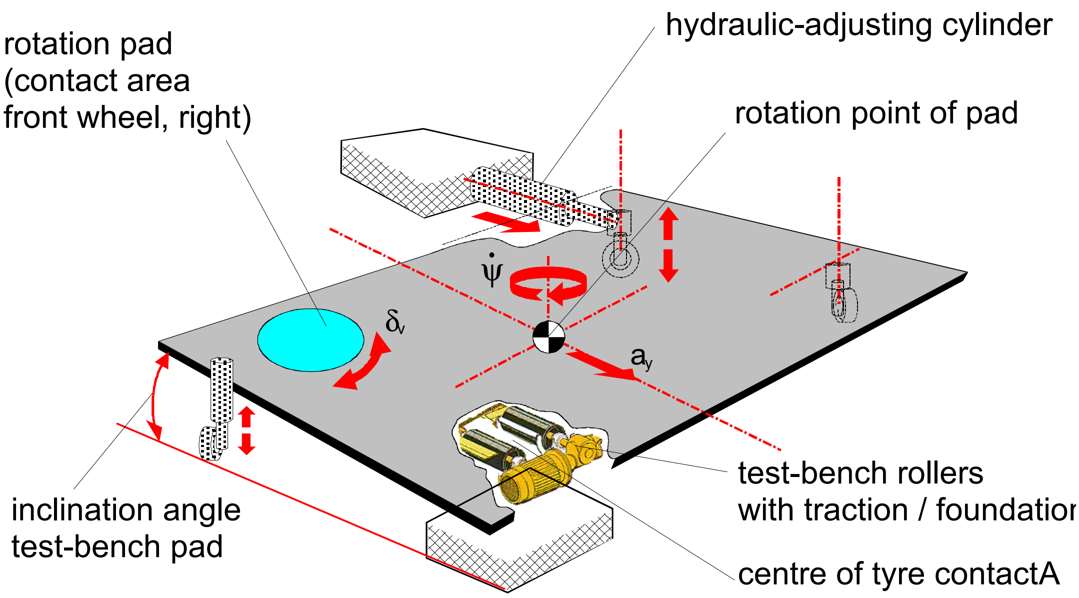

Fig. 5-2: Possible test-bench concept for a vehicle dynamics controller

However, both the tests of the suppliers and the test facilities of the vehicle manufacturers are an unsatisfactory starting point for any strategy of regular vehicle inspection, since detailed knowledge of a particular control unit is not relevant for vehicle inspection - not to mention the enormous space and cost requirements involved in acquiring such special test facilities. The same applies to driving tests. Their results are too subjective, require a good deal of space, and take too long. In some EU countries, vehicle inspection is carried out at the roadside. An examining procedure must be able to produce some meaningful results.

There are only four, practicable and respected strategies for the testing of electronically controlled systems as part of a regular vehicle testing procedure, Fig. 5-3. The first column documents the current situation which, for the above reasons, is considered an unsatisfactory solution for the future.

Warning device check	Communication with electronics via OBD-interface	Internal function test with mechanical influence	External function test with mechanical influence
Defined Faults are indicated by a warning device.	Defined Faults are indicated by a warning device. Additionally there is communication with the electronics.	Supplementary to the communication, test signals stored in the control unit are activated.	Supplementary to the communication, optional test signals are passed on to the control unit via a new interface.
Advantage: • Inexpensive method.	**Advantage:** • Inexpensive method, as interface exists in OBD. • Information about installed systems available (tamperproof).	**Advantage:** • High quality of Information. • Fast testing. • System safety, as no outside intervention occurs. • Information about installed systems available (tamperproof).	**Advantage:** • High quality of Information. • High test variability • Information about installed systems available (tamperproof).
Disadvantage: • No reliable information about the function of the systems. • No information about installed systems (less tamperproof).	**Disadvantage:** • No reliable information about the function of the systems.	**Disadvantage:** • More expensive than a mere fault read out.	**Disadvantage:** • More expensive, as technical modifications are necessary. • Enhanced risk due to possible access to hardware and software (intentional and involuntary).

Fig. 5-3: Concepts of tests during periodic vehicle inspection

The second column represents the current state of the technology. Since January 2000, all newly registered vehicles must comply with the EURO IV standard for exhaust gas quality. This is achieved with help of so-called OBD systems (on-board diagnosis) which permanently monitor the most important parameters of the vehicle's exhaust system. Part of the OBD system is a standardized interface, through which the system's error memory and the readiness code can be read, (The readiness code shows whether specific self diagnostic routines can be carried out). The valid norm - ISO 14230 "Keyword Protocol 2000" - is a general solution for all control units implemented on a serial databus (e.g. CAN bus). A standard interface has thus been available since the beginning of 2000, providing access, from a purely technical point of view, to the diagnostic functions of all control units (error memories, sensor values etc.....) as long as they are connected to the vehicle's CAN bus.

In reality, of course, the interface does make it possible to access the OBD system. However, only supplier-specific diagnostic test equipment can analyse other control units supplied by the manufacturer. From a technical point of view, it should be easy enough to check at least whether the built-in electronics components are present and work together properly. But it is still not possible to make any judgement as to the efficiency of the systems. For this reason, simply being able to communicate with the vehicle electronics cannot be considered a satisfactory inspection strategy.

A further inspection option involves storing test signals in the control unit. A simple diagnostic tool with the necessary interface (for example the current OBD components) would be capable of retrieving these test signals. The responses of the electronically controlled system would then be measured and compared with standard responses using available dynamic test facilities such as brake testing rigs. The advantage of this approach is that physical tests are carried out. This form of testing is very safe, since the electronics always receive the appropriate signals and all relevant functions can be properly tested. Furthermore, vehicle manufacturers are not obliged to provide an access point for test signals but can design the test signals themselves according to the requirements of their own systems.

These requirements are not met when the test signals are provided externally (4th test option). This testing procedure could be structured very flexibly, although an interface would be necessary for inserting test signals from the diagnostic equipment to the controller. This approach is expensive and prone to errors. This option only has benefits if the system responses measured are evaluated directly and serve as the basis for calculating of the next default values. This kind of "hardware in the loop" test rigs have become established for the development of electronically controlled systems. They are, however, too expensive for tests in the context of vehicle inspections.

Communication, in conjunction with the storage of test signals in the particular control units, is therefore considered the most expedient way to check electronically controlled systems, since real-life functional and operational testing can be carried out at acceptable cost.

Thus we have defined how testing should be carried out in principle. Yet to be defined are the overall scope of these tests and a strategy for testing the driving dynamics controller. Both of these are described in more detail in the following chapter.

5.1 Scope of testing

Electronically controlled systems consist basically of the following components:

- Sensors
- Cable harness
- Electronic Control Unit (ECU)
- Actuators

The main source or problems with electronically controlled systems are the sensors, the wiring and mechanical components, such as valves, pumps, etc. ...). The hardware is responsible for only 5% of the total number of the faults [TRW01]. However, a test of a vehicle's electronics should not be confined just to individual components like the sensors. All components should be checked.

Sensors

When checking a sensor signal, you must distinguish between the signal value and the signal quality (noise, drift, etc. ...).

a) Signal value

Signal values cannot for the most part be measured directly. For example, the whole vehicle must be tested to yaw velocity. Facilities that are already available, like the axle shaker, are not suitable for this.

However, signal results are constantly checked for plausibility by the control unit's self-diagnostic routines and are thus sufficiently well monitored. It only needs to be ensured that the self-diagnostic routines are properly carried out. This will always be the case as long as the hardware is in good condition (which is better checked in a different way, see below) and has been programmed correctly. This is scrutinized by the FMEA during vehicle homologation. It makes no sense to override badly defective signals and thus the operation of the self-diagnostic routines (indirect signal value check).

So-called master sensors are an exception to this (VDC: steering angle sensor). These sensors cannot be checked adequately by self-diagnosis, since they represent input variables for the control structures, to which all other signals refer. (An alignment of the steering angle sensor is unnecessary, since, even here, the steering angle can have arbitrary values.) For this reason master sensors currently perform their own self-diagnosis. For these reasons, a check of the signal values and the signal quality of sensors is recommended. Checking the signal values of the master sensors is advantageous, because they basically measure direct control variables of the driver and are therefore easily checkable.

b) Signal quality

Signals that have only slight noise or drift, or have a small offset are not yet classified as faulty (see Fig. 5-1). Such signals have considerable influence on the quality of the control system and can be symptomatic of the onset of problems. A judgment on the signal quality of all sensors should therefore be covered by the test procedure.

Cable harness

Direct measurement of individual cable resistances appears to have little benefit. Self-diagnosis carries out appropriate tests and will take action to protect the system from excessive resistance or broken wiring. Slight deterioration of the electrical characteristics of the cable harness that have not induced a reaction from self-diagnosis, but have noticeably impaired signal quality, can be included in a test of signal quality.

Electronic Control Unit

The entire control unit hardware is monitored by self-diagnosis, as all the other components ("Watch-Dog"). The control unit should store the history of the hardware test (similar to the readiness code of the OBD) in a separate memory. A reading from this memory stating that the hardware is working should be perfectly sufficient. Don't forget that every test of the complete system always includes a test of the control unit. Separate tests that only check the control unit functions do not seem particularly worthwhile.

Actuators

The actuators, on the other hand, are not adequately monitored by the vehicle's own electronics. For example, the trigger current to a valve is often checked. But you cannot check whether the valve will in fact actuate (e.g. corroded ABS valves). Any test procedure should certainly include the mechanical components of the electronically regulated systems. This is particularly important when you consider that these systems are sometimes only very rarely used (ABS, ESP) and that faulty actuators may remain unnoticed for a long time.

5.2 Testing stragegy

It has been stressed in the preceded chapter that it makes little sense in the context of the regular vehicle inspection to check whether the electronically controlled system actually works. This is already adequately ensured by the self-diagnostic systems. It is preferable to test how effectively the system is working, in order to diagnose system deterioration before the self-diagnostic systems are able to do so. The sensors and the wiring must be included in the test. We suggest the following testing strategy:

At the heart of the testing strategy for vehicle dynamics controllers should be a test for functionalily and effectiveness carried out on a brake test rig, during which test signals stored in the control unit are added to the sensor signals.

Since the vehicle is standing on the brake test rig, the vehicle's own sensors will all supply a signal value of zero. (Exception: rotational velocity sensors on the axle being tested. Which is easily taken care of). The test signals can be added as supplementary signals to the signals provided by the vehicle's own sensors. Noise or drifting or an offset of a sensor signal is still included in the test signal. This ensures that the signal quality of the vehicle's own sensor signals is taken into account in the test.

An alternative to this approach is offered by internal stimulation of individual sensors, to provide direct readings of sensor values. This method is already being used occasionally for sensor monitoring (e.g. ESP yaw rate sensor), see also Fig. 2-6. The advantage lies in the fact that the signal quality is considered not only at "zero". This approach is possible only with some sensors, since it is dependent on the measuring principle used.

The complete test procedure involves a mixture of data and sensor value readings, as well as the activation of the test signals. A diagnostic tool is needed here, which is able to communicate via a standard diagnostic interface with the vehicle electronics. In terms of features, this would be comparable with today's OBD testers. When this tool is initially connected to the electronics, it identifies the vehicle. Because of this identification, all the information required for the test can be downloaded from the Internet, for example, or from a workshop database. The test consists of four stages.

1) Hardware and software recognition

- You should first check if all system components are actually available, are suitable for the system under test and have correctly "identified themselves" to the control unit. To ascertain this, identify the hardware with the help of the diagnostic tools compare with the list of required hardware that you will be shown.

  -> *If individual components do not match the system, or are missing, the test has not been passed.*

- Check the version numbers of the software. An out of date piece of software should be replaced, with an upgrade if possible.

  -> *If an item of software cannot be installed, the test has not been passed.*

2) Reading the error memory and the readiness codes

- The error memory of the system is read out.

  -> *If there is an error, the test has not been passed (as OBD).*

- The readiness code for the hardware monitoring self-test is read out.

  -> *If the self-test has not been carried out for some time, the test has not been passed (as OBD).*

3) Testing the master sensor (steering wheel angle sensor)

- The value of the steering wheel angle sensor is read out with the steering wheel in its centre position and at the two extremes.

  -> *If the displayed value is not zero in the steering wheel centre position unequally or if the values at the two extremes do not agree with the standard values, the test has not been passed.*

- The quality of the steering wheel sensor signal (noise, drift, etc. ...) is measured with the steering wheel in its centre position.

  -> *If the quality does not agree with the manufacturer's specifications, then the test has not been passed.*

4) Effectiveness and function test with test signals

- At the start of the test procedure, the vehicle is driven with the front wheels on a conventional brake test rig, such as the one used for the brake test in the context of the regular vehicle inspection (the non-tested axle may have to be secured with brake chocks, see ABS). Using the diagnostic tool, the stored test signals for the front axle are retrieved and the braking responses of the system measured by the brake test rig.
- After completion of the front axle group of tests, the vehicle is driven onto the brake test rig with the rear wheels. The signals are then invoked, to cause the VDC to start braking interventions on the rear axle.
- An automated evaluation of predefined vehicle movement and measured braking force allows a reliable judgment to be made of the complete system.

  -> *If the braking force curves that have been measured do not agree with the standard curves, the test has not been passed.*

5.3 Test signals

The test signals are open-loop signals, which are stored directly in the control unit. This means that the examiner has only limited access to the control logic, that signals cannot be mixed up and that the vehicle manufacturer can guarantee that the test signals are actually designed for the control units.

The exact signal paths of all sensor variables are not fixed - only the associated driving manoeuvre and the expected system response. Depending on the vehicle, the test signals can be generated using knowledge of some basic vehicle parameters.

Different types of driving manoeuvre are consciously selected to provide as wide a range of stimulus signals as possible for judging the rule quality. Suggested driving manoeuvres for a driving dynamics controller test are listed and described in later sections.

5.3.1 Static test of yaw velocity control

The static tests of yaw velocity regulation are based on a steady state cornering with a constant radius R = 40 m at a constant driving speed of v = 54 km/h (15 m/s). This produces constant values for lateral acceleration a_y and yaw velocity $\dot{\psi}$. Both of these are calculated from radius of the track and the driving speed:

$$\dot{\psi} = \frac{v}{R} \qquad \text{Eq. 5-1}$$

$$a_y = \frac{v^2}{R} \qquad \text{Eq. 5-2}$$

The steering wheel angle can be calculated from the driving speed and yaw velocity, as with the bicycle model equation. The wheelbase l, the steering ratio i and the characteristic speed v_{char} represent vehicle-specific constants:

$$\delta = \frac{\dot{\psi}}{v} \cdot l \cdot \left(1 + \frac{v^2}{{v_{char}}^2}\right) \cdot i \qquad \text{Eq. 5-3}$$

The wheel velocities can easily be derived from the driving speeds. Since the driving speed is constant, the longitudinal acceleration is equal to zero. All the input variables of the driving dynamics controller have now been defined.

To induce the driving dynamics controller to act, a difference must be created between the actual and the target yaw velocity. The steering wheel angle is calculated from the latter. For the calculation of the steering angle according to Eq. 5-3 a deviation must be applied to the yaw velocity, which increases linearly up to the halfway point of the test, and then decreases. A critical driving situation is simulated in the calculation of the steering angle by this deviation in the yaw rate. Depending on whether the manipulated steering angle is too large or too small for the driving situation, and whether a right or left hand bend is provided, the driving dynamics controller reacts by applying the brakes at one of the four for wheels. The magnitude of the yaw rate difference is selected in such a way as to ensure that the full braking force is applied for a period of time. The duration of the manoeuvre is T = 10 s in each instance.

Fig. 5-4 to Fig. 5-7 show the result of four different driving situations for the Mercedes-Benz A-Class. The graphs for the BMW 330xi are the same. Also shown in the diagram of the yaw velocity, is the influence the braking force would have on the yaw movement of the vehicle, if it were to react to the movement of the vehicle. For this purpose, the lever on the vehicle's main centre of gravity multiplies the active braking force. The additional yaw velocity resulting from this is initially integrated and then deducted from the standard value for the yaw velocity. This calculation is carried out as long as the driving dynamics controller provides braking power. It is easily seen how the amount of the yaw velocity is reduced during driving manoeuvres with a tendency towards oversteer. Conversely, during driving manoeuvres tending towards understeer, the amount of yaw velocity is increased.

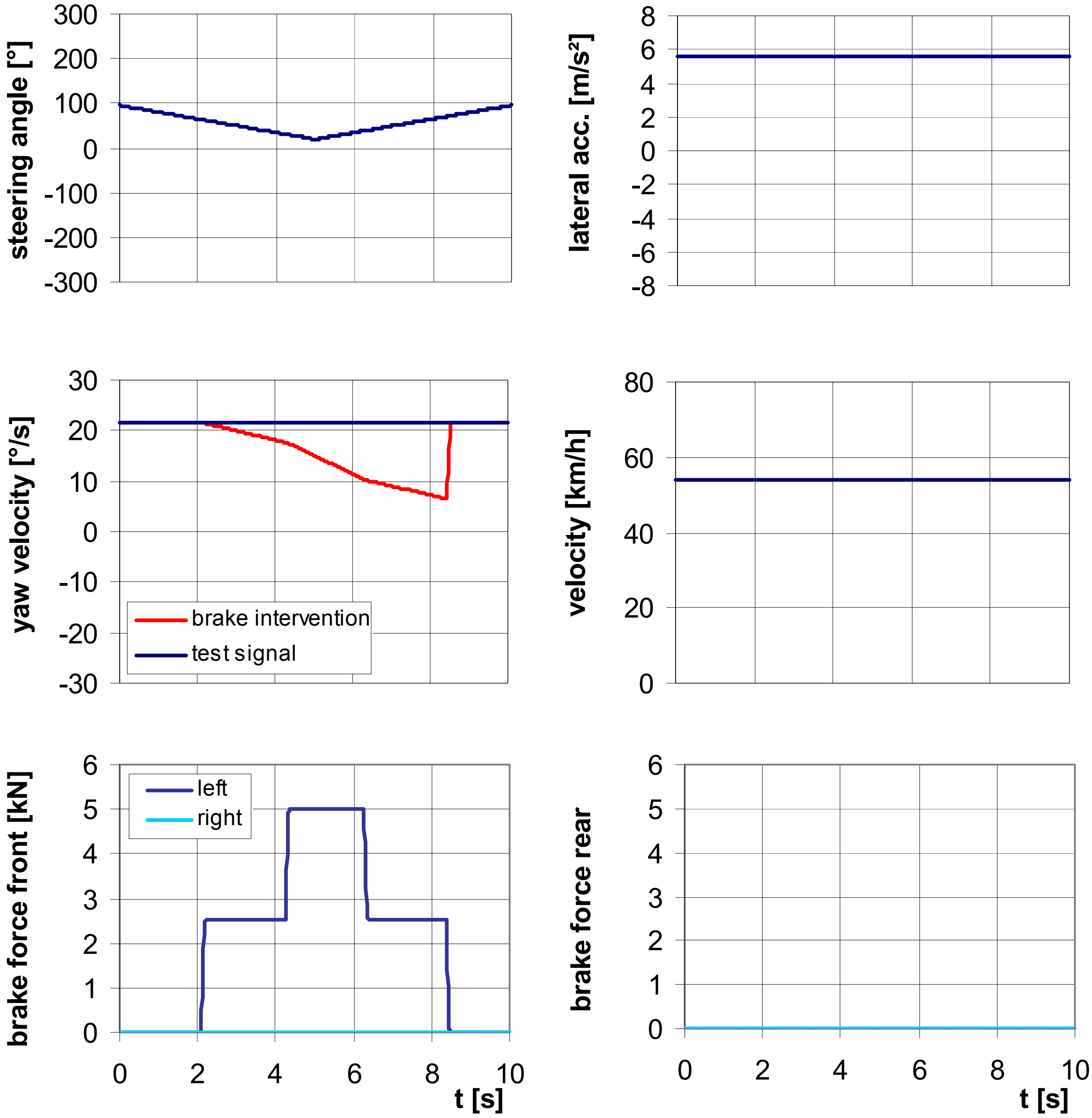

Fig. 5-4: Static oversteer in right hand bend

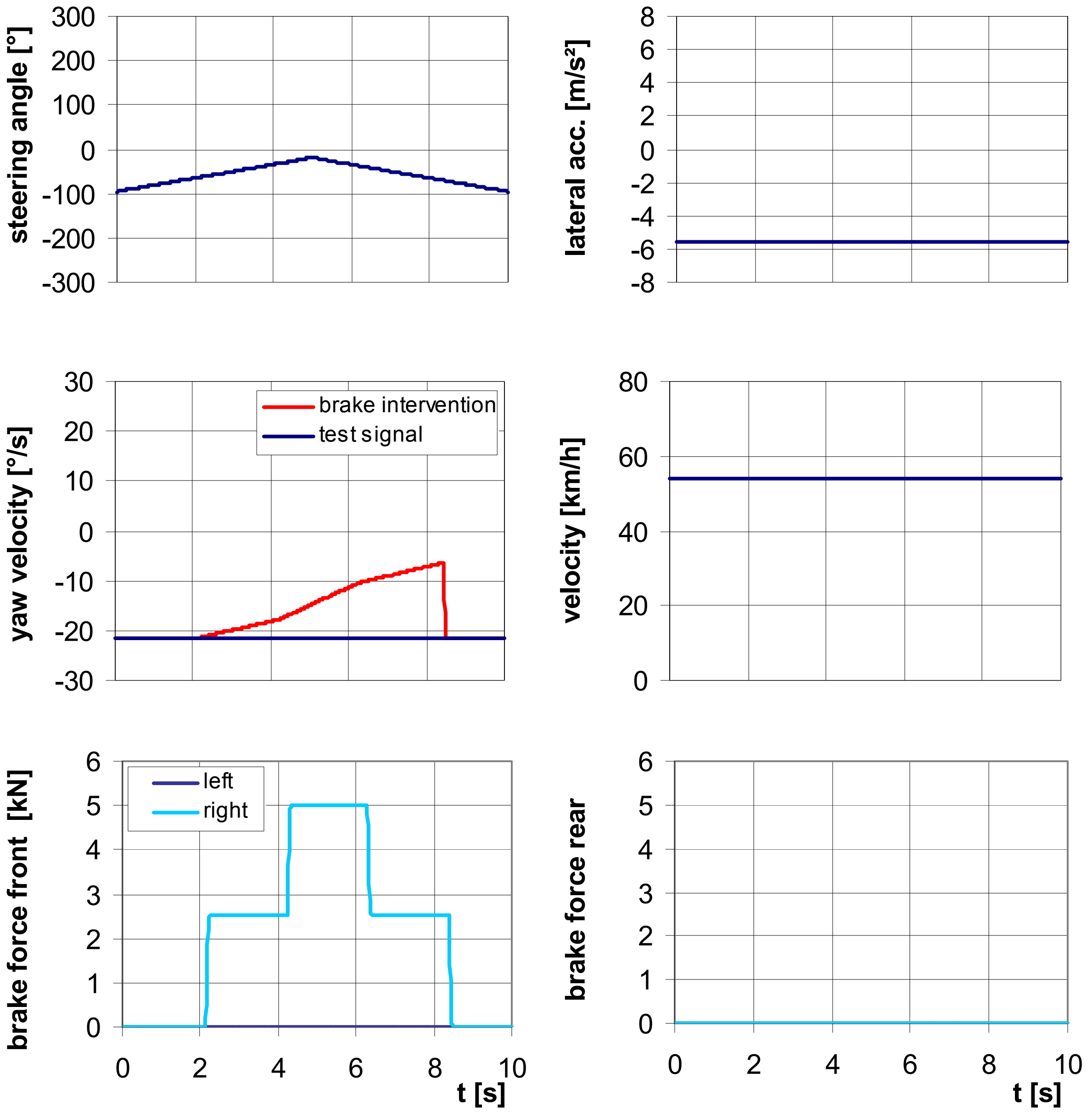

Fig. 5-5: Static oversteer in left hand curve

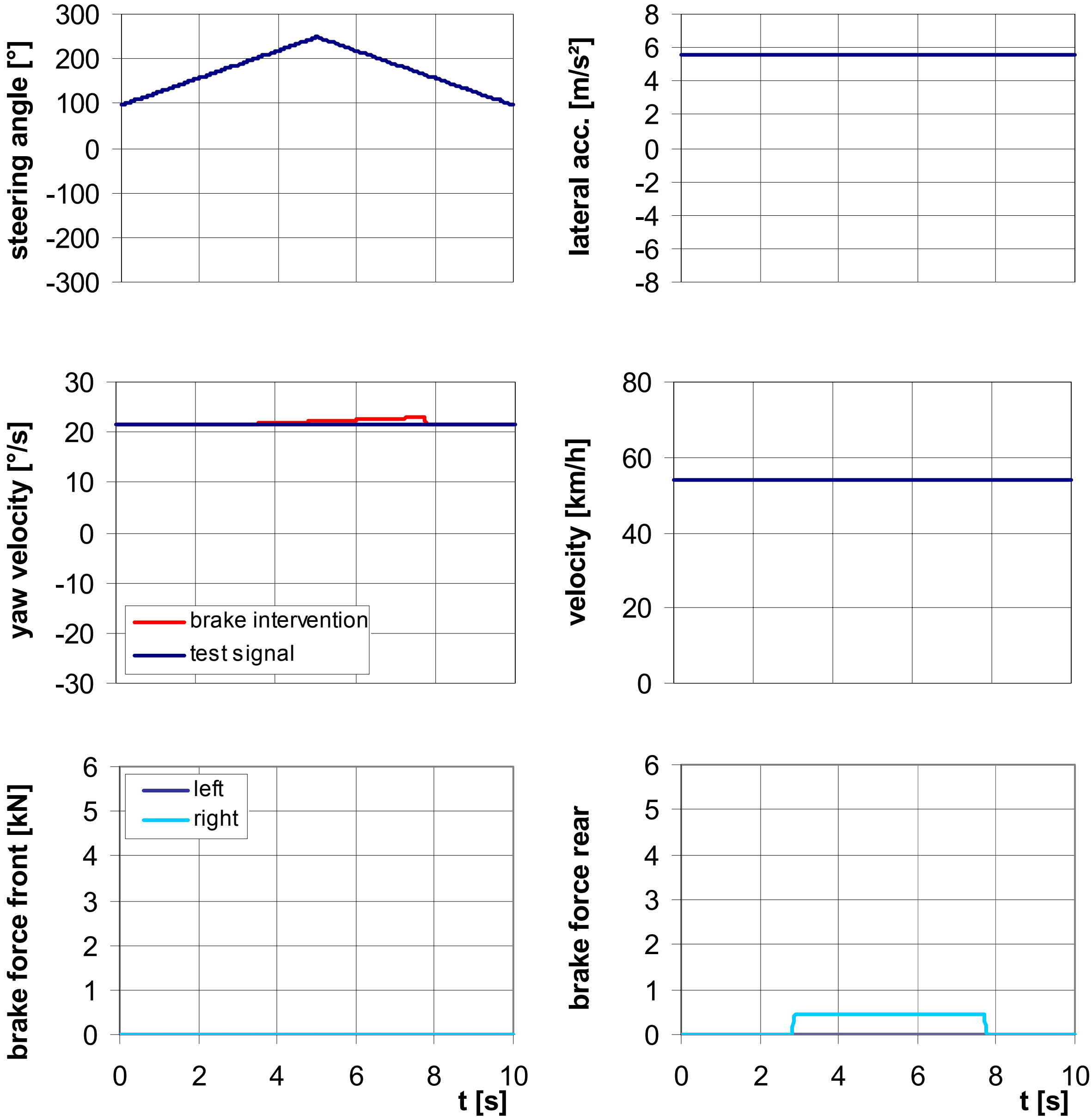

Fig. 5-6: Static understeer in right hand curve

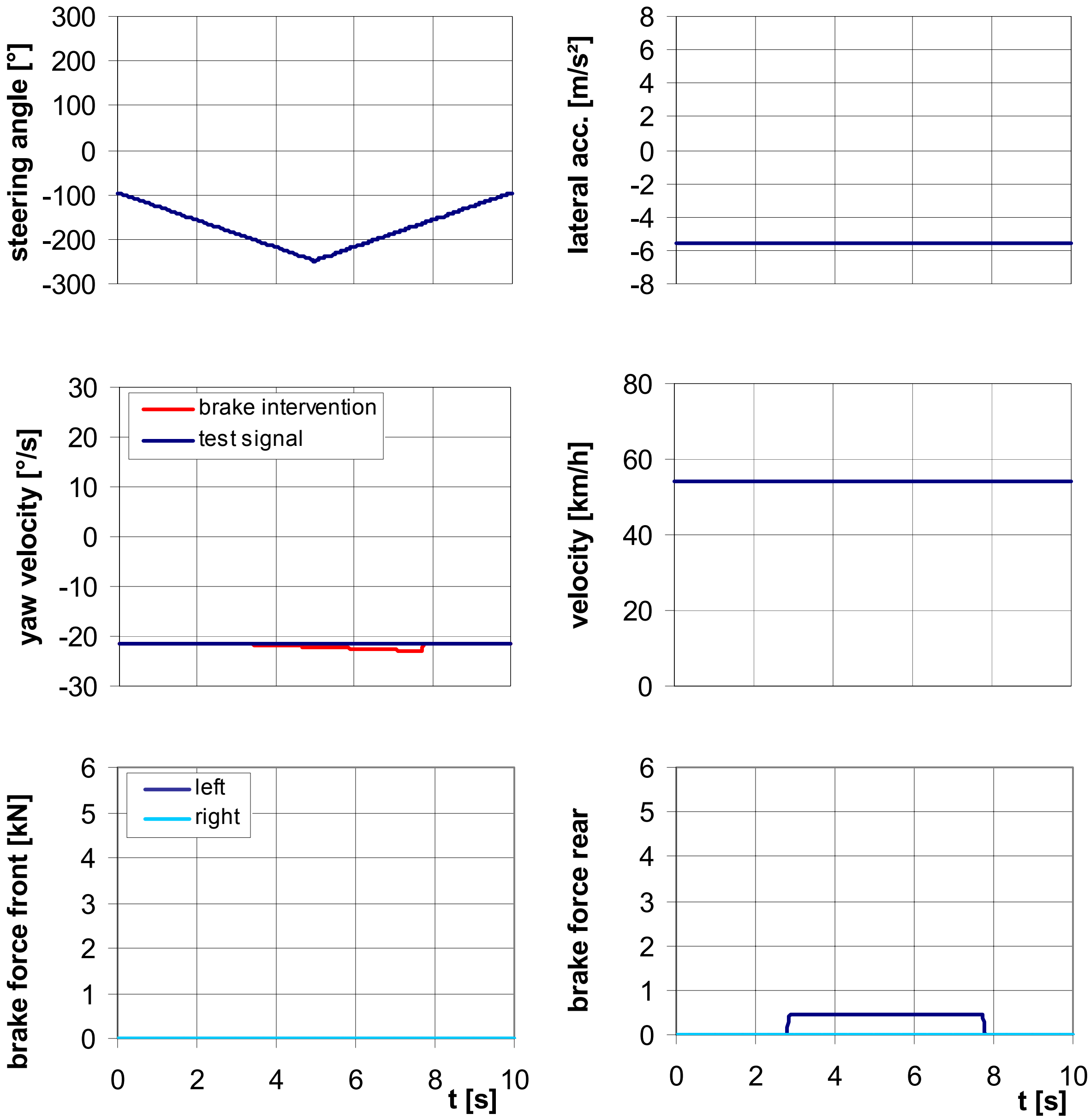

Fig. 5-7: Static understeer in left hand curve

It is highly likely that the static test will be considered implausible by the system's self-diagnostics. Nevertheless, the self-diagnosis created here judges the large difference between steering angle and yaw velocity or lateral acceleration to be a malfunction of the steering wheel angle sensor, because of its long duration, and consequently switches the controller off. It is still worthwhile having this kind of test in the programme, since only here is it feasible to apply braking power for an extended period of time in order to check whether the required braking force is fully available. As a consequence, it may be necessary to deactivate self-diagnostics for the duration of the test (although this should happen automatically) so that you can be sure that the self-diagnostics are definitely available when the tests are over.

5.3.2 Dynamic test of the yaw velocity control

For the dynamic test of the yaw velocity controller, sinusoidal steering at a constant steering frequency forms the basis of the driving manoeuvre for both oversteer and for understeer. However, yaw velocity and lateral acceleration signals of equal frequency but with an amplitude difference and a phase shift adapted to the particular vehicle, are suitably assigned to the selected driving speed, steering angle amplitude and steering frequency.

For the simulation of dynamic oversteer, an appropriate movement in the region of the yaw natural frequency is preset. This is achieved here with both vehicles by a steering frequency of 1 Hz and a steering angle amplitude of 90° (A-Class) or 80° (330xi) at an identical driving speed of 72 km/h (20 m/s). The duration of the simulation is 15 s. During this time, a steering angle amplitude is emitted only 12 s, allowing plenty of time for the system to settle before a new test signal is transmitted.

Fig. 5-8 shows the driving manoeuvre again for the vehicle parameters of the Mercedes Benz A-Class. The yaw velocity diagram also shows a second curve alongside the standard signal. This is the curve that the yaw velocity would take if the braking forces were to retroact on the yaw movement (see previous chapter). A section of both yaw velocity signals is included, to show that the driving dynamics controller is actually damping the yaw movement rather than the rear braking forces, which are zero here in any case. The damping is quite visible.

The dynamic understeer must be arranged, so that the vehicle is no longer able to follow the steering wheel standard, and is forced over the front wheels. Therefore, the steering frequency is increased to 3 Hz, the steering angle amplitude for both vehicles is increased to 120°, and the driving speed is reduced to 36 km/H (10 m/s). Because the steering frequency has been increased by a factor of 3, the duration of the simulation may be reduced to 5 s. Here too, the steering angle amplitude is not emitted until the end of the simulation, to allow for decay, Fig. 5-9.

A section of the yaw velocity can also be seen (this time, of course, instead of the front braking force). Even in this section, the increase in yaw velocity by the driving dynamics controller has to be assumed. This is because the braking forces are extremely low. Dynamic understeer in particular shows convincingly that it is wise to run the individual operating points statically as well, although doing this will most probably require the self-diagnostics to be deactivated temporarily.

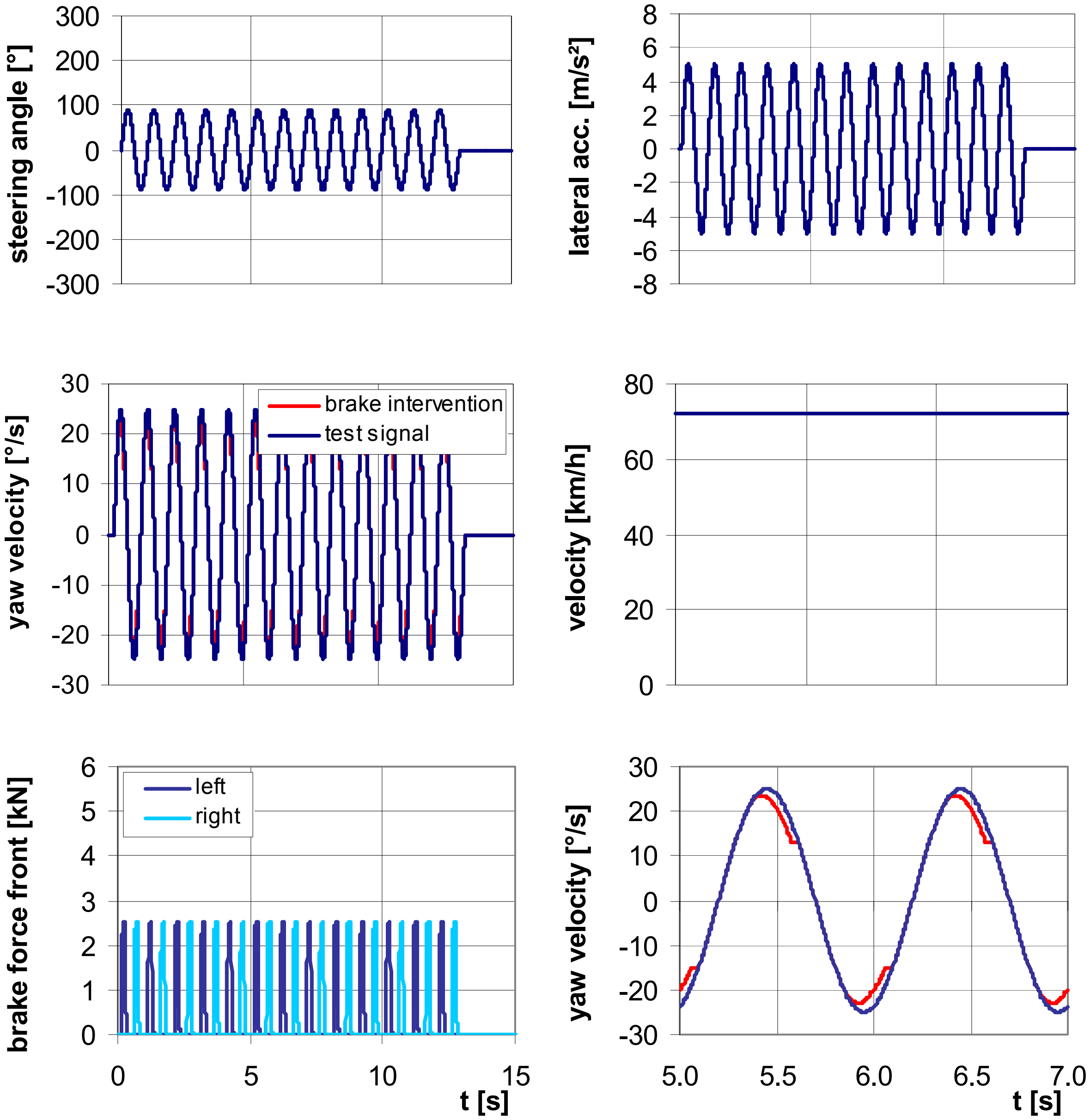

Fig. 5-8: Dynamic oversteer

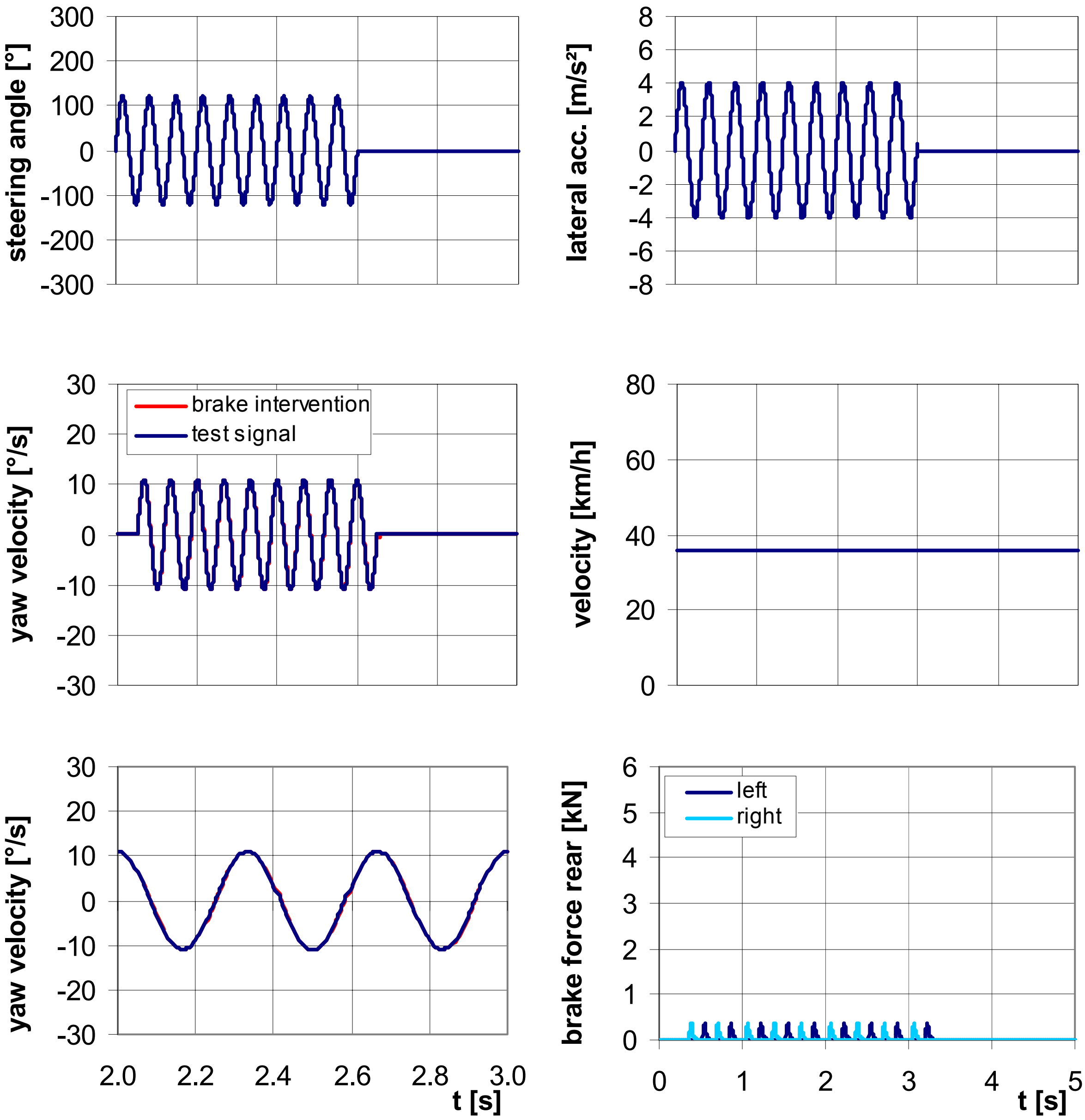

Fig. 5-9: Dynamic understeer

5.3.3 Test of the slip angle limitation

A test of the slip angle limitation is sensible, because lateral acceleration is normally included in the calculation of slip angle speed and thus of the slip angle:

$$\dot{\beta} = \dot{\psi} - \frac{a_y}{v} \qquad \text{Eq. 5-4}$$

The slip angle limitation is always activated when the driving dynamics controller is trying to adjust actual to target speed, and when the vehicle is twisting strongly, which can easily happen on μ low surfaces (see Chapt. 2.1.2). In this test, therefore, a circular route is simulated on a road surface with a frictional resistance of $\mu = 0.2$. To this end, the steering angle is increased after 3 s, and within 2 s, to 100°. The vehicle can no longer follow the large, prescribed steering angle on this low friction surface and moves accordingly towards its physical limit:

$$\dot{\psi} = \frac{\mu \cdot g}{v} \qquad \text{Eq. 5-5}$$

$$a_y = \mu \cdot g \qquad \text{Eq. 5-6}$$

This yaw velocity is considerably smaller than the target value, which is calculated from the fairly large steering wheel angle. The driving dynamics controller will try to use braking power at the rear axle to increase the yaw velocity. As a result, the yaw velocity does in fact increase. but only at the expense of a fast expanding slip angle, and not because of a reduced route radius. If the slip angle exceeds a limit of 10°, the slip angle limitation acts to brake the diagonally opposed front wheel, reducing the yaw velocity and slip angle once more. The test of the slip angle limitation is carried out for right-hand (Fig. 5-10) and a left-hand bend (Fig. 5-11) and lasts for T = 40 s respectively, since vehicle responses on the low friction road surface are very sluggish.

When this kind of test is carried out on a single-axle brake testing rig, such as the type normally available for the regular vehicle inspection, it is of course not possible to test braking forces on the front and the rear axle simultaneously. Intervention on the rear-axle brakes is a normal reaction to understeer. This has already been tested both statically and dynamically. It therefore is more important to measure the front braking forces, since these are activated from a specific slip angle. With the test signals it is assumed that the rear brakes are activated (as is in fact the case) without this being measured explicitly in this test. The oscillation of the reference signal for the yaw velocity after 5 s (frequency: 0.1 Hz, amplitude 0.1 rad/s, duration: 30 s) also is initiated only on the assumption that the rear wheel brakes will in fact be applied.

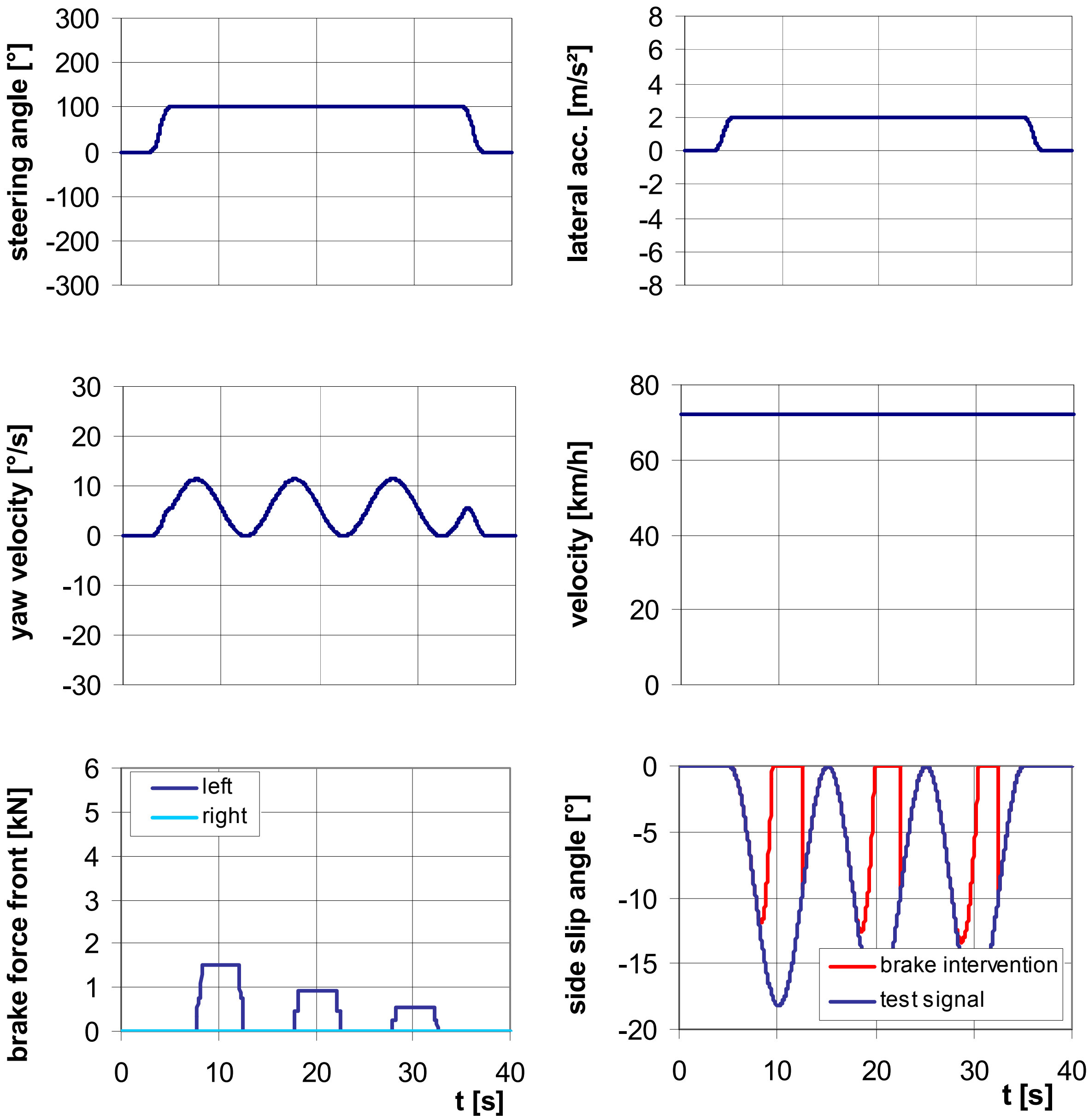

Fig. 5-10: Side slip angle limitation in right hand curve

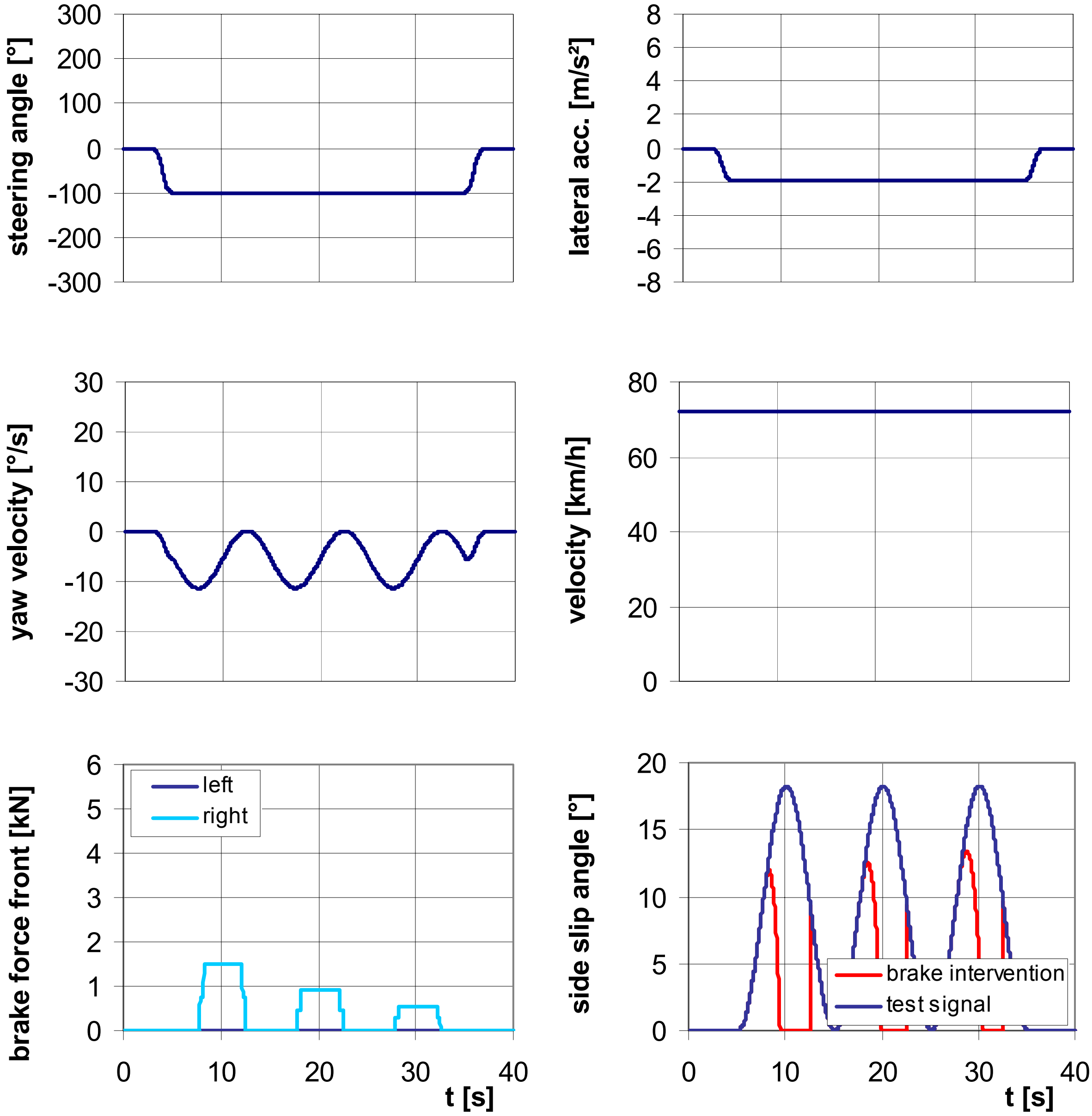

Fig. 5-11: Side slip limitation in left hand curve

It is clear that the slip angle really is reduced, if the slip angle is calculated once from the yaw velocity reference signal, and then once from the yaw velocity signal that has been extended by the braking responses (visible in place of the rear brake forces).

5.3.4 Complete test signal

The complete test signal is a composite of the individual tests described earlier. The complete signal is, of course, considerably longer than the sum of the individual tests, as attention must be given to ensuring plausible transitions in between the tests. In each case, the transitions are seen as stationary and calculated according to the Eq. 5-1 to Eq. 5-3 already described with sinusoidal modifications of yaw velocity and driving speed.

In addition, the order of individual tests is changed, so that all those tests that require a braking response at the front wheels can be carried out first, followed by the tests involving the rear axle. The complete signal has a length of 180 s (3 min). The changeover to the rear axle is carried out 135 s into this time (after 75% of the test cycle). Fig. 5-12 shows the composition of the test signal.

	driving manoeuvre	consequence for driving behaviour	time period [s]	time end [s]
1	acceleration up to 54 km/h		5	5
2	turn in righ hand curve with R=40m		2.5	7.5
3	take-back of steering angle	static oversteer in right hand curve	10	17.5
4	transition in left hand curve with R=40m		5	22.5
5	take-back of steering angle	static oversteer in left hand curve	10	32.5
6	straightline driving, acc. up to 72km/h		2.5	35
7	sinusodial steering input with f=1Hz	dynamic oversteer	15	50
8	step steer input up to 100° at μ=0.2	side slip limitation in right hand curve	40	90
9	step steer input up to -100° at μ=0.2	side slip limitation in left hand curve	40	130
10	deceleration up to 0 km/h	*(change to rear axle)*	5	135
11	acceleration up to 54 km/h		5	140
12	turn into right hand curve with R=40m		2.5	142.5
13	take-back of steering angle	static understeer in right hand curve	10	152.5
14	transition into left hand curve with R=40m		5	157.5
15	take-back of steering angle	static understeer in left hand curve	10	167.5
16	deceleration up to 36 km/h		2.5	170
17	sinusodial steering input with f=3Hz	dynamic understeer	5	175
18	deceleration up to 0 km/h		5	180

Fig. 5-12: Composition of the total test signal

Fig. 5-13 and Fig. 5-14 show, in conclusion, the complete test signals for Mercedes Benz A-Class and BMW 330 xi with the resultant braking forces.

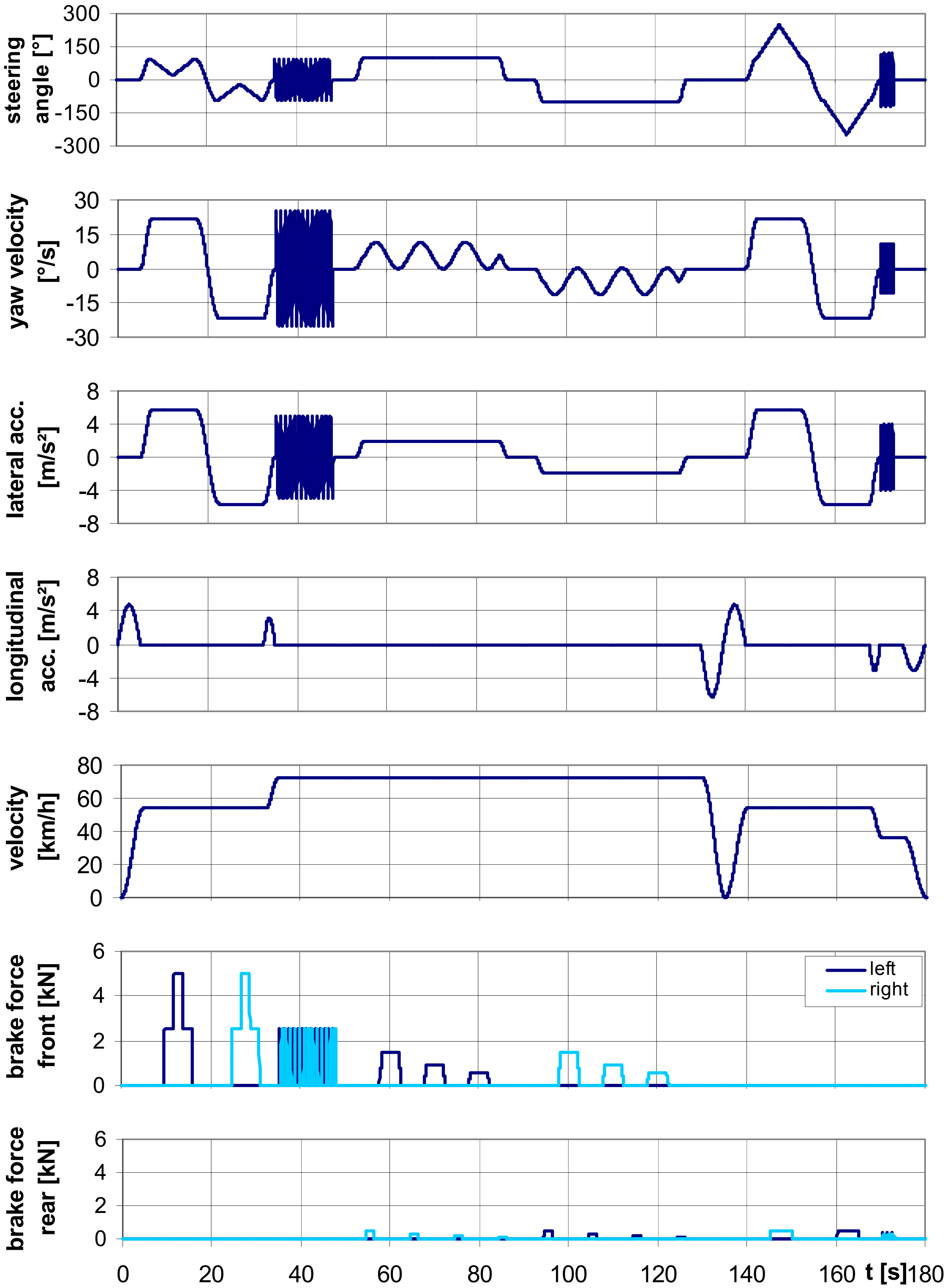

Fig. 5-13: Total test signal with resulting brake forces, Mercedes-Benz A-Klasse

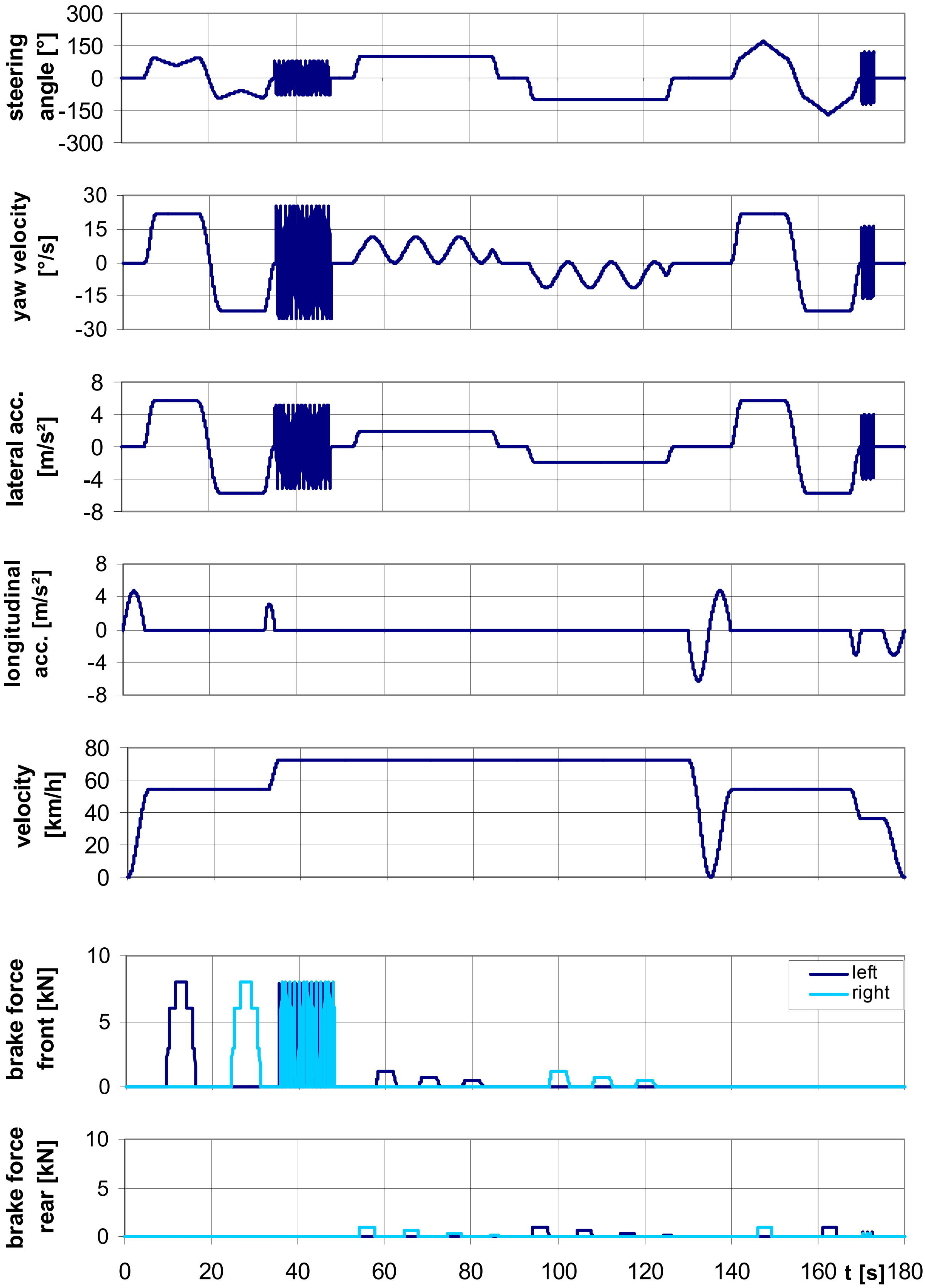

Fig. 5-14: Total test signal with resulting brake forces, BMW 330xi

5.4 Recognising gradual system deterioration

The aim of the test signals is to recognize system deteriorations that have already occurred and to reliably recognise potential system problems long before the self-diagnostics are able to do so. To do this, the test signals are added to the sensor values. How, for example, the noise of the yaw velocity sensor with a variance of only 0.002 rad can affect the braking force, can be seen in Fig. 5-15. A variance of this magnitude cannot be recognized by a self-diagnosis based on signal plausibility.

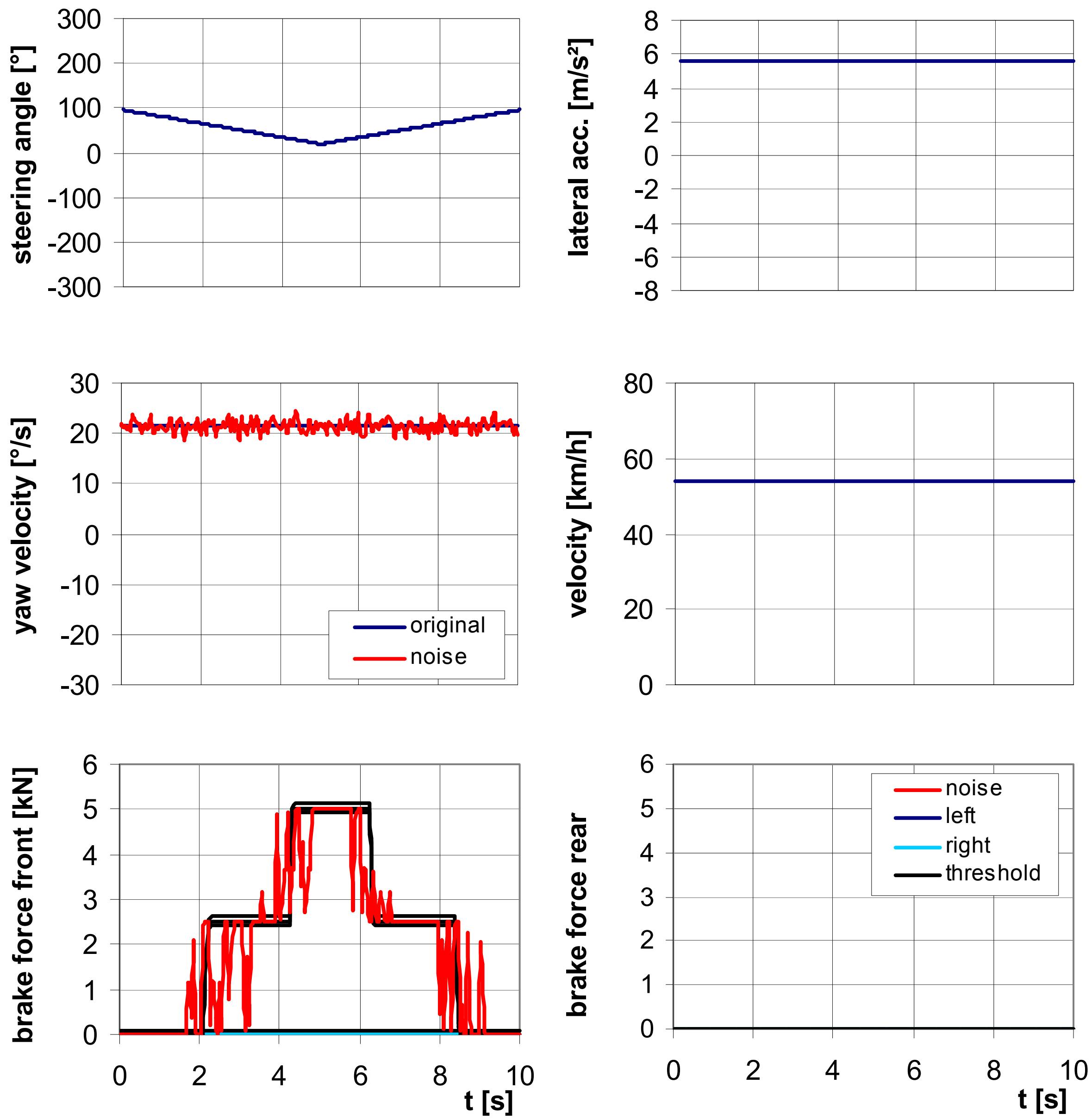

Fig. 5-15: Influence of minimum defects on quality of control – random of 0.002rad on the velocity sensor – oversteering in right bend

It is relatively simple to define a control criterion that will show whether the system is still working perfectly, or whether it is already suffering from major problems. Under this criterion, all braking forces that deviate by less 100 Nm from the standard curve are judged to be OK. If the braking power deviates more than 100 Nm from the standard curve, the relationship of the duration of the deviation to the duration of the entire standard curve is stated. The correlation to the standard braking power curve becomes one, minus this relationship.

$$\text{Correlation} = \left(1 - \frac{\text{duration of the deviation}}{\text{duration of the entire standard curve}}\right) \cdot 100\%$$

The correlation is 100% if the measured braking power remains within the tolerance band around the standard braking power curve at all times. If there is no braking at all at the wheel in question, the measured braking forces are outside the tolerance band for the complete duration of the standard braking period and the correlation is therefore 0%. For the braking forces at the rear axle, the tolerance band is restricted by the braking force distribution factor, since absolute braking momentums are considerably less at the rear.

Wie sich die Korrelationen an den einzelnen Räder bei den Gesamttestsignalen für die beiden Fahrdynamikreglermodelle verhalten, zeigen die

Fig. 5-16 and Fig. 5-17 show the correlations at the individual wheels for the two driving dynamics controller models during the complete test signals. In each case errors have occurred, which will not actuate the self-diagnosis systems. However, if your criterion states that there must be a correlation of at least 95% at all wheels, you will see the slight deterioration in signal quality in nearly every instance.

Recognising signal drifts is a difficult task. This error reduces the correlation in most cases only by few per cent, since the average deviation in these cases is zero and the absolute difference is only very low. This means that values generally do not fall below the threshold value of 95%. However, signal drifts with larger amplitudes would allow the correlations to fall further.

A deterioration in the quality of the lateral acceleration signal is only noticeable at the front axle. The reason for this is that the lateral acceleration signal is used only in the slip angle calculation and consequently only affects the slip angle limitation test. For this test, the front and rear axle brakes are actuated, but in the test procedure only the front axle signals are evaluated.

With both models it is clear that the deterioration in quality of the longitudinal acceleration signal is not recognized. Longitudinal acceleration is only used in the calculation of driving speed if there are large accelerations, or if the wheel velocity signal is not considered to be reliable because of large deviations in rotational velocity, or when wheel slip is large. When test signals are used, all driving conditions examined as part of the test procedure have a constant driving speed. That is why the signal has no influence on the operation of the driving dynamics controller.

			correlation [%]			
			front left	front right	rear left	rear right
steering angle	offset	0.05 rad	96.10	91.61	95.81	95.81
	offset	-0.05 rad	95.74	96.10	95.81	95.81
	noise	0.05 rad	73.59	76.54	83.96	86.24
	drift	0.05 rad	96.83	95.56	100.00	100.00
yaw velocity	offset	0.002 rad/s	87.87	88.64	97.45	100.00
	offset	-0.002 rad/s	88.64	87.87	100.00	97.45
	noise	0.002 rad/s	58.20	63.36	67.73	73.47
	drift	0.002 rad/s	99.07	98.48	100.00	100.00
lateral acc.	offset	0.05 m/s²	86.58	86.76	100.00	100.00
	offset	-0.05 m/s²	86.76	86.58	100.00	100.00
	noise	0.05 m/s²	94.74	95.28	100.00	100.00
	drift	0.05 m/s²	98.82	99.03	100.00	100.00
long. Acc.	offset	0.4 m/s²	100.00	100.00	100.00	100.00
	offset	-0.4 m/s²	100.00	100.00	100.00	100.00
	noise	0.4 m/s²	100.00	100.00	100.00	100.00
	drift	0.4 m/s²	100.00	100.00	100.00	100.00
wheel speed front left	offset	3 rad/s	100.00	100.00	100.00	100.00
	offset	-3 rad/s	95.24	90.59	100.00	100.00
	noise	3 rad/s	30.22	99.03	100.00	100.00
	drift	3 rad/s	98.25	98.25	100.00	100.00
wheel speed rear left	offset	3 rad/s	90.41	86.35	100.00	100.00
	offset	-3 rad/s	95.24	90.59	100.00	100.00
	noise	3 rad/s	97.66	96.92	18.05	100.00
	drift	3 rad/s	87.44	89.75	100.00	100.00
actuator front left	failure		0.00	100.00	100.00	100.00
	delay	0.10 s	78.19	100.00	100.00	100.00
	delay	0.25 s	64.14	100.00	100.00	100.00
actuator rear left	failure		100.00	100.00	0.00	100.00
	delay	0.10 s	100.00	100.00	75.39	100.00
	delay	0.25 s	100.00	100.00	69.92	100.00

Fig. 5-16: Influence of minimum defects on quality of control; Mercedes-Benz A-Class

			Correlation [%]			
			vl	vr	hl	hr
steering angle	offset	0.05 rad	84.69	85.37	87.93	86.88
	offset	-0.05 rad	88.73	82.25	86.78	85.88
	noise	0.05 rad	59.93	60.11	58.05	48.22
	drift	0.05 rad	92.97	90.09	92.53	92.58
yaw velocity	offset	0.002 rad/s	87.80	87.06	96.26	94.15
	offset	-0.002 rad/s	69.78	88.62	96.26	96.29
	noise	0.002 rad/s	36.67	52.96	61.06	32.95
	drift	0.002 rad/s	97.51	98.65	96.26	94.86
lateral acc.	offset	0.05 m/s²	86.94	88.77	100.00	100.00
	offset	-0.05 m/s²	88.51	87.23	100.00	100.00
	noise	0.05 m/s²	92.42	99.21	100.00	100.00
	drift	0.05 m/s²	99.39	99.40	100.00	100.00
long. acc.	offset	0.4 m/s²	100.00	100.00	100.00	100.00
	offset	-0.4 m/s²	100.00	100.00	100.00	100.00
	noise	0.4 m/s²	100.00	100.00	100.00	100.00
	drift	0.4 m/s²	100.00	100.00	100.00	100.00
wheel speed front left	offset	3 rad/s	87.29	89.49	98.13	98.15
	offset	-3 rad/s	97.51	88.49	98.13	96.01
	noise	3 rad/s	29.42	100.00	100.00	100.00
	drift	3 rad/s	91.09	88.08	98.13	100.00
wheel speed rear left	offset	3 rad/s	95.37	99.40	100.00	100.00
	offset	-3 rad/s	97.51	88.49	71.41	96.01
	noise	3 rad/s	97.29	97.35	15.23	98.57
	drift	3 rad/s	96.96	90.69	100.00	100.00
actuator front left	failure		0.00	100.00	100.00	100.00
	delay	0.10 s	72.22	100.00	100.00	100.00
	delay	0.25 s	54.25	100.00	100.00	100.00
actuator rear left	failure		100.00	100.00	0.00	100.00
	delay	0.10 s	100.00	100.00	81.03	100.00
	delay	0.25 s	100.00	100.00	72.41	100.00

Fig. 5-17: Influence of minimum defects on quality of control; BMW 330xi

The structure of the driving dynamics controller is also noticeable with wheel velocities. With the front-wheel drive A-Class model, both rear axle wheel speeds and the smaller front wheel speeds were used to calculate the driving speed. Increasing the rotational speed of the front, left wheel does not result in an error, since the larger signal does not enter into the calculation. A negative offset, however, does affect the result. With the BMW model, however, both front wheel velocities go into the calculation of the driving speed, because of the rear-wheel drive. Both positive and negative offset have their consequences. Noise in the rotational velocity signal is interpreted by the ABS system as strong acceleration, resulting in heavy interventions, which considerably reduce the correlation.

Similar behaviour can be seen with the two models with reduced signal quality at a rear wheel - rotational velocity signal. While increasing the wheel velocity affects the speed calculation of the A-Class, and is recognised as an error, the affect on the BMW, which uses only the smaller speed signal, is less, and does not lead under the 95% threshold.

Errors in the actuators affect both models almost identically, whether on the front or rear axle. If the actuator fails completely i.e. the braking momentum at the affected wheel is zero during the complete test cycle, then the correlation with the reference signal is also equal to zero. A delay in the response of the actuator, caused, for example, by a stuck valve, leads directly to a considerable reduction in the correlation. As the delay becoming longer, the correlation also becomes correspondingly smaller. As expected, this kind of error in the test has no effect on the other wheels.

6 Summary

In vehicle dynamic control systems, the driving condition of the vehicle is monitored by sensors and the vehicle is stabilised in critical driving situations by powerful interventions into the throttle and individual to each wheel by the brake.

As there is a "grey area" between the functioning of all components within normal parameters (green) and the recognition of an error by self-diagnosis (red) in and Fig. 6-1, Institut für Kraftfahrwesen of RWTH was requested to develop a test procedure to identify systems deterioration or wear during periodical inspection or in workshop tests. In the "grey area", the self-diagnosis system is unable to identify problems, even though they influence the quality of the control system itself. This is confirmed both by tests on real systems, for instance when electrical resistances were increased, as well as through simulation results.

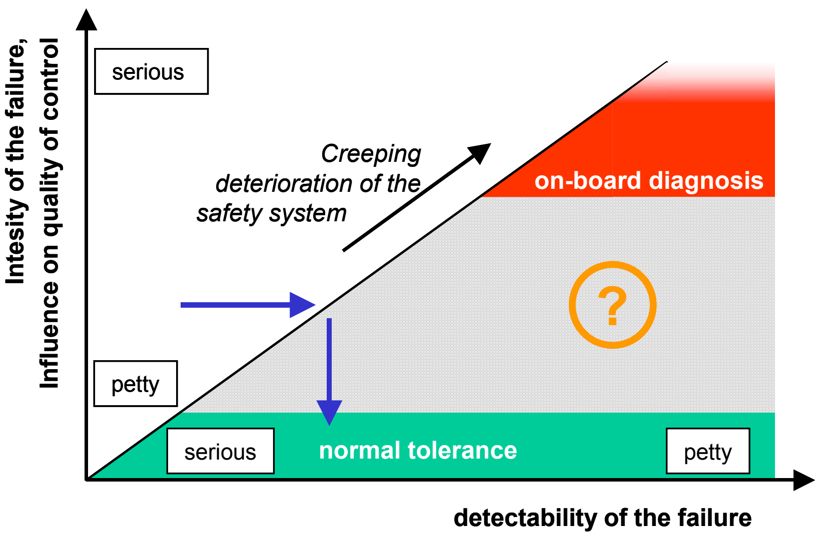

Fig. 6-1: Coherence between intensity of the failure and the identification possibilities

For a vehicle test to be useful to the vehicle owner, it should assess both of these aspects:

1) There are limited options for self-diagnosis.
2) Creeping system deterioration is only recognized late in the day.

Therefore a test procedure for vehicle dynamics controllers was developed by use of simulation models. During the driving tests of Mercedes-Benz A-Class and BMW 330xi the purely passive handling performance of the vehicles, as well as the performance with the intervention of the driving dynamics controller was measured. From the results of the test rig tests, it was possible to create the vehicle models as multi-body systems (SIMPACK). The driving dynamics controller model was created with MATLAB/Simulink and linked to the vehicle models. The close agreement between test and simulation model ensured the validity of the investigations that followed.

The present situation with looking to the Malfunction Indication Lamp (MIL) only is an unsatisfactory solution for the future. The same is valid for the pure communication with the electronic control unit through a standardized interface (like today's emission-OBD), although this would already mean a significant progress to the present situation, because it would allow to see whether the built-in electronic components are present and work together properly and it would allow to read the system's error memory and the readiness code. But as it is still not possible to make any judgement to the efficiency of the system, real function and performance tests should be carried out.

For the inspection option test signals are stored directly in the control unit. A simple diagnostic tool with the necessary interface (i.e. the current emission-OBD) would be capable of retrieving these test signals. The responses of the electronically controlled system would then be measured and compared with standard responses using available dynamic test facilities such as brake testing rigs. The advantage of this approach is that physical tests are carried out. This form of testing is very safe, since the electronics always receive the appropriate signals and all relevant functions can be properly tested. Furthermore, vehicle manufacturers are not obliged to provide an access point for test signals but can design the test signals themselves according to the requirements of their own systems.

These requirements are not met when the test signals are provided externally. This approach is expensive and prone to errors. This option only has benefits if the system responses measured are evaluated directly and serve as the basis for calculating of the next default values. This kind of "hardware in the loop" test rigs have become established for the development of electronically controlled systems. They are, however, too expensive for tests in the context of vehicle inspections.

Fig. 6-2 summarises the pros and cons of the discussed approaches.

Communication in conjunction with the storage of test signals in the particular control units, was therefore, considered the most reasonable way to check electronically controlled systems, since real-life functional and operational testing can be carried out at acceptable cost.

Electronically controlled systems consist basically of the components sensors, cable harness, Electronic Control Unit (ECU) and actuators. The main source or problems with electronically controlled systems are the sensors, the wiring and mechanical components, such as valves, pumps, etc. ... . However, a test of a vehicle's electronics should not be confined just to individual components like the sensors. All components should be checked.

Sensor-signals that have only slight noise or drift, or have a small offset are not yet classified as faulty. Such signals have considerable influence on the quality of the control system and can be symptomatic of the onset of problems. A judgment on the signal quality of all sensors should therefore be covered by the test procedure

Warning device check	Communication with electronics via OBD-interface	Internal function test with mechanical influence	External function test with mechanical influence
Defined Faults are indicated by a warning device.	Defined Faults are indicated by a warning device. Additionally there is communication with the electronics.	Supplementary to the communication, test signals stored in the control unit are activated.	Supplementary to the communication, optional test signals are passed on to the control unit via a new interface.
Advantage: • Inexpensive method.	**Advantage:** • Inexpensive method, as interface exists in OBD. • Information about installed systems available (tamperproof).	**Advantage:** • High quality of Information. • Fast testing. • System safety, as no outside intervention occurs. • Information about installed systems available (tamperproof).	**Advantage:** • High quality of Information. • High test variability • Information about installed systems available (tamperproof).
Disadvantage: • No reliable information about the function of the systems. • No information about installed systems (less tamperproof).	**Disadvantage:** • No reliable information about the function of the systems.	**Disadvantage:** • More expensive than a mere fault read out.	**Disadvantage:** • More expensive, as technical modifications are necessary. • Enhanced risk due to possible access to hardware and software (intentional and involuntary).

Fig. 6-2: Concepts of tests during periodic vehicle inspection

The actuators, on the other hand, are not adequately monitored by the vehicle's own electronics. Thus any test procedure should certainly include the mechanical components of the electronically controlled systems

As the self-diagnostic system provides already a lot of important checks, during periodical technical inspection it is preferable to test how effectively the system is working, in order to diagnose system deterioration before the self-diagnostic systems are able to do so. As the sensors and the wiring must be included in the test, the following testing strategy is suggested:

Vehicle dynamics controllers must be tested for functionality. Performance must be checked on a brake test rig, during which test signals, stored in the control unit, are added to the sensor signals.

The test signals are to be added as supplementary signals to the signals provided by the vehicle's own sensors. Noise or drifting or an offset of a sensor signal is still included in the test signal. This ensures that the signal quality of the vehicle's own sensor signals is taken into account in the test.

The complete test procedure involves a mixture of data and sensor value readings, as well as the activation of the test signals. A diagnostic tool is needed here, which is able to communicate via a standard diagnostic interface with the vehicle electronics. When this tool is initially connected to the electronics, it identifies the vehicle.

The total test consists out of four stages:

1) Hardware and software recognition

   First is checked if all system components are actually available, are suitable for the system under test and have correctly "identified themselves" to the control unit. Additionally, the version numbers of the software shall be checked. An out of date piece of software should be replaced, with an upgrade if possible.

2) Reading the error memory and the readiness codes

   The error memory of the system is read out. The test is not passed, if self-tests have not been performed, shown by the readiness code (as today’s emission-OBD).

3) Testing the master sensor (steering wheel angle sensor)

   The value of the steering wheel angle sensor is read out with the steering wheel in its center position and at the two extremes. Furthermore, the quality of this sensor signal (noise, drift, etc. ...) is measured with the steering wheel in its center position.

4) Effectiveness and function test with test signals

   At the start, the vehicle is with the front wheels on a conventional brake test rig, such as the one used for the brake test in regular vehicle inspection. Using the diagnostic tool, the stored test signals for the brake intervention of the front axle are retrieved and the braking responses of the system measured.

   Fig. 6-3 shows the complete test signals with the resultant braking forces.

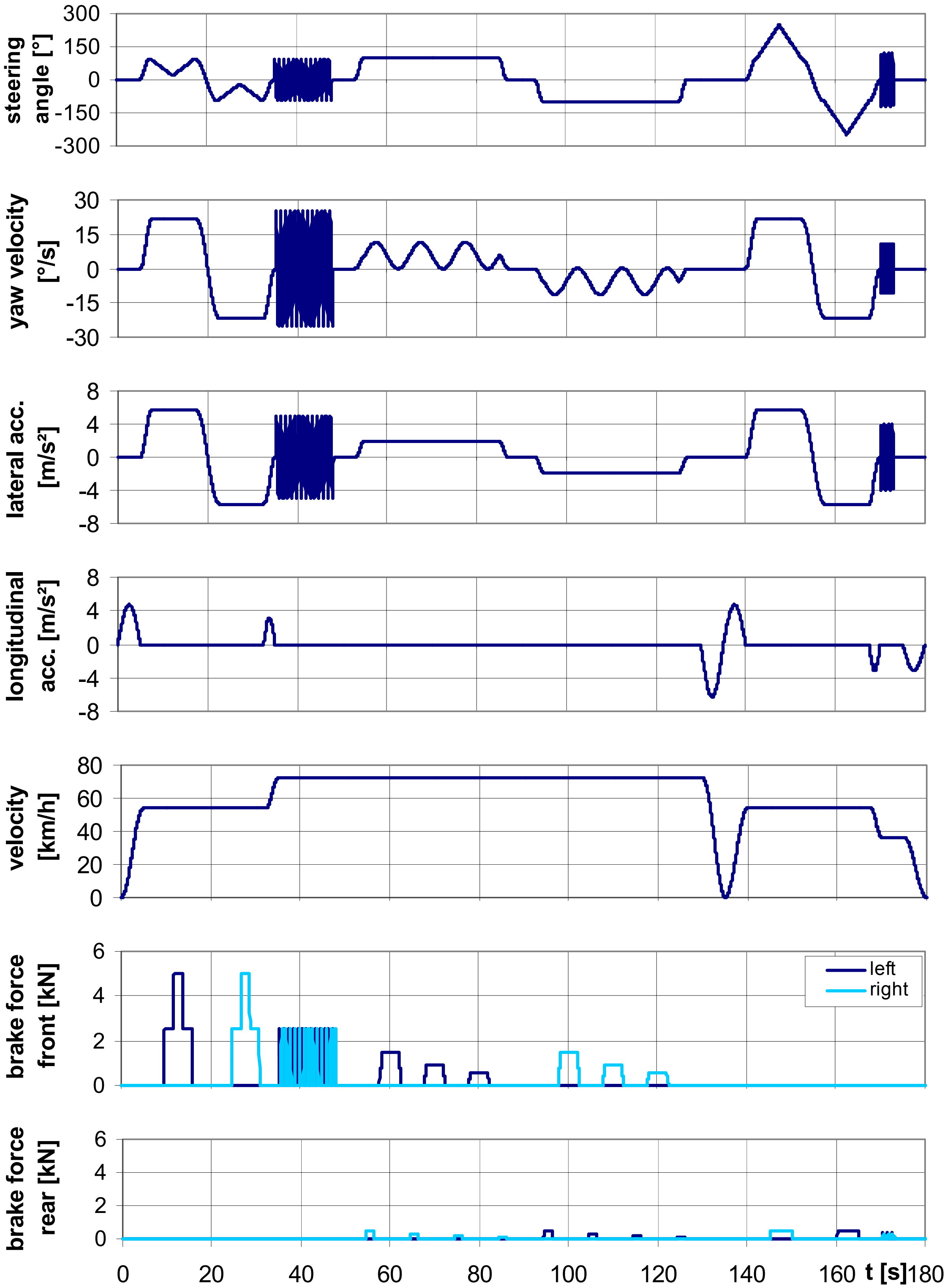

Fig. 6-3: Total test signal with resulting brake forces

Then the vehicle is driven onto the brake test rig with the rear wheels. The signals are started, to cause the VDC for braking interventions on the rear axle. An automated evaluation of measured braking force allows a reliable judgment to be made of the complete system.

The simulation results in this study have shown, that minimum signal deteriorations can be detected by comparing the actual brake forces to a master scan. In order to check the whole system, the driving tests behind the test signals shall cover all possible interferences of the vehicle dynamics controller.

The aim of the test signals is to recognize system deteriorations that have already occurred and to reliably recognize potential system problems long before the self-diagnostics are able to do so. To do this, the test signals are added to the sensor values.

How, for example, the noise of the yaw velocity sensor with a variance of only 0.002 rad can affect the braking force, can be seen in Fig. 6-4. A variance of this magnitude cannot be recognized by a self-diagnosis based on signal plausibility.

It is relatively simple to define a control criterion that will show whether the system is still working perfectly, or whether it is already suffering from major problems. Under this criterion, all braking forces that deviate by less than 100 Nm from the standard curve are judged to be OK. If the braking power deviates more than 100 Nm from the standard curve, the relationship of the duration of the deviation to the duration of the entire standard curve is stated.

The correlation to the standard braking power curve becomes one, minus this relationship.

$$\text{Correlation} = \left(1 - \frac{\text{duration of the deviation}}{\text{duration of the entire standard curve}}\right) \cdot 100\%$$

The correlation is 100% if the measured braking power remains within the tolerance band around the standard braking power curve at all times. If there is no braking at all at the wheel in question, the measured braking forces are outside the tolerance band for the complete duration of the standard braking period and the correlation is therefore 0%. For the braking forces at the rear axle, the tolerance band is restricted by the braking force distribution factor, since absolute braking moments are considerably less at the rear.

Fig. 6-5 shows the correlations at the individual wheels for the driving dynamic controller models during the complete test signals. In this case errors have occurred, which will not actuate the self-diagnosis systems. However, if your criterion states that there must be a correlation of at least 95% at all wheels, it can be seen that the slight deterioration in signal quality is occurring in nearly every instance.

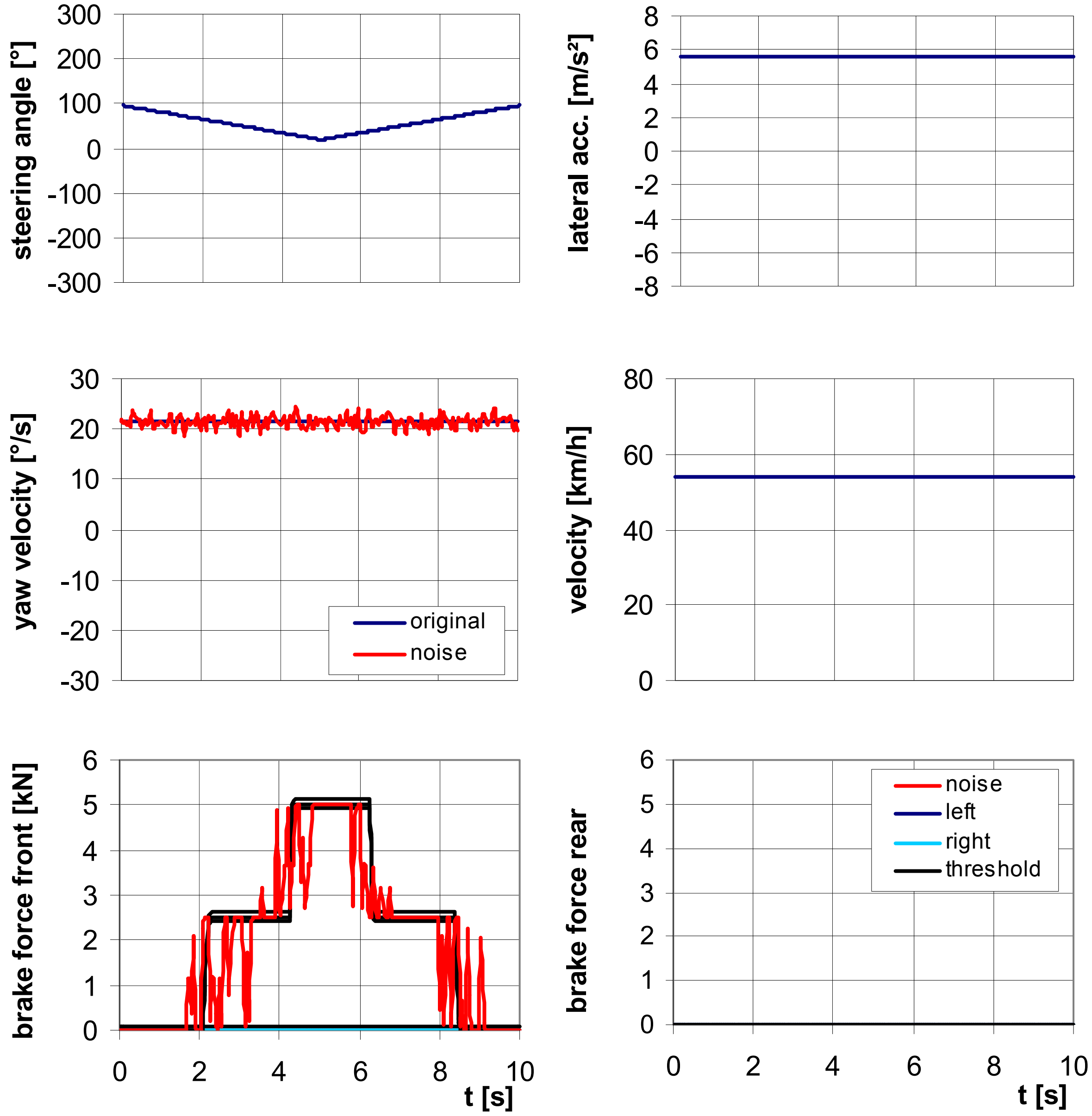

Fig. 6-4: Influence of minimum defects on quality of control – random of 0.002rad on the velocity sensor – oversteer - behaviour in right bends

With this method, it will be possible to test the driving dynamics controller as a complete system, since the actual sensor values also influence the measured braking responses. A meaningful analysis of the system will be possible, long before the problems are such that the system's self-diagnostics will have to completely or partially deactivate the system. Communication is possible using interfaces already fitted to today's vehicles. Available testing technology can be used to measure the braking responses, which means that investment in new equipment can be kept within limits. The test procedure is quick and can be integrated into the regular vehicle test inspection without any problem. The shown procedure in Fig. 6-3 can be developed for every car.

			correlation [%]			
			front left	front right	rear left	rear right
steering angle	offset	0.05 rad	96.10	91.61	95.81	95.81
	offset	-0.05 rad	95.74	96.10	95.81	95.81
	noise	0.05 rad	73.59	76.54	83.96	86.24
	drift	0.05 rad	96.83	95.56	100.00	100.00
yaw velocity	offset	0.002 rad/s	87.87	88.64	97.45	100.00
	offset	-0.002 rad/s	88.64	87.87	100.00	97.45
	noise	0.002 rad/s	58.20	63.36	67.73	73.47
	drift	0.002 rad/s	99.07	98.48	100.00	100.00
lateral acc.	offset	0.05 m/s²	86.58	86.76	100.00	100.00
	offset	-0.05 m/s²	86.76	86.58	100.00	100.00
	noise	0.05 m/s²	94.74	95.28	100.00	100.00
	drift	0.05 m/s²	98.82	99.03	100.00	100.00
long. Acc.	offset	0.4 m/s²	100.00	100.00	100.00	100.00
	offset	-0.4 m/s²	100.00	100.00	100.00	100.00
	noise	0.4 m/s²	100.00	100.00	100.00	100.00
	drift	0.4 m/s²	100.00	100.00	100.00	100.00
wheel speed front left	offset	3 rad/s	100.00	100.00	100.00	100.00
	offset	-3 rad/s	95.24	90.59	100.00	100.00
	noise	3 rad/s	30.22	99.03	100.00	100.00
	drift	3 rad/s	98.25	98.25	100.00	100.00
wheel speed rear left	offset	3 rad/s	90.41	86.35	100.00	100.00
	offset	-3 rad/s	95.24	90.59	100.00	100.00
	noise	3 rad/s	97.66	96.92	18.05	100.00
	drift	3 rad/s	87.44	89.75	100.00	100.00
actuator front left	failure		0.00	100.00	100.00	100.00
	delay	0.10 s	78.19	100.00	100.00	100.00
	delay	0.25 s	64.14	100.00	100.00	100.00
actuator rear left	failure		100.00	100.00	0.00	100.00
	delay	0.10 s	100.00	100.00	75.39	100.00
	delay	0.25 s	100.00	100.00	69.92	100.00

Fig. 6-5: Influence of minimum defects on quality of control

study4 (final)

7 Literature

[ALB96a] Alberti, V., u.a.
Fahrstabilitätsregelung durch Aktivbremsung einzelner Räder
Automatisierungstechnik 44 (1996), Oldenburg Verlag, S.213ff

[AUD01] PRESSEMITTEILUNG DER AUDI AG
Gerüttelt, geschüttelt und geschleudert: Innovationen der neuen Audi A4-Montage
Weltweit erster kombinierter ESP-/Rüttelrollen-Prüfstand
Ingolstadt, 21. August 2001

[CHE87] CHEN; Z.
Regelkreis Fahrer – Fahrzeug für Längs- und Querdynamik
Diplomarbeit , Institut für Fahrzeugtechnik, TU Braunschweig, 1987

[DAT98] Datron - Meßtechnik GmbH
MSW-Sensor, Schwalbach

[FEN98] Fennel, H.
ABS plus und ESP - Ein Konzept zur Beherrschung der Fahrdynamik
ATZ 100 (1998) Nr. 4

[HAR98] Hartig, F. und Reichel, M.
Das Fahrwerk des neuen 3er
Automobiltechnische Zeitschrift (ATZ), 1998

[KLU99] M. KLUMPF, u.a.
Automatisierter Test von Steuergeräten in der Automobilindustrie
VDI Berichte Nr. 1470, 1999,

[KOI96] Koibuchi, K., Yamamoto, M. ,Fukada, Y., Inagaki S.
Vehicle Stability Control in Limit Cornering by Active Brake
SAE-Paper Nr. 960487

[P4305] Patent Bosch P 43 05 155.3
Fahrdynamikregelsystem (FDR von Bosch)

[REI93] Reimpell, J.
Radschlupf – Regelsysteme
Vogel Verlag Würzburg, 1993

[TRW01] TRW
Schulung für KFZ-Überwachungsrganisationen
Thesen zu Fehlern in elektrischen Systemen, 2001

[VAN94] van Zanten, A., Erhardt, R., Pfaff, G.
FDR - Die Fahrdynamikregelung von Bosch
ATZ 96 (1994) 11, S.674-689

[VAN96a] van Zanten, A., Erhardt, R., Lutz, A., Neuwald, W., Bartels, H.
Simulation for the Developement of the Bosch-VDC
SAE-Paper Nr. 960486

[VAN96b] van Zanten, A.
Die FDR von Bosch
Automatisierungstechnik at 7/96, S. 354

[VAN96c] van Zanten, A.
Control aspects of the Bosch-VDC
AVEC 96, Aachen 1996

[VAN98] van Zanten, A., Erhardt, R., Landesfeind K. , Pfaff G.
VDC Systems Development and Perspective
SAE-Paper Nr. 980235

[WAL96] WALLENTOWITZ, H.
Rechentechnik im Kraftfahrwesen
Umdruck zur Vorlesung
Institut für Kraftfahrwesen Aachen, RWTH-Aachen, 1996

[WAL96b] Wallentowitz, H.
Vertikal-/ Querdynamik von Kraftfahrzeugen
Umdruck zur Vorlesung KFZ II, Schriftenreihe Automobiltechnik
ika Aachen, 1996

[WIE74] WIEGNER; P.
Über den Einfluss von Blockierverhinderern auf das Fahrverhalten von Personenkraftwagen bei Panikbremsungen
Dissertation TU Braunschweig, 1974

[WIT95] Witte, B.
Stabilisierung der Gierbewegung eines Kraftfahrzeugs im kritischen Fahrzustand
VDI-Berichte, Schriftenreihe 12, Nr. 254, 1995

8 Appendix

Sinusoidal steering 70 km/h

0,1 Hz			omega fl	omega fr	omega rl	omega rr	ax	ay	psi'	delta_H
omega fl	Zero		0.34							
	Offset	30 rad/s	0.34							
	Noise	30 rad/s	6.7							
	Drift	30 rad/s	1.38							
omega fr	Zero			0.34						
	Offset	30 rad/s		0.34						
	Noise	30 rad/s		6.7						
	Drift	30 rad/s		1.38						
omega rl	Zero				0.34					
	Offset	30 rad/s			0.34					
	Noise	30 rad/s			6.7					
	Drift	30 rad/s			1.38					
omega rr	Zero					0.34				
	Offset	30 rad/s				0.34				
	Noise	30 rad/s				6.7				
	Drift	30 rad/s				1.38				
ax	Zero						-			
	negative						-			
	Offset	2 m/s²					1			
	Noise	2 m/s²					2.69			
	Drift	2 m/s²					1.85			
ay	Zero							0.82		
	negative							0.6		
	Offset	2 m/s²						0.25		
	Noise	2 m/s²						0.42		
	Drift	2 m/s²						1.1		
psi'	Zero								1.48	
	negative								0.92	
	Offset	0,25 rad/s							0.3	
	Noise	0,25 rad/s							0.25	
	Drift	0,25 rad/s							1.78	
delta_H	Zero							0.6		1.4
	negative							0.6		0.9
	Offset	pi						0.62		0.65
	Noise	pi						0.45		10
	Drift	pi						0.64		0.88

Tab. 8-1: Simulation results of driving maneuver No. 1

Sinusoidal steering 70 km/h

0,5 Hz			omega				ax	ay	psi'	delta_H
			fl	fr	rl	rr				
omega fl	Zero		0.34							
	Offset	30 rad/s	0.34							
	Noise	30 rad/s	6.7							
	Drift	30 rad/s	1.38							
omega fr	Zero			0.34						
	Offset	30 rad/s		0.34						
	Noise	30 rad/s		6.7						
	Drift	30 rad/s		1.38						
omega rl	Zero				0.34					
	Offset	30 rad/s			0.34					
	Noise	30 rad/s			6.7					
	Drift	30 rad/s			1.38					
omega rr	Zero					0.34				
	Offset	30 rad/s				0.34				
	Noise	30 rad/s				6.7				
	Drift	30 rad/s				1.38				
ax	Zero						-			
	negative						-			
	Offset	2 m/s²					1			
	Noise	2 m/s²					2.69			
	Drift	2 m/s²					1.85			
ay	Zero							0.53		
	negative							0.37		
	Offset	2 m/s²						0.27		
	Noise	2 m/s²						0.57		
	Drift	2 m/s²						1.2		
psi'	Zero								0.6	
	negative								0.42	
	Offset	0,25 rad/s							0.3	
	Noise	0,25 rad/s							0.25	
	Drift	0,25 rad/s							1.35	
delta_H	Zero							0.42		0.62
	negative							0.37		0.45
	Offset	pi						0.62		0.65
	Noise	pi						0.48		9.2
	Drift	pi						0.8		1.18

Tab. 8-2: Simulation results of driving maneuver No. 2

Sinusoidal steering 70 km/h

1 Hz			omega				ax	ay	psi'	delta_H
			fl	fr	rl	rr				
omega fl	Zero		0.34							
	Offset	30 rad/s	0.34							
	Noise	30 rad/s	6.7							
	Drift	30 rad/s	1.38							
omega fr	Zero			0.34						
	Offset	30 rad/s		0.34						
	Noise	30 rad/s		6.7						
	Drift	30 rad/s		1.38						
omega rl	Zero				0.34					
	Offset	30 rad/s			0.34					
	Noise	30 rad/s			6.7					
	Drift	30 rad/s			1.38					
omega rr	Zero					0.34				
	Offset	30 rad/s				0.34				
	Noise	30 rad/s				6.7				
	Drift	30 rad/s				1.38				
ax	Zero						-			
	negative						-			
	Offset	2 m/s²					1			
	Noise	2 m/s²					2.69			
	Drift	2 m/s²					1.85			
ay	Zero							0.41		
	negative							0.34		
	Offset	2 m/s²						0.27		
	Noise	2 m/s²						0.48		
	Drift	2 m/s²						1.1		
psi'	Zero								0.73	
	negative								0.34	
	Offset	0,25 rad/s							0.32	
	Noise	0,25 rad/s							0.25	
	Drift	0,25 rad/s							1.35	
delta_H	Zero							0.4		0.75
	negative								0.36	0.43
	Offset	pi						0.62		0.65
	Noise	pi						0.49		7.9
	Drift	pi						0.78		0.81

Tab. 8-3: Simulation results of driving maneuver No. 3

Step steer input 52°

2 m/s² v = 40 km/h			omega fl	fr	rl	rr	ax	ay	psi'	delta_H
omega fl	Zero		0.34							
	Offset	30 rad/s	0.34							
	Noise	30 rad/s	2.18							
	Drift	30 rad/s	0.9							
omega fr	Zero			0.34						
	Offset	30 rad/s		0.34						
	Noise	30 rad/s		2.18						
	Drift	30 rad/s		0.9						
omega rl	Zero				0.34					
	Offset	30 rad/s			0.34					
	Noise	30 rad/s			2.18					
	Drift	30 rad/s			0.9					
omega rr	Zero					0.34				
	Offset	30 rad/s				0.34				
	Noise	30 rad/s				2.18				
	Drift	30 rad/s				0.9				
ax	Zero						-			
	negative						-			
	Offset	2 m/s²					1			
	Noise	2 m/s²					2.69			
	Drift	2 m/s²					1.85			
ay	Zero							0.28		
	negative							0.28		
	Offset	2 m/s²						0.28		
	Noise	2 m/s²						0.65		
	Drift	2 m/s²						1.15		
psi'	Zero								0.69	
	negative								0.31	
	Offset	0,25 rad/s							0.34	
	Noise	0,25 rad/s							0.32	
	Drift	0,25 rad/s							1.2	
delta_H	Zero							0.28		0.45
	negative							0.28		0.35
	Offset	pi						0.62		0.73
	Noise	pi						0.52		0.94
	Drift	pi						0.91		1.38

Tab. 8-4: Simulation results of driving maneuver No. 4

Step steer input 52°

4 m/s²			omega				ax	ay	psi'	delta_H
	v = 70 km/h		fl	fr	rl	rr				
omega fl	Zero		0.34							
	Offset	30 rad/s	0.34							
	Noise	30 rad/s	6.8							
	Drift	30 rad/s	1.38							
omega fr	Zero			0.34						
	Offset	30 rad/s		0.34						
	Noise	30 rad/s		6.8						
	Drift	30 rad/s		1.38						
omega rl	Zero				0.34					
	Offset	30 rad/s			0.34					
	Noise	30 rad/s			6.8					
	Drift	30 rad/s			1.38					
omega rr	Zero					0.34				
	Offset	30 rad/s				0.34				
	Noise	30 rad/s				6.8				
	Drift	30 rad/s				1.38				
ax	Zero						-			
	negative						-			
	Offset	2 m/s²					1			
	Noise	2 m/s²					2.69			
	Drift	2 m/s²					1.85			
ay	Zero							0.62		
	negative							0.62		
	Offset	2 m/s²						0.62		
	Noise	2 m/s²						2.7		
	Drift	2 m/s²						1.95		
psi'	Zero								0.31	
	negative								0.2	
	Offset	0,25 rad/s							0.36	
	Noise	0,25 rad/s							0.26	
	Drift	0,25 rad/s							1.72	
delta_H	Zero							0.28		0.42
	negative								0.26	0.27
	Offset	pi						0.62		0.74
	Noise	pi						0.62		1.21
	Drift	pi						0.87		1.06

Tab. 8-5: Simulation results of driving maneuver No. 5

Step steer input 52°

6 m/s²			omega				ax	ay	psi'	delta_H
	v = 140km/h		fl	fr	rl	rr				
omega fl	Zero		0.34							
	Offset	30 rad/s	1.1							
	Noise	30 rad/s	x							
	Drift	30 rad/s	1.86							
omega fr	Zero			0.34						
	Offset	30 rad/s		1.1						
	Noise	30 rad/s		x						
	Drift	30 rad/s		1.86						
omega rl	Zero				0.34					
	Offset	30 rad/s			1.1					
	Noise	30 rad/s			x					
	Drift	30 rad/s			1.86					
omega rr	Zero					0.34				
	Offset	30 rad/s				1.1				
	Noise	30 rad/s				x				
	Drift	30 rad/s				1.86				
ax	Zero						-			
	negative						-			
	Offset	2 m/s²					1			
	Noise	2 m/s²					2.69			
	Drift	2 m/s²					1.85			
ay	Zero							0.62		
	negative							0.62		
	Offset	2 m/s²						0.62		
	Noise	2 m/s²						2.08		
	Drift	2 m/s²						2.78		
psi'	Zero								0.68	
	negative								0.3	
	Offset	0,25 rad/s							0.3	
	Noise	0,25 rad/s							0.25	
	Drift	0,25 rad/s							0.82	
delta_H	Zero								0.35	0.42
	negative							0.29		0.37
	Offset	pi						0.62		0.73
	Noise	pi							1	4
	Drift	pi						1		1.12

Tab. 8-6: Simulation results of driving maneuver No. 6

Steady-state cornering

2 m/s^2	R = 60 m		omega				ax	ay	psi'	delta_H
	v =40 km/h		fl	fr	rl	rr				
omega fl	Zero		0.34							
	Offset	30 rad/s	0.34							
	Noise	30 rad/s	2.18							
	Drift	30 rad/s	0.9							
omega fr	Zero			0.34						
	Offset	30 rad/s		0.34						
	Noise	30 rad/s		2.18						
	Drift	30 rad/s		0.9						
omega rl	Zero				0.34					
	Offset	30 rad/s			0.34					
	Noise	30 rad/s			2.19					
	Drift	30 rad/s			0.9					
omega rr	Zero					0.34				
	Offset	30 rad/s				0.34				
	Noise	30 rad/s				2.19				
	Drift	30 rad/s				0.9				
ax	Zero						-			
	negative						-			
	Offset	2 m/s^2					1			
	Noise	2 m/s^2					2.69			
	Drift	2 m/s^2					1.85			
ay	Zero							0.28		
	negative							0.28		
	Offset	2 m/s^2						0.28		
	Noise	2 m/s^2						0.65		
	Drift	2 m/s^2						1.15		
psi'	Zero								0.69	
	negative								0.31	
	Offset	0,25 rad/s							0.34	
	Noise	0,25 rad/s							0.32	
	Drift	0,25 rad/s							1.2	
delta_H	Zero							0.27		0.45
	negative							0.28		0.34
	Offset	pi						0.62		0.74
	Noise	pi						0.58		0.68
	Drift	pi						0.95		1.49

Tab. 8-7: Simulation results of driving maneuver No. 7

Steady-state cornering

4 m/s²	R = 95 m		omega				ax	ay	psi'	delta_H
	v =70 km/h		fl	fr	rl	rr				
omega fl	Zero		0.34							
	Offset	30 rad/s	0.34							
	Noise	30 rad/s	6.78							
	Drift	30 rad/s	1.4							
omega fr	Zero			0.34						
	Offset	30 rad/s		0.34						
	Noise	30 rad/s		6.78						
	Drift	30 rad/s		1.4						
omega rl	Zero				0.34					
	Offset	30 rad/s			0.34					
	Noise	30 rad/s			6.78					
	Drift	30 rad/s			1.4					
omega rr	Zero					0.34				
	Offset	30 rad/s				0.34				
	Noise	30 rad/s				6.78				
	Drift	30 rad/s				1.4				
ax	Zero						-			
	negative						-			
	Offset	2 m/s²					1			
	Noise	2 m/s²					2.69			
	Drift	2 m/s²					1.85			
ay	Zero							0.31		
	negative							0.2		
	Offset	2 m/s²						0.36		
	Noise	2 m/s²						0.33		
	Drift	2 m/s²						1.74		
psi'	Zero								0.31	
	negative								0.2	
	Offset	0,25 rad/s							0.36	
	Noise	0,25 rad/s							0.33	
	Drift	0,25 rad/s							1.74	
delta_H	Zero							0.29		0.41
	negative							0.25		0.27
	Offset	pi						0.62		0.74
	Noise	pi						0.68		0.71
	Drift	pi						0.87		1.06

Tab. 8-8: Simulation results of driving maneuver No. 8

Steady-state cornering

6 m/s²	R = 250 m		omega				ax	ay	psi'	delta_H
	v =140 km/h		fl	fr	rl	rr				
omega fl	Zero		0.34							
	Offset	30 rad/s	1.11							
	Noise	30 rad/s	x							
	Drift	30 rad/s	1.87							
omega fr	Zero			0.34						
	Offset	30 rad/s		1.11						
	Noise	30 rad/s		x						
	Drift	30 rad/s		1.64						
omega rl	Zero				0.34					
	Offset	30 rad/s			1.11					
	Noise	30 rad/s			x					
	Drift	30 rad/s			1.91					
omega rr	Zero					0.34				
	Offset	30 rad/s				1.11				
	Noise	30 rad/s				x				
	Drift	30 rad/s				1.91				
ax	Zero						-			
	negative						-			
	Offset	2 m/s²					1			
	Noise	2 m/s²					2.69			
	Drift	2 m/s²					1.85			
ay	Zero							0.62		
	negative							0.62		
	Offset	2 m/s²						0,62		
	Noise	2 m/s²						2.38		
	Drift	2 m/s²						6.07		
psi'	Zero								0.69	
	negative								0.31	
	Offset	0,25 rad/s							0.3	
	Noise	0,25 rad/s							0.3	
	Drift	0,25 rad/s							0.82	
delta_H	Zero								0.35	0.55
	negative							0.29		0.4
	Offset	pi						0.62		0.73
	Noise	pi						1.15		4.14
	Drift	pi						0.98		1.14

Tab. 8-9: Simulation results of driving maneuver No. 9

Double lane change open-loop

45 km/h			omega				ax	ay	psi'	delta_H
			fl	fr	rl	rr				
omega fl	Zero		0.34							
	Offset	30 rad/s	0.34							
	Noise	30 rad/s	2.49							
	Drift	30 rad/s	0.97							
omega fr	Zero			0.34						
	Offset	30 rad/s		0.34						
	Noise	30 rad/s		2.49						
	Drift	30 rad/s		0.97						
omega rl	Zero				0.34					
	Offset	30 rad/s			0.34					
	Noise	30 rad/s			2.49					
	Drift	30 rad/s			0.97					
omega rr	Zero					0.34				
	Offset	30 rad/s				0.34				
	Noise	30 rad/s				2.49				
	Drift	30 rad/s				0.97				
ax	Zero						-			
	negative						-			
	Offset	2 m/s²					1			
	Noise	2 m/s²					2.71			
	Drift	2 m/s²					1.84			
ay	Zero							0.76		
	negative							0.65		
	Offset	2 m/s²						0.2		
	Noise	2 m/s²						0.69		
	Drift	2 m/s²						1.96		
psi'	Zero								0.84	
	negative								0.58	
	Offset	0,25 rad/s							0.31	
	Noise	0,25 rad/s							0.32	
	Drift	0,25 rad/s							1.21	
delta_H	Zero							0.45		0.64
	negative								0.58	0.65
	Offset	pi						0.51		0.58
	Noise	pi						1.14		5.58
	Drift	pi						0.52		0.93

Tab. 8-10: Simulation results of driving maneuver No. 10

Double lane change open-loop

50 km/h			omega				ax	ay	psi'	delta_H
			fl	fr	rl	rr				
omega fl	Zero		0.34							
	Offset	30 rad/s	0.34							
	Noise	30 rad/s	2.99							
	Drift	30 rad/s	1.04							
omega fr	Zero			0.34						
	Offset	30 rad/s		0.34						
	Noise	30 rad/s		2.99						
	Drift	30 rad/s		1.04						
omega rl	Zero				0.34					
	Offset	30 rad/s			0.34					
	Noise	30 rad/s			2.99					
	Drift	30 rad/s			1.04					
omega rr	Zero					0.34				
	Offset	30 rad/s				0.34				
	Noise	30 rad/s				2.99				
	Drift	30 rad/s				1.04				
ax	Zero						-			
	negative						-			
	Offset	2 m/s²					1			
	Noise	2 m/s²					2.72			
	Drift	2 m/s²					1.84			
ay	Zero							1.26		
	negative							1.16		
	Offset	2 m/s²						0.18		
	Noise	2 m/s²						0.31		
	Drift	2 m/s²						0.74		
psi'	Zero								1.32	
	negative								1.07	
	Offset	0,25 rad/s							0.31	
	Noise	0,25 rad/s							0.32	
	Drift	0,25 rad/s							1.69	
delta_H	Zero							0.94		1.13
	negative							1.07		1.16
	Offset	pi						0.62		0.69
	Noise	pi						0.6		5.45
	Drift	pi						0.51		0.71

Tab. 8-11: Simulation results of driving maneuver No. 11

Double lane change open-loop

55 km/h			omega				ax	ay	psi'	delta_H
			fl	fr	rl	rr				
omega fl	Zero		0.34							
	Offset	30 rad/s	0.34							
	Noise	30 rad/s	3.39							
	Drift	30 rad/s	1.12							
omega fr	Zero			0.34						
	Offset	30 rad/s		0.34						
	Noise	30 rad/s		3.43						
	Drift	30 rad/s		1.12						
omega rl	Zero				0.34					
	Offset	30 rad/s			0.34					
	Noise	30 rad/s			3.44					
	Drift	30 rad/s			1.12					
omega rr	Zero					0.34				
	Offset	30 rad/s				0.34				
	Noise	30 rad/s				3.44				
	Drift	30 rad/s				1.12				
ax	Zero						-			
	negative						-			
	Offset	2 m/s²					1			
	Noise	2 m/s²					2.97			
	Drift	2 m/s²					2.24			
ay	Zero							1.02		
	negative							0.82		
	Offset	2 m/s²						0.18		
	Noise	2 m/s²						0.31		
	Drift	2 m/s²						3.14		
psi'	Zero								1.18	
	negative								0.87	
	Offset	0,25 rad/s							0.31	
	Noise	0,25 rad/s							0.32	
	Drift	0,25 rad/s							1.79	
delta_H	Zero							0.72		0.95
	negative							0.82		0.87
	Offset	pi						0.62		0.69
	Noise	pi						0.52		5.49
	Drift	pi						0.5		0.69

Tab. 8-12: Simulation results of driving maneuver No. 12

Double lane change open-loop

60 km/h			omega				ax	ay	psi'	delta_H
			fl	fr	rl	rr				
omega fl	Zero		0.34							
	Offset	30 rad/s	0.34							
	Noise	30 rad/s	4							
	Drift	30 rad/s	1.2							
omega fr	Zero			0.34						
	Offset	30 rad/s		0.34						
	Noise	30 rad/s		4.11						
	Drift	30 rad/s		1.2						
omega rl	Zero				0.34					
	Offset	30 rad/s			0.34					
	Noise	30 rad/s			4.69					
	Drift	30 rad/s			1.2					
omega rr	Zero					0.34				
	Offset	30 rad/s				0.34				
	Noise	30 rad/s				4.69				
	Drift	30 rad/s				1.2				
ax	Zero						-			
	negative						-			
	Offset	2 m/s²					1			
	Noise	2 m/s²					2.9			
	Drift	2 m/s²					2.07			
ay	Zero							1.2		
	negative							1.1		
	Offset	2 m/s²						0.18		
	Noise	2 m/s²						0.31		
	Drift	2 m/s²						0.92		
psi'	Zero								1.28	
	negative								1.06	
	Offset	0,25 rad/s							0.31	
	Noise	0,25 rad/s							0.32	
	Drift	0,25 rad/s							1.23	
delta_H	Zero							0.84		1
	negative								1.06	1.1
	Offset	pi								0.49
	Noise	pi						0.5		
	Drift	pi						0.5		0.68

Tab. 8-13: Simulation results of driving maneuver No. 13

Double lane change open-loop

65 km/h			omega				ax	ay	psi'	delta_H
			fl	fr	rl	rr				
omega fl	Zero		0.34							
	Offset	30 rad/s	0.34							
	Noise	30 rad/s	4.67							
	Drift	30 rad/s	1.32							
omega fr	Zero			0.34						
	Offset	30 rad/s		0.34						
	Noise	30 rad/s		4.49						
	Drift	30 rad/s		1.35						
omega rl	Zero				0.34					
	Offset	30 rad/s			0.34					
	Noise	30 rad/s			4.99					
	Drift	30 rad/s			1.33					
omega rr	Zero					0.34				
	Offset	30 rad/s				0.34				
	Noise	30 rad/s				4.91				
	Drift	30 rad/s				1.33				
ax	Zero						-			
	negative						-			
	Offset	2 m/s²					1.33			
	Noise	2 m/s²					3.15			
	Drift	2 m/s²					2.63			
ay	Zero							1.02		
	negative							0.93		4.21
	Offset	2 m/s²						0.28		4.18
	Noise	2 m/s²						0.69		4.18
	Drift	2 m/s²						3.1		
psi'	Zero								1.11	
	negative								0.91	
	Offset	0,25 rad/s							0.31	
	Noise	0,25 rad/s							0.32	
	Drift	0,25 rad/s							1.21	
delta_H	Zero							0.65		0.82
	negative								0.91	0.93
	Offset	pi						0.62		0.64
	Noise	pi						0.48		4.16
	Drift	pi						0.51		0.67

Tab. 8-14: Simulation results of driving maneuver No. 14

Double lane change closed-loop

45 km/h			omega				ax	ay	psi'	delta_H
			fl	fr	rl	rr				
omega fl	Zero		0.34							
	Offset	30 rad/s	0.34							
	Noise	30 rad/s	2.49							
	Drift	30 rad/s	0.97							
omega fr	Zero			0.34						
	Offset	30 rad/s		0.34						
	Noise	30 rad/s		2.49						
	Drift	30 rad/s		0.97						
omega rl	Zero				0.34					
	Offset	30 rad/s			0.34					
	Noise	30 rad/s			2.49					
	Drift	30 rad/s			0.97					
omega rr	Zero					0.34				
	Offset	30 rad/s				0.34				
	Noise	30 rad/s				2.49				
	Drift	30 rad/s				0.97				
ax	Zero						-			
	negative						-			
	Offset	2 m/s²					1			
	Noise	2 m/s²					2.71			
	Drift	2 m/s²					1.84			
ay	Zero							1.18		
	negative							1.1		
	Offset	2 m/s²						0.18		
	Noise	2 m/s²						0.31		
	Drift	2 m/s²						0.87		
psi'	Zero								1.25	
	negative								1	
	Offset	0,25 rad/s							0.31	
	Noise	0,25 rad/s							0.32	
	Drift	0,25 rad/s							1.21	
delta_H	Zero							0.85		1.02
	negative								1	
	Offset	pi								0.44
	Noise	pi						0.59		6.92
	Drift	pi						0.53		0.73

Tab. 8-15: Simulation results of driving maneuver No. 15

Double lane change closed-loop

50 km/h			omega				ax	ay	psi'	delta_H
			fl	fr	rl	rr				
omega fl	Zero		0.34							
	Offset	30 rad/s	0.34							
	Noise	30 rad/s	2.99							
	Drift	30 rad/s	1.04							
omega fr	Zero			0.34						
	Offset	30 rad/s		0.34						
	Noise	30 rad/s		2.99						
	Drift	30 rad/s		1.04						
omega rl	Zero				0.34					
	Offset	30 rad/s			0.34					
	Noise	30 rad/s			2.99					
	Drift	30 rad/s			1.04					
omega rr	Zero					0.34				
	Offset	30 rad/s				0.34				
	Noise	30 rad/s				2.99				
	Drift	30 rad/s				1.04				
ax	Zero						-			
	negative						-			
	Offset	2 m/s²					1			
	Noise	2 m/s²					2.72			
	Drift	2 m/s²					1.84			
ay	Zero							1.18		
	negative							1.03		
	Offset	2 m/s²						0.18		
	Noise	2 m/s²						0.31		
	Drift	2 m/s²						2.21		
psi'	Zero								1.18	
	negative								0.97	
	Offset	0,25 rad/s							0.31	
	Noise	0,25 rad/s							0.32	
	Drift	0,25 rad/s							1.25	
delta_H	Zero							0.75		0.9
	negative								0.97	1.03
	Offset	pi								0.44
	Noise	pi						0.59		6.58
	Drift	pi						0.52		0.71

Tab. 8-16: Simulation results of driving maneuver No. 16

Double lane change closed-loop

55 km/h			omega				ax	ay	psi'	delta_H
			fl	fr	rl	rr				
omega fl	Zero		0.34							
	Offset	30 rad/s	0.34							
	Noise	30 rad/s	3.39							
	Drift	30 rad/s	1.12							
omega fr	Zero			0.34						
	Offset	30 rad/s		0.34						
	Noise	30 rad/s		3.38						
	Drift	30 rad/s		1.12						
omega rl	Zero				0.34					
	Offset	30 rad/s			0.34					
	Noise	30 rad/s			3.37					
	Drift	30 rad/s			1.12					
omega rr	Zero					0.34				
	Offset	30 rad/s				0.34				
	Noise	30 rad/s				3.42				
	Drift	30 rad/s				1.12				
ax	Zero						-			
	negative						-			
	Offset	2 m/s²					1			
	Noise	2 m/s²					2.82			
	Drift	2 m/s²					2.24			
ay	Zero							1.03		
	negative							0.96		
	Offset	2 m/s²						0.18		
	Noise	2 m/s²						0.31		
	Drift	2 m/s²						2.2		
psi'	Zero								1.11	
	negative								0.93	
	Offset	0,25 rad/s							0.31	
	Noise	0,25 rad/s							0.32	
	Drift	0,25 rad/s							1.21	
delta_H	Zero							0.67		0.81
	negative								0.93	0.96
	Offset	pi						0.62		0.64
	Noise	pi						0.54		6
	Drift	pi						0.5		0.7

Tab. 8-17: Simulation results of driving maneuver No. 17

Double lane change closed-loop

60 km/h			omega				ax	ay	psi'	delta_H
			fl	fr	rl	rr				
omega fl	Zero		0.34							
	Offset	30 rad/s	0.34							
	Noise	30 rad/s	4.35							
	Drift	30 rad/s	1.2							
omega fr	Zero			0.34						
	Offset	30 rad/s		0.34						
	Noise	30 rad/s		3.71						
	Drift	30 rad/s		1.21						
omega rl	Zero				0.34					
	Offset	30 rad/s			0.34					
	Noise	30 rad/s			4.69					
	Drift	30 rad/s			1.2					
omega rr	Zero					0.34				
	Offset	30 rad/s				0.34				
	Noise	30 rad/s				4.69				
	Drift	30 rad/s				1.21				
ax	Zero						-			
	negative						-			
	Offset	2 m/s²					1			
	Noise	2 m/s²					2.69			
	Drift	2 m/s²					2.07			
ay	Zero							0.97		
	negative							0.91		
	Offset	2 m/s²						0.18		
	Noise	2 m/s²						0.31		
	Drift	2 m/s²						3.26		
psi'	Zero								1.05	
	negative								0.89	
	Offset	0,25 rad/s							0.31	
	Noise	0,25 rad/s							0.32	
	Drift	0,25 rad/s							1.22	
delta_H	Zero							0.6		0.73
	negative								0.89	0.91
	Offset	pi							0.6	0.62
	Noise	pi						0.5		5.6
	Drift	pi						0.5		1.05

Tab. 8-18: Simulation results of driving maneuver No. 18

Double lane change closed-loop

65 km/h			omega				ax	ay	psi'	delta_H
			fl	fr	rl	rr				
omega fl	Zero		0.34							
	Offset	30 rad/s	0.34							
	Noise	30 rad/s	4.89							
	Drift	30 rad/s	1.35							
omega fr	Zero			0.34						
	Offset	30 rad/s		0.34						
	Noise	30 rad/s		4.54						
	Drift	30 rad/s		1.37						
omega rl	Zero				0.34					
	Offset	30 rad/s			0.34					
	Noise	30 rad/s			5.08					
	Drift	30 rad/s			1.38					
omega rr	Zero					0.34				
	Offset	30 rad/s				0.34				
	Noise	30 rad/s				5.18				
	Drift	30 rad/s				1.35				
ax	Zero						-			
	negative						3.58			
	Offset	2 m/s²					1.41			
	Noise	2 m/s²					2.92			
	Drift	2 m/s²					2.89			
ay	Zero							0.92		3.33
	negative							0.87		3.38
	Offset	2 m/s²						0.18		3.23
	Noise	2 m/s²						0.31		3.23
	Drift	2 m/s²						3.21		3.54
psi'	Zero								1.01	
	negative								0.86	
	Offset	0,25 rad/s							0.31	
	Noise	0,25 rad/s							0.32	
	Drift	0,25 rad/s							1.21	
delta_H	Zero							0.54		0.67
	negative								0.86	0.87
	Offset	pi							0.56	0.62
	Noise	pi						1.19		5.51
	Drift	pi						0.49		1.07

Tab. 8-19: Simulation results of driving maneuver No. 19

Straightline driving open-loop (delta_H = 0)

50 km/h			omega				ax	ay	psi'	delta_H
			fl	fr	rl	rr				
omega fl	Zero		0.34							
	Offset	30 rad/s	0.34							
	Noise	30 rad/s	3							
	Drift	30 rad/s	1.04							
omega fr	Zero			0.34						
	Offset	30 rad/s		0.34						
	Noise	30 rad/s		3						
	Drift	30 rad/s		1.04						
omega rl	Zero				0.34					
	Offset	30 rad/s			0.34					
	Noise	30 rad/s			3					
	Drift	30 rad/s			1.04					
omega rr	Zero					0.34				
	Offset	30 rad/s				0.34				
	Noise	30 rad/s				3				
	Drift	30 rad/s				1.04				
ax	Zero						-			
	negative						-			
	Offset	2 m/s²					1			
	Noise	2 m/s²					2.71			
	Drift	2 m/s²					1.83			
ay	Zero							-		
	negative							-		
	Offset	2 m/s²						0.18		
	Noise	2 m/s²						0.31		
	Drift	2 m/s²						0.7		
psi'	Zero								-	
	negative								-	
	Offset	0,25 rad/s							0.31	
	Noise	0,25 rad/s							0.32	
	Drift	0,25 rad/s							1.21	
delta_H	Zero									-
	negative									-
	Offset	pi								0.44
	Noise	pi						0.59		0.65
	Drift	pi						0.52		0.71

Tab. 8-20: Simulation results of driving maneuver No. 20

Straightline driving open-loop (delta_H = 0)

100 km/h			omega				ax	ay	psi'	delta_H
			fl	fr	rl	rr				
omega fl	Zero		0.34							
	Offset	30 rad/s	1.11							
	Noise	30 rad/s	21.97							
	Drift	30 rad/s	1.6							
omega fr	Zero			0.34						
	Offset	30 rad/s		1.11						
	Noise	30 rad/s		21.97						
	Drift	30 rad/s		1.6						
omega rl	Zero				0.34					
	Offset	30 rad/s			1.11					
	Noise	30 rad/s			21.97					
	Drift	30 rad/s			1.6					
omega rr	Zero					0.34				
	Offset	30 rad/s				1.11				
	Noise	30 rad/s				21.97				
	Drift	30 rad/s				1.6				
ax	Zero						-			
	negative						-			
	Offset	2 m/s²					1			
	Noise	2 m/s²					2.72			
	Drift	2 m/s²					1.82			
ay	Zero							-		
	negative							-		
	Offset	2 m/s²						0.18		
	Noise	2 m/s²						0.31		
	Drift	2 m/s²						0.7		
psi'	Zero								-	
	negative								-	
	Offset	0,25 rad/s							0.31	
	Noise	0,25 rad/s							0.32	
	Drift	0,25 rad/s							1.21	
delta_H	Zero									-
	negative									-
	Offset	pi								0.44
	Noise	pi						0.56		0.65
	Drift	pi						0.56		0.65

Tab. 8-21: Simulation results of driving maneuver No. 21

Straightline driving open-loop (delta_H = 0)

130 km/h			omega				ax	ay	psi'	delta_H
			fl	fr	rl	rr				
omega fl	Zero		0.34							
	Offset	30 rad/s	1.11							
	Noise	30 rad/s	x							
	Drift	30 rad/s	1.75							
omega fr	Zero			0.34						
	Offset	30 rad/s		1.11						
	Noise	30 rad/s		x						
	Drift	30 rad/s		1.75						
omega rl	Zero				0.34					
	Offset	30 rad/s			1.11					
	Noise	30 rad/s			x					
	Drift	30 rad/s			1.75					
omega rr	Zero					0.34				
	Offset	30 rad/s				1.11				
	Noise	30 rad/s				x				
	Drift	30 rad/s				1.75				
ax	Zero						-			
	negative						-			
	Offset	2 m/s²					1			
	Noise	2 m/s²					2.77			
	Drift	2 m/s²					1.82			
ay	Zero							-		
	negative							-		
	Offset	2 m/s²						0.18		
	Noise	2 m/s²						0.31		
	Drift	2 m/s²						0.7		
psi'	Zero								-	
	negative								-	
	Offset	0,25 rad/s							0.31	
	Noise	0,25 rad/s							0.32	
	Drift	0,25 rad/s							1.21	
delta_H	Zero									-
	negative									-
	Offset	pi							0.31	0.44
	Noise	pi							0.46	0.54
	Drift	pi						0.57		0.64

Tab. 8-22: Simulation results of driving maneuver No. 22

Straightline driving closed-loop (straight.asc)

50 km/h			omega				ax	ay	psi'	delta_H
			fl	fr	rl	rr				
omega fl	Zero		0.34							
	Offset	30 rad/s	0.34							
	Noise	30 rad/s	3							
	Drift	30 rad/s	1.04							
omega fr	Zero			0.34						
	Offset	30 rad/s		0.34						
	Noise	30 rad/s		3						
	Drift	30 rad/s		1.04						
omega rl	Zero				0.34					
	Offset	30 rad/s			0.34					
	Noise	30 rad/s			3					
	Drift	30 rad/s			1.04					
omega rr	Zero					0.34				
	Offset	30 rad/s				0.34				
	Noise	30 rad/s				3				
	Drift	30 rad/s				1.04				
ax	Zero						-			
	negative						-			
	Offset	2 m/s²					1			
	Noise	2 m/s²					2.71			
	Drift	2 m/s²					1.83			
ay	Zero							-		
	negative							-		
	Offset	2 m/s²						0.18		
	Noise	2 m/s²						0.31		
	Drift	2 m/s²						0.7		
psi'	Zero								-	
	negative								-	
	Offset	0,25 rad/s							0.31	
	Noise	0,25 rad/s							0.32	
	Drift	0,25 rad/s							1.21	
delta_H	Zero									-
	negative									-
	Offset	pi								0.44
	Noise	pi						0.59		0.65
	Drift	pi						0.52		0.71

Tab. 8-23: Simulation results of driving maneuver No. 23

Straightline driving closed-loop (straight.asc)

100 km/h			omega				ax	ay	psi'	delta_H
			fl	fr	rl	rr				
omega fl	Zero		0.34							
	Offset	30 rad/s	1.11							
	Noise	30 rad/s	21.97							
	Drift	30 rad/s	1.6							
omega fr	Zero			0.34						
	Offset	30 rad/s		1.11						
	Noise	30 rad/s		21.97						
	Drift	30 rad/s		1.6						
omega rl	Zero				0.34					
	Offset	30 rad/s			1.11					
	Noise	30 rad/s			21.97					
	Drift	30 rad/s			1.6					
omega rr	Zero					0.34				
	Offset	30 rad/s				1.11				
	Noise	30 rad/s				21.97				
	Drift	30 rad/s				1.6				
ax	Zero						-			
	negative						-			
	Offset	2 m/s²					1			
	Noise	2 m/s²					2.72			
	Drift	2 m/s²					1.82			
ay	Zero							-		
	negative							-		
	Offset	2 m/s²						0.18		
	Noise	2 m/s²						0.31		
	Drift	2 m/s²						0.7		
psi'	Zero								-	
	negative								-	
	Offset	0,25 rad/s							0.31	
	Noise	0,25 rad/s							0.32	
	Drift	0,25 rad/s							1.21	
delta_H	Zero									-
	negative									-
	Offset	pi								0.44
	Noise	pi						0.56		0.65
	Drift	pi						0.56		0.65

Tab. 8-24: Simulation results of driving maneuver No. 24

Straightline driving closed-loop (straight.asc)

130 km/h			omega				ax	ay	psi'	delta_H
			fl	fr	rl	rr				
omega fl	Zero		0.34							
	Offset	30 rad/s	1.11							
	Noise	30 rad/s	x							
	Drift	30 rad/s	1.75							
omega fr	Zero			0.34						
	Offset	30 rad/s		1.11						
	Noise	30 rad/s		x						
	Drift	30 rad/s		1.75						
omega rl	Zero				0.34					
	Offset	30 rad/s			1.11					
	Noise	30 rad/s			x					
	Drift	30 rad/s			1.75					
omega rr	Zero					0.34				
	Offset	30 rad/s				1.11				
	Noise	30 rad/s				x				
	Drift	30 rad/s				1.75				
ax	Zero						-			
	negative						-			
	Offset	2 m/s²					1			
	Noise	2 m/s²					2.77			
	Drift	2 m/s²					1.82			
ay	Zero							-		
	negative							-		
	Offset	2 m/s²						0.18		
	Noise	2 m/s²						0.31		
	Drift	2 m/s²						0.7		
psi'	Zero								-	
	negative								-	
	Offset	0,25 rad/s							0.31	
	Noise	0,25 rad/s							0.32	
	Drift	0,25 rad/s							1.21	
delta_H	Zero									-
	negative									-
	Offset	pi							0.31	0.44
	Noise	pi							0.46	0.54
	Drift	pi						0.57		0.64

Tab. 8-25: Simulation results of driving maneuver No. 25